INTRAOPERATIVE ULTRASOUND IN BRAIN TUMOR SURGERY: STATE-OF-THE-ART AND FUTURE PERSPECTIVES

EDITED BY: Massimiliano Del Bene, Francesco DiMeco and Geirmund Unsgård
PUBLISHED IN: Frontiers in Oncology

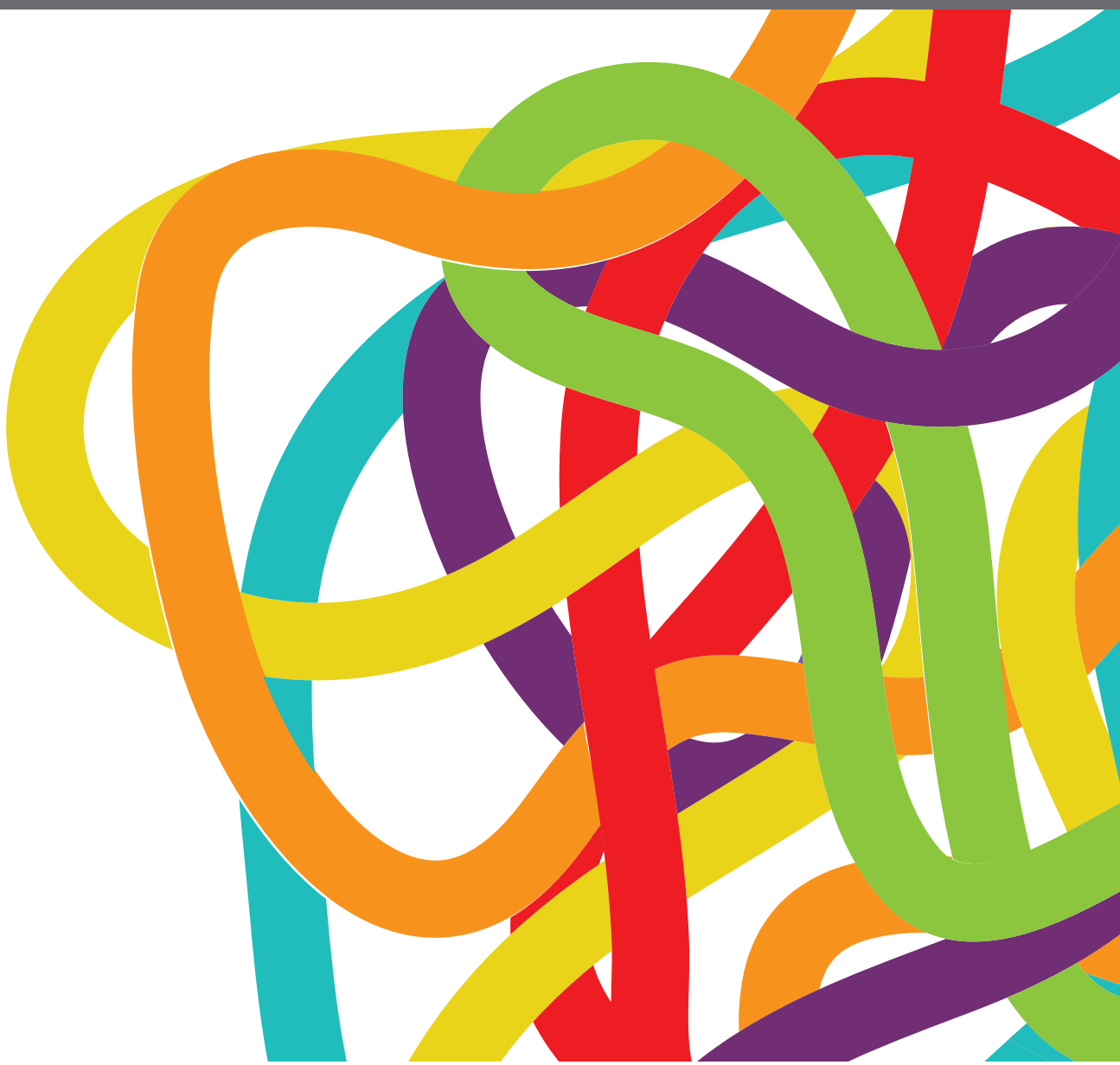

frontiers Research Topics

ISSN 1664-8714
ISBN 978-2-88971-933-4
DOI 10.3389/978-2-88971-933-4

About Frontiers

Frontiers is more than just an open-access publisher of scholarly articles: it is a pioneering approach to the world of academia, radically improving the way scholarly research is managed. The grand vision of Frontiers is a world where all people have an equal opportunity to seek, share and generate knowledge. Frontiers provides immediate and permanent online open access to all its publications, but this alone is not enough to realize our grand goals.

Frontiers Journal Series

The Frontiers Journal Series is a multi-tier and interdisciplinary set of open-access, online journals, promising a paradigm shift from the current review, selection and dissemination processes in academic publishing. All Frontiers journals are driven by researchers for researchers; therefore, they constitute a service to the scholarly community. At the same time, the Frontiers Journal Series operates on a revolutionary invention, the tiered publishing system, initially addressing specific communities of scholars, and gradually climbing up to broader public understanding, thus serving the interests of the lay society, too.

Dedication to Quality

Each Frontiers article is a landmark of the highest quality, thanks to genuinely collaborative interactions between authors and review editors, who include some of the world's best academicians. Research must be certified by peers before entering a stream of knowledge that may eventually reach the public - and shape society; therefore, Frontiers only applies the most rigorous and unbiased reviews.
Frontiers revolutionizes research publishing by freely delivering the most outstanding research, evaluated with no bias from both the academic and social point of view. By applying the most advanced information technologies, Frontiers is catapulting scholarly publishing into a new generation.

What are Frontiers Research Topics?

Frontiers Research Topics are very popular trademarks of the Frontiers Journals Series: they are collections of at least ten articles, all centered on a particular subject. With their unique mix of varied contributions from Original Research to Review Articles, Frontiers Research Topics unify the most influential researchers, the latest key findings and historical advances in a hot research area! Find out more on how to host your own Frontiers Research Topic or contribute to one as an author by contacting the Frontiers Editorial Office: frontiersin.org/about/contact

INTRAOPERATIVE ULTRASOUND IN BRAIN TUMOR SURGERY: STATE-OF-THE-ART AND FUTURE PERSPECTIVES

Topic Editors:
Massimiliano Del Bene, IRCCS Carlo Besta Neurological Institute Foundation, Italy
Francesco DiMeco, IRCCS Carlo Besta Neurological Institute Foundation, Italy
Geirmund Unsgård, Norwegian University of Science and Technology, Norway

Citation: Del Bene, M., DiMeco, F., Unsgård, G., eds. (2021). Intraoperative Ultrasound in Brain Tumor Surgery: State-Of-The-Art and Future Perspectives. Lausanne: Frontiers Media SA. doi: 10.3389/978-2-88971-933-4

Table of Contents

frontiers in Oncology

EDITORIAL
published: 02 November 2021
doi: 10.3389/fonc.2021.780517

Editorial: Intraoperative Ultrasound in Brain Tumor Surgery: State-Of-The-Art and Future Perspectives

Massimiliano Del Bene[1,2*], *Francesco DiMeco*[1,3,4] *and Geirmund Unsgård*[5]

[1] *Department of Neurosurgery, Fondazione Istituto di Ricovero e Cura a Carattere Scientifico (IRCCS) Istituto Neurologico Carlo Besta, Milan, Italy,* [2] *Department of Experimental Oncology, European Institute of Oncology (IEO), Istituto di Ricovero e Cura a Carattere Scientifico (IRCCS), Milan, Italy,* [3] *Department of Pathophysiology and Transplantation, University of Milan, Milan, Italy,* [4] *Department of Neurological Surgery, Johns Hopkins Medical School, Baltimore, MD, United States,* [5] *Norwegian University of Science and Technology, Trondheim, Norway*

Keywords: intra-operative ultrasound, neurosurgery, oncology, brain tumour, advanced ultrasound

Editorial on the Research Topic

Intraoperative Ultrasound in Brain Tumor Surgery: State-Of-The-Art and Future Perspectives

OPEN ACCESS

Edited and reviewed by:
David D. Eisenstat,
Royal Children's Hospital, Australia

***Correspondence:**
Massimiliano Del Bene
massimiliano.delbene@istituto-besta.it

Specialty section:
This article was submitted to Neuro-Oncology and Neurosurgical Oncology, a section of the journal Frontiers in Oncology

Received: *21 September 2021*
Accepted: *13 October 2021*
Published: *02 November 2021*

Citation:
Del Bene M, DiMeco F and Unsgård G (2021) Editorial: Intraoperative Ultrasound in Brain Tumor Surgery: State-Of-The-Art and Future Perspectives. Front. Oncol. 11:780517. doi: 10.3389/fonc.2021.780517

Ultrasound (US) is undoubtedly the most versatile imaging modality in medicine. It can provide real-time, high-resolution images in almost every setting, (e.g. ward, emergency room, outpatients clinic, operating room, etc) and in almost every anatomical region (e.g. abdomen, thorax, limbs, intra-cranial, etc). The central nervous system, owing to its optimal mechanical/acoustic properties, represents the ideal substrate for US propagation and image generation (1). The earliest reports on intraoperative ultrasound (ioUS) in neurosurgery date back to the late 1970s (2). Since this time, US applications have been described both in brain and spine surgery. Intriguingly, after initial enthusiasm, ioUS has mainly been confined to marginal applications because of several intrinsic limitations such as poor resolution, user dependency, difficult semiology/orientation, and lack of specific training (1, 3). More recently, the introduction of major technical improvements has gradually framed ioUS as one of the most versatile and valuable techniques for intra-operative imaging in neurosurgery even if it is still under utilized, mainly because of the lack of specific training.

The multi-modal nature of ioUS can guide surgery, offering both structural and functional information in real-time. The classical B-mode US has reached an exceptional spatial and temporal resolution, providing mainly structural information (4–6). In the effort to overcome B-mode limitations [e.g. specific semiotics, orientation (5, 6)], fusion imaging has been introduced, which enables practitioners to match the ioUS images to the pre-operative magnetic resonance imaging (MRI) to better understand semiotics, facilitate orientation, and compensate brain shift occurrence (7–10). Doppler imaging (color-, spectral-, power-, micro-vessels) permits the study of blood flow and at the same time, the anatomy of the vessels (8, 11, 12), providing valuable information for both vascular and oncological neurosurgery (8, 12–15). Further evolution of Doppler imaging has been enabled by contrast-enhanced ultrasound (CEUS), which relies on purely endovascular contrast agents, namely gas-filled micro-bubbles, to provide a dynamic and continuous representation of the

vascular tree, from a structural and a functional standpoint, and of the tissue perfusion pattern (16–18). Its applications, in oncological surgery, encompass tumor identification and characterization, assessment of the pattern of vascularization, and the identification of residual tumours (12, 15, 18–20). The last modality, even if still at its dawn, is elasto-sonography (ESG). ESG provides a mechanical characterization of the tissues, relying on the distortion obtained through a mechanical stimulus, which can be delivered by US impulses (quantitative representation- shear wave elastography) or by brain pulsation and probe motion (qualitative representation – strain elastography) (21). Interestingly, by assessing the mechanical properties of the tissues, it is possible to highlight most of the lesions and characterize their features such as degree and histotype (12, 21–27). Regardless of the employed modality, during the process of surgery, ioUS semiotics and image quality are subjected to modifications and deterioration. Different explanations have been proposed leading to specific adjuncts, such as mini-probes (28, 29), specific fluid to fill the cavity (30), contrast-enhanced ultrasound (19), and tangential trans-cortical scanning (5), which have further improved ioUS potential. We are still witnessing innovation and research in the field of ioUS applications in neurosurgery.

This Research Topic reports the experiences of leading experts in the field, presenting an updated portrait of the state-of-the-art and future perspectives of ioUS. Carai et al. present their experience on ioUS in pediatric neurosurgical oncology, where they observed a good predictive value on the extent of resection of ioUS in children. Šteňo et al. address ioUS from a different perspective by presenting on current limitations, such as suboptimal quality in some pathologies, different types of artifacts, patient positioning, and the unavailability of probes to depict the entire sellar region finally presenting valuable insights and solutions. Bastos et al. describe the use of 3D ioUS with intra-operative MRI, demonstrating that ioUS, in most cases, defines tumor location, tumor margins, relevant landmarks for orientation, and predicts the extent of resection. Incekara et al. performed a randomized controlled trial in glioblastoma patients (NCT03531333), demonstrating that ioUS (B-mode) leads to a complete resection in a higher number of patients if compared to standard surgery. Chan et al., relying on their experience with Shear Wave Elastography (SWE), observed a higher sensitivity of SWE and an improved ability to detect residual tumor, thus sustaining the combination of surgeon's opinion and ioUS to enhance the extent of resection. Gueziri et al. present a novel US-based registration for spinal procedures which yields an acceptable accuracy if compared to CT-based procedures. Saß et al. present a novel approach to amend the brain shift in intra-axial tumor surgery. In particular, they developed a method based on 3D ioUS color Doppler to estimate the amount of brain shift intraoperatively, thus potentially allowing an update of the navigation system. Gerard et al. undertook a comprehensive review, dissecting the limitation and impact of brain-shift in neuro-navigation and focusing on ioUS-based technologies for measuring and compensating its occurrence. Different ioUS approaches are presented, together with the major unmet clinical need for newer openly available clinical datasets. Notably, ioUS would benefit not only from US technical improvements but also from emerging technologies such as machine learning and modern graphics processing units (GPUs), which strictly depend on the databases of ioUS images to train the algorithms. In this context, Reinertsen et al. present the current situation of the large number of projects that have profited from the publicly available datasets that include MR and US data from brain tumor cases, finally advocating for the realization of an organized platform to prospectively collect data to develop and validate machine learning algorithms. On this line, Cepeda et al. exploited an automated deep learning approach for image analysis. They demonstrate that the automated processing of ioUS through deep learning can generate high-precision algorithms to differentiate glioblastomas from metastases, in particular with strain elastography.

This collection of articles provides a wide overview of ioUS applications in neurosurgery, enhancing the level of evidence in favor of the use of ioUS in neurosurgical oncology, and shedding light on some promising research lines and unmet needs in this field.

AUTHOR CONTRIBUTIONS

MB, FD, and GU: manuscript concept and design. FD and GU: final revision. All authors contributed to the article and approved the submitted version.

REFERENCES

1. Makuuchi M, Torzilli G, Machi J. History of Intraoperative Ultrasound. *Ultrasound Med Biol Elsevier* (1998) 24:1229–42. doi: 10.1016/S0301-5629(98)00112-4
2. Reid MH. Ultrasonic Visualization of a Cervical Cord Cystic Astrocytoma. *Am J Roentgenol* (1978) 131(5):907–8. doi: 10.2214/ajr.131.5.907
3. Van Velthoven V. Intraoperative Ultrasound Imaging: Comparison of Pathomorphological Findings in US *Versus* CT, MRI and Intraoperative Findings. In: *Acta Neurochirurgica, Supplement. Acta Neurochir Suppl;* Switzerland AG: Springer Nature (2003). p. 95–9.
4. Martegani A, Mattei L, Aiani L. US Physics, Basic Principles, and Clinical Application. In: *Intraoperative Ultrasound (IOUS) in Neurosurgery: From Standard B-Mode to Elastosonography*. Cham, Switzerland: Springer. (2016). p. 9–17.
5. Coburger J, König RW. Intraoperative Findings in Brain Tumor Surgery. In: *Intraoperative Ultrasound (IOUS) in Neurosurgery: From Standard B-Mode to Elastosonography*. Cham, Switzerland: Springer. (2016). p. 41–58.
6. Prada F, Del Bene M, Moiraghi A, DiMeco F. Echographic Brain Semeiology and Topographic Anatomy According to Surgical Approaches. In: *Intraoperative Ultrasound (IOUS) in Neurosurgery: From Standard B-Mode to Elastosonography*. Cham, Switzerland: Springer. (2016). p. 29–39.
7. Unsgaard G, Rygh OM, Selbekk T, Müller TB, Kolstad F, Lindseth F, et al. Intra-Operative 3D Ultrasound in Neurosurgery. *Acta Neurochirurgica Acta Neurochir (Wien);* (2006) 148:235–53. doi: 10.1007/s00701-005-0688-y

8. Unsgård G, Rao V, Solheim O, Lindseth F. Clinical Experience With Navigated 3D Ultrasound Angiography (Power Doppler) in Microsurgical Treatment of Brain Arteriovenous Malformations. *Acta Neurochir (Wien)* (2016) 158(5):875–83. doi: 10.1007/s00701-016-2750-3
9. Moiyadi AV, Unsgård G. Navigable Ultrasound, 3D Ultrasound and Fusion Imaging in Neurosurgery. In: *Intraoperative Ultrasound (IOUS) in Neurosurgery: From Standard B-Mode to Elastosonography*. Cham, Switzerland: Springer. (2016). p. 135–45.
10. Prada F, Del Bene M, Mattei L, Lodigiani L, DeBeni S, Kolev V, et al. Preoperative Magnetic Resonance and Intraoperative Ultrasound Fusion Imaging for Real-Time Neuronavigation in Brain Tumor Surgery. *Ultraschall Med* (2015) 36(2):174–86. doi: 10.1055/s-0034-1385347
11. Caldiera V, Caputi L, Ciceri E. Doppler Imaging: Basic Principles and Clinical Application. In: *Intraoperative Ultrasound (IOUS) in Neurosurgery: From Standard B-Mode to Elastosonography*. Cham, Switzerland: Springer. (2016). p. 101–20.
12. Del Bene M, Perin A, Casali C, Legnani F, Saladino A, Mattei L, et al. Advanced Ultrasound Imaging in Glioma Surgery: Beyond Gray-Scale B-Mode. *Front Oncol* (2018) 8(DEC):576. doi: 10.3389/fonc.2018.00576
13. Griffith S, Pozniak MA, Mitchell CC, Ledwidge ME, Dempsey R, Peters A, et al. Intraoperative Sonography of Intracranial Arteriovenous Malformations: How We Do It. *J Ultrasound Med* (2004) 23:1065–72. doi: 10.7863/jum.2004.23.8.1065
14. Malferrari G, Pulito G, Pizzini AM, Carraro N, Meneghetti G, Sanzaro E, et al. MicroV Technology to Improve Transcranial Color Coded Doppler Examinations. *J Neuroimaging* (2018) 28(4):350–8. doi: 10.1111/jon.12517
15. Prada F, Del Bene M, Mauri G, Lamperti M, Vailati D, Richetta C, et al. Dynamic Assessment of Venous Anatomy and Function in Neurosurgery With Real-Time Intraoperative Multimodal Ultrasound: Technical Note. *Neurosurg Focus* (2018) 45(1):E6. doi: 10.3171/2018.4.FOCUS18101
16. Sidhu PS, Cantisani V, Dietrich CF, Gilja OH, Saftoiu A, Bartels E, et al. The EFSUMB Guidelines and Recommendations for the Clinical Practice of Contrast-Enhanced Ultrasound (CEUS) in Non-Hepatic Applications: Update 2017 (Long Version). *Ultraschall der Medizin* (2018) 39(2):e2–44. doi: 10.1055/a-0586-1107
17. Dietrich CF, Averkiou M, Nielsen MB, Barr RG, Burns PN, Calliada F, et al. How to Perform Contrast-Enhanced Ultrasound (CEUS). *Ultrasound Int Open Thieme Med Publishers* (2018) 4:E2–15. doi: 10.1055/s-0043-123931
18. Prada F, Perin A, Martegani A, Aiani L, Solbiati L, Lamperti M, et al. Intraoperative Contrast-Enhanced Ultrasound for Brain Tumor Surgery. *Neurosurgery* (2014) 74(5):542–52. doi: 10.1227/NEU.0000000000000301
19. Prada F, Bene MD, Fornaro R, Vetrano IG, Martegani A, Aiani L, et al. Identification of Residual Tumor With Intraoperative Contrast-Enhanced Ultrasound During Glioblastoma Resection. *Neurosurg Focus* (2016) 40(3):E7. doi: 10.3171/2015.11.FOCUS15573
20. Prada F, Mattei L, Del Bene M, Aiani L, Saini M, Casali C, et al. Intraoperative Cerebral Glioma Characterization With Contrast Enhanced Ultrasound. *BioMed Res Int* (2014) 2014:484261. doi: 10.1155/2014/484261
21. Chan HW, Bamber J, Dorward N, Chakraborty A, Uff C. Ultrasound Elastography. In: *Intraoperative Ultrasound (IOUS) in Neurosurgery: From Standard B-Mode to Elastosonography*. Cham, Switzerland: Springer. (2016). p. 173–87.
22. Prada F, Del Bene M, Rampini A, Mattei L, Casali C, Vetrano IG, et al. Intraoperative Strain Elastosonography in Brain Tumor Surgery. *Oper Neurosurg (Hagerstown Md).* (2019) 17(2):227–36. doi: 10.1093/ons/opy323
23. Cepeda S, Barrena C, Arrese I, Fernandez-Pérez G, Sarabia R. Intraoperative Ultrasonographic Elastography: A Semi-Quantitative Analysis of Brain Tumor Elasticity Patterns and Peritumoral Region. *World Neurosurg* (2020) 135:e258–70. doi: 10.1016/j.wneu.2019.11.133
24. Chauvet D, Imbault M, Capelle L, Demene C, Mossad M, Karachi C, et al. *In Vivo* Measurement of Brain Tumor Elasticity Using Intraoperative Shear Wave Elastography. *Ultraschall der Medizin* (2016) 37(6):584–90. doi: 10.1055/s-0034-1399152
25. Cepeda S, García-García S, Velasco-Casares M, Fernández-Pérez G, Zamora T, Arrese I, et al. Is There a Relationship Between the Elasticity of Brain Tumors, Changes in Diffusion Tensor Imaging, and Histological Findings? A Pilot Study Using Intraoperative Ultrasound Elastography. *Brain Sci* (2021) 11(2):1–13. doi: 10.3390/brainsci11020271
26. Alawaji G, Alhothali W, Albakr A, Amer A, Al-Habib A, Ajlan A. Shear Wave Elastography for Intracranial Epidermoid Tumors. *Clin Neurol Neurosurg* (2021) 207:106531. doi: 10.1016/j.clineuro.2021.106531
27. Pepa GMD, Menna G, Stifano V, Pezzullo AM, Auricchio AM, Rapisarda A, et al. Predicting Meningioma Consistency and Brain-Meningioma Interface With Intraoperative Sstrain Ultrasound Elastography: A Novel Application to Guide Surgical Strategy. *Neurosurg Focus* (2020) 50(1):1–11. doi: 10.3171/2020.10.FOCUS20797
28. Šteňo A, Matejčík V, Šteňo J. Intraoperative Ultrasound in Low-Grade Glioma Surgery. *Clin Neurol Neurosurg Clin Neurol Neurosurg* (2015) 135:96–9. doi: 10.1016/j.clineuro.2015.05.012
29. Šteňo A, Matejčík V, Šteňo J. Letter to the Editor: Identification of Residual Glioma Using Ultrasound Miniprobes. *Neurosurg Focus* (2016) 41(4):E15. doi: 10.3171/2016.5.FOCUS16180
30. Unsgård G, Sagberg LM, Müller S, Selbekk T. A New Acoustic Coupling Fluid With Ability to Reduce Ultrasound Imaging Artefacts in Brain Tumour Surgery—a Phase I Study. *Acta Neurochir (Wien)* (2019) 161(7):1475–86. doi: 10.1007/s00701-019-03945-x

Conflict of Interest: The authors declare that the research was conducted in the absence of any commercial or financial relationships that could be construed as a potential conflict of interest.

frontiers in Oncology

ORIGINAL RESEARCH
published: 02 February 2021
doi: 10.3389/fonc.2020.590756

Comparison of Intraoperative Ultrasound B-Mode and Strain Elastography for the Differentiation of Glioblastomas From Solitary Brain Metastases. An Automated Deep Learning Approach for Image Analysis

Santiago Cepeda[1], Sergio García-García[1], Ignacio Arrese[1], Gabriel Fernández-Pérez[2], María Velasco-Casares[2], Manuel Fajardo-Puentes[2], Tomás Zamora[3] and Rosario Sarabia[1]*

[1] Neurosurgery Department, University Hospital Río Hortega, Valladolid, Spain, [2] Radiology Department, University Hospital Río Hortega, Valladolid, Spain, [3] Pathology Department, University Hospital Río Hortega, Valladolid, Spain

OPEN ACCESS

Edited by:
Geirmund Unsgård,
Norwegian University of Science and Technology, Norway

Reviewed by:
David Bouget,
SINTEF, Norway
Erik Magnus Berntsen,
Norwegian University of Science and Technology, Norway
Tormod Selbekk,
SonoClear AS, Norway

***Correspondence:**
Santiago Cepeda
cepeda_santiago@hotmail.com
orcid.org/0000-0003-1667-8548

Specialty section:
This article was submitted to Neuro-Oncology and Neurosurgical Oncology, a section of the journal Frontiers in Oncology

Received: 02 August 2020
Accepted: 17 December 2020
Published: 02 February 2021

Citation:
Cepeda S, García-García S, Arrese I, Fernández-Pérez G, Velasco-Casares M, Fajardo-Puentes M, Zamora T and Sarabia R (2021) Comparison of Intraoperative Ultrasound B-Mode and Strain Elastography for the Differentiation of Glioblastomas From Solitary Brain Metastases. An Automated Deep Learning Approach for Image Analysis. Front. Oncol. 10:590756. doi: 10.3389/fonc.2020.590756

Background: The differential diagnosis of glioblastomas (GBM) from solitary brain metastases (SBM) is essential because the surgical strategy varies according to the histopathological diagnosis. Intraoperative ultrasound elastography (IOUS-E) is a relatively novel technique implemented in the surgical management of brain tumors that provides additional information about the elasticity of tissues. This study compares the discriminative capacity of intraoperative ultrasound B-mode and strain elastography to differentiate GBM from SBM.

Methods: We performed a retrospective analysis of patients who underwent craniotomy between March 2018 to June 2020 with glioblastoma (GBM) and solitary brain metastases (SBM) diagnoses. Cases with an intraoperative ultrasound study were included. Images were acquired before dural opening, first in B-mode, and then using the strain elastography module. After image pre-processing, an analysis based on deep learning was conducted using the open-source software Orange. We have trained an existing neural network to classify tumors into GBM and SBM *via* the transfer learning method using Inception V3. Then, logistic regression (LR) with LASSO (least absolute shrinkage and selection operator) regularization, support vector machine (SVM), random forest (RF), neural network (NN), and k-nearest neighbor (kNN) were used as classification algorithms. After the models' training, ten-fold stratified cross-validation was performed. The models were evaluated using the area under the curve (AUC), classification accuracy, and precision.

Results: A total of 36 patients were included in the analysis, 26 GBM and 10 SBM. Models were built using a total of 812 ultrasound images, 435 of B-mode, 265 (60.92%)

corresponded to GBM and 170 (39.8%) to metastases. In addition, 377 elastograms, 232 (61.54%) GBM and 145 (38.46%) metastases were analyzed. For B-mode, AUC and accuracy values of the classification algorithms ranged from 0.790 to 0.943 and from 72 to 89%, respectively. For elastography, AUC and accuracy values ranged from 0.847 to 0.985 and from 79% to 95%, respectively.

Conclusion: Automated processing of ultrasound images through deep learning can generate high-precision classification algorithms that differentiate glioblastomas from metastases using intraoperative ultrasound. The best performance regarding AUC was achieved by the elastography-based model supporting the additional diagnostic value that this technique provides.

Keywords: brain tumor, elastography, intraoperative ultrasound, deep learning, convolutional neural network

INTRODUCTION

Glioblastomas (GBM) represent approximately 40% to 50% of all malignant brain tumors (1). Brain metastases range from 9 to 17% in patients diagnosed with cancer; they may appear as single lesions and be the first manifestation of malignancy in 30%–50% of cases (2–4). The proper distinction of these tumors is essential because they have different treatments and prognosis.

The differential diagnosis of GBM and solitary brain metastases (SBM) can be difficult due to the similarity in conventional neuroimaging tests; both can present like single lesions, contrast-enhancing, with a cystic necrotic appearance and extensive involvement of perilesional white matter. Distinguishing them is particularly complicated when there is no evidence of a previous neoplasm. In these cases, more specific techniques such as PET (Positron Emission Tomography), specialized magnetic resonance imaging (MRI) sequences such as spectroscopy, diffusion/perfusion, and other forms of quantitative analysis can be used to clarify the origin of these lesions (5–18); however, in many centers, these techniques are not available, their acquisition and interpretation can sometimes be challenging and have a non-negligible margin of error.

Intraoperative diagnosis using frozen samples enables discriminating glial tumors from SBM obtaining a histopathological diagnosis after starting the tumor resection. Thus, it would be helpful to establish a surgical planning in the earliest stage of surgery. In the case of GBM, in our center, as in many others, the policy adopted is to try to carry out a supratotal resection whenever possible, taking into account the relationship with functional areas. In lobectomies, for example, resection includes non-enhancing tumor regions. This technique has been shown to improve the overall survival of these patients (19–25).

On the other hand, in metastases, resection is limited exclusively to the contrast-enhancing tumor component, because it is recognized that peritumoral MRI signal alterations are exclusively produced by vasogenic edema (26); therefore, there is still insufficient evidence to support supramarginal resections in these patients (27). Besides, in some cases, partial resections of brain metastases near functional areas might be indicated as a previous step to adjuvant therapies.

Intraoperative ultrasound is a low-cost, portable, fast technique that provides dynamic information in a real-time fashion. It has been widely used in brain tumor resection (28, 29); the simplicity of its application makes it a valuable intraoperative imaging option. Elastography is a relatively new technique in brain tumor pathology. Several publications highlight the importance of this technique because it provides better image contrast compared to B-mode and especially because it allows the characterization of elasticity patterns of the tumor and peritumoral regions, through which it is possible to differentiate between several histological types (30–37).

One of the disadvantages of medical imaging techniques is, of course, their interpretation. Regarding ultrasound, this technique presents challenges such as operator dependency, noise and artifacts. Deep learning is a branch of machine learning that has emerged to improve classification tasks using visual computer systems. The basic idea is that medical images have much more information than the human eye can process and distinguish. Deep learning involves the computation of hierarchical features or representations of a sample, in which high-level abstract features are defined by combining them with other low-level features (38). A deep learning approach based on convolutional neural networks (CNN) is getting attention in the medical image field. Artificial neural networks use a multi-step process that automatically learns features from an image and then extracts them to perform a classification task using an algorithm. CNN's are designed to automatically and adaptively learn features from data through backpropagation using multi-block reconstruction called convolution layers, pooling layers, and fully connected layers (39). Transfer learning is a technique that allows the use of a pre-trained CNN model. It has been previously used in oncological classification tasks with high accuracy. Several studies have demonstrated the ability of transfer learning to work with small datasets using minimal image pre-processing (40–44).

The objective of our work is to use intraoperative ultrasound images and a CNN-based deep learning model in order to differentiate GBM from SBM. We seek to assess the intraoperative ultrasound accuracy on this task while comparing B-mode against an emerging technique such as elastography.

MATERIAL AND METHODS

Patient Selection

A retrospective analysis of patients diagnosed with supratentorial tumors who underwent surgery by craniotomy between March 2018 and June 2020 was performed. Those cases with histopathological diagnosis of glioblastomas and metastases that had an intraoperative ultrasound study were included. Approval was obtained from the ethics committee of our center as well as patient's informed consent in all cases. Clinical, radiological and histopathological variables were collected.

Acquisition and Pre-Processing of Ultrasound Images

For the intraoperative ultrasound study, we used the Hitachi Noblus with a C42 convex probe, 8-10 MHz frequency range, 20 mm scan width radius and 80° scan angle of field of view. The images were acquired after the craniotomy and before the dural opening. The probe is placed perpendicular to the dura; manual compressions were performed maintaining a constant rhythm and intensity. More details of the elastogram acquisition technique are described in a previous publication by our group (34). The ultrasound machine generates a real-time color map called elastogram simultaneously with B-mode. **Figure 1**. The color scale represents the tissue's elasticity/consistency, with tones ranging from red (soft) to blue (hard). Elastograms and B-mode images attempted to cover the highest possible tumor volume and peritumoral areas with evident echogenicity changes. Several slices in different planes were acquired. The images were stored in DICOM format for offline processing.

The open-source software ImageJ version 1.50i (National Institutes of Health, Maryland, United States) was used to pre-process the ultrasound images. The first step was to convert DICOM files to 8-bit TIFF format. For the B-mode images, the tumor and peritumoral area were cropped, removing possible small peripheral artifacts and dark areas. Images with significant artifacts or with unrecognizable areas on elastography were excluded. In the case of elastograms, the area of the elastogram was cut out by removing the periphery that corresponded to zones in B-mode. A rescaling was then performed at 299 x 299 pixels; the intensities were normalized, despeckling, and smoothing by Gaussian blur filter was carried out; thus, we obtained images with similar intensities and standardized size for the analysis. **Figure 2**.

Analysis Using Deep CNN *via* Transfer Learning

For the generation of an image classification system, the open-source software Orange version 3.26 (University of Ljubljana, Slovenia) was used. The software has a user-friendly interface based on a work panel and the use of widgets. **Supplementary Figure 1**. After importing the images into the workspace, the first step consisted in the process called embedding. Using preprocessed ultrasound images, we have trained an existing neural network to classify tumors into GBM and SBM. Thus, we have used a transfer learning method applying Inception V3, one of the most popular image recognition models that have been previously adapted to the analysis of medical images with excellent results (45–47). Inception V3 is a 48-layer convoluted neural network trained in 1.2 million images from the ImageNet repository (48); each image in the ImageNet Large Scale Visual

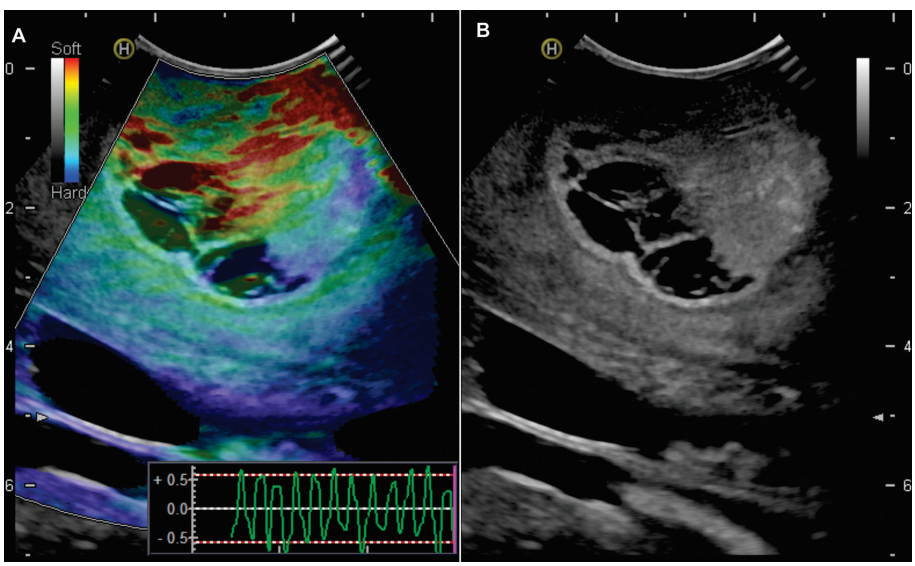

FIGURE 1 | Example of intraoperative ultrasound images. 65-year-old man with a right frontal glioblastoma. **(A)** Elastogram showing the difference in consistency between the tumor and the peritumoral region (green - red) from the rest of the healthy parenchyma (blue). In the right-lower part of the image, a graphic representation of the external compression waves is observed. **(B)** Simultaneous image in B-mode.

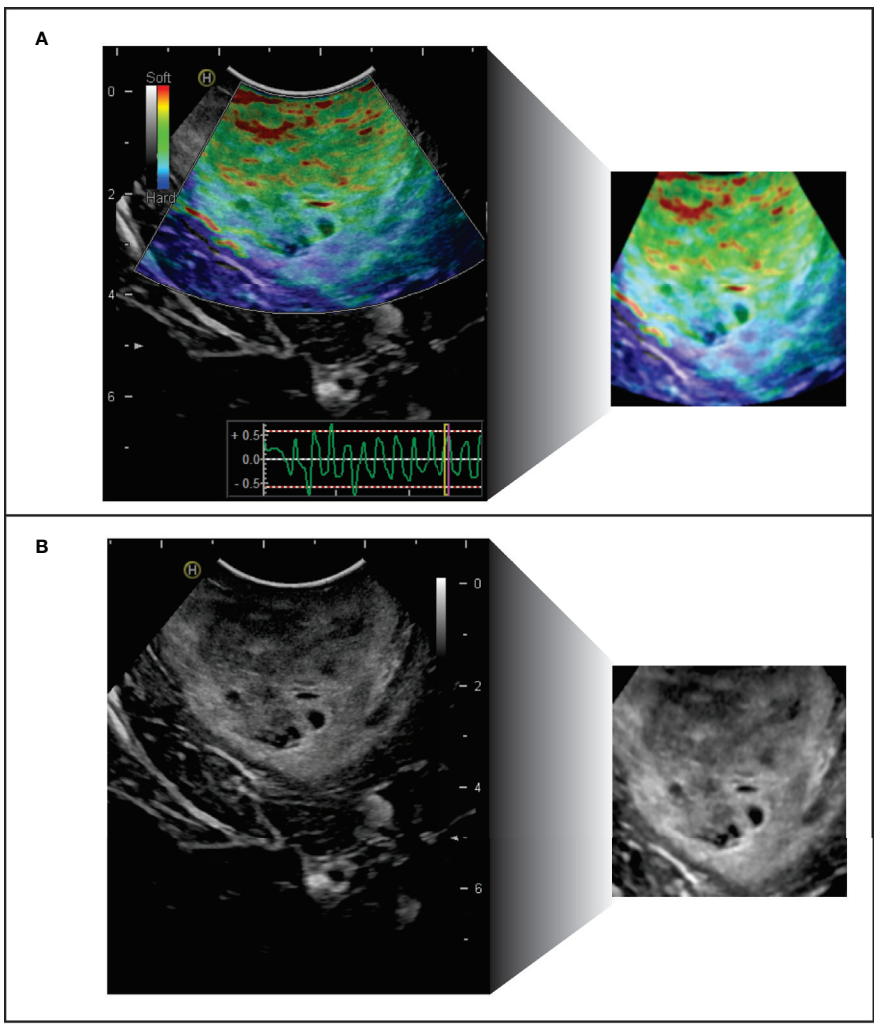

FIGURE 2 | Intraoperative ultrasound images pre-processing. Left: original images of **(A)** elastogram and **(B)** B-mode. Right: Final image available for automatic analysis.

Recognition Challenge repository belongs to one of the 1000 defined classes. Inception architecture is schematically summarized in **Figure 3**. Embedding process relies on the penultimate of these deep networks, where transfer learning is achieved by encoding images with characteristics of this layer, so each image is embedded in a 2048-element vector, followed by classic machine learning algorithms.

Hierarchical Clustering

In the first phase of machine learning, and without previously establishing categories or classes, the distances of the vector representations of all the images were calculated using the cosine as a distance metric. From the distance matrix, a hierarchical classification was made into groups called clusters. The software automatically detects related elements in search of patterns. To determine the elements included in each cluster, an analysis of the GBM and SBM categories' distribution within each subgroup was performed, both in B-mode and elastography. These groups are represented graphically through the development of a dendrogram.

Classifiers and Model Validation

In order to develop a prediction model, the following classification algorithms were used: logistic regression (LR) applying LASSO (least absolute shrinkage and selection operator) regularization, Neural Network (NN), Random Forest (RF), Support Vector Machine (SVM), and k-Nearest Neighbor. Model validation was performed using a ten-fold stratified cross-validation. Most of the sample was used in the construction or learning process of the model, leaving a portion of the sample for the validation of its predictions, the stratification maintains the proportion of both categories, namely GBM and SBM, this step is repeated several times guaranteeing that the cases were distributed randomly as part of the training and test group. For this reason, cross-validation has proved to be superior to the simple split random sampling.

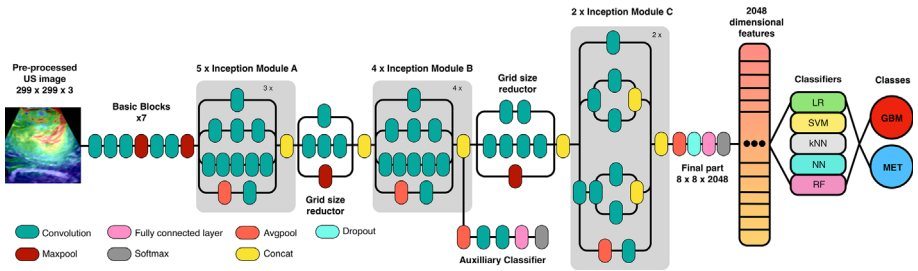

FIGURE 3 | Schematic representation of Inception v3 architecture (adapted from GoogLeNet) and the workflow used in the transfer learning process *via* convolutional neural network and classification algorithms.

The models were evaluated using the AUC (area under the curve)/ROC (receiver operating characteristics), classification accuracy (CA) and precision scores. Furthermore, confusion matrices were developed to determine the correct and misclassified cases for each algorithm.

Comparison of the Automatic Model Versus Experienced Human Observers

After establishing the best classification algorithm, a training set made up of 70% of the sample was randomly selected, a predictive model was built and then was validated in the test-data set, 30% remaining of the sample, keeping the proportion of each of the classes. Using the same test-data set, two expert observers analyzed the images, classifying them as GBM and SBM according to their judgment. One of them is a senior neuroradiologist with ten years of experience, and the second observer is a neurosurgeon with thirty years of experience and knowledge about intraoperative ultrasound images. Both observers were blinded to the definitive histopathological diagnosis. Their results were compared with the automatic algorithm.

TABLE 1 | Patient characteristics.

Variable	n
Age	
Sex	64.58 ± 8.76
Female	10 (27.8%)
Male	26 (72.2%)
Preoperative KPS	77.78 ± 9.88
Histopathology	
Glioblastoma	26 (72.2%)
Metastases	10 (27.8%)
Lung	6 (60%)
Breast	1 (10%)
Ovarian	1 (10%)
Colorectal	1 (10%)
Prostate	1 (10%)
Tumor location	
Frontal	16 (44.4%)
Parietal	8 (22.2%)
Temporal	8 (22.2%)
Occipital	4 (11.1%)
Initial volume (cm^3)	25.31 ± 24.27

Values are expressed as the mean ± standard deviation or as the frequency (%). KPS, Karnofsky Performance Score.

RESULTS

Thirty-six patients were included during the study period. Twenty-six cases corresponded to GBM and 10 to metastases. The histological diagnoses, radiological and demographic characteristics, are summarized in **Table 1**. Illustrative cases and their appearance on MRI and intraoperative ultrasound images are shown in **Figure 4**.

Models were built using a total of 812 ultrasound images, 435 of B-mode, 265 (60.92%) corresponded to GBM and 170 (39.8%) to metastases. In addition, 377 elastograms, 232 (61.54%) GBM and 145 (38.46%) metastases were analyzed. **Figure 5**. The average of B-mode images was twelve images per patient, while for elastography, an average of eleven images was analyzed for each case. The difference in the number of images between the two modalities is because several images were discarded due to their low quality or to the presence of noise/artifacts.

By hierarchical clustering, two main groups of images were identified. For B-mode, the first cluster included 65% of GBM images and the second cluster 46.45% metastasis. For elastography, the first cluster contained 80.3% GBM and the second cluster 82.3% metastases. The dendrogram of **Figure 6** graphically demonstrated the distribution and results of the classification.

The performance of the classification algorithms was represented graphically using the ROC (Receiver Operating Characteristics) curves. **Figure 7**. For B-mode, the classification algorithms' AUC and accuracy values ranged from 0.790 to 0.943 and from 72 to 89%, respectively. **Table 2**. Elastography-based model demonstrated the best performance since AUC and accuracy values ranged from 0.847 to 0.985 and 79 to 95%. **Table 3** and **Supplementary Figure 2**.

After the random selection of cases, the human observers' results versus the automatic selection algorithm are summarized in **Table 4**. The accuracy achieved by the experienced observers was up to 61% in the case of B-mode and 68% for elastography. For the CNN-based automatic system, the accuracy was 88% in B-mode and 93% in elastography.

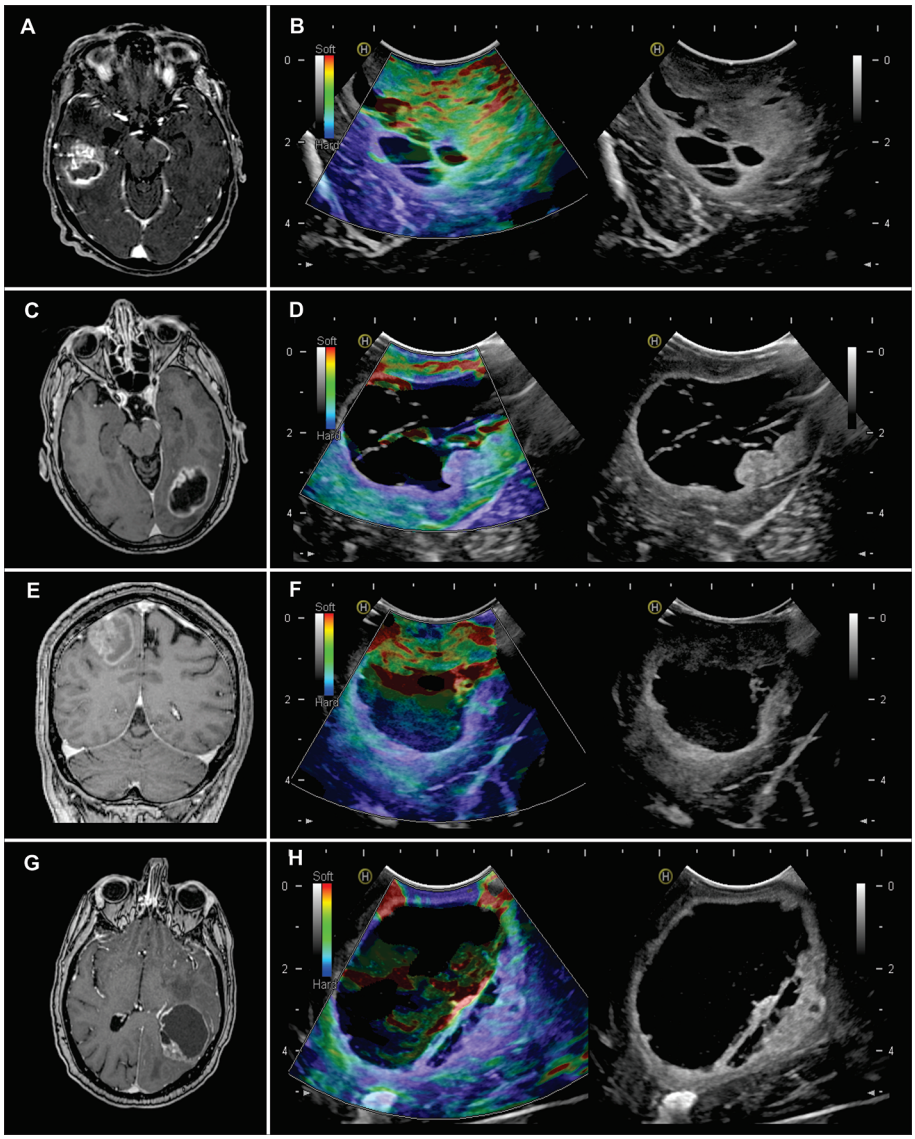

FIGURE 4 | Illustrative cases of the use of intraoperative ultrasound. **(A)** Axial T1 weighted post-contrast (T1WC) image of a 50-year-old man with a right temporal glioblastoma. **(B)** Elastogram (left) and B-mode (right). It is a soft tumor with small cystic regions and a peritumoral region of low stiffness compared to the healthy parenchyma. **(C)** Axial T1WC image of a 70-year-old woman with a left occipital glioblastoma. **(D)** The elastogram shows a cystic/necrotic lesion with a nodular component of intermediate consistency and a relatively soft peritumoral region. **(E)** Coronal T1WC image of a 45-year-old man with a right parietal lung metastasis. **(F)** The elastography image shows a solid/cystic lesion with a soft nodular component and a stiffer peritumoral region. **(G)** Axial T1WC image of a 52-year-old man with no history of systemic cancer with a left parieto-occipital metastasis. **(H)** The elastogram shows a large cystic lesion with a small hard region and a peritumoral region of similar consistency.

DISCUSSION

In the present study, we have developed a highly accurate classification system that allows GBM to be differentiated from SBM using automatic intraoperative ultrasound image processing through convolutional neural networks. Furthermore, elastography showed slightly better performance for the classification of these tumors compared to the B-mode.

Among the strengths of our work, we can mention that it is the first time that intraoperative ultrasound B-mode and elastography are applied to discriminate glioblastomas from metastases. Besides, our study follows a cutting-edge methodology, in which deep learning techniques are applied in the analysis of ultrasound images, the combination of these two technologies in brain tumor pathology has no previous references in the literature.

We are aware of our limitations, it is worth mentioning that the sample size from which we started is relatively small. This aspect can cause an overfitting problem and the creation of an over-optimistic predictive model. Our strategy to overcome this

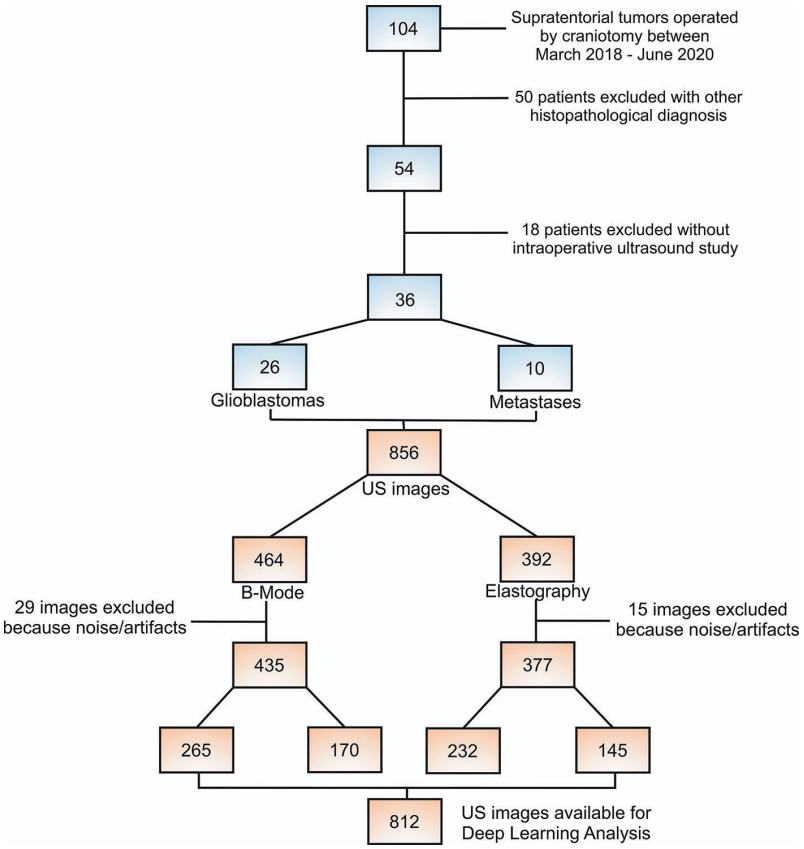

FIGURE 5 | Flow chart of patient and ultrasound image selection process.

issue was to use all the images available in each case, including different sections and projections of each tumor. We reached a sample size and a balance of classes enough to carry out an analysis based on artificial intelligence techniques.

On the other hand, we recognize the limitations that elastography holds, such as the variability of elasticity threshold values and the absence of an image quality control; also, they often contain irrelevant patterns that can difficult both handcrafted feature extraction and DL methods such as CNN.

Deep learning, a branch of machine learning, can automatically process and learn mid-level and high-level abstract characteristics acquired from raw data, in this case, ultrasound images. Still, tumor classification into subtypes is difficult due to variations in shape, size, intensities, and because different histological types can show similar patterns.

The image acquisition and processing methodology are rigorous and clear in every step. Strain type elastography is a technique used in previous studies, and with promising results regarding its application in the resection of brain tumors (34, 36). Pre-processing ultrasound images is a fundamental step, which has been performed with the highest reliability, applying a user-friendly open-source software that performs robust analysis without adding complexity (49, 50).

The analysis through deep learning has been demonstrated to be superior in image recognition compared to conventional radiological techniques and handcrafted radiomics (51, 52). The methods applied in our study, suppress some cumbersome steps such as tumor segmentation, which implies a significant limitation in this type of work and may bias the selection of variables of interest, such as texture features. The difference is that CNN, through transfer learning, takes advantage of a previously trained network of proven validity, to generate classification systems that automatically and without human intervention can distinguish between one class or another, in our case, GBM from SBM. A disadvantage of these systems is the inability to know which characteristics the software has used to generate its predictions, sometimes compared to a "black box" (53). Although feature selection techniques could be applied after converting images to vector representations, these techniques are still not validated. Using DL models, we can lose interpretability in exchange for gaining more robust and generalizable prediction systems based on much more complex characteristics.

A comparison has been conducted between the classification algorithms and experienced human observers to discriminate these tumor types using ultrasound images in our study. According to our results, the DL based model

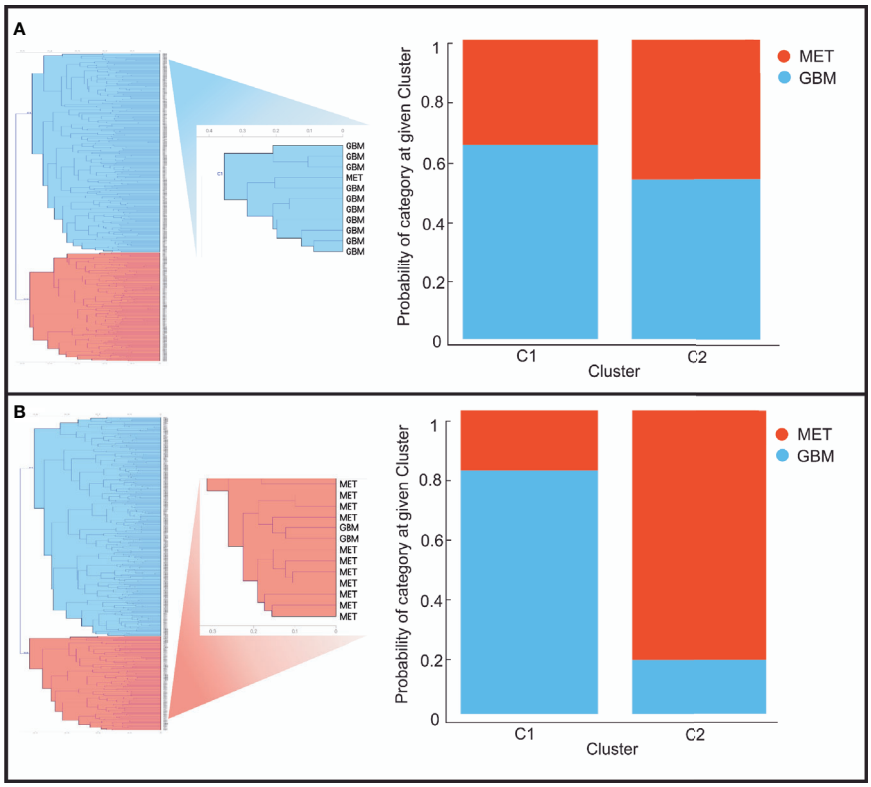

FIGURE 6 | Graphical representation of the clusters generated from the distance matrices after analyzing images in **(A)** B-mode and **(B)** Elastography. Left: dendrograms of the top two clusters. Right: Bar graph of the probabilities of being assigned to each cluster of glioblastomas (blue) and metastases (red).

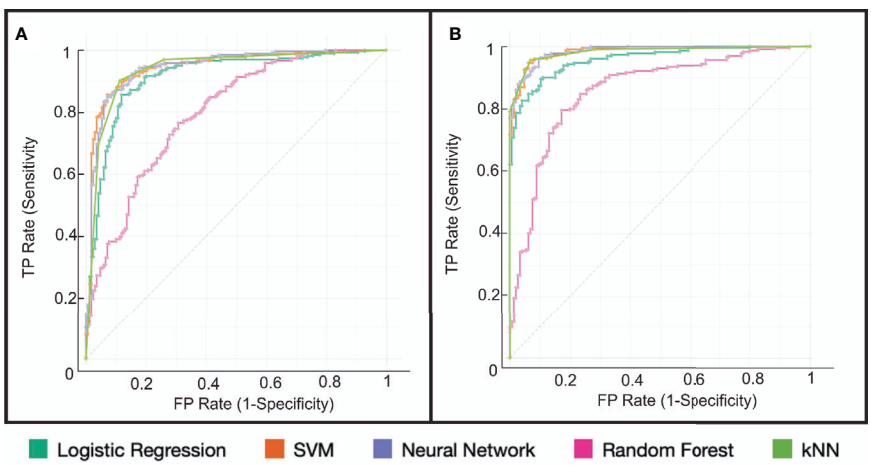

FIGURE 7 | Representation of classifier performance using the ROC (Receiver Operating Characteristics) curve for **(A)** B-mode and **(B)** Elastography. The best results were obtained by the Support Vector Machine (SVM) and K-Nearest Neighbor (k-NN) algorithms.

seems to be more precise and accurate to differentiate one tumor type from another. These findings make it necessary to improve our knowledge about how artificial intelligence works, only in this way, these new technological resources will serve as support tools in neurosurgical and radiological fields.

In our study, the best performance regarding AUC and accuracy was achieved by the elastography-based model compared to B-mode in the classification task of SBM and GBM. One possible explanation for this advantage could be the better contrast offered by the color images of the elastograms, as

TABLE 2 | Diagnostic performance of classification algorithms based on Ultrasound B-mode images.

Classifier	AUC	CA	F1-Score	Precision	Recall
kNN	0.938	0.897	0.897	0.898	0.897
Logistic Regression	0.915	0.871	0.871	0.871	0.871
Neural Network	0.945	0.876	0.877	0.879	0.876
Random Forest	0.791	0.749	0.724	0.779	0.749
SVM	0.944	0.887	0.887	0.887	0.887

AUC, Area Under the Curve; CA, Classification Accuracy; kNN, k-Nearest Neighbor; SVM, Support Vector Machine.

TABLE 3 | Diagnostic performance of classification algorithms based on Ultrasound Elastography images.

Classifier	AUC	CA	F1-Score	Precision	Recall
kNN	0.983	0.947	0.947	0.947	0.947
Logistic Regression	0.960	0.889	0.888	0.888	0.889
Neural Network	0.985	0.918	0.918	0.922	0.918
Random Forest	0.861	0.796	0.786	0.803	0.796
SVM	0.985	0.941	0.941	0.942	0.942

AUC, Area Under the Curve; CA, Classification Accuracy; kNN, k-Nearest Neighbor; SVM, Support Vector Machine.

TABLE 4 | Comparison between convolutional neural network (CNN)-SVM model performance and the two expert observers.

Ultrasound Modality	Classifier	AUC	CA	Precision
B-mode	SVM	0.937	0.877	0.883
	Observer 1	0.573	0.608	0.659
	Observer 2	0.545	0.569	0.642
Elastography	SVM	0.976	0.929	0.930
	Observer 1	0.622	0.681	0.693
	Observer 2	0.587	0.612	0.686

AUC, Area Under the Curve; CA, Classification Accuracy; SVM, Support Vector Machine.

previously published (33). Furthermore, we believe that one of the fundamental differences between the two tumor types is the correlation between the peritumoral regions' histology and their radiological appearance. Although this correlation has not been proven, previous studies indicate that the elasticity patterns differ in gliomas and metastases (34, 54). These differences do not seem to be captured with the B-mode; thus, the peritumoral areas' elastographic pattern could differentiate both histological types through automatic analysis of this imaging modality. It is worth mentioning that the elastograms are produced in an RGB (red-green-blue) image format. Therefore, the elastogram results from the superposition of the B-mode image and the colorimetric scale of the tissues' elasticity. Our study has been carried out based on the original image produced by the ultrasound machine because we wanted to use the same pictures in the classification task by human observers. Another alternative for future studies could be to perform an image decomposition in HSB (hue-saturation-brightness) format and then extract the hue component.

Regarding the differentiation of GBM from SBM, we know that there are multiple radiological techniques available for pre-operative or non-invasive applications (5, 8–11, 13, 15–17, 55); besides, intraoperative histopathological techniques are currently the reference parameter for decision-making (56). Our study does not intend to make a comparison with the techniques mentioned above but to demonstrate, on the one hand, the high value that ultrasound and especially elastography owns in the study of brain tumors, and on the other hand, highlight that automatic image processing is a highly reliable technique. Therefore, we believe that it is essential to develop automatic ultrasound image analysis methods to increase the precision in the diagnosis, evaluation, and interventionism based on this technique.

Our work demonstrates that automated processing of ultrasound images through deep learning can generate high-precision classification algorithms that differentiate glioblastomas from metastases using intraoperative ultrasound. The best performance regarding AUC and accuracy was achieved by the elastography-based model, supporting the additional value that this technique provides by analyzing brain tumor elasticity. With our results, the next step will be to obtain real-time feedback based on intraoperative image analysis, allowing the surgeon to adapt the surgical strategy and even guide tumor resection.

DATA AVAILABILITY STATEMENT

The raw data supporting the conclusions of this article will be made available by the authors, without undue reservation.

ETHICS STATEMENT

The studies involving human participants were reviewed and approved by University Hospital Río Hortega Ethics Committee. The patients/participants provided their written informed consent to participate in this study.

AUTHOR CONTRIBUTIONS

Conception and design: SC and RS. Material preparation, data collection, and analysis were performed by SC, SG-G, MV-C, GF-P, IA, MF-P, and TZ. The first draft of the manuscript was written by SC and all authors commented on previous versions of the manuscript. All authors contributed to the article and approved the submitted version.

SUPPLEMENTARY MATERIAL

The Supplementary Material for this article can be found online at: https://www.frontiersin.org/articles/10.3389/fonc.2020.590756/full#supplementary-material

Supplementary Figure 1 | Orange visual environment and the workflow used in the construction of the predictive model.

Supplementary Figure 2 | Confusion matrices generated by the different classification algorithms based on (left) B-Mode and (right) Elastography. **(A)** k-Nearest Neighbor; **(B)** Logistic Regression; **(C)** Neural Network; **(D)** Random Forest and **(E)** Support Vector Machine. The number of instances correctly (purple) and misclassified (pink) are shown.

REFERENCES

1. Sherwood PR, Stommel M, Murman DL, Given CW, Given BA. Primary malignant brain tumor incidence and Medicaid enrollment. *Neurology* (2004) 62:1788–93. doi: 10.1212/01.WNL.0000125195.26224.7C
2. Schiff D. Single Brain Metastasis. *Curr Treat Options Neurol* (2001) 3:89–99. doi: 10.1007/s11940-001-0027-4
3. Giordana MT, Cordera S, Boghi A. Cerebral metastases as first symptom of cancer: a clinico-pathologic study. *J Neurooncol* (2000) 50:265–73. doi: 10.1023/a:1006413001375
4. Nayak L, Lee EQ, Wen PY. Epidemiology of brain metastases. *Curr Oncol Rep* (2012) 14:48–54. doi: 10.1007/s11912-011-0203-y
5. Abdel Razek AAK, Talaat M, El-Serougy L, Abdelsalam M, Gaballa G. Differentiating Glioblastomas from Solitary Brain Metastases Using Arterial Spin Labeling Perfusion– and Diffusion Tensor Imaging–Derived Metrics. *World Neurosurg* (2019) 127:e593–8. doi: 10.1016/j.wneu.2019.03.213
6. Maurer MH, Synowitz M, Badakshi H, Lohkamp LN, Wüstefeld J, Schäfer ML, et al. Glioblastoma multiforme versus solitary supratentorial brain metastasis: Differentiation based on morphology and magnetic resonance signal characteristics. *RoFo Fortschr auf dem Gebiet der Rontgenstrahlen und der Bildgeb Verfahren* (2013) 185:235–40. doi: 10.1055/s-0032-1330318
7. Zhang G, Chen X, Zhang S, Ruan X, Gao C, Liu Z, et al. Discrimination Between Solitary Brain Metastasis and Glioblastoma Multiforme by Using ADC-Based Texture Analysis: A Comparison of Two Different ROI Placements. *Acad Radiol* (2019) 26:1466–72. doi: 10.1016/j.acra.2019.01.010
8. Qian Z, Li Y, Wang Y, Li L, Li R, Wang K, et al. Differentiation of glioblastoma from solitary brain metastases using radiomic machine-learning classifiers. *Cancer Lett* (2019) 451:128–35. doi: 10.1016/j.canlet.2019.02.054
9. Petrujkić K, Milošević N, Rajković N, Stanisavljević D, Gavrilović S, Dželebdžić D, et al. Computational quantitative MR image features - a potential useful tool in differentiating glioblastoma from solitary brain metastasis. *Eur J Radiol* (2019) 119:108634. doi: 10.1016/j.ejrad.2019.08.003
10. Askaner K, Rydelius A, Engelholm S, Knutsson L, Lätt J, Abul-Kasim K, et al. Differentiation between glioblastomas and brain metastases and regarding their primary site of malignancy using dynamic susceptibility contrast MRI at 3T. *J Neuroradiol* (2019) 46:367–72. doi: 10.1016/j.neurad.2018.09.006
11. Sunwoo L, Yun TJ, You SH, Yoo RE, Kang KM, Choi SH, et al. Differentiation of glioblastoma from brain metastasis: Qualitative and quantitative analysis using arterial spin labeling MR imaging. *PloS One* (2016) 11:1–13. doi: 10.1371/journal.pone.0166662
12. Byrnes TJD, Barrick TR, Bell BA, Clark CA. Diffusion tensor imaging discriminates between glioblastoma and cerebral metastases in vivo. *NMR BioMed* (2011) 24:54–60. doi: 10.1002/nbm.1555
13. Artzi M, Bressler I, Ben Bashat D. Differentiation between glioblastoma, brain metastasis and subtypes using radiomics analysis. *J Magn Reson Imaging* (2019) 50:519–28. doi: 10.1002/jmri.26643
14. She D, Xing Z, Cao D. Differentiation of Glioblastoma and Solitary Brain Metastasis by Gradient of Relative Cerebral Blood Volume in the Peritumoral Brain Zone Derived from Dynamic Susceptibility Contrast Perfusion Magnetic Resonance Imaging. *J Comput Assist Tomogr* (2019) 43:13–7. doi: 10.1097/RCT.0000000000000771
15. Tsougos I, Svolos P, Kousi E, Fountas K, Theodorou K, Fezoulidis I, et al. Differentiation of glioblastoma multiforme from metastatic brain tumor using proton magnetic resonance spectroscopy, diffusion and perfusion metrics at 3 T. *Cancer Imaging* (2012) 12:423–36. doi: 10.1102/1470-7330.2012.0038
16. Bauer AH, Erly W, Moser FG, Maya M, Nael K. Differentiation of solitary brain metastasis from glioblastoma multiforme: a predictive multiparametric approach using combined MR diffusion and perfusion. *Neuroradiology* (2015) 57:697–703. doi: 10.1007/s00234-015-1524-6
17. Skogen K, Schulz A, Helseth E, Ganeshan B, Dormagen JB, Server A. Texture analysis on diffusion tensor imaging: discriminating glioblastoma from single brain metastasis. *Acta Radiol* (2019) 60:356–66. doi: 10.1177/0284185118780889
18. Kadota Y, Hirai T, Azuma M, Hattori Y, Khant ZA, Hori M, et al. Differentiation between glioblastoma and solitary brain metastasis using neurite orientation dispersion and density imaging. *J Neuroradiol* (2020) 47:197–202. doi: 10.1016/j.neurad.2018.10.005
19. Eyüpoglu IY, Hore N, Merkel A, Buslei R, Buchfelder M, Savaskan N. Supra-complete surgery via dual intraoperative visualization approach (DiVA) prolongs patient survival in glioblastoma. *Oncotarget* (2016) 7:25755–68. doi: 10.18632/oncotarget.8367
20. Esquenazi Y, Friedman E, Liu Z, Zhu J-J, Hsu S, Tandon N. The Survival Advantage of "Supratotal" Resection of Glioblastoma Using Selective Cortical Mapping and the Subpial Technique. *Neurosurgery* (2017) 81:275–88. doi: 10.1093/neuros/nyw174
21. Roh TH, Kang S-G, Moon JH, Sung KS, Park HH, Kim SH, et al. Survival benefit of lobectomy over gross-total resection without lobectomy in cases of glioblastoma in the noneloquent area: a retrospective study. *J Neurosurg* (2020) 132:895–901. doi: 10.3171/2018.12.JNS182558
22. Al-Holou WN, Hodges TR, Everson RG, Freeman J, Zhou S, Suki D, et al. Perilesional Resection of Glioblastoma Is Independently Associated With Improved Outcomes. *Neurosurgery* (2020) 86:112–21. doi: 10.1093/neuros/nyz008
23. Mampre D, Ehresman J, Pinilla-Monsalve G, Osorio MAG, Olivi A, Quinones-Hinojosa A, et al. Extending the resection beyond the contrast-enhancement for glioblastoma: feasibility, efficacy, and outcomes. *Br J Neurosurg* (2018) 32:528–35. doi: 10.1080/02688697.2018.1498450
24. Jiang H, Cui Y, Liu X, Ren X, Li M, Lin S. Proliferation-dominant high-grade astrocytoma: survival benefit associated with extensive resection of FLAIR abnormality region. *J Neurosurg* (2019) 22:1–8. doi: 10.3171/2018.12.JNS182775
25. Glenn CA, Baker CM, Conner AK, Burks JD, Bonney PA, Briggs RG, et al. An Examination of the Role of Supramaximal Resection of Temporal Lobe Glioblastoma Multiforme. *World Neurosurg* (2018) 114:e747–55. doi: 10.1016/j.wneu.2018.03.072
26. Pekmezci M, Perry A. Neuropathology of brain metastases. *Surg Neurol Int* (2013) 4:245. doi: 10.4103/2152-7806.111302
27. Hardesty DA, Nakaji P. The Current and Future Treatment of Brain Metastases. *Front Surg* (2016) 25:3–30. doi: 10.3389/fsurg.2016.00030
28. Jakola AS, Unsgård G, Solheim O. Quality of life in patients with intracranial gliomas: the impact of modern image-guided surgery. *J Neurosurg* (2011) 114:1622–30. doi: 10.3171/2011.1.JNS101657
29. Munkvold BKR, Jakola AS, Reinertsen I, Sagberg LM, Unsgård G, Solheim O. The Diagnostic Properties of Intraoperative Ultrasound in Glioma Surgery and Factors Associated with Gross Total Tumor Resection. *World Neurosurg* (2018) 115:e129–36. doi: 10.1016/j.wneu.2018.03.208
30. Chauvet D, Imbault M, Capelle L, Demene C, Mossad M, Karachi C, et al. In Vivo Measurement of Brain Tumor Elasticity Using Intraoperative Shear Wave Elastography. *Ultraschall Med - Eur J Ultrasound* (2015) 37:584–90. doi: 10.1055/s-0034-1399152
31. Chan HW. Optimising the Use and Assessing the Value of Intraoperative Shear Wave Elastography in Neurosurgery. Doctoral thesis. University of London (2016).
32. Selbekk T, Bang J, Unsgaard G. Strain processing of intraoperative ultrasound images of brain tumours: Initial results. *Ultrasound Med Biol* (2005) 31:45–51. doi: 10.1016/j.ultrasmedbio.2004.09.011
33. Selbekk T, Brekken R, Indergaard M, Solheim O, Unsgård G. Comparison of contrast in brightness mode and strain ultrasonography of glial brain tumours. *BMC Med Imaging* (2012) 12:11. doi: 10.1186/1471-2342-12-11
34. Cepeda S, Barrena C, Arrese I, Fernandez-Pérez G, Sarabia R. Intraoperative Ultrasonographic Elastography: A Semi-Quantitative Analysis of Brain Tumor Elasticity Patterns and Peritumoral Region. *World Neurosurg* (2020) 135:e258–70. doi: 10.1016/j.wneu.2019.11.133
35. Prada F, Del Bene M, Moiraghi A, Casali C, Legnani FG, Saladino A, et al. From Grey Scale B-Mode to Elastosonography: Multimodal Ultrasound Imaging in Meningioma Surgery—Pictorial Essay and Literature Review. *BioMed Res Int* (2015) 2015:1–13. doi: 10.1155/2015/925729
36. Prada F, Del Bene M, Rampini A, Mattei L, Casali C, Vetrano IG, et al. Intraoperative Strain Elastosonography in Brain Tumor Surgery. *Oper Neurosurg* (2019) 17:227–36. doi: 10.1093/ons/opy323
37. Chakraborty A, Berry G, Bamber J, Dorward N. Intra-operative Ultrasound Elastography and Registered Magnetic Resonance Imaging of Brain Tumours: A Feasibility Study. *Ultrasound* (2006) 14:43–9. doi: 10.1179/174313406x82461

38. Sermanet P, Eigen D, Zhang X, Mathieu M, Fergus R, LeCun Y. OverFeat: Integrated Recognition, Localization and Detection using Convolutional Networks. (2013). http://arxiv.org/abs/1312.6229.
39. Shin H-C, Roth HR, Gao M, Lu L, Xu Z, Nogues I, et al. Deep Convolutional Neural Networks for Computer-Aided Detection: CNN Architectures, Dataset Characteristics and Transfer Learning. *IEEE Trans Med Imaging* (2016) 35:1285–98. doi: 10.1109/TMI.2016.2528162
40. Zhou L, Zhang Z, Chen Y-C, Zhao Z-Y, Yin X-D, Jiang H-B. A Deep Learning-Based Radiomics Model for Differentiating Benign and Malignant Renal Tumors. *Transl Oncol* (2019) 12:292–300. doi: 10.1016/j.tranon.2018.10.012
41. Deniz E, Şengür A, Kadiroğlu Z, Guo Y, Bajaj V, Budak Ü. Transfer learning based histopathologic image classification for breast cancer detection. *Health Inf Sci Syst* (2018) 6:18. doi: 10.1007/s13755-018-0057-x
42. Deepak S, Ameer PM. Brain tumor classification using deep CNN features via transfer learning. *Comput Biol Med* (2019) 111:103345. doi: 10.1016/j.compbiomed.2019.103345
43. Maki S, Furuya T, Horikoshi T, Yokota H, Mori Y, Ota J, et al. A Deep Convolutional Neural Network With Performance Comparable to Radiologists for Differentiating Between Spinal Schwannoma and Meningioma. *Spine (Phila Pa 1976)* (2020) 45:694–700. doi: 10.1097/BRS.0000000000003353
44. Godec P, Pančur M, Ilenič N, Čopar A, Stražar M, Erjavec A, et al. Democratized image analytics by visual programming through integration of deep models and small-scale machine learning. *Nat Commun* (2019) 10:1–7. doi: 10.1038/s41467-019-12397-x
45. Coudray N, Ocampo PS, Sakellaropoulos T, Narula N, Snuderl M, Fenyö D, et al. Classification and mutation prediction from non-small cell lung cancer histopathology images using deep learning. *Nat Med* (2018) 24:1559–67. doi: 10.1038/s41591-018-0177-5
46. Esteva A, Kuprel B, Novoa RA, Ko J, Swetter SM, Blau HM, et al. Dermatologist-level classification of skin cancer with deep neural networks. *Nature* (2017) 542:115–8. doi: 10.1038/nature21056
47. Gulshan V, Peng L, Coram M, Stumpe MC, Wu D, Narayanaswamy A, et al. Development and Validation of a Deep Learning Algorithm for Detection of Diabetic Retinopathy in Retinal Fundus Photographs. *JAMA* (2016) 316:2402–10. doi: 10.1001/jama.2016.17216
48. Szegedy C, Vanhoucke V, Ioffe S, Shlens J, Wojna Z. Rethinking the Inception Architecture for Computer Vision. (2015). http://arxiv.org/abs/1512.00567.
49. Van Sloun RJG, Cohen R, Eldar YC. Deep Learning in Ultrasound Imaging. *Proc IEEE* (2020) 108:11–29. doi: 10.1109/JPROC.2019.2932116
50. Liu S, Wang Y, Yang X, Lei B, Liu L, Li SX, et al. Deep Learning in Medical Ultrasound Analysis: A Review. *Engineering* (2019) 5:261–75. doi: 10.1016/j.eng.2018.11.020
51. Brehar R, Mitrea DA, Vancea F, Marita T, Nedevschi S, Lupsor-Platon M, et al. Comparison of deep-learning and conventional machine-learning methods for the automatic recognition of the hepatocellular carcinoma areas from ultrasound images. *Sensors (Switzerland)* (2020) 20:1–22. doi: 10.3390/s20113085
52. Burlina P, Billings S, Joshi N, Albayda J. Automated diagnosis of myositis from muscle ultrasound: Exploring the use of machine learning and deep learning methods. *PloS One* (2017) 12:1–15. doi: 10.1371/journal.pone.0184059
53. Parekh VS, Jacobs MA. Deep learning and radiomics in precision medicine. *Expert Rev Precis Med Drug Dev* (2019) 4:59–72. doi: 10.1080/23808993.2019.1585805
54. Scholz M, Noack V, Pechlivanis I, Engelhardt M, Fricke B, Linstedt U, et al. Vibrography during tumor neurosurgery. *J Ultrasound Med* (2005) 24:985–92. doi: 10.7863/jum.2005.24.7.985
55. Chen C, Ou X, Wang J, Guo W, Ma X. Radiomics-based machine learning in differentiation between glioblastoma and metastatic brain tumors. *Front Oncol* (2019) 9:806. doi: 10.3389/fonc.2019.00806
56. Chand P, Amit S, Gupta R, Agarwal A. Errors, limitations, and pitfalls in the diagnosis of central and peripheral nervous system lesions in intraoperative cytology and frozen sections. *J Cytol* (2016) 33:93–7. doi: 10.4103/0970-9371.182530

Conflict of Interest: The authors declare that the research was conducted in the absence of any commercial or financial relationships that could be construed as a potential conflict of interest.

frontiers in Oncology

TECHNOLOGY AND CODE
published: 02 February 2021
doi: 10.3389/fonc.2020.619274

The Essential Role of Open Data and Software for the Future of Ultrasound-Based Neuronavigation

Ingerid Reinertsen[1,2], *D. Louis Collins*[3] *and Simon Drouin*[4*]

[1] Department of Health Research, SINTEF Digital, Trondheim, Norway, [2] Department of Circulation and Medical Imaging, Norwegian University of Science and Technology (NTNU), Trondheim, Norway, [3] NIST Laboratory, McConnell Brain Imaging Center, Montreal Neurological Institute and Hospital, McGill University, Montréal, QC, Canada, [4] Laboratoire Multimédia, École de Technologie Supérieure, Montréal, QC, Canada

OPEN ACCESS

Edited by:
Massimiliano Del Bene, Istituto Neurologico Carlo Besta (IRCCS), Italy

Reviewed by:
Francesco Maria Crisà, Niguarda Ca' Granda Hospital, Italy
Carlo Giussani, University of Milano-Bicocca, Italy

***Correspondence:**
Simon Drouin
simon.drouin@etsmtl.ca

Specialty section:
This article was submitted to Neuro-Oncology and Neurosurgical Oncology, a section of the journal Frontiers in Oncology

Received: 19 October 2020
Accepted: 11 December 2020
Published: 02 February 2021

Citation:
Reinertsen I, Collins DL and Drouin S (2021) The Essential Role of Open Data and Software for the Future of Ultrasound-Based Neuronavigation. Front. Oncol. 10:619274. doi: 10.3389/fonc.2020.619274

With the recent developments in machine learning and modern graphics processing units (GPUs), there is a marked shift in the way intra-operative ultrasound (iUS) images can be processed and presented during surgery. Real-time processing of images to highlight important anatomical structures combined with in-situ display, has the potential to greatly facilitate the acquisition and interpretation of iUS images when guiding an operation. In order to take full advantage of the recent advances in machine learning, large amounts of high-quality annotated training data are necessary to develop and validate the algorithms. To ensure efficient collection of a sufficient number of patient images and external validity of the models, training data should be collected at several centers by different neurosurgeons, and stored in a standard format directly compatible with the most commonly used machine learning toolkits and libraries. In this paper, we argue that such effort to collect and organize large-scale multi-center datasets should be based on common open source software and databases. We first describe the development of existing open-source ultrasound based neuronavigation systems and how these systems have contributed to enhanced neurosurgical guidance over the last 15 years. We review the impact of the large number of projects worldwide that have benefited from the publicly available datasets "Brain Images of Tumors for Evaluation" (BITE) and "Retrospective evaluation of Cerebral Tumors" (RESECT) that include MR and US data from brain tumor cases. We also describe the need for continuous data collection and how this effort can be organized through the use of a well-adapted and user-friendly open-source software platform that integrates both continually improved guidance and automated data collection functionalities.

Keywords: ultrasound, neurosurgical navigation, open source software, machine learning, open data

INTRODUCTION

Ultrasound (US) is the most affordable and least invasive modality for intra-operative imaging of the brain. It is portable, flexible and provides real time imaging whenever needed during the procedure. The progress of surgery can therefore be closely monitored without major delays or interruptions in the workflow. When combined with neuronavigation, US images can be acquired directly in the patient's frame of reference and are therefore independent of any image-to-patient registration. Consequently, the most recently acquired US images provide the most accurate and up-to-date information about the patient's anatomy at any given time (1. Despite these advantages, US-guided neurosurgery is still not widely adopted in routine clinical practice. The availability of fully integrated US solutions for neuronavigation systems remains limited. Only a few specialized centers can afford costly extensions to their navigation systems such as BrainLab™'s US navigation module [1], and these solutions only provide a simple display of live US images in the context of preoperative scans. All other neurosurgeons who use US imaging must rely on real-time 2D US displayed on the monitor of the scanner, separate from the neuronavigation system, which makes it difficult to map the information on the scans back to the patient. Furthermore, US images present unfamiliar contrast, noise, and artefacts, which further limits its clinical usefulness.

To address these limitations, more research is needed on the processing, visualization, and integration of US images with existing navigation systems. To fuel the next wave of research on those topics, large amounts of data gathered from real surgical cases is needed. Over the past 15 years, our respective research groups have developed world leading expertise in the acquisition, processing and display of intra-operative ultrasound (iUS) data through the development of open source software platforms CustusX (2) and Ibis Neuronav (3). Despite the availability of such platforms, the efforts to collect and distribute the resulting data have remained limited to one center. However, recent efforts from the open source community have enabled the standardization of interfaces between research software and proprietary medical equipment installed in different centers [e.g. the Plus Toolkit (4)], and the interoperability between existing software platforms for the acquisition and processing of US images (e.g., IGSIO[2]). These recent developments open the possibility for multi-center efforts for large-scale data collection. Such efforts would provide researchers with the quantity and variability of ultrasound data required for the technical developments needed for ultrasound to become a truly widespread and useful tool in neurosurgery.

In this paper, we describe the development of existing open-source ultrasound based neuronavigation systems and how these systems have contributed to enhanced neurosurgical guidance over the last 15 years. We also review the impact of the large number of projects worldwide that have benefited from the existing publicly available datasets "Brain Images of Tumors for Evaluation" BITE (5) and "Retrospective evaluation of Cerebral Tumors" (RESECT) (6) that include MR and US data from brain tumor cases. Finally, we describe the increasing need for collecting large amounts of data to meet the requirements of recently developed machine learning algorithms, the possible organization of data collection through the use of an open-source software platform and the potential for new developments in ultrasound guided neurosurgery.

[1] https://www.brainlab.com/surgery-products/overview-neurosurgery-products/intraoperative-ultrasound/

[2] https://github.com/IGSIO

MATERIALS AND METHODS

In this section, we describe existing open source systems and how, together with the public datasets they have helped to acquire, these systems have contributed to the advancement of iUS-based navigation in neurosurgery.

Existing Systems

Commercial image-guided neurosurgery (IGNS) systems such as Medtronics™, BrainLab™, Stryker™, Synaptive™, and others are widely used for surgical planning and guidance worldwide. These systems are built for routine clinical use and their user interfaces are designed for easy use by surgeons and clinical staff. However, these systems are largely closed and are not built for systematic data collection for research purposes. In general, the mechanism provided to export data gathered during an operation is restricted to a certain portion of the information available and can only be done after the end of the procedure. In some cases, a software development kit allows for third parties to develop application that can capture real-time data such as 3D pose of certain tracked surgical tools using a separate computer (e.g., Medtronic's StealthLink™ or BrainLab™'s support for OpenIGTLink). However, these development kits are either costly or require specific research agreements between the hospital and the manufacturer, and their interfaces tend to change frequently, which is likely to disrupt long-term or multi-center research projects.

To address the limitations of the commercial systems, our respective research groups have developed world leading expertise in the acquisition of various types of intraoperative data through the development of open source software platforms. The two systems, Ibis Neuronav, developed by the Montreal group, and CustusX developed by the Trondheim group are described in the following sections.

Ibis Neuronav

Ibis neuronav (3) is an open source surgical navigation platform originally developed at the Montreal Neurological Institute (MNI) in Canada. The platform provides all the basic functionality common to most commercial systems mentioned above. It can visualize a wide variety of 3D brain scans in the operating room (OR) and register the patient with the scans in order to display the location of tracked surgical tools in relation to the images displayed on a computer screen. The goal of the platform is to enable research projects that aim to improve upon existing commercial systems by providing an open implementation that

can easily be modified and extended. The platform enables the validation of novel visualization, image processing and human-computer interaction methods in the OR and can be run in parallel with state of the art commercial solutions to enable comparison. Over the years, the Ibis system has been used for a variety of clinical applications such as brain tumor resection, neurovascular interventions (7), spine surgery (8), electrode implantation for deep brain stimulation (9), and the monitoring of epilepsy (10). However, the most notable contributions of the platform come from its ability to correct for brain shift based on intraoperative US imaging (11, 12) and its augmented reality visualization functionality (3). The system is able to capture and display images from a tracked US probe. It can acquire a sequence of such images and automatically reconstruct a volume from the individual slices. The computed US volume can then be used to compensate for mis-registration and tissue deformation by registering preoperative scans to the acquired US volume. The validation process for the brain shift correction functionality involved acquisition of tracked US sequences during a large number of neurosurgical procedures. Following these acquisitions, it rapidly became clear that the acquired US images together with other corresponding patient scans would be of interest for a wider community of medical image processing researchers, most of whom do not have access to neurosurgical operating rooms. The acquired data sets were thus made publicly available as the "Online database of clinical MR and ultrasound images of brain tumors" (BITE). We will describe this database in a later section. **Figure 1A**) shows an example of the main interface of Ibis Neuronav where the MR volume, iUS volume and iUS slices for one of the cases in the BITE database was loaded.

CustusX

The CustusX platform (2) in its current form was initiated in 2007 as the software platform for the Norwegian National Advisory Unit for Ultrasound and Image-Guided Therapy (USIGT)[3]. The platform is built on a number of open source libraries and toolkits and includes all the key components of a surgical navigation system. The system includes many of the same functionalities as Ibis Neuronav such as visualization of pre-operative MR/CT images in 2D and 3D, image-to-patient registration with various methods, tracking of ultrasound probes and surgical instruments, acquisition of 2D freehand ultrasound images, reconstruction of 3D ultrasound volumes and rigid MR-to-US registration for correction of brain shift. The main focus of the development has been intra-operative ultrasound imaging in different neurosurgical applications such as of brain tumor resection and neurovascular procedures procedures (13–15). The platform is also used in other clinical areas such as broncoscopy (16, 17), vascular surgery (18), and laparascopic surgery (19). **Figure 1B** shows how CustusX is being used in the OR for iUS-based navigation and **Figure 1C** presents an overview of the main interface during an iUS acquisition session.

[3]https://usigt.org

Other Systems

A wide variety of open source guidance systems have been proposed over the years. Although several of them included some form of support for iUS, it has not been their main focus. These systems include 3D Slicer (20) and MITK (21). 3DSlicer, initiated and mainly developed by the Surgical Planning Laboratory (SPL) at Brigham and Women's Hospital and Harvard Medical School in Boston, USA, is an open source software system for medical image processing and visualization. In recent years, 3DSlicer has been enhanced to support intraoperative navigation, ultrasound acquisition and advanced visualization (22). 3DSlicer is largely built on the same low-level libraries as Ibis and CustusX but has the additional advantage of being supported by a large and active community of developers and users worldwide. Although 3D Slicer has been used in various research prototypes of guidance systems based on US imaging, the setup of such systems from the distributed software components remains technically very challenging and the interface is not appropriate for use by clinicians. An important aspect to note however is that the SlicerIGT extension provides a mechanism to replace the user interface, enabling the creation of custom applications for specific clinical contexts and more appropriate for their use by clinicians.

The Medical Imaging Interaction Toolkit (MITK) (21, 23) is developed and maintained by the German Cancer Research Center (DKFZ) in Heidelberg, Germany. The platform was initiated more than 15 years ago as an open-source solution for image analysis, treatment planning and intervention support. The system has also been enhanced with support for real time ultrasound imaging (24). MITK has been used in applications such as robot-assisted ultrasound-guided radiation therapy (25) but not for ultrasound guided neurosurgery.

Comparison of Existing Systems

Amongst the existing open source systems, we can distinguish two categories. Both Ibis Neuronav and CustusX are built specifically to be used as intraoperative navigation systems and are designed with a focus on iUS-based navigation, while 3D Slicer and MITK are general purpose imaging platforms that can be customized as navigation systems by installing extensions and/or modifying configuration scripts. Although the interfaces of Ibis and CustusX are designed by engineers and for engineers, they are simple enough to envision training clinicians to use them without technical assistance, but it is not the ideal scenario for a multi-center research projects. On the other hand, both 3D Slicer and MITK allow developers to completely overwrite the default user interface, which opens the possibility of developing a simplified, clinician-centered interface specialized for iUS-based navigation and intraoperative data acquisition. In the case of 3D Slicer, the interface can be overwritten with a simple Python script, which can greatly ease the development process. One important aspect to consider in choosing an open source system is the level of activity in the community of developers and users. On this aspect, 3D Slicer has the most active community by far, even though its developers spread their efforts over a much larger number of features. **Table 1** summarizes the differences between existing systems.

FIGURE 1 | **(A)** The main interface of Ibis Neuronav where a case from the BITE databased was loaded, **(B)** iUS-based navigation in the OR using the CustusX system. **(C)** The main interface of CustusX during the acquisition of a US image sequence.

TABLE 1 | Comparison of features provided by different open source navigation platforms in regard of acquisition, rendering and navigation using US imaging (NT, Non-trivial).

Feature	CustusX	IBIS	Slicer	MITK
Configurable 2D/3D graphic window layout	Yes	No	Yes	Yes
Comprenhensive 3D Transforms system	Yes	Yes	Yes	Yes
Overwrite user interface	No	No	Yes	Yes
2D Slice rendering	Yes	Yes	Yes	Yes
3D Surface rendering	Yes	Yes	Yes	Yes
Volume Rendering	Yes	Yes	Yes	Yes
Augmented Reality	No	Yes	No	No
US capture	Yes	Yes	NT	NT
3D Display of US slice	Yes	Yes	NT	NT
US Volume Reconstruction	Yes	Yes (GPU)	No	No
Linear MR-US or CT-US registration	Yes	Yes (GPU)	NT	NT
US probe calibration	NT	Yes	No	No
3D tools tracking	Yes	Yes	NT	NT

Existing Databases

MNI BITE

The "Brain Images of Tumors for Evaluation" (BITE) database (5) is a publicly available dataset composed of MR and iUS images captured during 14 surgical procedures to remove brain tumors.[4]

All patients were operated at the Montreal Neurological Institute (MNI) by two different surgeons, and the iUS data was acquired using the IBIS Neuronav system described above. All patients presented with gliomas of varying grades. For each of the cases, the database contains a preoperative MR, multiple sequences of iUS and a postoperative MR. Here is a detailed description of the images:

- Preoperative scans: T1 weighted gadolinium-enhanced MR images acquired at 1.5T, with 1 mm slice thickness and a 0.5 mm in-plane resolution, except for one case that was acquired at 3T, with 1 mm slice thickness and 1 mm in-plane resolution.
- Postoperative scans: T1 weighted gadolinium-enhanced MR images acquired at 1.5T with 0.5 mm in-plane resolution, but have varying slice thicknesses (between 1 and 5 mm).
- iUS sequences: US images acquired from a Philips HDI 5000 scanner by capturing the analog video output. A P7-4MHz phased array transducer was used and set for a scanning depth of 6.5 or 8 cm, depending on the size and location of the tumor. The probe was tracked in 3D using an NDI Polaris optical tracking system. Each of the acquisitions consists of an approximately linear sweeps of 200–600 frames where the probe is moved at approximately 3 mm/s. In addition to the images themselves, the database contains a rigid transform obtained from the tracking system for every image. Each patient has multiple US sweeps and all of them, except for one, have sweeps pre- and post resection.

In addition to the raw data described above, the database contains the following processed/manually specified data for each case:

- A set of 10 homologous landmarks identified by a neuroradiologist that maps one pair of pre and post resection sweeps
- A US volume obtained by concatenating all the slices from a single iUS sweep.
- A set of between 19 and 37 homologous landmarks that maps preoperative MR and pre-resection US.
- The patient to preoperative MR transform obtained by aligning a set of homologous points identified on the scans prior to the operation and acquired on the patient using a tracked pointer during the operation.

[4]The BITE database is avilable at http://nist.mni.mcgill.ca/?page ¡d= 672

Following the success of the BITE database, 25 more tumor cases were acquired to form the basis for a second version of the database. An initial set of 9 cases have already been released and described in (26). The new version of the database contains essentially the same information as the first version and has been complemented with preoperative FLAIR and T2 weighted MR scans when available. In addition to the various sets of homologous landmarks that can be used as ground truth for the registration of the different imaging modalities, the new version of the database contains a segmentation of the tumor based on all preoperative modalities available, namely the T2 tumor hyperintensities (edema), the enhancing tumor core and the non-enhancing tumor core. The complete database comprising all 25 cases is in preparation and will be released shortly.

RESECT

The "Retrospective evaluation of Cerebral Tumors" (RESECT) database (6) consists of MR and ultrasound images of 23 low grade gliomas that have been resected at St. Olavs University Hospital, Trondheim, Norway by one neurosurgeon. [5]The database includes pre-operative contrast enhanced T1-weighted images, pre-operative FLAIR images and 3D ultrasound images acquired before, during and after tumor resection. More specifically, the database contains:

- Preoperative MR images: T1 weighted gadolinium (Gd)-enhanced and fluid attenuated inversion recovery (FLAIR) MR images acquired at 3T, both with 1 mm isotropic voxel size. For three patients, pre-operative images were acquired at 1.5T with a slice thickness of 1 mm and a 0.5 mm in-plane resolution for the Gd-enhanced T1 images and 1mm isotropic voxel size for the FLAIR images. The MR images include the patient registration transform.
- Intra-operative US images: US images acquired using the Sonowand Invite neuronavigation system (Sonowand AS, Trondheim, Norway) which includes a digitally integrated ultrasound scanner. A 12FLA-L linear transducer with a frequency range of 6–12 MHz was used. Depth and gain were adjusted depending on the size and location of the tumor. The probe was tracked in 3D using the NDI Polaris optical tracking system integrated in the Sonowand Invite system. The raw ultrasound data were reconstructed into 3D volumes using the reconstruction method included in the Sonowand Invite system. For all patients, the database includes one ultrasound volume acquired before resection (after opening of the dura), one ultrasound volume acquired during the resection and one ultrasound volume acquired after the resection.

In addition to the images, the database contains for each patient:

- Two sets of between 10 and 34 landmarks mapping the first (before resection) ultrasound volume and the second (during resection) and third (after resection) ultrasound volumes.
- Two sets of between 12 and 16 homologous landmarks mapping the pre-operative FLAIR volume to the first (before resection) ultrasound volume or the third (after resection) ultrasound volume.

The database does not contain any post-operative data or segmentations.

[5]The RESECT database is available at https://archive.norstore.no

RESULTS—IMPACT OF EXISTING DATABASES BITE AND RESECT

Together, the BITE and RESECT databases have been downloaded more than 1,000 times and have enabled the publication of more than 110 (number of citations as of Oct 2020) research articles, which illustrates the need and interest from the research community. Most of theses articles concerned the development and evaluation of registration algorithms for correction of brain shift, which is in line with the initial intended use. The public availability of the databases has enabled the development of alternative approaches to brain shift correction by groups with different expertise. The availability of BITE and RESECT has also enabled research on previously unforeseen applications.

MR-US and US-US Registration

The main purpose of the RESECT and BITE database was to provide a public dataset with real clinical data for evaluation of MR-US and US-US registration algorithms for correction of brain shift. These methods include the use of different similarity metrics (27–33), segmentation-based registration (34), and deep learning (35–37). So far, the conventional registration methods using similarity metrics well adapted to ultrasound images have proven to be the most successful (38). The work of Machado et al. (32) is particularly interesting in the way it focuses on robustness, and not only accuracy, of the registration and validate their results on BITE and RESECT in addition to MIBS, a proprietary database from Brigham and Women's Hospital. The article highlights the need for larger publicly available datasets collected from different centers as robustness is key to the adoption of iUS-based correction of brain shift in the standard of care.

As the databases do not contain any segmentations of tumors or other structures, segmentation-based approaches require the authors to perform their own segmentations to obtain a ground truth. This is challenging and time consuming, and limits the development of such methods. Several groups have tested deep learning approaches. However, the databases only contains data from 46 patients, which is probably insufficient for these methods to perform well and presents a high risk of overfitting. The RESECT database has also enabled the organization of registration challenges (CuRIOUS 2018 and 2019, Learn2Reg 2020) in conjunction with the International Conference on Medical Image Computing and Computer Assisted Interventions (MICCAI) where a number of different approaches have been benchmarked. The methods and results from the CuRIOUS 2018 challenge are summarized in (38).

The provided images have also been used together with other available databases for evaluation of registration metrics. Luo et al. analyzed the validity and distribution of landmark points provided with both RESECT and BITE (39). The paper highlights the need for a mechanism that allows users of such databases to contribute back improved data generated by users, in this case an improved version of landmark positions for points with a potentially high fiducial localization error (FLE).

Segmentation

One of the most promising avenues to facilitate the interpretation of iUS images is to automatically segment anatomical structures to enhance the visualized image with annotations. Several projects have used the data in BITE and RESECT to develop and validate segmentation methods for different structures. Canalini et al. used data from both databases to segment sulci and falx cerebri in US volumes using a convolutional neural network (CNN) (34). The segmented structures were then used to register together multiple US acquisitions at different stage of the resection and study the evolution of the procedure. It is interesting to note that for this paper, a manual segmentation of the sulci and falx cerebri has been performed using a custom tool built into the MevisLab platform[6]. Unfortunately, the current distribution systems for BITE and RESECT do not include functionality to contribute back this kind of annotation, which might be useful for other research groups. In many situations, it is important for a surgeon to determine the location of the boundary between gray and white matter. In Demiray et al., (40), authors use a CNN to perform the segmentation of gray and white matter from the 3D iUS images of the RESECT database. Given the difficulty for a clinician to manually segment those structures from iUS images alone, a ground truth segmentation was obtained automatically from the co-registered MR images distributed with RESECT. Another structure that has been segmented from the RESECT data is the resection cavity. This information can not only facilitate modeling of tissue deformation during surgery, but it can also help to identify residual tumor tissue that needs to be resected in order to prevent the recurrence of a tumor. Carton et al. used both BITE and RESECT to train a U-NET based model to perform surgical resection cavity segmentation in US images (41). For their work, they produced a manual segmentation of the resection cavity in US images. Again, this sort of annotation of the data could be beneficial to many other research teams if it could be contributed back to the databases. A more difficult, but very important problem in US image processing is that of segmenting brain tumors. This type of tissue can have a variety appearance depending on tumor type. Golb and al. used the RESECT database to develop and validate a tumor segmentation method based on US images (42). Maani et al. use the MR images from the BITE database to validate their tissue classification method based on volumetric texture analysis (43).

[6]https://www.mevislab.de/

Other Applications

The availability of the open databases has also enabled research in other areas related to US guided neurosurgery. One example is the work of Sagheer et al. (44) who used the BITE database to validate their US image denoising algorithm. Other examples include a US probe calibration method (45) where the authors used the BITE database in the validation process, simulation of 2D US from 3D MR (46) and sorting of DICOM images (47). Open image databases such as BITE and RESECT can also be used for more clinically oriented research. Petrecca et al. (48) used images from BITE to analyze the patterns of recurrence of glioblastomas.

DISCUSSION

In the previous sections, we have demonstrated that the public availability of US image databases such as BITE and RESECT has had an impact far beyond the initial intended purpose of the data collection process. Despite the relatively limited number of cases released in the databases, their availability has enabled significant progress in the development of algorithms that increase the usefulness and accuracy of iUS-based neuronavigation. First and foremost, a wide variety of MR-US registration algorithms have been proposed to compensate for brain shift and restore navigation accuracy at any moment during an operation. The databases have also enabled early successes in the development of multiple US image segmentation algorithms and a variety of other algorithms that are key to increasing the usefulness of US imaging in neurosurgery. In this section, we review the limitations of existing data sets, we show the importance of open source software to accelerate and standardize the acquisition process and we lay out a plan for the next generation of publicly available US imaging data.

Current Limitations and Future Needs for Technical Development and Data Collection

Registration

Despite the great advances in the iUS-based correction of brain shift we have seen with the previous generation of databases, the technology has yet to be adopted in commercial navigation systems and to be used as the standard of care. As a result, surgeons tend to simply stop relying on navigation systems once tissues have moved and deformed beyond a certain threshold. One of the reasons for this slow adoption by the major commercial systems is the lack of scientific evidence on the robustness of existing registration algorithms. Several questions remain as to the quantity, quality and acquisition protocol that will guarantee a stable and accurate correction of brain shift in every case. To be able to validate the robustness of MR-iUS registration algorithms, future data collection efforts will need to include a much larger number of patients from several centers and clinicians with different levels of training. Such data sets will not only enable the validation of the robustness of registration algorithms but will also allow for the development of iUS image acquisition guides that will help ensure that the quality and

quantity of data is sufficient to result in a stable registration every time.

Segmentation

With the recent developments in machine learning, we have started to see some progress in the area of segmentation of US images, a problem that was previously considered notoriously difficult. Segmented structures can be used to either improve image registration and further correct for brain shift, or improve visualization by highlighting different structures in real-time. For deep learning methods to perform well, large amounts of data are needed for training and testing. The number of cases needed depends on the difficulty of the segmentation problem (the image contrast between the structure to be segmented and its surroundings), the morphological variability of the structure to be segmented and the required accuracy. The training dataset needs to cover the full spectrum of anatomical and pathological variability in addition to differences due to scanners type, settings, and operators. Examples of segmentation of US using deep learning in other clinical areas are 1) Smistad et al. (49), where the authors segmented nerves for guiding regional anesthesia using data from 49 subjects and, 2) Anas et al. (50) where they segmented the prostate for targeted biopsies using data from 18 patients. These and other studies show promising results, but the number of included subjects is still limited. It is unlikely that the variability is fully covered, and the external validity of the results might therefore be limited. So far, there are no studies on the amount of ultrasound data required to detect or segment brain structures using deep learning methods. However, a study of deep learning for automatic segmentation in echocardiography suggests that 2D ultrasound images from 250 patients are needed for accurate segmentation of the left ventricle of the heart (51). As part of this study, a dataset with images from 500 patients, including expert annotations, was made publicly available (CAMUS data set) and it is now widely used for deep learning in the field of echocardiography (55 citations since 2019 as of Oct 2020). Even in cases with poor image quality in echocardiography, the image contrast is higher than in many ultrasound images of brain tumors. For segmentation of brain tumors, where contrast might be low and high accuracy is needed, it is reasonable to expect that at least a comparable number of cases is needed. For other relevant brain structures such as the lateral ventricles, the sulci and the falx that usually have higher contrast, fewer cases might be needed. These structures are important landmarks for the neurosurgeons, and automatic delineation would greatly ease the interpretation of the ultrasound images and thus address one of the main hurdles for widespread use of ultrasound in neurosurgery. However, as ultrasound images do not typically cover the entire brain, not all patient datasets will contain information about all structures. To collect several hundred data sets from brain tumor patients, multi-center data collection is the only possible way forward.

Visualization

One of the usability problems of iUS most often reported by neurosurgeons is the difficulty to simultaneously acquire and visualize the images. When imaging other parts of the anatomy such as abdominal organs, experienced ultrasonographers typically look at the screen of the scanner to locate the anatomy of interest and rely mostly on their sense of proprioception to physically position the US probe on the skin of the patient and maintain the appropriate amount of pressure. Imaging the brain is different because acquisition has to be performed on the very limited surface of the dura or cerebral cortex exposed by a craniotomy and almost no pressure can be applied to the delicate tissues of the brain. Thus, the surgeon's attention has to remain on the surgical field at all time, which results in an acquisition being performed without visual feedback first, and then visualized. This can force a surgeon to perform multiple cycles of acquisition and visualization to obtain the desired information. Several groups have proposed the use of augmented reality (AR) to solve this problem. The technology of AR enables the display of US images in-situ, allowing neurosurgeons to visualize the images being acquired while maintaining their attention on the surface of the operating field. So far, most of the research on neurosurgical AR has focused on the integration of hardware and software components required to accurately overlay virtual content such as US images, with a live view of the operating field. However, one of the main obstacles to the adoption of AR remain the various depth perception problems generated by the live mix of real and virtual content. In order to accelerate research on neurosurgical AR and in particular on live in-situ display of iUS images, a future intraoperative image database should include live video of the operating field allowing researchers working on the improvement of AR rendering techniques to evaluate their method on realistic models of the operating field. Images can be captured from a variety of sensors. For example, the Ibis Neuronav system includes a built-in module to produce AR images from a surgical microscope that has the ability to record live images (3). An extension of Ibis called MARIN adds similar capabilities to produce AR image from a tablet computer (52).

Interrelationship of Software and Data

The development of the Ibis Neuronav system and the following acquisition of the BITE dataset exemplify the interrelationship between software and data and the value of an open source surgical navigation system in the data acquisition process and in the advancement of iUS based surgical navigation. The version of the Ibis system used to acquire iUS images for the BITE database included only rudimentary functionality to reconstruct a 3D volume for 2D iUS slices, a process which took on average 10 min (5). Similarly, Ibis implemented a well-established method to linearly register an iUS volume with preoperative MR scans (53) to correct for brain shift, which also ran in approximately 10 min. Overall, the process of correcting for the patient-to-image misregistration took on average 20 min once the surgeon had finished a US image sweep. Given such delays, it was difficult to convince clinicians of the benefits of the method. It also made the data acquisition process error prone as once the reconstruction and registration process finished, it was already too late to perform a second acquisition if it turned out the first one did

not contain enough information to obtain a reliable registration. The release of the first BITE database stimulated the research on registration algorithms that were more appropriate for MR-US registration. One of the most robust methods proposed was based on the alignment of image gradient (33) and provided a GPU implementation that authors agreed to contribute to the source code of Ibis as an extension of the platform, together with a GPU implementation of iUS volume reconstruction. The new volume registration algorithm ran in under 5 s, while MR-iUS registration took under 1 s (3). The improved system generated much more interest on the part of the clinicians as they were able to appreciate the results of the registration correction algorithm as soon as they finished acquisition. It also provided instant feedback on the quality of the acquisition, allowing them to improve faster on their acquisition skills, resulting in an increased pace of data acquisition. As a result, a second version of the BITE database (soon to be released), containing double the number of cases of the first one (25), has been acquired in a shorter time frame.

Similarly, a GPU implementation of a MR-iUS registration algorithm (54) was integrated into CustusX and validated intra-operatively in a series of 13 brain tumor cases (14). This method provided registration results within a few seconds and ran seamlessly within the CustusX software.

While research platforms such as Ibis and CustusX have been useful and successful in a large number of research projects, they might not be suitable for a large scale data collection effort. The systems have clearly improved over the years, but they are still highly complex. The use of these systems requires the presence of a dedicated technical researcher in the operating room during every single procedure in order to ensure the correct functioning of the system. The complexity of their numerous options and configurations combined with a sub-optimal user interfaces makes these systems unsuited for clinical users, and thus unsuited for efficient collection of high volumes of intra-operative data from hundreds and possibly thousands of patients.

Requirements and Architecture for the Software and Database of the Future

In order to efficiently collect a large number of patient cases, a simplified software solution better adapted to brain tumor surgery is required. The software needs to include all the basic components of a neuronavigation system like Ibis and CustusX, but the user-interface should be redesigned and adapted with clinical users in mind. This means a highly intuitive interface with only the essential components, fewer buttons, menus, and configurations than the existing systems.

The user-interface should be designed to provide the right information at the right time and to fit into the clinical workflow in neurosurgery. The system should be adapted to run in parallel with commercial navigation systems without imposing additional preparation or manipulation by the surgeon. More specifically, the following steps should be performed simultaneously for both systems:

- Calibration of tools such as navigation pointer and ultrasound probe
- Pre-operative image-to-patient registration
- Ultrasound acquisition (when available in commercial systems)
- Pointer-based navigation

In addition to replicating the functionality of the commercial systems, the proposed platform should provide a fast mechanism to reconstruct a 3D volume from a sequence of iUS images and register preoperative scans to the reconstructed volume to correct for brain shift. From a developer's point of view, it should be straightforward to replace the default volume reconstruction and registration algorithm with newly developed methods as they become available.

The proposed system should also include improved visualization capabilities to provide visual feedback during the acquisition of iUS images. It should be capable of displaying the result of real-time automatic segmentation of arbitrary structures during the acquisition. For developers, a simple software development interface should allow to easily integrate new segmentation algorithms as they become available, without having to deal with the visualization aspect that would be natively supported by the system. The proposed system should also include modules to produce AR views of the operating field in order to provide visual feedback to the surgeons during the acquisition process, while allowing them to keep their attention focused on the operating field. The additional data captured during the AR visualization sequences should be automatically recorded. For example, when creating AR images with a tracked tablet computer like it is done with the MARIN system mentioned earlier, live video and tablet tracking transforms should be recorded to enable the improvement of AR rendering techniques in the laboratory.

The proposed system should automate the process to transfer the collected datasets from different centers to a common cloud-based database. In addition to various national and local solutions, large-scale international solutions for such cloud-based systems include:

- The "Imaging Data Commons" (https://imagingdatacommons.github.io/)
- ELIXIR Data Platform (https://elixir-europe.org/platforms/data)
- HRIC (55)

This infrastructure must ensure data storage and processing within the relevant ethical, legal, and regulatory frameworks such as EU's General Data Protection Regulation (GDPR). Following data collection, all datasets should be automatically anonymized and controlled for completeness and quality. The format of the database for each case should be flexible enough to take into account differences in imaging protocols at different centers. For example, certain centers might not acquire FLAIR images in their standard protocol for brain tumor cases, so the database should support uploading data without this type of image. The database should allow users to filter cases based on the information available. The proposed database should also support the addition of new types of data that were not planned for during development.

In order to be used for image analysis and machine learning, different levels of data annotation is needed. Annotation needs to be performed by clinical experts through the use of dedicated software solutions such as a secure web-based platform for example. The images, video, position information etc. should be made available in widely used open formats directly compatible with the most commonly used open source imaging and machine learning toolkits and libraries such as TensorFlow and Keras.

CONCLUSION

In this paper, we have reviewed the impact that the open source neuronavigation platforms Ibis Neuronav and CustusX and their associated databases BITE and RESECT have had on the progress iUS-based navigation. We have particularly emphasized how the synergy between open source software and publicly available data has contributed to accelerate this progress. Building on these successes, we have proposed to combine the effort of multiple research groups to build a simplified and improved combination of open software and tumor case database that is likely to enable gathering the large amounts of data needed to train new machine learning models to improve iUS-based navigation. The main goal of this data collection effort is to provide the international research community with high quality data. This will accelerate research in the field, especially among research groups who do not have the possibility to collect their own data but rely on publicly available datasets. With more research groups working actively in the field, the development of new tools and methods will also accelerate. New, innovative, and well validated tools can then be included in the open software platform which will enhance the usefulness for clinician and thus accelerate data collection through an increased rate of new cases. This cycle can thus be a positive self-reinforcing process that will lead to more robust and accurate tools, acceleration of the translation from the laboratory to industry and more accurate, safer, and more minimally invasive procedures for patients.

DATA AVAILABILITY STATEMENT

The original contributions presented in the study are included in the article/supplementary material; further inquiries can be directed to the corresponding author.

AUTHOR CONTRIBUTIONS

IR and SD drafted the manuscript. All authors contributed to the article and approved the submitted version.

FUNDING

This work has received funding from the Norwegian National Advisory Unit for Ultrasound and Image-Guided Therapy (usigt.org) as well as from the Natural Sciences and Engineering Research Council of Canada (CHRP 385864) and the Canadian Institute for Health Research (MOP-97820).

REFERENCES

1. Lindseth F, Bang J, Langø T. A robust and automatic method for evaluating accuracy in 3-dultrasound-based navigation. *Ultrasound Med Biol* (2003) 29:1439–52. doi: 10.1016/S0301-5629(03)00967-0
2. Askeland C, Solberg OV, Bakeng JB, Reinertsen I, Tangen GA, Hofstad EF, et al. CustusX: an open-source research platform for image-guidedtherapy. *Int J Comput Assist Radiol Surg* (2016)11:505–19. doi: 10.1007/s11548-015-1292-0
3. Drouin S, Kochanowska A, Kersten-Oertel M, Gerard IJ, Zelmann R, De Nigris D, et al. IBIS: an OR ready open-source platform for image-guidedneurosurgery. *Int J Comput Assist Radiol Surg* (2016) 12:363–78. doi: 10.1007/s11548-016-1478-0
4. Lasso A, Heffter T, Rankin A, Pinter C, Ungi T, Fichtinger G. Plus: Open-source toolkit for ultrasound-guided interventionsystems. *IEEE Trans Biomed Eng* (2014) 61:2527–37. doi: 10.1109/TBME.2014.2322864
5. Mercier L, Del Maestro R, Petrecca K, Araujo D, Haegelen C, Collins D. Online database of clinical MR and ultrasound images of brain tumors. *Med Phys* (2012) 39:3253–61. doi: 10.1118/1.4709600
6. Xiao Y, Fortin M, Unsgård G, Rivaz H, Reinertsen I. Retrospective evaluation of cerebral tumors (resect): A clinical database of pre-operative mri and intra-operative ultrasound in low-grade glioma surgeries. *Med Phys* (2017) 44:3875–82. doi: 10.1002/mp.12268
7. Kersten-Oertel M, Gerard IJ, Drouin S, Mok K, Sirhan D, Sinclair DS, et al. Augmented reality in neurovascular surgery: feasibility and firstuses in the operating room. *Int J Comput Assist Radiol Surg*(2015) 10:1823–36. doi: 10.1007/s11548-015-1163-8
8. Gueziri HE, Yan CX, Collins DL. Open-source software for ultrasound-based guidance in spinal fusionsurgery. *Ultrasound Med Biol* (2020) 46:3353–68. doi: 10.1016/j.ultrasmedbio.2020.08.005
9. Bériault S, Sadikot AF, Alsubaie F, Drouin S, Collins DL, Pike GB. Neuronavigation using susceptibility-weighted venography:application to deep brain stimulation and comparison with gadolinium contrast. *J Neurosurgery* (2014) 121:131–41. doi: 10.3171/2014.3.JNS131860
10. Frauscher B, von Ellenrieder N, Zelmann R, Rogers C, Nguyen DK, Kahane P, et al. High-Frequency Oscillations in the Normal HumanBrain. *Ann Neurol* (2018) 84:374–85. doi: 10.1002/ana.25304
11. Rivaz H, Collins DL. Deformable registration of preoperative mr, pre-resectionultrasound, and post-resection ultrasound images of neurosurgery. *Int J Comput Assist Radiol Surg* (2015a) 10:1017–28. doi: 10.1007/s11548-014-1099-4
12. Rivaz H, Collins DL. Near real-time robust non-rigid registration of volumetric ultrasound images for neurosurgery. *Ultrasound Med Biol* (2015b) 41:574–87. doi: 10.1016/j.ultrasmedbio.2014.08.013
13. Reinertsen I, Lindseth F, Askeland C, Iversen DH, Unsgård G. Intra-operative correction of brain-shift.*Acta Neurochirurgica* (2014) 156:1301–10. doi: 10.1007/s00701-014-2052-6
14. Iversen DH, Wein W, Lindseth F, Unsgard G, Reinertsen I. Automatic intraoperative correction of brain shift for accurate neuronavigation. *World Neurosurgery* (2018). doi: 10.1016/j.wneu.2018.09.012
15. Iversen DH, Løvstakken L, Unsgard G, Reinertsen I. Automatic intraoperative estimation of blood flow direction duringneurosurgical interventions. *Int J Comput Assist Radiol Surg* (2018) 13:693–701. doi: 10.1007/s11548-018-1711-0

16. Sorger H, Hofstad EF, Amundsen T, Langø T, Bakeng JBL, Leira HO. A multimodal image guiding system for navigated ultrasound bronchoscopy (ebus): A human feasibility study. *PloS One* (2017) 12:1–15. doi: 10.1371/journal.pone.0171841
17. Bakeng JBL, Hofstad EF, Solberg OV, Eiesland J, Tangen GA, Amundsen T, et al. Using the custusx toolkit to create an image guided bronchoscopy application: Fraxinus. *PloS One* (2019) 14:1–15. doi: 10.1371/journal.pone.0211772
18. Manstad-Hulaas F, Tangen GA, Dahl T, Hernes TAN, Aadahl P. Three-dimensional electromagnetic navigation vs. fluoroscopy forendovascular aneurysm repair: A prospective feasibility study in patients. *J Endovascular Ther* (2012) 19:70–78. doi: 10.1583/11-3557.1
19. Solberg OV, Langø T, Tangen GA, Mårvik R, Ystgaard B, Rethy A, et al. Navigated ultrasound in laparoscopic surgery. *Minimally Invasive Ther Allied Technol* (2009) 18:36–53. doi: 10.1080/13645700802383975
20. Fedorov A, Beichel R, Kalpathy-Cramer J, Fillion-Robin JFJC, Pujol S, Bauer C, et al. 3d slicer as an image computing platform for the quantitativeimaging network. *Magn Reson Imaging* (2012) 30:1323–41. doi: 10.1016/j.mri.2012.05.001
21. Wolf I, Vetter M, Wegner I, Böttger T, Nolden M, Schöbinger M, et al. The medical imaging interaction toolkit. *Med Image Anal* (2005) 9:594–604. doi: 10.1016/j.media.2005.04.005
22. Ungi T, Lasso A, Fichtinger G. Open-source platforms for navigated image-guidedinterventions. *Med Image Anal* (2016) 33:181–6. doi: 10.1016/j.media.2016.06.011
23. Nolden M, Zelzer S, Seitel A, Wald D, Müller M, Franz AM, et al. The medical imaging interaction toolkit: challenges and advances. *Int J Comput Assist Radiol Surg* (2013). doi: 10.1007/s11548-013-0840-8
24. März K, Franz AM, Seitel A, Winterstein A, Bendl R, Zelzer S, et al. Mitk-us: real-time ultrasound support within mitk. *Int J CARS* (2014) 9:411–20. doi: 10.1007/s11548-013-0962-z
25. Seitz PK, Baumann B, Johnen W, Lissek C, Seidel J, Bendl R. Development of a robot-assisted ultrasound-guided radiation therapy(USgRT). *Int J Comput Assist Radiol Surg* (2020) 15:491–501. doi: 10.1007/s11548-019-02104-y
26. Gerard IJ, Couturier C, Kersten-Oertel M, Drouin S, De Nigris D, Hall JA, et al. Towards a Second Brain Images of Tumours for Evaluation (BITE2) Database. In: *International Workshop on Brain lesion: Glioma, Multiple Sclerosis, Stroke and Traumatic Brain Injuries*. Cham: Springer (2016). p. 16–22. doi: 10.1007/978-3-319-55524-9_2
27. Masoumi N, Xiao Y, Rivaz H. Arena: Inter-modality affine registration using evolutionarystrategy. *Int J CARS* (2019) 14:441–50. doi: 10.1007/s11548-018-1897-1
28. Heinrich MP. Intra-operative ultrasound to mri fusion with a public multimodal discrete registration tool. In: *Simulation, Image Processing, and Ultrasound Systems for Assisted Diagnosis and Navigation*. Springer International Publishing (2018). doi: 10.1007/978-3-030-01045-4_19
29. Hong J, Park H. Non-linear approach for mri to intra-operative us registration using structural skeleton. In: *Simulation, Image Processing, and Ultrasound Systems for Assisted Diagnosis and Navigation*. Springer International Publishing (2018). doi: 10.1007/978-3-030-01045-4_16
30. Wein W. Brain-shift correction with image-based registration and landmark accuracy evaluation. In: *Simulation, Image Processing, and Ultrasound Systems for Assisted Diagnosis and Navigation*. Springer International Publishing (2018). doi: 10.1007/978-3-030-01045-4_17
31. Shams R, Boucher M-A, Kadoury S. Intra-operative brain shift correction with weighted locally linear correlations of 3DUS and MRI. In: *Simulation, Image Processing, and Ultrasound Systems for Assisted Diagnosis and Navigation. Springer* (2018). doi: 10.1007/978-3-030-01045-4_22
32. Machado I, Toews M, George E, Unadkat P, Essayed W, Luo J, et al. Deformable MRI Ultrasound registration using correlation-basedattribute matching for brain shift correction: Accuracy and generality in multi-site data. *NeuroImage* (2019) 202:116094. doi: 10.1016/j.neuroimage.2019.116094
33. De Nigris D, Collins DL, Arbel T. Fast rigid registration of pre-operative magnetic resonance images to intra-operative ultrasound for neurosurgery based on high confidence gradient orientations. *Int J Comput Assist Radiol Surg* (2013) 8:649–61. doi: 10.1007/s11548-013-0826-6
34. Canalini L, Klein J, Miller D, Kikinis R. Segmentation-based registration of ultrasound volumes for gliomaresection in image-guided neurosurgery. *Int J Comput Assist RadiolSurg* (2019) 14:1697–713. doi: 10.1007/s11548-019-02045-6
35. Sun L, Zhang S. Deformable MRI-ultrasound registration using 3D convolutional neural network. In: *Simulation, Image Processing, and Ultrasound Systems for Assisted Diagnosis and Navigation*. Springer International Publishing (2018). doi: 10.1007/978-3-030-01045-4_18
36. Zhong X, Bayer S, Ravikumar N, Strobel N, Birkhold A, Kowarschik M, et al. Resolve intraoperative brain shift as imitation game. In: *Simulation, Image Processing, and Ultrasound Systems for Assisted Diagnosis and Navigation*. Springer International Publishing (2018). doi: 10.1007/978-3-030-01045-4_15
37. Zeineldin RA, Karar ME, Coburger J, Wirtz CR, Mathis-Ullrich F, Burgert O. Towards automated correction of brain shift using deep deformablemagnetic resonance imaging intraoperative ultrasound (MRI-iUS) registration.*Curr Dir Biomed Eng* (2020) 6. doi: 10.1515/cdbme-2020-0039
38. Xiao Y, Rivaz H, Chabanas M, Fortin M, Machado I, Ou Y, et al. Evaluation of mri to ultrasound registration methods for brain shiftcorrection: The curious2018 challenge. *IEEE Trans Med Imaging* (2020) 39:777–86. doi: 10.1109/TMI.2019.2935060
39. Luo J, Ma G, Frisken S, Juvekar P, Haouchine N, Xu Z, et al. Do public datasets assure unbiased comparisons for registration evaluation? *arXiv* (2020). 2003.09483.
40. Demiray B, Rackerseder J, Bozhinoski S, Navab N. Weakly-supervised white and grey matter segmentation in 3d brain ultrasound. *arXiv* (2019). 1904.05191.
41. Carton F-X, Chabanas M, Lann FL, Noble JH. Automatic segmentation of brain tumor resections in intraoperativeultrasound images using U-Net. *J Med Imaging*(2020) 7:031503. doi: 10.1117/1.JMI.7.3.031503
42. Göbl R, Rackerseder J, Navab N, Hennersperger C. Fully automatic segmentation of 3d brain ultrasound: Learning from coarse annotations. *arXiv* (2018). 1904.08655.
43. Maani R, Kalra S, Yang YH. Robust volumetric texture classification of magnetic resonanceimages of the brain using local frequency descriptor. *IEEE Trans ImageProcess* (2014) 23:4625–36. doi: 10.1109/TIP.2014.2351620
44. Sagheer SVM, N.George S, Kurien SK. Despeckling of 3D ultrasound image using tensor low rank approximation. *Biomed Signal Process Control* (2019) 54:101595. doi: 10.1016/j.bspc.2019.101595
45. Toews M, Wells WM. Phantomless Auto-Calibration and Online Calibration Assessment for aTracked Freehand 2-D Ultrasound Probe. *IEEE Trans Med Imaging* (2018) 37:262–72. doi: 10.1109/TMI.2017.2750978
46. Salehi M, Ahmadi S-A, Prevost R, Navab N, Wein W. Patient-specific 3D Ultrasound Simulation Based on ConvolutionalRay-tracing and Appearance Optimization. In: *Medical image computing and computer-assisted intervention – MICCAI 2015.* vol. 9350. Cham: Springer (2015). p. 510–18. doi: 10.1007/978-3-319-24571-3_61
47. van der Voort S, Smits M, Klein S. Deepdicomsort: An automatic sorting algorithm for brain magneticresonance imaging data. *Neuroinform* (2020) 19:159–84. doi: 10.1007/s12021-020-09475-7
48. Petrecca K, Guiot MC, Panet-Raymond V, Souhami L. Failure pattern following complete resection plus radiotherapy and temozolomide is at the resection margin in patients with glioblastoma. *J Neuro Oncol* (2013) 111:19–23. doi: 10.1007/s11060-012-0983-4
49. Smistad E, Johansen KF, Iversen DH, Reinertsen I. Highlighting nerves and blood vessels for ultrasound-guided axillarynerve block procedures using neural networks. *J Med Imaging* (2018) 5:044004. doi: 10.1117/1.JMI.5.4.044004
50. Anas EMA, Mousavi P, Abolmaesumi P. A deep learning approach for real time prostate segmentation in freehand ultrasound guided biopsy. *Med Image Anal* (2018) 48:107–16. doi: 10.1016/j.media.2018.05.010
51. Leclerc S, Smistad E, Pedrosa J, Østvik A, Cervenansky F, Espinosa F, et al. Deep learning for segmentation using an open large-scale dataset in2d echocardiography. *IEEE Trans Med Imaging* (2019)38:2198–210. doi: 10.1109/TMI.2019.2900516
52. Léger É, Reyes J, Drouin S, Popa T, Hall JA, Collins DL, et al. MARIN: an open-source mobile augmented reality interactiveneuronavigation system. *Int*

J Comput Assist Radiol Surg(2020) 15:1013–21. doi: 10.1007/s11548-020-02155-6

53. Collignon A, Maes F, Delaere D, Vandermeulen D, Suetens P, Marchal G. Automated multi-modality image registration based on informationtheory. *In Inf Process Med Imaging (Citeseer)* (1995) 3:263–74.
54. Fuerst B, Wein W, Müller M, Navab N. Automatic ultrasound–mri registration for neurosurgery usingthe 2d and 3d lc2 metric. *Med Image Anal* (2014) 18:1312–9. doi: 10.1016/j.media.2014.04.008
55. Aarestrup FM, Albeyatti A, Oyen HV. Towards a european health research and innovation cloud(hric). *Genome Med* (2020) 12:1–14. doi: 10.1186/s13073-020-0713-z

Conflict of Interest: The authors declare that the research was conducted in the absence of any commercial or financial relationships that could be construed as a potential conflict of interest.

frontiers in Oncology

REVIEW
published: 08 February 2021
doi: 10.3389/fonc.2020.618837

Brain Shift in Neuronavigation of Brain Tumors: An Updated Review of Intra-Operative Ultrasound Applications

Ian J. Gerard[1]*, *Marta Kersten-Oertel*[2], *Jeffery A. Hall*[3], *Denis Sirhan*[3] *and D. Louis Collins*[3]

[1] Department of Radiation Oncology, McGill University Health Centre, Montreal, QC, Canada, [2] Department of Computer Science, Concordia University, Montreal, QC, Canada, [3] Department of Neurology and Neurosurgery, McGill University, Montreal, QC, Canada

OPEN ACCESS

Edited by:
Francesco DiMeco,
Fondazione IRCCS Istituto Neurologio Carlo Besta, Italy

Reviewed by:
Andrej Steno,
Comenius University, Slovakia
Francesco Prada,
Fondazione IRCCS Istituto Neurologio Carlo Besta, Italy

***Correspondence:**
Ian J. Gerard
ian.gerard@mail.mcgill.ca

Specialty section:
This article was submitted to Neuro-Oncology and Neurosurgical Oncology, a section of the journal Frontiers in Oncology

Received: 18 October 2020
Accepted: 22 December 2020
Published: 08 February 2021

Citation:
Gerard IJ, Kersten-Oertel M, Hall JA, Sirhan D and Collins DL (2021) Brain Shift in Neuronavigation of Brain Tumors: An Updated Review of Intra-Operative Ultrasound Applications. Front. Oncol. 10:618837. doi: 10.3389/fonc.2020.618837

Neuronavigation using pre-operative imaging data for neurosurgical guidance is a ubiquitous tool for the planning and resection of oncologic brain disease. These systems are rendered unreliable when brain shift invalidates the patient-image registration. Our previous review in 2015, *Brain shift in neuronavigation of brain tumours: A review* offered a new taxonomy, classification system, and a historical perspective on the causes, measurement, and pre- and intra-operative compensation of this phenomenon. Here we present an updated review using the same taxonomy and framework, focused on the developments of intra-operative ultrasound-based brain shift research from 2015 to the present (2020). The review was performed using PubMed to identify articles since 2015 with the specific words and phrases: *"Brain shift" AND "Ultrasound"*. Since 2015, the rate of publication of intra-operative ultrasound based articles in the context of brain shift has increased from 2–3 per year to 8–10 per year. This efficient and low-cost technology and increasing comfort among clinicians and researchers have allowed unique avenues of development. Since 2015, there has been a trend towards more mathematical advancements in the field which is often validated on publicly available datasets from early intra-operative ultrasound research, and may not give a just representation to the intra-operative imaging landscape in modern image-guided neurosurgery. Focus on vessel-based registration and virtual and augmented reality paradigms have seen traction, offering new perspectives to overcome some of the different pitfalls of ultrasound based technologies. Unfortunately, clinical adaptation and evaluation has not seen as significant of a publication boost. Brain shift continues to be a highly prevalent pitfall in maintaining accuracy throughout oncologic neurosurgical intervention and continues to be an area of active research. Intra-operative ultrasound continues to show promise as an effective, efficient, and low-cost solution for intra-operative accuracy management. A major drawback of the current research landscape is that mathematical tool validation based on retrospective data outpaces prospective clinical evaluations decreasing the strength of the evidence. The need for newer and

more publicly available clinical datasets will be instrumental in more reliable validation of these methods that reflect the modern intra-operative imaging in these procedures.

Keywords: brain shift, neuronavigation, intra-operative ultrasound, registration, neurosurgery, image-guided neurosurgery

INTRODUCTION

Neuronavigation using pre-operative imaging data for neurosurgical guidance is a ubiquitous tool for the planning and resection of oncologic disease in the brain and has become common practice in many centers. It is well known that these systems are rendered unreliable when brain shift is present. Any factor, physical, surgical, or biological, that violates the rigid body assumption of neuronavigation causes the tissues of the brain to shift and move away from the pre-operative images creating a difference between the reported location of anatomy in the virtual image and patient spaces. Simply put, brain shift invalidates the patient-to-image mapping (1). In our previous 2015 review of brain shift in neuronavigation (1), we offered a new taxonomy, classification system, and a historical perspective related to the causes, measurement, and pre- and intra-operative compensation of this phenomenon. In this work, we present an updated and focused review using the same taxonomy and framework on the developments of intra-operative ultrasound-based brain shift applications over the last five years, *i.e.* from 2015 to the present. A visual representation of the previously described classification system along with the highlighted trajectory of the focus of this review can be seen in **Figure 1**.

The first use of A-mode (1D) ultrasound (US) for adult neurosurgery was completed by Dr. William Peyton in 1951 and reported by Wild and Reid in 1953 (2). The first use of B-mode (2D) US in adult neurosurgery of the spine was in 1978 by Reid (3) and in the brain in 1980 by Rubin et al. (4). In the latter, they observed intra-cranial anatomy with real-time ultrasound as well as a grade III astrocytoma and postulated that there may be benefit for this technology as a tool for surgical planning and biopsy procedures. Since then, and throughout the 2000s, intra-operative ultrasound (iUS) has been used in many capacities to evaluate, quantify, and correct for brain shift and modify surgical plans in real-time without the use of ionizing radiation exposure (*e.g.* from CT) all while minimizing any disruption to the surgical workflow. Over the last 5 years the rate of publication for intra-operative based ultrasound intervention for brain shift evaluation, quantification, and correction has dramatically increased. In the context of these advances, we review the current state, potential, and challenges that remain in the context of iUS for neuronavigation of brain tumors.

BRAIN SHIFT TAXONOMY

In order to assist with the clarity of the review and the discussions to follow, this review follows the same taxonomy and classification system as the 2015 publication: *Brain shift in neuronavigation of brain tumours: A review* (1). To begin, brain shift is defined as—*any factor, physical, surgical, or biological, that violates the rigid body assumption of neuronavigation creating a difference between the reported location of anatomy in the virtual image and patient spaces*. The discussion of brain shift is further separated into three categories; 1) factors that cause brain shift, 2) methods for quantifying brain shift, and 3)

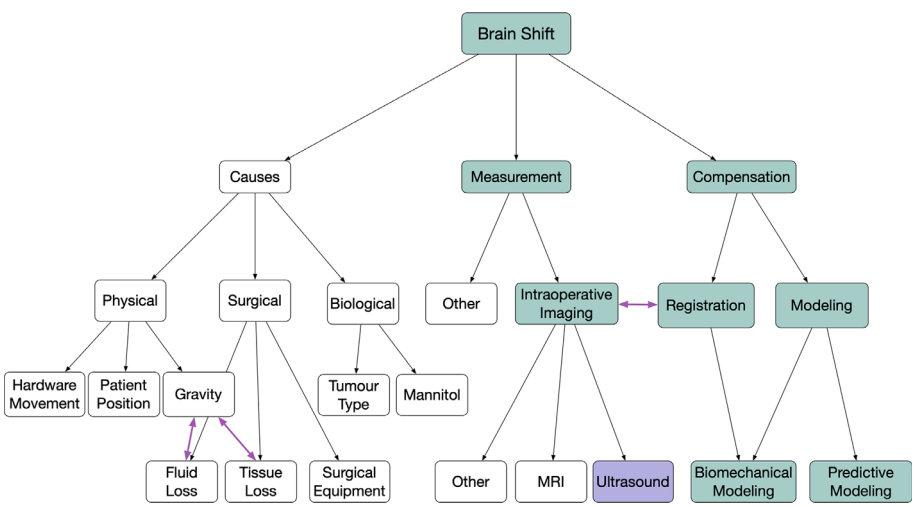

FIGURE 1 | Highlighted flow chart following classification from (1) showing the focused coverage of this review.

methods to correct or account for brain shift, followed by more specific subclassifications. As highlighted in **Figure 1**, the articles in this review are primarily those that describe either the measurement or compensation of brain shift using intra-operative ultrasound imaging in the context of image registration, biomechanical modeling, or predictive modeling.

INTRA-OPERATIVE ULTRASOUND FOR NEUROSURGERY

Ultrasound imaging uses high frequency sound waves that are emitted and detected by different probes and transducers. In the context of neurosurgery, the optimal choice of transducer and type of acquisition frequency will depend on the location and sonographic properties of the lesion of interest, the size of the craniotomy in which the probe can be placed, the surrounding anatomy, and of course, surgeon preference. The intensity of structures in these images directly reflects the amplitude of the detected signal driven by micro reflectors within tissue and the interfaces between tissues with different acoustic impedance. As a general principle, tissues that are acoustically homogeneous will generate low intensity signals, while structures with high gradients of acoustic impedance, such as bone or necrotic tissue, generate strong echoes and can obscure other structures deeper in the imaging plane. In a normal human brain, anatomical structures that give a hyperechoic signal on ultrasound imaging include the sulci, falx cerebri, choroid plexus, and vessel walls. In contrast, the ventricles and other spaces filled with cerebrospinal fluid are generally acoustically homogenous and create a low intensity hypoechoic signal. Lesions in the brain can have varying appearance depending on the mass density, necrotic infiltration, or fluid filled cavities but generally appear hyperechoic with areas of mixed echogenicity depending on the above specific features.

Intra-operative ultrasound, in the context of brain shift, was first introduced in 1997 by Bucholz (5) where they provided the first documented quantitative measurement of brain shift during hematoma and tumor neurosurgery. Before this, ultrasound had been previously introduced as an intra-operative neurosurgical tool to assist in small lesion identification in the context of arterio-venous malformation surgery by Chandler in 1987 (6). Since these initial publications, numerous investigators have implemented unique applications and procedures to harness this low-cost and widely available intra-operative imaging tool to gather real-time anatomical information for measuring and compensating for brain shift. The primary link between intra-operative imaging, such as ultrasound, and brain shift measurement or compensation is a registration procedure that relates intra-operative and pre-operative images to each other. In the context of iUS, the main challenge stemming from these registration procedures relates the widely different nature and quality of the iUS images as compared with the pre-operative MRI images. While voxel intensity of both modalities is directly dependent on the specific tissues imaged, there is an additional dependence for iUS on probe orientation and depth that leads to significant image intensity non-uniformity due to the presence of acoustic impedance transitions. The quality of individual ultrasound images is known to vary among users adding another obstacle when developing tools and methods to use this modality reliably for brain shift related interventions.

METHODS

This review followed the Preferred Reporting Items for Systematic Reviews and Meta-Analyses (PRISMA) 2009 guidelines without prior publication of the review protocol (7) and was performed using PubMed[1] on August 17, 2020, to identify articles since 2015 with the specific words and phrases:

("brain shift" OR brainshift) AND "ultrasound"

The returned titles were screened for any non-English, duplicate, or clearly irrelevant entries, which were excluded. The inclusion criterion used during the selection was that the work must be focused on brain shift in the paradigm of image-guided neurosurgery of brain tumors. Exclusion criteria included review papers and work with animal-based studies and no clinical validation. For publications that were more mathematical in nature focusing on modeling, compensation, or prediction, validation of the methods on clinical datasets was required. Thirty-eight (38) relevant publications were found using the search query, of which 22 were included in this review. A PRISMA diagram is presented in **Figure 2**.

RESULTS

A summary of the papers reviewed, as they relate to the described taxonomy, location of the measured brain shift, pre-resection *vs*. post-resection measurement, and quantitative findings can be found in **Table 1**. In total, the list includes four qualitative retrospective case reviews, eight brain shift compensation methods papers, and the remaining 10 articles focused on prospective evaluation of brain shift measurement and/or compensation.

Qualitative Retrospective Case Reviews

Since 2015, four groups have published qualitative analysis in the form of a retrospective case review of their center's experience with using intra-operative ultrasound for neurosurgical guidance. The first was published in 2015 by Petridis et al. (23) that reviewed 34 patients undergoing low grade glioma (LGG) resection between 2011 and 2014 in a German center. The retrospective analysis compared iUS use for localization of surgical targets with cases where iUS was not performed. They found in the 15 cases where iUS was used that the surgical target was properly found for either resection or biopsy, whereas in five of 19 cases where iUS was not used, the target was missed. The improvement was qualitatively attributed to intra-operative

[1] http://www.ncbi.nlm.nih.gov/pubmed

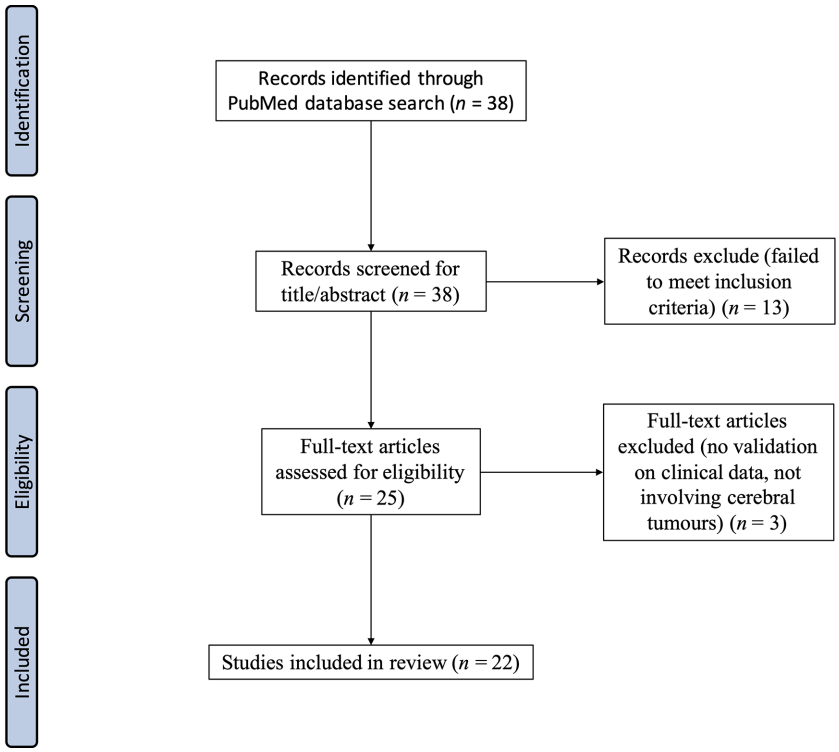

FIGURE 2 | PRISMA diagram high-lighting the search strategy for reviewed articles.

update of real-time information about brain shift as provided by the iUS imaging during these cases.

In 2016, Steno et al. (26) described a qualitative use of iUS during resection of insular low grade gliomas (LGG) during awake resections but with a focus on visualization of the lenticulostriate arteries. These landmarks served to measure brain shift compensation and to guide increased extent of resection, when compared to non-iUS interventions, without creating any new deficit while being nearby anatomic brain structures with important functional roles. Overall, their retrospective review of six cases demonstrated this to be a useful tool for this anatomical location of LGG. In 2018 (27), this group published a follow-up cohort case series of 49 patients undergoing awake resections for insular LGG nearby eloquent cortical and subcortical structures with 21 cases using only neuronavigation and the remaining 28 using iUS guidance. The mean extent of resection was significantly improved with iUS guidance (87 *vs.* 76%) without the addition of any new functional neurologic deficit.

Altieri et al. (8) describe a retrospective analysis of 264 patients with high-grade gliomas undergoing resection with neuronavigation and iUS guidance at the University of Turin between 2013 and 2016. The goal of their work was to improve the detection and characterize the echogenicity—the visual characteristics on ultrasound—of both normal and pathologic anatomical structures using different probes. The main challenge identified by the analysis, as often reported, was related to the surgeon's comfort in interpreting the anatomy in oblique planes, a characteristic that increased with iUS experience.

Finally, in 2019, Liang et al. (18) published a retrospective case review on a cohort of patients that underwent iUS alone without registration during resection and iUS with pre-operative MRI registration to review the extent of resection (EOR) improvement. Of the 45 total patients reviewed, only 6/19 cases using iUS alone achieved gross total resection (GTR) whereas 22/26 (85%) cases using MRI registered to iUS had GTR. This significant clinical improvement was attributed primarily to the comfort and quality of using MRI images for guidance after registration as compared to iUS images alone. The authors also described a significantly lower postoperative morbidity rate in the iUS registration group and concluded that iUS–MRI registration is an essential tool to improve EOR and functional protection.

Brain Shift Compensation Based on Clinical Datasets

Currently, there exists only two widely used and publicly available clinical databases with pre-operative MRI and iUS images that can be used for new brain shift compensation registration or predictive modeling algorithm validation: the Brain Images of Tumors for Evaluation (BITE) (31) and the REtroSpective Evaluation of Cerebral Tumors (RESECT) (30). Both databases have different internal limitations; however, they provide a necessary tool for comparison of brain shift

TABLE 1 | Summary of the classification and quantitative results of reviewed articles (alphabetic order).

Reference	Classification	Measurement Locations	Mean Brain Shift (mm)	Compensation (mm)
Altieri et al. (8)	Qualitative Measurement	Retrospective review of cases	n/a	n/a
Canalini et al. (9)	Compensation (clinical)	Manual landmarks and segmented falx cerebri and sulci	Data from RESECT and BITE databases 3.49 ± 1.55 (RESECT, pre-resect) 3.54 ± 1.75 (RESECT, post-resect) 3.55 ± 2.28 (BITE)	1.56 ± 0.82 (RESECT, pre-resect, parametric) 1.36 ± 0.61 (RESECT, pre-resect, non-parametric) 2.29 ± 1.37 (RESECT, post-resect, parametric) 2.05 ± 1.12 (RESECT, post-resect, non-parametric) 2.98 ± 1.8 (BITE, parametric) 2.48 ± 2.67 (BITE, non-parametric)
Farnia et al. (10)	Compensation (phantom and clinical)	Sulci	Data from BITE database	2.14 ± 0.34 (BITE—13.71% improvement)
Farnia et al. (11)	Compensation (clinical)	Sulci, tumor boundary	Data from BITE database	1.87 ± 0.37 (BITE)
Farnia et al. (12)	Compensation (clinical)	Sulci, tumor boundary	Data from BITE database	1.83 ± 0.11 (BITE—15.37% improvement)
Frisken et al. (13)	Measurement and Compensation (clinical/modelling with thin plate splines [TPS] and finite element modelling [FEM])	Manual landmarks (ML) and automatic features (AF)	1.37 ± 0.81 (ML pre-resect) 2.79 ± 1.05 (ML mid-resect) 1.08 ± 0.65 (AF pre-resect) 2.31 ± 0.78 (AF mid-resect)	1.28 ± 0.63 (ML, TPS pre-resect) 1.82 ± 1.3 (ML, TPS mid-resect) 1.23 ± 0.68 (ML, FEM pre-resect) 1.37 ± 0.84 (ML, FEM mid-resect) 0.90 ± 0.62 (AF, FEM pre-resect) 1.05 ± 0.25 (AF, FEM mid-resect)
Frisken et al. (14)	Measurement and Compensation (clinical/modelling with TPS and FEM)	Manual landmarks (ML) and automatic features (AF)	5.3 ± 0.8 (ML, iUS_1-MRI) 3.1 ± 2.2 (AF, iUS_1-iUS_2) 2.5 ± 1.8 (AF, iUS_1-iUS_3) 3.1 ± 1.7 (ML iUS_1-iUS_2) 2.5 ± 1.3 (ML iUS_1-iUS_3)	1.9 ± 0.6 (ML, iUS_1–MRI) 2.2 ± 1.9 (AF, FEM, iUS_1–iUS_2) 1.8 ± 1.3 (AF, FEM, iUS_1–iUS_3) 3.6 ± 3.7 (ML, TPS, iUS_1–iUS_2) 2.4 ± 2.6 (ML, TPS, iUS_1–iUS_3)
Gerard et al. (15)	Measurement and Compensation (clinical)	ML and pixel misalignment (PM)	6.17 ± 2.21 (ML pre-resect) 5.62 (PM pre-resect)	2.43 ± 1.45 (ML pre-resect) 1.74 (PM pre-resect)
Ilunga et al. (16)	Compensation (algorithm validation)	Vascular segmentation	n/a	n/a
Iversen et al. (17)	Measurement and Compensation (clinical)	Manual landmarks (ML)	7.71 (mean, ML pre-resect) 5.12 (median, ML pre-resect)	4.47 (mean, ML pre-resect) 2.72 (median, ML pre-resect)
Liang et al. (18)	Qualitative Measurement and Compensation	Retrospective case review of gross total resection (GTR)	Image quality improved from poor/moderate to moderate/good	GTR in 22/26 cases using iUS–MRI fusion navigation vs. 6/19 using iUS without fusion
Machado et al. (19)	Measurement and Compensation (clinical)	ML for validation AF for registration	3.25 ± 1.93 Other data from BITE/RESECT	1.75 (AF, affine registration) 1.54 (AF, TPS registration) 1.85 (BITE, ML, affine) 1.52 (BITE, ML, TPS) 1.54 (RESECT, ML, affine) 1.49 (RESECT, ML, TPS)
Machado et al. (20)	Compensation (clinical)	Three database sets using ML	Data from BITE, RESECT, MIBS databases	2.28 ± 0.71 (BITE) 2.08 ± 0.37 (RESECT) 2.24 ± 0.78 (MIBS)
Masoumi et al. (21)	Compensation (clinical)	BITE and RESECT databases	Data from BITE and RESECT databases	2.77 ± 1.13 (RESECT) 2.82 ± 0.72 (BITE)
Morin et al. (22)	Compensation (modelling)	Vascular manual landmarks	2.63 ± 1.55	1.78 ± 1.42 (rigid registration) 1.83 ± 1.25 (constraint-based registration)
Petridis et al. (23)	Qualitative (clinical)	Retrospective review of iUS or no iUS for tumor resection	n/a	Target missed 0/15 cases (iUS) Target missed 5/19 cases (no iUS)
Prada et al. (24)	Compensation (clinical)	Anatomical and vascular landmarks	n/a	Reported as <2 mm in 42/58 cases and <3 mm in 58/58 cases after iUS–MRI registration
Riva et al. (25)	Measurement and Compensation (clinical)	Anatomic ML (sulci, gyri, ventricle, vessel)	5.9 ± 1.9 (pre-dura reflect) 6.2 ± 2.3 (post-dura reflect) 7.5 ± 2.1 (post-resect)	2.7 ± 1.0 [pre-dura reflect (rigid)] 4.2 ± 1.6 [post-dura reflect (rigid)] 6.7 ± 2.5 [post resect (rigid)]

(Continued)

TABLE 1 | Continued

Reference	Classification	Measurement Locations	Mean Brain Shift (mm)	Compensation (mm)
Steno et al. (26)	Qualitative	Lenticulostriate arteries (LSA) visualization	n/a	n/a
Steno et al. (27)	Compensation (clinical)	Extent of resection (EOR)	n/a	86.79% EOR (mean, with iUS) 75.85% EOR (mean, no iUS)
Xiao et al. (28)	Measurement and Compensation (clinical)	Manual landmarks (ML)–tumor border, sulci, gyri	7.22 ± 3.35 (ML, pre-resect)	1.73 ± 0.62 (ML, pre-resect)
Zhou and Rivaz (29)	Compensation (algorithm validation)	Manual landmarks (ML)	Data from BITE database	1.5 ± 1.4 (ML, pre-resect, non-rigid symmetric registration [NSR])

RESECT, REtroSpective Evaluation of Cerebral Tumors database (30); BITE, Brain Images of Tumors for Evaluation database (31); MIBS, Multimodal Images of Brain Shift database (19).

compensation method development. Many authors (over 80 citations for BITE and over 30 for RESECT) have used these databases for the development and validation of innovative techniques. The quantitative results of the eight articles reviewed are in **Table 1**, and described below in more detail.

Farnia et al. have recently described brain shift compensation in a series of three articles (10–12) through matching of echogenic structures, specifically sulci, and optimization of the residual complexity value in the wavelet domain, a strategy to balance between feature and intensity-based registration approach advantages in multi-modal registration. With the introduction of the method in 2015, they validated the novel approach on both phantom and the BITE datasets, demonstrating a noted robustness to noise which is commonly encountered in iUS imaging. The following updates to their methods in 2016 and 2018 focused on improving computational time and the addition of a joint co-sparsity function to obtain a clinically acceptable and useful algorithm for intra-operative use. They report a registration accuracy of 0.90–1.82 mm depending on the method being evaluated. In all three of their works, they have shown significant improvement for both accuracy and efficiency that only lacks validation in a prospective setting.

Zhou and Rivaz 2016 (29) propose a non-rigid symmetric registration framework focused on pre- and post-resection ultrasound images to compensate for brain shift and assess for residual tumor that is difficult to assess on normal post-resection images due to the immense post-operative changes when compared with pre-operative MRI. This novel framework was validated on pre- and post-resection ultrasound images from the BITE database to identify "outlier regions" that may be consistent with possible residual tumor. The registration showed acceptable registration with reported accuracy, on the order of 1.5 mm, between the sets of images with the main drawback being long computation times not conducive to clinical workflow.

Continuing with the theme of novel registration strategies for brain shift compensation, in 2019, Masoumi et al. (21) describe an approach based on affine transformation that utilized a covariance matrix adaptation evolutionary strategy (CMA-ES) to optimize the registration. This work built upon their previous work in 2018 (32) that used a gradient descent optimization[2]. The method was evaluated on both the BITE and RESECT databases with statistically significant improvement of the mean target registration error (mTRE) on the order of 2.8 mm. Their proposed fully automatic registration improvement offers another option for iUS–MRI brain shift correction. The main advantages of this work compared to similar methods include an optimization step that is less susceptible to patch sizes and noise and is reported as the first use of CMA-ES specifically for MRI and US images.

In 2019, Canalini et al. (9) described a segmentation-based registration approach for brain shift compensation where the falx cerebri and different sulci were automatically segmented in pre-resection iUS volumes on the dura mater and used to register with iUS at different phases of the operation. The method is based on a trained convolutional neural network using manually annotated structures in the pre-resection ultrasound that are then used to segment and register the corresponding structures ad different phases of the operation. In contrast to previous work done, in this domain their solution focuses on iUS–iUS registration rather than iUS–MRI registration. They validated their method by comparing the mTRE between manually identified landmarks from the BITE and RESECT databases and showed significant improvement among both.

In one of the more complete series of brain shift compensation methodology papers, Machado et al. (19) published a registration procedure based on automatic feature detection followed by nearest-neighbor descriptor matching and probabilistic voting models similar to a Hough transform focused on scale-invariant features (SIFT). Their method was validated on two publicly available databases (BITE and RESECT) and, additionally, prospectively validated on a nine patient case series that they describe as the Multimodal Images of Brain Shift (MIBS) database. They report accuracy on the order of 2.2 mm with efficient registration results on all three data sets without the need to manually identify landmarks for evaluation. Within the same vein, in 2019 (20), this group described a correlation-based approach for brain shift compensation through extraction of multi-scale and multi-orientation attribute vectors with robust similarity measures on these attributes while simultaneously explicitly handling field-of-view differences between images as an approach to improve generalization and accuracy across different publicly available datasets. Their approach was validated on the BITE, RESECT, and MIBS databases, and tested against 15 other accepted multimodal registration algorithms. They consistently obtained one of the best results across the three datasets without deviation from their predefined parameters (compared to the often dataset

specific tuning described in other papers). This approach highlights the potential need for more robust similarity functions and automatic feature detection frameworks that can be generalizable to the limited public data for future algorithm development.

Prospective Brain Shift Measurement and Compensation

While retrospective data is important for method development and testing, it is critical to evaluate with prospective data to see how well methods generalize. The first of 10 prospective brain shift evaluation papers is from Prada et al. (24). They described their experience in 58 cases using an iUS-guided neuronavigation system. The measurements and compensation details for each individual case are not included in the article; however, they report that in 42 cases they were able to restore accuracy of the navigation system to below a critical threshold of 2 mm when compared with manually selected anatomic and vascular landmarks. In the 16 remaining cases, despite not reaching this critical clinical threshold, they were accurate to within 3 mm, and visualization of cerebral structures intra-operatively with iUS was achieved. Despite the lack of quantitative details on brain shift measurement and compensation this article highlights the expanding reach of iUS within the neurosurgical clinical community.

In 2017, Riva et al. (25) published an eight-patient case series to measure and compensate brain shift using 3D-iUS and an iterative deformation correction framework. Ultrasound was acquired at three time points during surgery: before dural opening, after dural opening, and following complete resection of the brain tumor. The goal of their work was to evaluate the robustness of mono-modal registration from serial iUS acquisitions at different time points in surgery in its ability to maintain accuracy of the navigation system and compensate for brain shift. The initial iUS volume is registered with a rigid transformation to the pre-operative MRI planning images using linear correlation of linear combination as a similarity metric. Following dural opening, iUS volumes are registered with the initial pre-dural iUS using both rigid normalized cross-correlation registration and deformable B-spline registration procedures and then applied to the original pre-operative planning volume. Their method was evaluated using expert neurosurgeon anatomic landmark identification to evaluate the target registration error. They report significant compensation of brain shift between the rigid registration of the initial iUS and pre-operative images both before (5.9 to 2.7 mm) and after (6.2 to 4.2 mm) dural removal with no significant improvement following complete resection (7.5 to 6.7 mm). The authors conclude that combining both mono- and multi-modal iUS registration in an iterative framework successfully measured and compensated brain shift and was easily integrated into the surgical workflow. This technique also has the potential to easily be expanded in other user-defined time points between those investigated in this work that could further help for more real-time brain shift correction throughout resection.

Xiao et al. (28) described a five patient case series evaluating a registration procedure between MRI tractography and iUS based on a correlation-ratio non-linear deformation framework. While the analysis was performed in a retrospective fashion and not intra-operatively, this article was included as the clinical data for which the algorithm was evaluated was not part of any previously published, publicly available database. This is the only report to describe MRI tractography–iUS registration in the context of brain shift measurement and compensation, and registration accuracy on the order of 1.7 mm was reported. As a relatively new imaging modality for surgical planning, tractography offers important information that, when accurately registered with pre-operative imaging, can help preserve white matter tracts important for proper brain function. The main limitation of this study results from the lack of data to validate their method and limited literature from which to draw for comparison. Despite this, they were successfully able to measure and compensate for brain shift in this short case series making it an intriguing avenue for future research.

In another prospective study, Gerard et al. (15) presented a unique approach to brain shift measurement and compensation with the combined use of iUS and augmented reality in a pilot study of eight cases using the Intraoperative Brain Imaging neuronavigation System (IBIS) (33). Brain shift was measured both with iUS and a compensation method based on gradient orientation alignment multimodal registration, as well as a calibrated augmented reality view where two-dimensional pixel misalignment error in a specified view was reported to provide both a qualitative and quantitative assessment of the associated brain shift. The main drawback in this work relates to the reporting of non-universal metric of pixel misalignment errors and the limited number and subjectivity of the manually identified landmarks. Despite these limitations, the authors demonstrate a combination of complementary technologies but require more extensive validation.

In 2019, Frisken et al. (13) describe a two-patient proof of concept study for brain shift measurement and compensation using thin plate spline registration and finite element method (FEM) modeling using physical and geometric constraints along with different material known biophysical properties of different tissues. During these two cases, they measured brain shift with both manually identified landmarks and automatic features using the SIFT method (19) with similar results for both the manual and automatically detected features. The brain shift was then compensated using two independent methods, thin-plate splines and FEM modeling, and the results were compared with one another. The main drawback, as stated by the authors, is that they were unable to compare the behavior of FEM and thin-plate splines for the automatically detected features since these features were used to train the splines and resulted in near-zero residuals; however, the FEM method had better results when compared with the thin-plate spine method for the manually identified landmarks, and given the similarity of brain shift measured between both the automatic features and manual

[2] Masoumi et al. (32) was published as an extended abstract at a conference and thus, as a full article, did not meet inclusion criteria for full review.

landmarks, it is possible the FEM may have outperformed on these features as well if the splines had been trained on different features. This preliminary work motivated a more complete study which was published in 2020 (14) using a similar methodology with additional measurement and compensation of brain shift with serial iUS (*i.e.*, ultrasounds at multiple time points during the operations) and registration in a series of 19 cases. In their follow-up prospective study, the authors conclude that the FEM method provided more consistent brain shift correction and better compensation at locations further from the driving feature displacement than the thin-plate splines; however, in the cases with smaller deformations, the thin-plate splines performed better but without statistical significance. These results highlight the fact that multiple strategies are likely to be required when trying to account for brain shift in real-time and may evolve even throughout a single procedure.

Prospective Brain Shift Measurement and Compensation Using Cerebral Vasculature

Contrast-enhanced ultrasound (CEUS) is a technique not often used in neurosurgical procedures; however, in 2016, Ilunga-Mbuyamba et al. (16) report on using CEUS for vascular structure identification and brain shift compensation in a series of 10 patients. The difficulty in reviewing this work for this article stems from the fact that only the similarity measures between the pre-segmented MRI images and the CEUS segmentation after registration are reported with no absolute registration error. Looking past this limitation, nine of the 10 cases evaluated in this report had successful brain shift compensation—reported as usable for clinical guidance—suggesting this unique approach could provide useful in highly vascular regions of operation.

Morin et al. (22) also focus on cerebral vasculature in a constraint-based biomechanical simulation of brain shift compensation for a series of five patients undergoing neurosurgery with iUS guidance. Each patient underwent a patient-specific biomechanical model built from pre-operative imaging which is intra-operatively registered with both iUS B-mode and Doppler imaging after a constraint-based simulation of the shift of the cerebral vascular tree. Manually chosen landmarks are used to assess the total brain shift and validate the compensation with reported accuracy on the order of 1.8 mm. The authors compared their work to their previously described rigid registration methods/techniques with successful results and having a workflow that is efficient for clinical integration.

In another prospective study, Iversen et al. (17) describe their experience using the CustusX platform (34) in a series of 13 patients. Intra-operative ultrasound was acquired pre-resection to update the guidance system in all 13 cases, and the amount of brain shift and subsequent compensation following registration with pre-operative MRI was evaluated using manual placed anatomic landmarks. They report that their system was deemed accurate enough for tumor resection guidance in nine of 13 cases following neurosurgeon evaluation and showed significant brain shift compensation in all 13 of their cases. The mean reported registration error was on the order of 4 mm with the median being 2.7 mm. This work highlights experience with one of the few open-source neuronavigation systems that support intra-operative ultrasound acquisition prospectively during navigation.

DISCUSSION AND CONCLUSION

Brain shift is a very complex problem that has many pre- and intra-operative contributing factors. Strategies for measuring and compensating for brain shift continue to evolve, and intra-operative ultrasound continues to show promise as an effective, efficient, and low-cost solution for intra-operative accuracy management. Indeed, the rate of publication of intra-operative ultrasound brain shift related work has seen an increase from two to three articles per year, from 2005 to 2015, to eight to 10 articles per year since 2015. One of the primary issues with the current research landscape is that mathematical tool development in the form of registration, FEM, and predictive modeling continues to progress at a fast rate, but validation is repeatedly performed on a small cohort of publicly available retrospective data, that, while invaluable to the field, is nearly a decade old and may not accurately portray the quality and character of imaging used for guidance and surgical planning today. Additionally, as highlighted in Macahado et al. (19), many of these publicly available datasets require cohort-specific parameter tuning, and the compensation methods presented do not generalize well over the entirety of available data.

Indeed, one of the major needs for the field is newer and larger publicly available clinical datasets, such as that in the Brain Images of Tumors for Evaluation (BITE) (31), Retrospective Evaluation of Cerebral Tumors (ResECT) (30) databases. The Multimodal Images of Brain Shift (MIBS) (19) dataset is interesting, but not publicly available. Currently there are roughly 50 cases of pre-operative and intra-operative data freely available for research, a small number that reduces the strength and quality of validation and generalization of these compensation procedures. Another database that has yet to be published publicly but that has been described is the Brain Images of Tumors for Evaluation 2 (BITE2) database (35) which aims to build on the strengths of the original BITE database from the same group. This form of data sharing will be instrumental in more reliable and appropriate validation of these methods that reflect the modern pre- and intra-operative imaging landscape in neurosurgical oncologic procedures.

Among the many advances in the field since our last published review, the variety of applications that iUS has seen in neurosurgery over the last half-decade speaks to the extent to which the potential of the technology is being realized. Applications in cerebral vasculature, both as a tool for measuring brain shift, a feature for brain shift compensation, and a landmark for improving extent of resection are exciting for the field in terms of the broadness of how this tool will be used to treat patients and maintain accuracy for clinicians. With the advancement in technology comes additional challenges; as highlighted in the articles above there are numerous metrics

reported for evaluation of brain shift compensation ranging from fiducial registration errors, target registration errors, extent of resection, segmentation similarity metrics, qualitative evaluations, and pixel misalignment errors. The difference in evaluation metrics and limited number of cases that techniques are evaluated makes comparison of new methodology especially difficult. In the context of extent of resection, for example, it is hard to know if the percentage increase in improvement is clinically significant and difficult to characterize and is attributed completely to brain shift compensation as opposed to specific patient and tumor anatomy.

Two additional points can be made with respect to reporting of results. While a standard for reporting target registration accuracy is desirable and some of the methods described here report accuracies better than 2mm, are these results useful clinically? Resection metrics, such as EOR and GTR provide valuable clinical information but given their value being relative in nature, it is difficult to compare them with other objective measures not specifically related to the tumor volumes. For example, Steno 2018 (27) reports a small but statistically significant improvement in EOR (from 76 to 87%), while Liang 2019 (18) reports an increase of tumor GTR from 32% without ultrasound navigation to 85% with ultrasound-corrected navigation. Both studies demonstrate statistically significant objective and clinical benefits of using iUS-based technology but are near impossible to compare with work that uses registration errors to quantify their results. The lack of a universally accepted evaluation metric and the non-reporting of absolute registration errors when assessing brain shift compensation remain a major challenge in the field for which there is no clear solution currently.

Intra-operative ultrasound for surgical guidance is a well-established tool and has seen applications in many organ systems including: hepatobiliary, genitourinary, lung, mediastinum, vascular, and breast (36). In many of the above applications, US has evolved from a complementary tool to one that has become almost standard-of-care for therapeutic intervention, especially within the hepatobiliary system. In vascular surgery, both within the cardiac and peripheral systems, both B-mode and Doppler iUS have been used, often to assist with surgical repair and to assess the adequacy of the repaired tissue (36, 37). It also plays a very important role in the vascular reconstruction phase of transplantation surgery for flow assessment and minimizing vascular complications (37). Additionally, there has been significant work using iUS navigation in the context of skull-based (38, 39). One of the main challenges during skull base tumor surgery is identifying the relationships between the lesion and principal intracranial vessels which are often mediated by neuronavigation systems. While inaccuracies due to brain shift at the skull base are generally minimal, there can still be other sources of inaccuracy making the pre-operative navigation images less reliable (39). Intra-operative US, often in the form of Doppler imaging and contrast-enhanced B-mode, can help improve the understanding of the skull-base and intracranial vessel relationship to avoid vascular damage and assist with lesion resection (38). The application of this technology in the brain adds an additional level of complexity as it is primarily used as a tool for re-calibrating MRI images for guidance as opposed to direct guidance. Despite this, it is important to learn from both the successes and failures from the many years of experience in these other surgical domains to maximize the potential of this technology and to avoid repeat failures or strategies that have proven to be inefficient from both clinical and technical points of view.

A final point of discussion stems from the timing of brain shift correction. While accurate navigation seems to be imperative for pre- and early perioperative planning, it is unclear on both how often and at which specific time points during surgery accurate brain shift correction correlated with pre-operative MRI is necessary. Once a neurosurgeon has begun operating and has an open cavity from which they can then see the surrounding anatomy comfortably, are highly accurate navigation images imperative to improve the success measure of that operation? As we saw reported in this review, Steno et al. (26, 27). evaluated the improvement of EOR with frequently updated navigation images for resections; however, very few studies report on these types of clinical outcomes, and there currently does not exist any report evaluating both perceived need for improved navigation images from surgeons or the objective analysis on the effects of the workflow and large-scale clinical outcomes. As iUS technology becomes more reliable and easily accessible, it will be important to have studies that identify optimal times of surgery where navigation accuracy is of high importance to improve clinical outcomes while not disrupting surgical workflow. To push the discussion to a further extreme, one may ask if we need to update navigation at all. With real-time imaging, like that provided through iUS, showing up-to-date anatomy and even functional information when Doppler mode is used, perhaps a better strategy would be to focus on improving surgeon comfort and technical proficiency with iUS image interpretation to remove the need for correlation with pre-operative MRI images which seems to have an upper limit of accuracy. In some select cases; however, where resection and anatomy are complex and iUS images difficult to interpret, it may serve beneficial to combine the information with pre-operative MRI as is the practice now for a more complete integration of information.

It is clear from the increasing rate of publication, specifically in qualitative retrospective case reviews and quasi-quantitative analysis from different neurosurgery centers across the world that the comfort and training in using iUS during surgery is expanding and its potential being realized by more clinicians. Unfortunately, the lack of prospective evidence continues to limit the overall reliability of the technology. Moving forward it will be imperative for multi-center prospective trials that focus on improving clinical criteria among patients undergoing iUS surgical guidance for tumor resections for this technology to make the next step and broaden into more clinical practices worldwide. With continued improvement on ultrasound hardware including portable probes with a smaller footprint such as the Clarius, Lumify, and Butterfly IQ, further support and easier clinical workflow integration for future trials is possible.

In conclusion, the growth of iUS in the field of neurosurgery is exciting and encouraging for both clinicians and researchers and continues to show major promise as a multi-faceted tool for measuring and compensating brain shift and improving both the safety and completeness of neurosurgical tumor resections.

AUTHOR CONTRIBUTIONS

IG—literature review, data analysis, manuscript writing. MK-O—Figure development, data analysis, manuscript editing and writing. JH—Expert neurosurgical critique and manuscript review/writing. DS—Expert neurosurgical critique and manuscript review/writing. DC—Supervisor, expert neurosurgical critique and manuscript review/writing, data analysis verification. All authors contributed to the article and approved the submitted version.

FUNDING

The following grants supported this research: Canadian Institute of Health Research (MOP-97820) and Natural Science and Engineering Research Council of Canada (CHRP 385864).

REFERENCES

1. Gerard IJ, Kersten-Oertel M, Petrecca K, Sirhan D, Hall JA, Collins DL. Brain shift in neuronavigation of brain tumors: A review. *Med Image Anal* (2017) 35:403–20. doi: 10.1016/j.media.2016.08.007
2. Wild J, Reid JM. The Effects of Biological Tissues on 15-mc Pulsed Ultrasound. *J Acoust Soc Am* (1953) 25(2):270–80. doi: 10.1121/1.1907031
3. Reid MH. Ultrasonic visualization of a cervical cord cystic astrocytoma. *AJR Am J Roentgenol* (1978) 131(5):907–8. doi: 10.2214/ajr.131.5.907
4. Rubin JM, Mirfakhraee M, Duda EE, Dohrmann GJ, Brown F. Intraoperative ultrasound examination of the brain. *Radiology* (1980) 137(3):831–2. doi: 10.1148/radiology.137.3.6255514
5. Bucholz RD, Yeh DD, Trobaugh J, McDurmont LL, Sturm CD, Baumann C, et al. The correction of stereotactic inaccuracy caused by brain shift using an intraoperative ultrasound device. In: *CVRMed-MRCAS'97*. Berlin, Heidelberg: Springer (1997). p. 459–66.
6. Chandler WF, Knake JE, McGillicuddy JE, Lillehei KO, Silver TM. Intraoperative use of real-time ultrasonography in neurosurgery. *J Neurosurg* (1982) 57(2):157–63. doi: 10.3171/jns.1982.57.2.0157
7. Moher D, Liberati A, Tetzlaff J, Altman DGPrisma Group. Preferred reporting items for systematic reviews and meta-analyses: the PRISMA statement. *BMJ* (2009) 339(b2535):e1000097. doi: 10.1136/bmj.b2535
8. Altieri R, Melcarne A, Di Perna G, Specchia FMC, Fronda C, La Rocca G, et al. Intra-Operative Ultrasound: Tips and Tricks for Making the Most in Neurosurgery. *Surg Technol Int* (2018) 33:353–60.
9. Canalini L, Klein J, Miller D, Kikinis R. Segmentation-based registration of ultrasound volumes for glioma resection in image-guided neurosurgery. *Int J Comput Assist Radiol Surg* (2019) 14(10):1697–713. doi: 10.1007/s11548-019-02045-6
10. Farnia P, Ahmadian A, Shabanian T, Serej ND, Alirezaie J. Brain-shift compensation by non-rigid registration of intra-operative ultrasound images with preoperative MR images based on residual complexity. *Int J Comput Assist Radiol Surg* (2015) 10(5):555–62. doi: 10.1007/s11548-014-1098-5
11. Farnia P, Makkiabadi B, Ahmadian A, Alirezaie J. Curvelet based residual complexity objective function for non-rigid registration of pre-operative MRI with intra-operative ultrasound images. *Annu Int Conf IEEE Eng Med Biol Soc* (2016) 2016:1167–70. doi: 10.1109/EMBC.2016.7590912
12. Farnia P, Najafzadeh E, Ahmadian A, Makkiabadi B, Alimohamadi M, Alirezaie J. Co-Sparse Analysis Model Based Image Registration to Compensate Brain Shift by Using Intra-Operative Ultrasound Imaging. *Annu Int Conf IEEE Eng Med Biol Soc* (2018) 2018:1–4. doi: 10.1109/EMBC.2018.8512375
13. Frisken S, Luo M, Machado I, Unadkat P, Juvekar P, Bunevicius A, et al. Preliminary Results Comparing Thin Plate Splines with Finite Element Methods for Modeling Brain Deformation during Neurosurgery using Intraoperative Ultrasound. *Proc SPIE Int Soc Opt Eng* (2019) 10951:1095120. doi: 10.1117/12.2512799
14. Frisken S, Luo M, Juvekar P, Bunevicius A, Machado I, Unadkat P, et al. A comparison of thin-plate spline deformation and finite element modeling to compensate for brain shift during tumor resection. *Int J Comput Assist Radiol Surg* (2020) 15(1):75–85. doi: 10.1007/s11548-019-02057-2
15. Gerard IJ, Kersten-Oertel M, Drouin S, Hall JA, Petrecca K, De Nigris D, et al. Combining intraoperative ultrasound brain shift correction and augmented reality visualizations: a pilot study of eight cases. *J Med Imaging (Bellingham)* (2018) 5(2):21210. doi: 10.1117/1.JMI.5.2.021210
16. Ilunga-Mbuyamba E, Avina-Cervantes JG, Lindner D, Cruz-Aceves I, Arlt F, Chalopin C. Vascular Structure Identification in Intraoperative 3D Contrast-Enhanced Ultrasound Data. *Sensors (Basel)* (2016) 16(4):497. doi: 10.3390/s16040497
17. Iversen DH, Wein W, Lindseth F, Unsgard G, Reinertsen I. Automatic Intraoperative Correction of Brain Shift for Accurate Neuronavigation. *World Neurosurg* (2018) 120:e1071–8. doi: 10.1016/j.wneu.2018.09.012
18. Liang C, Li M, Gong J, Zhang B, Lin C, He H, et al. A new application of ultrasound-magnetic resonance multimodal fusion virtual navigation in glioma surgery. *Ann Transl Med* (2019) 7(23):736. doi: 10.21037/atm.2019.11.113
19. Machado I, Toews M, Luo J, Unadkat P, Essayed W, George E, et al. Non-rigid registration of 3D ultrasound for neurosurgery using automatic feature detection and matching. *Int J Comput Assist Radiol Surg* (2018) 13(10):1525–38. doi: 10.1007/s11548-018-1786-7
20. Machado I, Toews M, George E, Unadkat P, Essayed W, Luo J, et al. Deformable MRI-Ultrasound registration using correlation-based attribute matching for brain shift correction: Accuracy and generality in multi-site data. *NeuroImage* (2019) 202:116094. doi: 10.1016/j.neuroimage.2019.116094
21. Masoumi N, Xiao Y, Rivaz H. ARENA: Inter-modality affine registration using evolutionary strategy. *Int J Comput Assist Radiol Surg* (2019) 14(3):441–50. doi: 10.1007/s11548-018-1897-1
22. Morin F, Courtecuisse H, Reinertsen I, Le Lann F, Palombi O, Payan Y, et al. Brain-shift compensation using intraoperative ultrasound and constraint-based biomechanical simulation. *Med Image Anal* (2017) 40:133–53. doi: 10.1016/j.media.2017.06.003
23. Petridis AK, Anokhin M, Vavruska J, Mahvash M, Scholz M. The value of intraoperative sonography in low grade glioma surgery. *Clin Neurol Neurosurg* (2015) 131:64–8. doi: 10.1016/j.clineuro.2015.02.004
24. Prada F, Del Bene M, Mattei L, Lodigiani L, DeBeni S, Kolev V, et al. Preoperative magnetic resonance and intraoperative ultrasound fusion imaging for real-time neuronavigation in brain tumor surgery. *Ultraschall Med* (2015) 36(2):174–86. doi: 10.1055/s-0034-1385347
25. Riva M, Hennersperger C, Milletari F, Katouzian A, Pessina F, Gutierrez-Becker B, et al. 3D intra-operative ultrasound and MR image guidance: pursuing an ultrasound-based management of brainshift to enhance neuronavigation. *Int J Comput Assist Radiol Surg* (2017) 12(10):1711–25. doi: 10.1007/s11548-017-1578-5
26. Steno A, Jezberova M, Holly V, Timarova G, Steno J. Visualization of lenticulostriate arteries during insular low-grade glioma surgeries by navigated 3D ultrasound power Doppler: technical note. *J Neurosurg* (2016) 125(4):1016–23. doi: 10.3171/2015.10.JNS151907
27. Steno A, Hollý V, Mendel P, Šteňová V, Petričková L, Timárová G, et al. Navigated 3D-ultrasound versus conventional neuronavigation during awake

resections of eloquent low-grade gliomas: a comparative study at a single institution. *Acta Neurochir* (2018) 160(2):331–42. doi: 10.1007/s00701-017-3377-8

28. Xiao Y, Eikenes L, Reinertsen I, Rivaz H. Nonlinear deformation of tractography in ultrasound-guided low-grade gliomas resection. *Int J Comput Assist Radiol Surg* (2018) 13(3):457–67. doi: 10.1007/s11548-017-1699-x
29. Zhou H, Rivaz H. Registration of Pre- and Postresection Ultrasound Volumes With Noncorresponding Regions in Neurosurgery. *IEEE J BioMed Health Inform* (2016) 20(5):1240–9. doi: 10.1109/JBHI.2016.2554122
30. Xiao Y, Fortin M, Unsgard G, Rivaz H, Reinertsen I. REtroSpective Evaluation of Cerebral Tumors (RESECT): A clinical database of pre-operative MRI and intra-operative ultrasound in low-grade glioma surgeries. *Med Phys* (2017) 44 (7):3875–82. doi: 10.1002/mp.12268
31. Mercier L, Del Maestro RF, Petrecca K, Araujo D, Haegelen C, Collins DL. Online database of clinical MR and ultrasound images of brain tumors. *Med Phys* (2012) 39(6):3253–61. doi: 10.1118/1.4709600
32. Masoumi N, Xiao Y, Rivaz H. MARCEL (Inter-Modality Affine Registration with CorrELation Ratio): An Application for Brain Shift Correction in Ultrasound-Guided Brain Tumor Resection. In: *Brainlesion: Glioma, Multiple Sclerosis, Stroke and Traumatic Brain Injuries*. Cham: Springer International Publishing (2018). p. 55–63.
33. Drouin S, Kochanowska A, Kersten-Oertel M, Gerard IJ, Zelmann R, De Nigris D, et al. IBIS: an OR ready open-source platform for image-guided neurosurgery. *Int J Comput Assist Radiol Surg* (2017) 12(3):363–78. doi: 10.1007/s11548-016-1478-0
34. Askeland C, Solberg OV, Bakeng JB, Reinertsen I, Tangen GA, Hofstad EF, et al. CustusX: an open-source research platform for image-guided therapy. *Int J Comput Assist Radiol Surg* (2016) 11(4):505–19. doi: 10.1007/s11548-015-1292-0
35. Gerard IJ, Couturier C, Kersten-Oertel M, Drouin S, De Nigris D, Hall JA, et al. Towards a second brain images of tumours for evaluation (BITE2) database. In: *International Workshop on Brainlesion: Glioma, Multiple Sclerosis, Stroke and Traumatic Brain Injuries*. Cham: Springer (2016). p. 16–22.
36. Machi J, Oishi AJ, Furumoto NL, Oishi RH. Intraoperative ultrasound. *Surg Clin North Am* (2004) 84(4):1085–111, vi-i. doi: 10.1016/j.suc.2004.04.001
37. Makuuchi M, Torzilli G, Machi J. History of intraoperative ultrasound. *Ultrasound Med Biol* (1998) 24(9):1229–42. doi: 10.1016/s0301-5629(98)00112-4
38. Prada F, Del Bene M, Casali C, Saladino A, Legnani FG, Perin A, et al. Intraoperative Navigated Angiosonography for Skull Base Tumor Surgery. *World Neurosurg* (2015) 84(6):1699–707. doi: 10.1016/j.wneu.2015.07.025
39. Unsgaard G, Rygh OM, Selbekk T, Müller TB, Kolstad F, Lindseth F, et al. Intra-operative 3D ultrasound in neurosurgery. *Acta Neurochir (Wien)* (2006) 148(3):235–53; discussion 253. doi: 10.1007/s00701-005-0688-y

Conflict of Interest: The authors declare that the research was conducted in the absence of any commercial or financial relationships that could be construed as a potential conflict of interest.

frontiers in Oncology

ORIGINAL RESEARCH
published: 01 March 2021
doi: 10.3389/fonc.2021.619286

Clinical Application of Shear Wave Elastography for Assisting Brain Tumor Resection

Huan Wee Chan[1,2]*, *Christopher Uff*[3], *Aabir Chakraborty*[2], *Neil Dorward*[4] and *Jeffrey Colin Bamber*[1]

[1] Joint Department of Physics, Institute of Cancer Research and the Royal Marsden Hospital, Sutton, United Kingdom, [2] Neurosurgery Department, Southampton General Hospital, Southampton, United Kingdom, [3] Neurosurgery Department, Royal London Hospital, London, United Kingdom, [4] Neurosurgery Department, The National Hospital for Neurology and Neurosurgery, London, United Kingdom

Background: The clinical outcomes for brain tumor resection have been shown to be significantly improved with increased extent of resection. To achieve this, neurosurgeons employ different intra-operative tools to improve the extent of resection of brain tumors, including ultrasound, CT, and MRI. Young's modulus (YM) of brain tumors have been shown to be different from normal brain but the accuracy of SWE in assisting brain tumor resection has not been reported.

Aims: To determine the accuracy of SWE in detecting brain tumor residual using post-operative MRI scan as "gold standard".

Methods: Thirty-four patients (aged 1–62 years, M:F = 15:20) with brain tumors were recruited into the study. The intraoperative SWE scans were performed using Aixplorer® (SuperSonic Imagine, France) using a sector transducer (SE12-3) and a linear transducer (SL15-4) with a bandwidth of 3 to 12 MHz and 4 to 15 MHz, respectively, using the SWE mode. The scans were performed prior, during and after brain tumor resection. The presence of residual tumor was determined by the surgeon, ultrasound (US) B-mode and SWE. This was compared with the presence of residual tumor on post-operative MRI scan.

Results: The YM of the brain tumors correlated significantly with surgeons' findings (ρ = 0.845, $p < 0.001$). The sensitivities of residual tumor detection by the surgeon, US B-mode and SWE were 36%, 73%, and 94%, respectively, while their specificities were 100%, 63%, and 77%, respectively. There was no significant difference between detection of residual tumor by SWE, US B-mode, and MRI. SWE and MRI were significantly better than the surgeon's detection of residual tumor ($p = 0.001$ and $p < 0.001$, respectively).

Conclusions: SWE had a higher sensitivity in detecting residual tumor than the surgeons (94% vs. 36%). However, the surgeons had a higher specificity than SWE (100% vs. 77%). Therefore, using SWE in combination with surgeon's opinion may optimize the detection of residual tumor, and hence improve the extent of brain tumor resection.

Keywords: brain tumor, detecting brain tumor residual, elastography, shear wave, intraoperative ultrasound

OPEN ACCESS

Edited by:
Francesco DiMeco, Fondazione IRCCS Istituto Neurologio Carlo Besta, Italy

Reviewed by:
Francesco Prada, Fondazione IRCCS Istituto Neurologio Carlo Besta, Italy
Quan Cheng, Central South University, China

***Correspondence:**
Huan Wee Chan
chanhuanwee@gmail.com

Specialty section:
This article was submitted to Neuro-Oncology and Neurosurgical Oncology, a section of the journal Frontiers in Oncology

Received: *19 October 2020*
Accepted: *08 January 2021*
Published: *01 March 2021*

Citation:
Chan HW, Uff C, Chakraborty A, Dorward N and Bamber JC (2021) Clinical Application of Shear Wave Elastography for Assisting Brain Tumor Resection. Front. Oncol. 11:619286. doi: 10.3389/fonc.2021.619286

INTRODUCTION

The clinical outcomes for brain tumor resection have been shown to be significantly improved with increased extent of resection (1–18). To achieve this, neurosurgeons employ different intra-operative tools to improve the extent of resection of brain tumors (19–22). Although neuronavigation with pre-operative imaging is indispensable in providing useful information for craniotomy planning, it is susceptible to structural shift during resection (23). Intra-operative MRI (iMRI) has been shown to significantly improve the extent of resection and clinical outcomes (21) of brain tumors by providing high resolution imaging. However, iMRI increases operative time by up to 107 min (21, 24) and is not widely available, especially in the less affluent neurosurgical units. Furthermore, it provides only infrequent (one or two) opportunities to image during surgery. Fluorescence imaging with 5-ALA (5-aminolevulinic acid) has been shown to improve the extent of resection and therefore survival in patients with malignant glioma (22). However, this method is limited to the application in malignant gliomas. The fluorescence is only limited to tumor surface and can be obscured by blood and normal brain tissue (25). By providing real-time intra-operative imaging with nearly unlimited imaging opportunity and minimal effect on operative time, intraoperative US (IOUS) has also been shown to provide significant improvement the extent of resection (26, 27), even without integration with neuronavigation (28). It can also improve quality of life in patients who had brain tumor surgery (29). However, the artifacts of IOUS such as post-resection hyperechoic rim (30, 31), post-surgical and post-radiation artifacts (26), acoustic shadowing from Surgicel (30), peritumoural-oedema hyperechogenicity (32), and hyperechoic blood (32), may pose difficulty in IOUS interpretation. Furthermore, in some cases, IOUS cannot distinguish the surrounding tissue from the tumor (33). Due to artifacts and limitations in IOUS and inaccuracies of neurosurgeons in estimating residual tumor intra-operatively (34, 35), ultrasound elastography may provide differentiation between residual tumor from artifacts on IOUS. Intraoperative contrast-enhanced ultrasound (iCEUS) has been shown to add anatomic and biological information but its utility in detecting tumor remnants have not been studied (36).

For a long time, neurosurgeons rely on visual inspection and tactile feedback to help determine the nature of the tissue being resected during surgery. Ultrasound elastography is an ultrasound-based method of obtaining biomechanical properties of tissue. There are two main types of ultrasound elastography, i.e., qualitative and quantitative elastography. Quasistatic strain elastography (QSE) is a qualitative elastography method whereby the operator applies a certain amount of pressure to deform the tissue (37). The degree to which the tissue deforms is defined as strain. The stiffness will be inversely proportional to the strain. As the amount of pressure applied by the operator, i.e., stress, cannot be accurately quantified, this method can only determine the strain of the tumor in relation to the surrounding brain tissue. On the other hand, shear wave elastography (SWE) is a quantitative elastography technique where stiffness of tissue was obtained by measuring the speed of the shear waves generated in the tissue.

Shear Wave Elastography

SWE is a type of elasticity imaging technique, which allows quantification of soft tissue elastic modulus. This technique requires generation of shear waves in the tissue either by ARF (38, 39) or mechanically (40–42). Shear waves are secondary waves that propagate perpendicular to the direction of displacement, analogous to circular ripples on the water surface that travels outward when a disturbance is introduced. The shear wave propagation speed is dependent on the Young's (elastic) modulus of the medium by the equation $E = 3\rho c^2$, where E is the Young's modulus, ρ is the medium density, and c is the shear wave propagation speed. Assuming that the medium through which the shear waves travel has a density of approximately 1,000 kg/m^3, the equation becomes $E \approx c^2$.

In this study, SWE is performed using SSI (SuperSonic shear imaging) where ARF (acoustic radiation force) is applied to soft tissue to induce displacement to generate perpendicularly propagating shear waves, the speed of which are subsequently estimated with cross-correlation function, thus allowing quantitative real-time mapping of elastic modulus (38). This system is capable of producing an ARF sweep to successively focus on different depths along the line of excitation in a Mach cone, thus allowing generation of shear waves at multiple depths, known as quasi-plane shear waves (43). As a result of the Mach cone, the shear waves generated are shaped like a cone, which is at an angle to the axis of excitation travelling in opposite directions to each other.

Ultrafast imaging acquisition is performed using plane wave transmit-receive. This means that the whole 128 elements are fired at the same time, therefore, for a 3-cm imaging depth, the achievable frame rate is ~25 kHz, more than 100 times that of conventional ultrasound. This means that the ultrafast imaging regime can capture up to three frames of the shear waves travelling within 1 mm, thus allowing real-time elasticity mapping or elastography.

METHODS

Patient Selection

Patients were recruited prospectively from Great Ormond Street Hospital for Children and The National Hospital for Neurology and Neurosurgery between September 2011 and May 2013. This study was approved by the National Research Ethics Service Committee London – Queen Square. The inclusion criteria were as follows:

1. They were diagnosed with brain tumor.
2. They had consented to undergo craniotomy and resection or open biopsy of the tumor.
3. They have given their consent for this study, or their parents have given their consent on their behalf for this study if they are under 16 years old.

Those who had consented for craniotomy but underwent neuronavigation-guided biopsy (burr hole biopsy), were excluded because the surgeon would be unable to comment on the stiffness of the tumor, and it would not be possible to perform intra-operative SWE with the SuperSonic® Aixplorer.

Operating Room Protocol

The operating room setup is depicted in **Figure 1**. After anesthesia, the patient was transferred to the operating table and his/her head was pinned with a Mayfield clamp to immobilize the head. Stealth® neuronavigation registration was performed to plan the craniotomy placement. The location of the tumor was determined with neuronavigation. For intrinsic tumors, SWE was performed after durotomy and prior to corticotomy, whereas SWE was performed prior to durotomy for extrinsic tumors as they are often adhere to the dura. After the initial scan, the resection was initiated. The resection was continued until such time when the surgeon felt that he wanted to check the extent of resection or to confirm the location of the tumor. At this time, IOUS was again performed with SWE simultaneously to assess the extent of resection or to confirm the location of the tumor. Final SWE was performed to assess the final extent of resection prior to closure of craniotomy.

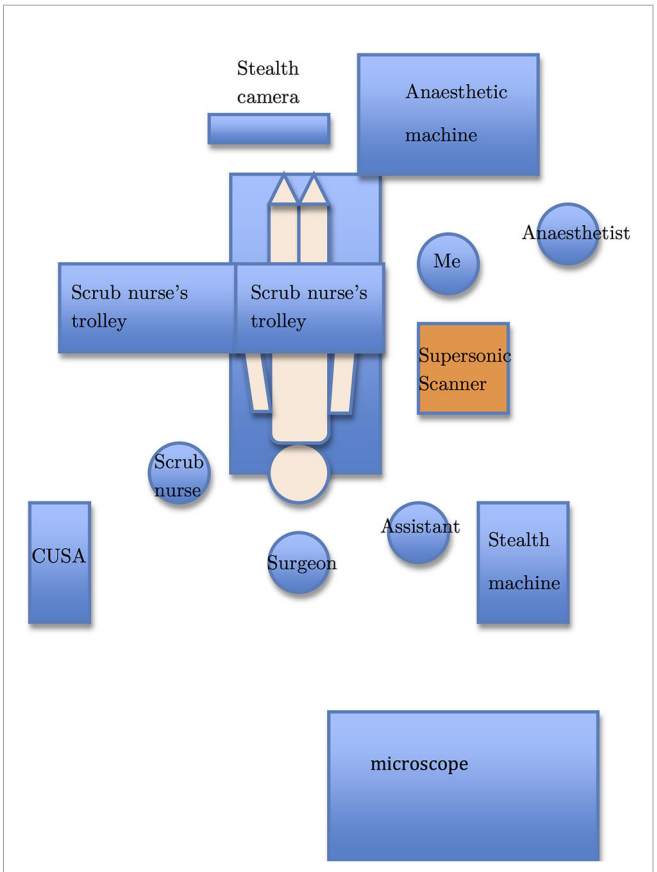

FIGURE 1 | The operating room setup. The Supersonic Aixplorer® scanner (orange) is placed next to the patient body (beige) with the monitor swivelled to face the surgeon. I stand next to the scanner so that I can optimize the scanner settings as well as acquire images for this thesis.

Data Acquisition

After craniotomy, the ultrasound transducer was placed in a sterile sheath filled with acoustic coupling gel. The SWE mode on the SuperSonic Aixplorer® scanner was then activated. The scans were performed on exposed cortex for intrinsic tumors and on closed dura for extrinsic tumors. The intraoperative SWE scans were performed using Aixplorer® (SuperSonic Imagine, France) using a sector transducer (SE12-3) and a linear transducer (SL15-4) with a bandwidth of 3-12 MHz and 4-15 MHz, respectively, using the SWE mode. The sector transducer was used at Great Ormond Street Hospital whereas the linear transducer at the National Hospital for Neurology and Neurosurgery. Without informing the surgeon about the SWE findings beforehand, the surgeon was asked to grade the stiffness of the lesions from 1 to 5 as follows:

1. The lesion is very soft like cyst.
2. The lesion is softer than brain.
3. The lesion is similar to brain.
4. The lesion is stiffer than brain.
5. The lesion is very stiff like cartilage.

After the resection was deemed complete by the surgeon, SWE was performed to determine if there was tumor residual. The tumor residual was graded by the author as either present or absent on both SWE and B-mode. The Q-box function was used to measure the Young's modulus for the tumor bed and adjacent brain. The YM contrast (YMC) was calculated using the following equation:

$$YMC = \frac{E_l - E_b}{E_l + E_b},$$

where E_l is the YM of the lesion and E_b is the YM of adjacent normal brain. A negative YMC denotes a soft tumor whereas a positive YMC a stiff tumor.

Data Analysis

The intra-operative findings by SWE, B-mode and the surgeon were compared with post-operative MRI.

Statistical analysis using Spearman's rank correlation, a non-parametric statistical test, was performed for comparison of Young's modulus measurements and Young's modulus contrast with surgical findings, because the grading of stiffness was ordinal and discrete whereas Young's modulus and Young's modulus contrast were continuous. McNemar's test was used to compare SWE, B-mode and surgeon's opinions with post-operative MRI, which was considered the "gold standard", and also SWE with surgeon's opinions. This test uses 2 × 2 contingency tables with dichotomous, that is either a "Yes" or "No" in this case, result for paired data. Statistical analysis was performed using Student's t-test and Mann Whitney U test to compare Young's modulus measurements for different histological diagnoses, when the Young's modulus distribution was Gaussian and non-Gaussian, respectively. For paired data comparing Young's modulus measurements for brain tumors and corresponding surrounding brain, paired Student's t-test and Wilcoxon signed-rank test were used for normally and non-normally distributed data.

RESULTS

A total of 34 patients were recruited into the study. The summary of the cases is given in **Table 1**.

The patient characteristics are summarized in **Table 2**.

Comparison of Young's Modulus Measurements With Surgical Findings

One patient (Patient 13) was excluded for comparison because the surgeons could not ascertain the stiffness of the tumor due excessive bleeding upon opening the dura, which resulted in the operation being abandoned.

There was overall a significant correlation between Young's modulus measurements and surgical grading (Spearman's rank correlation coefficient (ρ) = 0.845, $p < 0.001$), illustrated in **Figure 2**. The correlation between the Young's modulus contrast and surgical grading was also significant (ρ = 0.780, $p < 0.001$), as illustrated in **Figure 3**. The calculation of Young's modulus contrast for Patients 7 and 8 was not possible as the tumor, SEGA, was located under the ventricle and the adjacent brain could not be imaged with SWE due to lack of signal (see **Figures 4** and **5**).

Figure 6 shows the plot for Young's modulus of normal brain and all tumors. The median Young's modulus for the normal brain was 14.9 kPa, which was significantly lower than that for all tumors (median 33.5 kPa, $p = 0.003$). Wilcoxon's signed-rank test was used to perform paired statistical analysis, as the values for both the tumor and normal brain were not normally distributed. **Figure 7** shows the Young's modulus for various tumor types. The tumors with WHO grades of I and II were graded as low grade while those with WHO grades of III and IV

TABLE 1 | Summary of brain resection cases recruited into this study.

Patient number	Age	Gender	Diagnosis	YM (kPa) (mean ± SD)	YMC	Stiffness grading	Residual (Surgeon)	Residual (B-mode)	Residual (SWE)	Residual (MRI)	US Probe
1	12	M	Low grade astrocytoma	26.2 ± 3.1	0.297	2	No	Yes	No	No	Sector
2	11	F	sPNET[£]	35.6 ± 4.5	0.361	2	No	Yes	Yes	Yes	Sector
3	1	F	Choroid plexus papilloma	13.2 ± 2.6	–0.064	2	No	Not done	Not done	No	Sector
4	6	F	Epidermoid cyst	182.4 ± 15.6	0.772	4	No	No	No	Yes	Sector
5	11	F	Residual sPNET[£]	164.4 ± 48.4	0.692	4	No	No	No	No	Sector
6	15	M	Pilomyxoid astrocytoma	9.7 ± 1.7	–0.224	2	Yes	Yes	Yes	Yes	Sector
7[$]	8	F	SEGA[§§]	300 ± 0	N/A	4	No	No	Yes	No	Sector
8[$]	6	F	SEGA[§§]	300 ± 0	N/A	4	No	No	No signal	No	Sector
9	6	M	Metastasis from clear cell sarcoma of the kidney	241.6 ± 21	0.788	5	No	No	Yes	Yes	Sector
10	15	M	GBM[$$]	154.4 ± 20.9	0.748	4	Yes	Yes	Yes	Yes	Sector
11	2	F	Pilocytic astrocytoma	17.8 ± 1.5	–0.285	2	No	Yes	Yes	Yes	Sector
12	2	M	ATRT[&&]	159.1 ± 82.3	0.802	5	Yes	No	Yes	Yes	Sector
13	14	M	Recurrent pleomorphic xanthoastrocytoma	197.8 ± 2.4	0.681	N/A	Yes	Yes	Yes	Not done*	Sector
14	1	F	ETANTR[££]	4.2 ± 0.9	–0.720	2	Yes	Yes	Yes	Not done[§]	Sector
15	3.3	M	Pineoblastoma	196.3 ± 23.6	0.920	4	Yes	Yes	Yes	Yes	Sector
16	1.1	M	Choroid plexus papilloma	11.9 ± 5.9	–0.290	2	No	No	No	No	Sector
17	7	F	Anaplastic ganglioglioma	11 ± 3.9	–0.102	2	No	No	No	No	Sector
18	17	F	Pleomorphic xanthoastrocytoma with anaplasia	11.2 ± 1.4	–0.138	2	Yes	Yes	Yes	Yes	Sector
19	15	M	Recurrent pilocytic astrocytoma	146.4 ± 14.1	0.889	4	Yes	Yes	Yes	Yes	Sector
20	43	F	Meningioma	39.5 ± 1.2	0.771	4	No	Yes	No	No	Linear
21	1	M	ATRT[&&]	33.6 ± 8.6	0.559	2	No	Yes	No	No	Sector
22	1	F	Residual choroid plexus papilloma	178.9 ± 57.6	0.921	4	No	Yes	Yes	Yes	Sector
23	53	M	GBM[$$]	7.3 ± 3.2	–0.170	2	No	No	Yes	Yes	Linear
24[&]	39	M	Residual medulloblastoma	33.1 ± 8.6	0.458	3	No	N/A	N/A	No	Linear
25	61	F	GBM[$$]	12.3 ± 1.3	0.070	2	No	No	Yes	Yes	Linear
26	46	F	GBM[$$]	3 ± 0.9	–0.439	2	No	Yes	Yes	Yes	Linear
27	62	M	Vestibular schwannoma	153.8 ± 56.3	0.870	4	Yes	Yes	Yes	Yes	Linear
28	49	F	Meningioma	5.6 ± 2	–0.158	2	No	Yes	No signal	Yes	Linear
29	40	M	GBM[$$]	9.9 ± 4.9	–0.823	2	No	Yes	No signal	Yes	Linear
30	35	F	Pilocytic astrocytoma	31.8 ± 5.7	0.216	2	No	Yes	Yes	No	Linear
31	49	F	Metastasis from breast	97.6 ± 42	0.711	4	No	Yes	Yes	Yes	Linear
32	56	F	Meningioma	46.2 ± 24.2	0.505	4	No	No	No	No	Linear
33	5	F	Pilocytic astrocytoma	11.4 ± 0.7	–0.088	2	No	Yes	Yes	Yes	Sector
34	10	M	Anaplastic ependymoma	77.1 ± 11.4	0.858	2	No	No	No signal	No	Sector

[¶]*Standard deviation. *It was converted to biopsy due to excessive bleeding.* [§]*It was a case of known residual due to invasion into brainstem.* [&]*The patient developed air embolus during surgery so the post-operative scan was abandoned.* [$]*The calculation of YMC for these cases was not possible as the lesions were subventricular and the adjacent brain was too deep for shear wave to penetrate.* [£]*Supratentorial primitive neuroectodermal tumor.* [§§]*Subependymal giant cell astrocytoma.* [&&]*Atypical teratoid/rhabdoid tumor.* [$$]*Glioblastoma multiforme.* [££]*Embryonal tumor with abundant neuropil and true rosettes.*

TABLE 2 | Summary to patient and tumor characteristics.

Variables		n
Age		20.7y (range: 1–62y)
Sex	Female	19
	Male	15
Hispathology	High grade glioma	8
	Low grade glioma	9
	Metastasis	2
	Meningioma	3
	Choroid plexus papilloma	3
	Developmental	1
	Vestibular schwannoma	1
	Malignant embryonal tumor	6
Tumor locations	Frontal	11
	Temporal	7
	Parietal	5
	Thalamus	1
	Posterior fossa	9
	Pineal	1

were graded as high grade. As demonstrated, the low grade and high grade tumors were not normally distributed, hence the Mann Whitney U test was used to judge whether the difference between the values in the two groups were statistically significant. Low grade tumors tended to be stiffer than high grade tumors, and metastases even stiffer. However, differences between the Young's moduli were not significant for low grade versus high grade ($p = 0.220$), low grade versus metastasis ($p = 0.288$), and high grade versus metastasis ($p = 0.101$).

Residual Tumor Detection

Table 3 shows the 2 × 2 contingency table comparing SWE with MRI findings on the presence of residual tumor. Using MRI as the "gold standard", the sensitivity and specificity of SWE for detection of residual tumor identified by MRI were 94% and 77%, respectively. McNemar's test showed no statistically significant difference between SWE and MRI in the number of cases in which residual tumor was and was not detected ($p = 1.000$).

The sensitivity and specificity of US B-mode for the same task were 73% and 63%, respectively, using MRI as the "gold standard" (*see* **Table 4**). McNemar's test showed no statistically significance between US B-mode and MRI for detecting residual tumor ($p = 1.000$).

When comparing surgeon's findings with MRI, there was a statistically significant difference ($p < 0.001$), as illustrated in **Table 5**. The sensitivity and specificity of surgeon's opinion on whether residual tumor was present were 36% and 100%, respectively.

When comparing SWE with US B-mode, there was no statistically significant difference between them ($p = 0.727$), as shown in **Table 6**.

When comparing SWE against surgeon's findings, there was a statistically significant difference between them ($p = 0.001$), as shown in **Table 7**. Although surgeon agreed with SWE when SWE demonstrated no residual tumor, SWE detected residual tumor in significantly more cases than surgeon.

Of the 34 patients, only 26 patients were included in the comparison between intra-operative SWE and post-operative MRI in detecting residual tumor. Patients 13 and 14 were excluded because post-operative MRI was not performed. Patient 13 developed excessive bleeding during surgery resulting in the surgeons abandoning the operation. Patient 14 had extensive invasion into the brainstem on pre-operative MRI. Therefore, the surgeons decided to perform only debulking surgery with intended residual tumor. Patients 8, 11, 28, 29, and 34 did not have SWE signal post-operatively despite using "penetration mode" and the probe being held as close to the

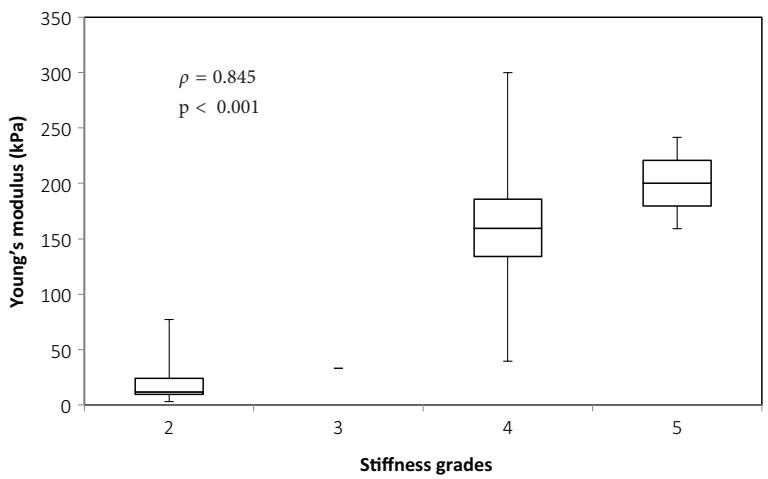

FIGURE 2 | Box and whiskers plot for Young's modulus measurements according to stiffness grade assessed by independent surgical opinion (n = 34). The upper and lower bounds of the box were the third and first quartiles, respectively, while the line within the box was the median. The upper and lower whiskers were maximum and minimum values, respectively.

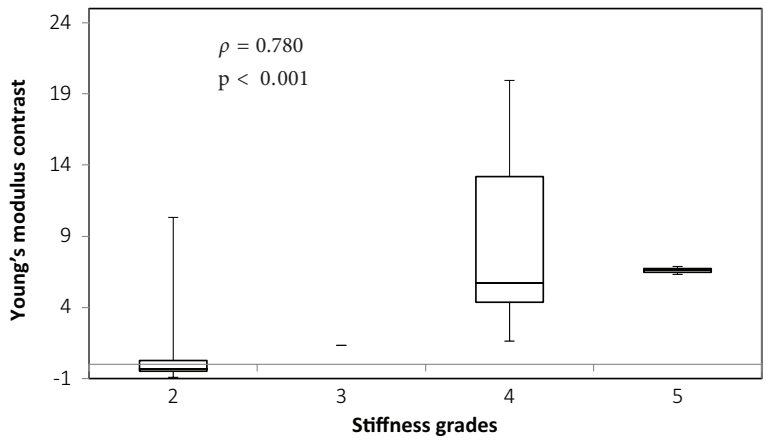

FIGURE 3 | Box and whiskers plot for Young's modulus contrast according to stiffness grade assessed by independent surgical opinion (n = 32). The upper and lower bounds of the box were the third and first quartiles, respectively, while the line within the box was the median. The upper and lower whiskers were maximum and minimum values, respectively.

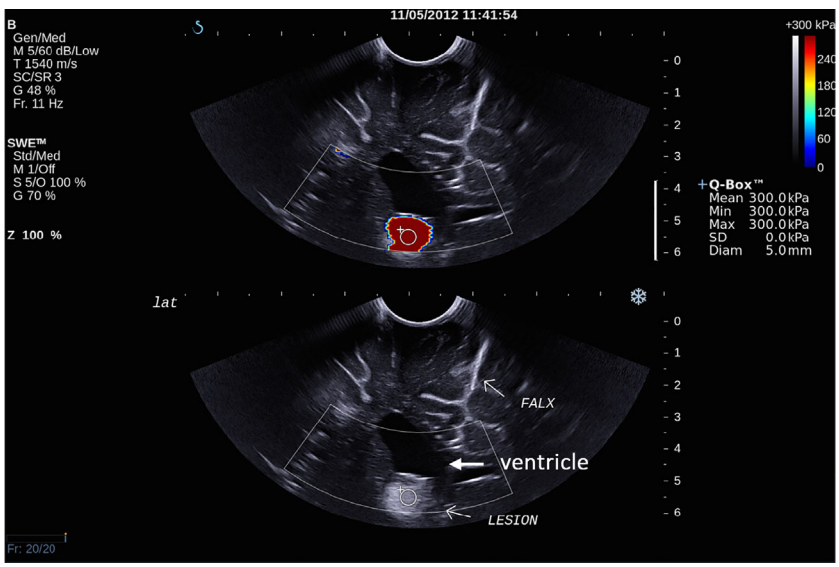

FIGURE 4 | Intra-operative SWE for Patient 7 showing the tumor lying under the ventricles. The adjacent deep grey matter did not have any SWE signal. This scan was acquired using the sector probe (SE12-3) insonating in the coronal plane. The histology of this lesion is subependymal giant cell astrocytoma (SEGA).

cavity as possible. The tumor in Patient 8 was situated at a depth of >5 cm, and there was no SWE signal. In contrast, Patient 7, similar case to Patient 8, had SWE signal down to a depth of 5-cm post-resection, but the signal was of questionable reliability as it gave a very high Young's modulus of 300 kPa. For Patient 34, the water standoff could not be maintained in the resection cavity. For cases performed at the National Hospital for Neurology and Neurosurgery, as the acquisition was performed using a linear array probe, which was a lot larger than the sector array probe, all the post-resection scans were performed with the probe above the cavity using a water standoff. Patient 28 had Surgicel® in the resection cavity prior to the scan because of excessive bleeding, thereby causing a lack of SWE signal. Patient 29 had a large GBM prior to resection, resulting in a very deep post-resection cavity. Due to the large linear array probe, it was not possible to insert the probe in the cavity. Patient 3 did not have a post-resection scan, as it was one of the earlier cases where the primary aim was to investigate the feasibility and determine the artifacts associated with clinical scanning. Patient 24 did not have a post-resection scan as the patient developed an air embolus and the surgery had to be abandoned.

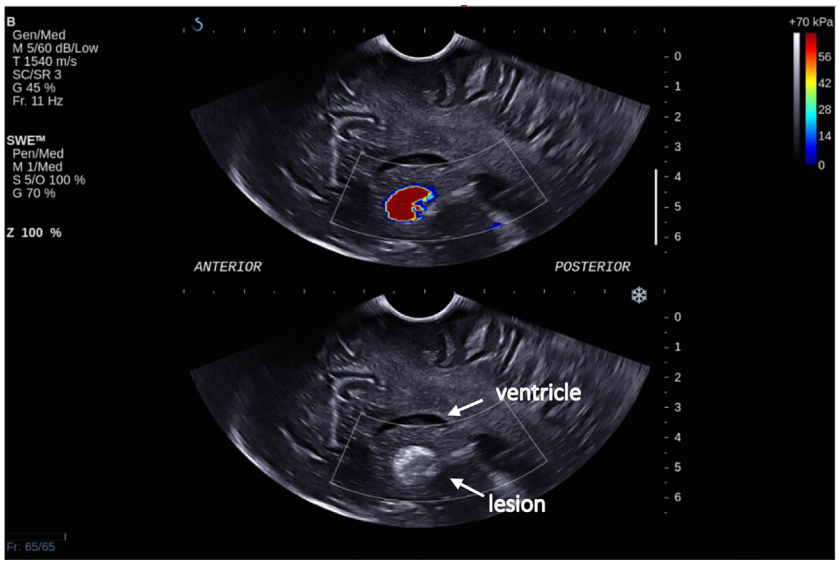

FIGURE 5 | Intra-operative SWE for Patient 8 showing the tumor lying under the ventricles at a depth of 5 cm from the transducer. There was a lack of SWE signal in the adjacent brain. This scan was acquired using the sector probe (SE12-3) insonating in the sagittal plane. The histology of this lesion again is subependymal giant cell astrocytoma (SEGA).

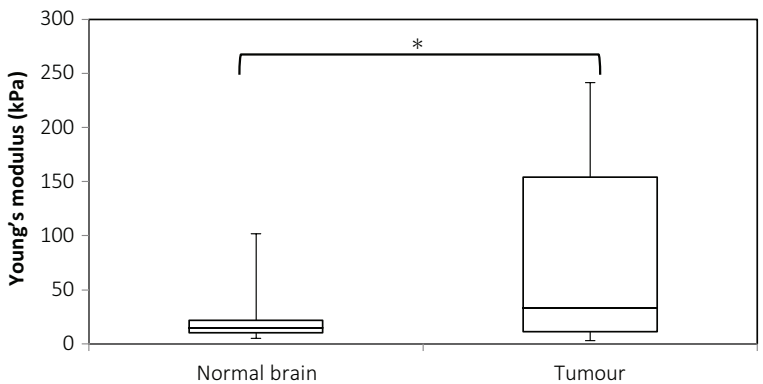

FIGURE 6 | Box and whiskers plot for Young's modulus measurements of normal brain and tumor. The upper and lower bounds of the box were the third and first quartiles, respectively, while the line within the box was the median. The upper and lower whiskers were maximum and minimum values, respectively. *There was a significant difference between the two groups (p = 0.003, Wilcoxon's signed-rank test).

DISCUSSION

Neurosurgeons usually employ intra-operative tools, which offer spatial orientation, navigational guidance, and up-to-date imaging to achieve maximal brain tumor resection. However, as these intra-operative tools do not offer elasticity imaging, to gain information on tissue mechanics neurosurgeons ultimately rely on visual inspection and tactile feedback during surgery. Neurosurgeons tend to overestimate the extent of resection of brain tumors by up to three times, as judged by post-operative MRI (34, 35). This could be due to the similarity in appearance of tumor and brain resulting in the neurosurgeon having difficulty in differentiating tumor from brain.

Elastography is a term coined in 1991 to describe a method of quasistatic ultrasound strain imaging (37). Nowadays, there are three main types of ultrasound elastography, namely: quasistatic strain elastography (QSE) (37), shear wave elastography (SWE) (38–42), and acoustic radiation force impulse (ARFI) imaging (44). Ultrasound elastography has been employed in clinical practice to characterize lesions in other parts of the body including the salivary gland, the thyroid, the breast, the gastrointestinal tract, the prostate, and the liver (45). Although

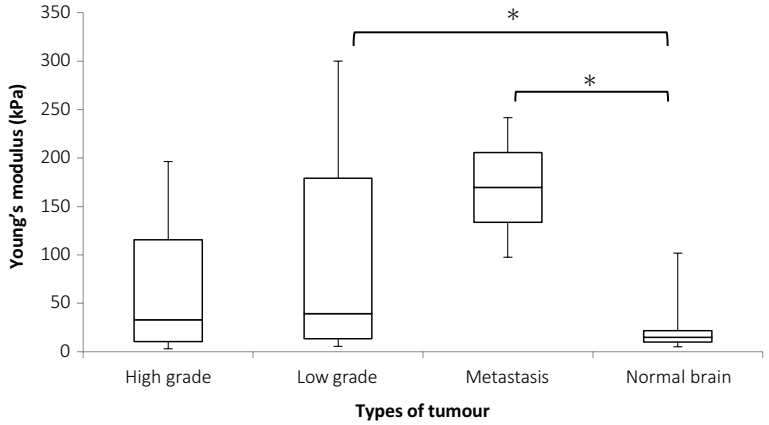

FIGURE 7 | Box and whiskers plot of Young's modulus distributions for various tumor types. The upper and lower bounds of the box were the third and first quartiles, respectively, while the line within the box was the median. The upper and lower whiskers were maximum and minimum values, respectively. *There was a significant difference between the Young's modulus values for low grade tumor and normal brain ($p = 0.036$) and between metastases and normal brain ($p = 0.007$) but the differences between high grade and normal brain ($p = 0.125$), high grade and low grade ($p = 0.220$), metastases and high grade ($p = 0.132$), and low grade and metastasis ($p = 0.288$), were not significant. Mann Whitney U test was used to perform statistical analysis.

TABLE 3 | McNemar's 2 × 2 contingency table comparing intra-operative SWE with post-operative MRI for detecting residual tumor.

SWE \ MRI	Residual tumor	No residual tumor	Total
Residual tumor	16	2	**18**
No residual tumor	1	7	**8**
Total	**17**	**9**	**26**

No statistically significant difference was detected between SWE and MRI for detecting residual tumor ($p = 1.000$).

TABLE 4 | McNemar's 2 × 2 contingency table for comparing intra-operative US B-mode with post-operative MRI scan in detecting residual tumor.

MRI \ B-mode	Residual tumor	No residual tumor	Total
Residual tumor	14	4	**18**
No residual tumor	5	7	**12**
Total	**19**	**11**	**30**

No statistically significant difference was detected between US B-mode and MRI for detecting residual tumor ($p = 1.000$).

TABLE 5 | McNemar's 2 × 2 contingency table for comparing surgeon's intra-operative opinion with post-operative MRI scan in detecting residual tumor.

Surgeon \ MRI	Residual tumor	No residual tumor	Total
Residual tumor	7	0	**7**
No residual tumor	12	13	**25**
Total	**19**	**13**	**32**

A statistically significant difference was detected between surgeons' opinion and MRI for determining whether there was residual tumor or not ($p < 0.001$).

TABLE 6 | McNemar's 2 × 2 contingency table for comparing intra-operative SWE with B-mode in detecting residual tumor.

SWE \ B-mode	Residual tumor	No residual tumor	Total
Residual tumor	15	5	**20**
No residual tumor	3	5	**8**
Total	**18**	**10**	**28**

No statistically significant difference was detected for SWE and B-mode for detecting residual tumor ($p = 0.727$).

TABLE 7 | McNemar's 2 × 2 contingency table for comparing intra-operative SWE and surgeon's opinion in detecting residual tumor.

SWE \ Surgeon	Residual tumor	No residual tumor	Total
Residual tumor	9	11	**20**
No residual tumor	0	8	**8**
Total	**9**	**19**	**28**

A statistically significant difference was deteted for SWE and surgeon's opinion of the presence of residual tumor. ($p = 0.001$).

ultrasound elastography in the brain has not been used in clinical practice, there have been studies looking at the application in brain tumor surgery using QSE (46–51) and SWE (52, 53). Chakraborty et al. (47) demonstrated feasibility of using QSE co-registered with MRI in brain tumor resection whereas Uff et al. (46) showed that real-time QSE was able to demonstrate good correlation between surgeon and elastograms in determining tumor stiffness and surgical plane. Selbekk et al. (50) and Selbekk, Bang, and Unsgaard (51) demonstrated that arterial pulsations were able to generate elastograms to improve

visualization of tumors. Cepeda et al. (49) showed that peritumoural tissue of glial tumors have different elasticity compared to other tumor types. Prada et al. (48) showed that elastograms were superimposable to US B-mode and had sharper tumor margins than US B-mode. Besides brain tumor surgery, ultrasound elastography has also been studied in paediatric (54, 55) and epilepsy surgery (56). Su et al. (54) showed that the brains in preterm babies have lower stiffness compared to those in term babies whereas Kim et al. (55) demonstrated different stiffness in different parts of neonatal brains. Chan et al. (56) demonstrated a case report of the detection of MRI-negative epileptogenic lesion using SWE. There have also been studies using ultrasound elastography in animal models looking at changes in brain elasticity after stroke (57) and trauma brain injury (58).

Comparison of Young's Modulus Measurements With Surgical Findings

This study showed that there was significant correlation between both Young's modulus and Young's modulus contrast measured by SWE and surgical opinion of tumor stiffness relative to normal brain. In the brain tumors, the Young's modulus measurements agreed better than Young's modulus contrast with surgical grading of the stiffness. This is consistent with the findings in other studies using QSE where strain was correlated with surgical opinion on tumor stiffness (47, 53, 59, 60). In Patient 34, although the tumor was thought to be softer than brain by the surgeon, the Young's modulus measurement was 77.1 ± 11.4 kPa (mean ± SD) and Young's modulus contrast was 0.858, indicating that it was stiffer than brain by SWE. This could be due to undue pressure on the brain surface when performing the scan. The location of the tumor, which was parietal, was particularly vulnerable to saline irrigation flowing out making water standoff almost impossible. Therefore, in order to acquire a good quality B-mode or SWE, the surgeon might have applied too much pressure, which was known to cause artifactual stiffness due to the non-linear effects of pre-compression in the area of stress concentration caused by the transducer. As the lesion was superficial, this effect could be unintentionally produced by small pressure.

This study showed that the Young's modulus for all tumor types was significantly higher than normal brain ($p = 0.003$), thereby showing that SWE was capable of differentiating various brain tumors from the surrounding brain. The paired statistical analysis, Wilcoxon's signed rank test in this case, showed that the difference in Young's modulus measurements was significant between brain tumors and normal brain. In this study low grade tumors tended to be stiffer than high grade tumors, and metastases stiffer still, although the differences between median values was not significant. However, the low grade tumors ($p = 0.036$) and metastasis ($p = 0.007$) were shown to be significantly stiffer than brain. Murphy et al. (61) showed that meningiomas have shear modulus of 2–10 kPa, that is, Young's modulus of 6–30 kPa. From the intraoperative SWE study by Chauvet et al. (62), the meningiomas was found to have a Young's modulus of 33.1 ± 5.9 kPa. From **Table 1**, the meningioma cases (patients 13, 30, and 31) showed that the Young's modulus ranged from 5.6 to 46.2 kPa (mean 30.4 kPa; SD 21.8 kPa), which agreed with the literature. In a case of breast metastasis (NHNN 14), the Young's modulus was 97.6 kPa ± 42 kPa (mean ± SD), which agrees with the reported values of 61–165 kPa in the literature (63, 64). This study attempts to examine whether Young's modulus is characteristic of brain tumor type, showing that there is considerable variability within groups but due to small numbers of different tumor types, the result was not conclusive. This means that SWE was capable in distinguishing brain tumors from normal brain but was unable to separate different tumor types from each other intraoperatively prior to resection. Chauvet et al. (62) showed that low grade gliomas, meningiomas, and metastasis were significantly stiffer than normal brain. The high grade glioma is stiffer than normal brain but the result was not statistically significant. In this study the normal brain only had Young's modulus of 6.3 to 7.2 kPa, which was much lower than the findings from this thesis (median Young's modulus of 31.0 kPa and 18.8 kPa for grey and white matter, respectively). This study also showed that the different tumor types had significantly different Young's modulus, which was not shown by this study. This could be due to the much larger number of patients in this study (63 patients) than this study (34 patients).

Residual Tumor Detection

Using post-operative MRI as the "gold standard", detection of residual tumor by SWE was shown to have a sensitivity and specificity of 94% and 77%, respectively. Currently, there has been no literature reporting the sensitivity and specificity of SWE in detecting residual brain tumor. SWE was shown to be comparable to post-operative MRI in detecting residual tumor.

Compared to post-operative MRI, US B-mode was shown to have a sensitivity and specificity of 73% and 63%, respectively, for detecting residual tumor. This result agrees with current literature results, which showed a sensitivity of 67%–85% (26, 27, 30). US B-mode was also shown to be comparable to both post-operative MRI findings and SWE in detecting residual tumor.

Surgeon's intraoperative opinion of the presence or absence of residual tumor was shown to be significantly different from post-operative MRI findings. The sensitivity of surgeon's opinion in detecting residual tumor was also lower than both SWE and US B-mode. This agrees with Albert et al. (34) and Orringer et al. (35), where surgeons were less likely to detect residual tumor than post-operative MRI. The reason underpinning this could be that tumor can have similar appearance to normal surrounding brain, making visual inspection less reliable. Furthermore, after manipulation and dissection, the tumor typically becomes softer and loses its pre-resection appearance, thereby making it harder for the surgeon to differentiate it from normal surrounding brain. Most surgeons would err on the side of caution to prevent neurological deficit, thereby explaining the lower sensitivity of surgeon detecting residual tumor. Having said that, surgeons had a specificity of 100%, higher than both SWE and US B-mode, in detecting residual tumor. This means that when there was no residual tumor on the MRI scan, surgeon would correctly identify this intraoperatively. Comparing SWE with surgeon's findings, SWE significantly detected more cases of residual tumor than surgeon. This could be explained by the ability of SWE to visualize the tumor deep to the "manipulated" tumor. Therefore, using

SWE in combination with surgeon's opinion may optimize the detection of residual tumor as SWE has a higher sensitivity than surgeon while the surgeon has a higher specificity than SWE.

LIMITATIONS

This study has a few limitations. Firstly, the small sample size with a heterogeneous tumor types in this study, has led to statistically non-significant results in the ability for SWE to differentiate different tumor types. This can be overcome with a larger study focusing on main tumor types undergoing resection. Secondly, the use of two different of US probes in the two different hospitals in which the study was performed, may pose some skepticism regarding the validity of the SWE measurements. However, the measurements of the normal brain Young's modulus were shown to be similar using these two different probes. Furthermore, the bandwidths for these probes were very similar—3-12 MHz and 4-15 MHz for the sector and the linear probes, respectively, thereby producing very similar image quality. Thirdly, due to SWE signal insufficiency, there were eight patients (24%) excluded from SWE analysis compared to four patients (12%) and two patients (6%) excluded from B-mode and surgeons' opinion analyses. This may have biased the result, which again can be overcome with a larger sample.

CONCLUSION

This study showed that the SWE measurements of Young's modulus and Young's modulus contrast correlated significantly with surgical grading of stiffness. This means that clinically, the SWE measurements are reliable in predicting stiffness.

It also showed that there was high sensitivity and specificity of SWE in detecting residual tumor compared to post-operative MRI scan as the "gold standard". It also showed that when there is residual tumor, SWE is better than the surgeon at detecting residual tumor by 2.5 times (94% versus 37%). When there is an absence of residual tumor, the surgeon is better at predicting the absence of residual tumor (100% versus 77%). These results imply that intraoperative SWE can be a useful tool in assisting neurosurgeons in identifying residual tumor during resection. However, these results are preliminary due to the small sample size with heterogeneous tumors. A larger study with less heterogeneous tumor types will be required to show reproducibility of these findings.

DATA AVAILABILITY STATEMENT

The raw data supporting the conclusions of this article will be made available by the authors, without undue reservation.

ETHICS STATEMENT

The studies involving human participants were reviewed and approved by National Research Ethics Service (NRES) Committee London—Queen Square (REC reference: 08/H0716/92; amendment number: AM04). Written consents were provided by the participants, or the participants' legal guardian/next of kin if the participants were unable to provide consents.

AUTHOR CONTRIBUTIONS

HC conceived and designed the analysis, collected the data, performed the analysis, and wrote the paper. CU, AC, ND, and JB contributed data and analysis tools, and performed the analysis. All authors contributed to the article and approved the submitted version.

FUNDING

The authors would like to thank the Royal Free Charity and Royal Free Clinical Research Fellowship for funding the study. The authors would also like to thank the Engineering and Physical Sciences Research Council (EPSRC) for funding the equipment.

ACKNOWLEDGMENTS

I would like to acknowledge that the content of the manuscript has previously appeared online in a thesis (65) and been presented in a conference (66). I would also like to acknowledge the neurosurgeons at the Great Ormond Street Hospital (Messrs William Harkness, Dominic Thompson, Owase Jeelani, and Kristian Aquilina) and the National Hospital for Neurology and Neurosurgery (Messrs Andrew McEvoy, Lewis Thorne, George Samandouras, Robert Bradford, Andrew McEvoy, and Miss Anna Miserocchi) for their assistance.

REFERENCES

1. Capelle L, Fontaine D, Mandonnet E, Taillandier L, Golmard JL, Bauchet L, et al. Spontaneous and therapeutic prognostic factors in adult hemispheric World Health Organization Grade II gliomas: a series of 1097 cases: clinical article. *J Neurosurg* (2013) 118(6):1157–68. doi: 10.3171/2013.1.JNS121
2. Claus EB, Horlacher A, Hsu L, Schwartz RB, Dello-Iacono D, Talos F, et al. Survival rates in patients with low-grade glioma after intraoperative magnetic resonance image guidance. *Cancer* (2005) 103(6):1227–33. doi: 10.1002/cncr.20867
3. Oszvald A, Güresir E, Setzer M, Vatter H, Senft C, Seifert V, et al. Glioblastoma therapy in the elderly and the importance of the extent of resection regardless of age. *J Neurosurg* (2012) 116(2):357–64. doi: 10.3171/2011.8.JNS102114
4. Sanai N, Polley M-Y, McDermott MW, Parsa AT, Berger MS. An extent of resection threshold for newly diagnosed glioblastomas. *J Neurosurg* (2011) 115(1):3–8. doi: 10.3171/2011.2.JNS10998
5. Shaw E, Arusell R, Scheithauer B, O'Fallon J, O'Neill B, Dinapoli R, et al. Prospective randomized trial of low- versus high-dose radiation therapy in adults with supratentorial low-grade glioma: initial report of a North Central Cancer Treatment Group/Radiation Therapy Oncology Group/Eastern

Cooperative Oncology Group Study. *J Clin Oncol* (2002) 20(9):2267–76. doi: 10.1200/JCO.2002.09.126
6. Smith JS, Chang EF, Lamborn KR, Chang SM, Prados MD, Cha S, et al. Role of extent of resection in the long-term outcome of low-grade hemispheric gliomas. *J Clin Oncol* (2008) 26(8):1338–45. doi: 10.1200/JCO.2007.13.9337
7. Stummer W, Reulen H-J, Meinel T, Pichlmeier U, Schumacher W, Tonn J-C, et al. Extent of resection and survival in glioblastoma multiforme: identification of and adjustment for bias. *Neurosurgery* (2008) 62(3):564–76. doi: 10.1227/01.neu.0000317304.31579.17
8. Ushio Y, Kochi M, Hamada J, Kai Y, Nakamura H. Effect of surgical removal on survival and quality of life in patients with supratentorial glioblastoma. *Neurol Med Chir (Tokyo)* (2005) 45(9):454–60; discussion 460-1. doi: 10.2176/nmc.45.454
9. Vuorinen V, Hinkka S, Färkkilä M, Jääskeläinen J. Debulking or biopsy of malignant glioma in elderly people - a randomised study. *Acta Neurochir (Wien)* (2003) 145(1):5–10. doi: 10.1007/s00701-002-1030-6
10. Yeh S-A, Ho J-T, Lui C-C, Huang Y-J, Hsiung C-Y, Huang E-Y. Treatment outcomes and prognostic factors in patients with supratentorial low-grade gliomas. *Br J Radiol* (2005) 78(927):230–5. doi: 10.1259/bjr/28534346
11. Hervey-Jumper SL, Berger MS. Role of surgical resection in low- and high-grade gliomas. *Curr Treat Options Neurol* (2014) 16(4):284. doi: 10.1007/s11940-014-0284-7
12. Keles GE, Lamborn KR, Berger MS. Low-grade hemispheric gliomas in adults: a critical review of extent of resection as a factor influencing outcome. *J Neurosurg* (2001) 95(5):735–45. doi: 10.3171/jns.2001.95.5.0735
13. Lacroix M, Abi-Said D, Fourney DR, Gokaslan ZL, Shi W, DeMonte F, et al. A multivariate analysis of 416 patients with glioblastoma multiforme: prognosis, extent of resection, and survival. *J Neurosurg* (2001) 95(2):190–8. doi: 10.3171/jns.2001.95.2.0190
14. Laws ER, Parney IF, Huang W, Anderson F, Morris AM, Asher A, et al. Survival following surgery and prognostic factors for recently diagnosed malignant glioma: data from the Glioma Outcomes Project. *J Neurosurg* (2003) 99(3):467–73. doi: 10.3171/jns.2003.99.3.0467
15. McGirt MJ, Chaichana KL, Attenello FJ, Weingart JD, Than K, Burger PC, et al. Extent of surgical resection is independently associated with survival in patients with hemispheric infiltrating low-grade gliomas. *Neurosurgery* (2008) 63(4):700–7; author reply 707-8. doi: 10.1227/01.NEU.0000325729.41085.73
16. McGirt MJ, Chaichana KL, Gathinji M, Attenello FJ, Than K, Olivi A, et al. Independent association of extent of resection with survival in patients with malignant brain astrocytoma. *J Neurosurg* (2009) 110(1):156–62. doi: 10.3171/2008.4.17536
17. Nakamura M, Konishi N, Tsunoda S, Nakase H, Tsuzuki T, Aoki H, et al. Analysis of prognostic and survival factors related to treatment of low-grade astrocytomas in adults. *Oncology* (2000) 58(2):108–16. doi: 10.1159/000012087
18. Nomiya T, Nemoto K, Kumabe T, Takai Y, Yamada S. Prognostic significance of surgery and radiation therapy in cases of anaplastic astrocytoma: retrospective analysis of 170 cases. *J Neurosurg* (2007) 106(4):575–81. doi: 10.3171/jns.2007.106.4.575
19. Gronningsaeter A, Kleven A, Ommedal S, Aarseth TE, Lie T, Lindseth F, et al. SonoWand, an ultrasound-based neuronavigation system. *Neurosurgery* (2000) 47(6):1373–9; discussion 1379-80. doi: 10.1093/neurosurgery/47.6.1373
20. Lunsford LD, Parrish R, Albright L. Intraoperative imaging with a therapeutic computed tomographic scanner. *Neurosurgery* (1984) 15(4):559–61. doi: 10.1227/00006123-198410000-00017
21. Senft C, Bink A, Franz K, Vatter H, Gasser T, Seifert V. Intraoperative MRI guidance and extent of resection in glioma surgery: a randomised, controlled trial. *Lancet Oncol* (2011) 12(11):997–1003. doi: 10.1016/S1470-2045(11)70196-6
22. Stummer W, Pichlmeier U, Meinel T, Wiestler OD, Zanella F, Reulen H-J. Fluorescence-guided surgery with 5-aminolevulinic acid for resection of malignant glioma: a randomised controlled multicentre phase III trial. *Lancet Oncol* (2006) 7(5):392–401. doi: 10.1016/S1470-2045(06)70665-9
23. Dorward NL, Alberti O, Velani B, Gerritsen FA, Harkness WF, Kitchen ND, et al. Postimaging brain distortion: magnitude, correlates, and impact on neuronavigation. *J Neurosurg* (1998) 88(4):656–62. doi: 10.3171/jns.1998.88.4.0656
24. Shah MN, Leonard JR, Inder G, Gao F, Geske M, Haydon DH, et al. Intraoperative magnetic resonance imaging to reduce the rate of early reoperation for lesion resection in pediatric neurosurgery. *J Neurosurg Pediatr* (2012) 9(3):259–64. doi: 10.3171/2011.12.PEDS11227
25. Stummer W, Stocker S, Wagner S, Stepp H, Fritsch C, Goetz C, et al. Intraoperative detection of malignant gliomas by 5-aminolevulinic acid-induced porphyrin fluorescence. *Neurosurgery* (1998) 42(3):518–26. doi: 10.1097/00006123-199803000-00017
26. Hammoud MA, Ligon BL, elSouki R, Shi WM, Schomer DF, Sawaya R. Use of intraoperative ultrasound for localizing tumors and determining the extent of resection: a comparative study with magnetic resonance imaging. *J Neurosurg* (1996) 84(5):737–41. doi: 10.3171/jns.1996.84.5.0737
27. Le Roux PD, Berger MS, Wang K, Mack LA, Ojemann GA. Low grade gliomas: comparison of intraoperative ultrasound characteristics with preoperative imaging studies. *J Neurooncol* (1992) 13(2):189–98. doi: 10.1007/BF00172770
28. Renovanz M, Hickmann A, Henkel C, Nadji-Ohl M, Hopf N. Navigated versus non-navigated intraoperative ultrasound: is there any impact on the extent of resection of high-grade gliomas? A retrospective clinical analysis. *J Neurol Surg A Cent Eur Neurosurg* (2014) 75:224–30. doi: 10.1055/s-0033-1356486
29. Jakola AS, Unsgård G, Solheim O. Quality of life in patients with intracranial gliomas: the impact of modern image-guided surgery. *J Neurosurg* (2011) 114(6):1622–30. doi: 10.3171/2011.1.JNS101657
30. Erdoğan N, Tucer B, Mavili E, Menkü A, Kurtsoy A. Ultrasound guidance in intracranial tumor resection: correlation with postoperative magnetic resonance findings. *Acta Radiol* (2005) 46(7):743–9. doi: 10.1080/02841850500223208
31. Woydt M, Krone A, Becker G, Schmidt K, Roggendorf W, Roosen K. Correlation of intra-operative ultrasound with histopathologic findings after tumour resection in supratentorial gliomas. A method to improve gross total tumour resection. *Acta Neurochir* (1996) 138(12):1391–8. doi: 10.1007/BF01411117
32. van Velthoven V, Auer LM. Practical application of intraoperative ultrasound imaging. *Acta Neurochir (Wien)* (1990) 105(1–2):5–13. doi: 10.1007/BF01664851
33. Shinoura N, Takahashi M, Yamada R. Delineation of brain tumor margins using intraoperative sononavigation: implications for tumor resection. *J Clin Ultrasound* (2006) 34(4):177–83. doi: 10.1002/jcu.20219
34. Albert FK, Forsting M, Sartor K, Adams H-P, Kunze S. Early postoperative magnetic resonance imaging after resection of malignant glioma: objective evaluation of residual tumor and its influence on regrowth and prognosis. *Neurosurgery* (1994) 34(1):45–61. doi: 10.1227/00006123-199401000-00008
35. Orringer D, Lau D, Khatri S, Zamora-Berridi G, Zhang K, Wu C, et al. Extent of resection in patients with glioblastoma: limiting factors, perception of resectability, and effect on survival. *J Neurosurg* (2012) 117(5):851–9. doi: 10.3171/2012.8.JNS12234
36. Prada F, Perin A, Martegani A, Aiani L, Solbiati L, Lamperti M, et al. Intraoperative Contrast Enhanced Ultra-Sound (iCEUS) for brain surgery. *Neurosurgery* (2014) 74:542–52. doi: 10.1227/NEU.0000000000000301
37. Ophir J, Cespedes I, Ponnekanti H, Yazdi Y, Li X. Elastography: a quantitative method for imaging the elasticity of biological tissues. *Ultrason Imaging* (1991) 13(2):111–34. doi: 10.1177/016173469101300201
38. Bercoff J, Tanter M, Fink M. Supersonic shear imaging: a new technique for soft tissue elasticity mapping. *IEEE Trans Ultrason Ferroelectr Freq Control* (2004) 51(4):396–409. doi: 10.1109/TUFFC.2004.1295425
39. Sarvazyan AP, Rudenko OV, Swanson SD, Fowlkes JB, Emelianov SY. Shear wave elasticity imaging: a new ultrasonic technology of medical diagnostics. *Ultrasound Med Biol* (1998) 24(9):1419–35. doi: 10.1016/S0301-5629(98)00110-0
40. Catheline S, Wu F, Fink M. A solution to diffraction biases in sonoelasticity: the acoustic impulse technique. *J Acoust Soc Am* (1999) 105(5):2941–50. doi: 10.1121/1.426907
41. Sandrin L, Fourquet B, Hasquenoph J-M, Yon S, Fournier C, Mal F, et al. Transient elastography: a new noninvasive method for assessment of hepatic fibrosis. *Ultrasound Med Biol* (2003) 29(12):1705–13. doi: 10.1016/j.ultrasmedbio.2003.07.001

42. Wu Z, Hoyt K, Rubens DJ, Parker KJ. Sonoelastographic imaging of interference patterns for estimation of shear velocity distribution in biomaterials. *J Acoust Soc Am* (2006) 120(1):535. doi: 10.1121/1.2203594
43. Deffieux T, Gennisson J-L, Larrat B, Fink M, Tanter M. The variance of quantitative estimates in shear wave imaging: theory and experiments. *IEEE Trans Ultrason Ferroelectr Freq Control* (2012) 59(11):2390–410. doi: 10.1109/TUFFC.2012.2472
44. Nightingale K, Soo MS, Nightingale R, Trahey G. Acoustic radiation force impulse imaging: in vivo demonstration of clinical feasibility. *Ultrasound Med Biol* (2002) 28(2):227–35. doi: 10.1016/S0301-5629(01)00499-9
45. Cosgrove D, Piscaglia F, Bamber J, Bojunga J, Correas J-M, Gilja OH, et al. EFSUMB guidelines and recommendations on the clinical use of ultrasound elastography. Part 2: clinical applications. *Ultraschall Med* (2013) 34(3):238–53. doi: 10.1055/s-0033-1335375
46. Uff CE, Garcia L, Fromageau J, Dorward N, Bamber JC. Real-time ultrasound elastography in neurosurgery. *IEEE Int Ultrasound Symp Proc* (2009), 467–70. doi: 10.1109/ULTSYM.2009.5441629
47. Chakraborty A, Berry G, Bamber J, Dorward N. Intra-operative ultrasound elastography and registered magnetic resonance imaging of brain tumours: a feasibility study. *Ultrasound* (2006) 14(1):43–9. doi: 10.1179/174313406X82461
48. Prada F, Del Bene M, Rampini A, Mattei L, Casali C, Vetrano IG, et al. Intraoperative strain elastosonography in brain tumor surgery. *Oper Neurosurg* (2019) 17(2):227–36. doi: 10.1093/ons/opy323
49. Cepeda S, Barrena C, Arrese I, Fernandez-Pérez G, Sarabia R. Intraoperative ultrasonographic elastography: a semi-quantitative analysis of brain tumor elasticity patterns and peritumoral region. *World Neurosurg* (2020) 135:e258–70. doi: 10.1016/j.wneu.2019.11.133
50. Selbekk T, Brekken R, Indergaard M, Solheim O, Unsgård G. Comparison of contrast in brightness mode and strain ultrasonography of glial brain tumours. *BMC Med Imaging* (2012) 12(1):11. doi: 10.1186/1471-2342-12-11
51. Selbekk T, Bang J, Unsgaard G. Strain processing of intraoperative ultrasound images of brain tumours: initial results. *Ultrasound Med Biol* (2005) 31(1):45–51. doi: 10.1016/j.ultrasmedbio.2004.09.011
52. Imbault M, Demene C, Mossad M, Gennisson J-L, Tanter M, Chauvet D, et al. Intraoperative quantitative measurement of brain tumor stiffness and intracranial pressure assessment using ultrasound shear wave elastography. *IEEE Int Ultrasound Symp Proc* (2014), 201–4. doi: 10.1109/ULTSYM.2014.0051
53. Scholz M, Noack V, Pechlivanis I, Engelhardt M, Fricke B, Linstedt U, et al. Vibrography during tumor neurosurgery. *J Ultrasound Med* (2005) 24(7):985–92. doi: 10.7863/jum.2005.24.7.985
54. Su Y, Ma J, Du L, Xia J, Wu Y, Jia X, et al. Application of acoustic radiation force impulse imaging (ARFI) in quantitative evaluation of neonatal brain development. *Clin Exp Obstet Gynecol* (2015) 42(6):797–800.
55. Kim HG, Park MS, Lee JD, Park SY. Ultrasound elastography of the neonatal brain: preliminary study. *J Ultrasound Med* (2017) 36(7):1313–9. doi: 10.7863/ultra.16.06079
56. Chan HW, Pressler R, Uff C, Gunny R, St Piers K, Cross H, et al. A novel technique of detecting MRI-negative lesion in focal symptomatic epilepsy: intraoperative shear wave elastography. *Epilepsia* (2014) 55(4):e30–3. doi: 10.1111/epi.12562
57. Xu ZS, Lee RJ, Chu SS, Yao A, Paun MK, Murphy SP, et al. Evidence of changes in brain tissue stiffness after ischemic stroke derived from ultrasound-based elastography. *J Ultrasound Med* (2013) 32:485–94. doi: 10.7863/jum.2013.32.3.485
58. Xu ZS, Yao A, Chu SS, Paun MK, McClintic AM, Murphy SP, et al. Detection of mild traumatic brain injury in rodent models using shear wave elastography: preliminary studies. *J Ultrasound Med* (2014) 33(10):1763–71. doi: 10.7863/ultra.33.10.1763
59. Rygh OM, Nagelhus Hernes TA, Lindseth F, Selbekk T, Brostrup Müller T, Unsgaard G. Intraoperative navigated 3-dimensional ultrasound angiography in tumor surgery. *Surg Neurol* (2006) 66(6):581–92; discussion 592. doi: 10.1016/j.surneu.2006.05.060
60. Uff CE. *The evaluation of advanced ultrasound elastographic techniques in neurosurgery*. London: Institute of Cancer Research, University of London, UK (2011).
61. Murphy MC, Huston J, Glaser KJ, Manduca A, Meyer FB, Lanzino G, et al. Preoperative assessment of meningioma stiffness using magnetic resonance elastography. *J Neurosurg* (2013) 118(3):643–8. doi: 10.3171/2012.9.JNS12519
62. Chauvet D, Imbault M, Capelle L, Demene C, Mossad M, Karachi C, et al. In vivo measurement of brain tumor elasticity using intraoperative shear wave elastography. *Ultraschall der Med* (2016) 37(6):584–90. doi: 10.1055/s-0034-1399152
63. Chang JM, Park IA, Lee SH, Kim WH, Bae MS, Koo HR, et al. Stiffness of tumours measured by shear-wave elastography correlated with subtypes of breast cancer. *Eur Radiol* (2013) 23(9):2450–8. doi: 10.1007/s00330-013-2866-2
64. Youk JH, Gweon HM, Son EJ, Kim J-A, Jeong J. Shear-wave elastography of invasive breast cancer: correlation between quantitative mean elasticity value and immunohistochemical profile. *Breast Cancer Res Treat* (2013) 138 (1):119–26. doi: 10.1007/s10549-013-2407-3
65. Chan HW. *Optimising the use and assessing the value of intraoperative shear wave elastography in neurosurgery. Phd Thesis*. London: Institute of Neurology, University College London (2016).
66. Chan HW, Uff C, Chakraborty A, Dorward N, Bamber J. (2016). Clinical application of shear wave elastography for assisting brain tumour resection, in: *Fifteenth International Tissue Elasticity Conference*, Lake Morey, Vermont, USA, October 16 – 19, 2016. p. 38.

Conflict of Interest: The authors declare that the research was conducted in the absence of any commercial or financial relationships that could be construed as a potential conflict of interest.

frontiers in Oncology

ORIGINAL RESEARCH
published: 04 March 2021
doi: 10.3389/fonc.2021.619204

Evaluation of an Ultrasound-Based Navigation System for Spine Neurosurgery: A Porcine Cadaver Study

Houssem-Eddine Gueziri[1]*, *Oded Rabau*[2], *Carlo Santaguida*[2] and *D. Louis Collins*[1]

[1] McConnell Brain Imaging Centre, Montreal Neurological Institute and Hospital, McGill University, Montreal, QC, Canada,
[2] Department of Neurology and Neurosurgery, McGill University, Montreal, QC, Canada

Background: With the growing incidence of patients receiving surgical treatment for spinal metastatic tumours, there is a need for developing cost-efficient and radiation-free alternatives for spinal interventions. In this paper, we evaluate the capabilities and limitations of an image-guided neurosurgery (IGNS) system that uses intraoperative ultrasound (iUS) imaging for guidance.

Methods: Using a lumbosacral section of a porcine cadaver, we explored the impact of CT image resolution, ultrasound depth and ultrasound frequency on system accuracy, robustness and effectiveness. Preoperative CT images with an isotropic resolution of , and were acquired. During surgery, vertebrae L1 to L6 were exposed. For each vertebra, five iUS scans were acquired using two depth parameters (5 cm and 7 cm) and two frequencies (6 MHz and 12 MHz). A total of 120 acquisition trials were evaluated. Ultrasound-based registration performance is compared to the standard alignment procedure using intraoperative CT. We report target registration error (TRE) and computation time. In addition, the scans' trajectories were analyzed to identify vertebral regions that provide the most relevant features for the alignment.

Results: For all acquisitions, the median TRE ranged from 1.42 mm to 1.58 mm and the overall computation time was 9.04 s ± 1.58 s. Fourteen out of 120 iUS acquisitions (11.66%) yielded a level-to-level mismatch (and these are included in the accuracy measurements reported). No significant effect on accuracy was found with CT resolution ($F_{(2,10)} = 1.70$, $p = 0.232$), depth ($F_{(1,5)} = 0.22$, $p = 0.659$) nor frequency ($F_{(1,5)} = 1.02$, $p = 0.359$). While misalignment increases linearly with the distance from the imaged vertebra, accuracy was satisfactory for directly adjacent levels. A significant relationship was found between iUS scan coverage of laminae and articular processes, and accuracy.

Conclusion: Intraoperative ultrasound can be used for spine surgery neuronavigation. We demonstrated that the IGNS system yield acceptable accuracy and high efficiency compared to the standard CT-based navigation procedure. The flexibility of the iUS acquisitions can have repercussions on the system performance, which are not fully identified. Further investigation is needed to understand the relationship between iUS acquisition and alignment performance.

Keywords: ultrasound neuronavigation, spine surgery, image-guided neurosurgery, registration, evaluation, accuracy

OPEN ACCESS

Edited by:
Massimiliano Del Bene, Istituto Neurologico Carlo Besta (IRCCS), Italy

Reviewed by:
Luca Raspagliesi, University of Milan, Italy
Francesco Maria Crisà, Niguarda Ca' Granda Hospital, Italy

***Correspondence:**
Houssem-Eddine Gueziri
houssem.gueziri@mcgill.ca

Specialty section:
This article was submitted to Neuro-Oncology and Neurosurgical Oncology, a section of the journal Frontiers in Oncology

Received: *19 October 2020*
Accepted: *18 January 2021*
Published: *04 March 2021*

Citation:
Gueziri H-E, Rabau O, Santaguida C and Collins DL (2021) Evaluation of an Ultrasound-Based Navigation System for Spine Neurosurgery: A Porcine Cadaver Study. Front. Oncol. 11:619204. doi: 10.3389/fonc.2021.619204

INTRODUCTION

Advancing technology and improvement in surgical techniques have contributed to the rising incidence of patients receiving surgical treatment for spinal metastatic tumours (1, 2). In the last two decades, significant efforts have been made to develop image-guided neurosurgery (IGNS) systems for spine oncology in traditional open surgery (3, 4), in minimally invasive and robotic surgeries (5–7) and in ablative therapy (8–11). Neuronavigation performed by IGNS allows the digital tracking of surgical instruments with respect to diagnostic imaging, therefore facilitating tumour localization, anatomy visualization and monitoring surgical progress. For most commercial IGNS systems, computed tomography (CT) is the preferred imaging modality for spine interventions. CT images yield good visualization of bone anatomy, suitable for fusion instrumentation. In addition, the accessibility of mobile scanners offers some flexibility for intraoperative imaging in the operating room (OR). However, there is a non-negligible risk of ionizing radiation exposure to the patient and, perhaps more impotently to the surgical staff, associated with intraoperative CT imaging (12). Alternative approaches have investigated magnetic resonance (MR) imaging to reduce radiation exposure (13–16). Although intraoperative MR provides high image resolution and good soft tissue contrast, restrictions due to high costs and ferromagnetic compatibility of surgical instruments limit its application in the OR.

Recently, the use of intraoperative ultrasound (iUS) has gained attention for spinal neuronavigation (17). While the many advantages to using iUS imaging include safety, real-time acquisition, cost-efficiency and reduced footprint in the OR, the role of iUS in spinal surgery is not fully defined and remains under investigation (18). Ultrasound acquisition has some limitations in the OR. For example, the small field of view obtained from an iUS scan reduces the ability to observe deep structures, limiting its application to mostly posterior surgical approaches. Moreover, low ultrasound signal propagation through dense bone tissues induces shadow artifacts and makes navigation using iUS images challenging. To address these limitations, iUS-based IGNS systems do not use ultrasound images for diagnosis or visual navigation. Rather, iUS is used to collect anatomical features in order to establish patient alignment with preoperative CT or MR images. Then, the navigation is performed on the preoperative images.

In our previous work (19), we introduced an open-source and freely available IGNS system based on iUS imaging which allows for CT-to-iUS image alignment for spine instrumentation. Although the system was able to achieve satisfactory results for the alignment of one vertebra at a time, the full capabilities of such a system in variable acquisition conditions are unknown. This paper investigates the limitations associated with the usability of the system on a porcine cadaver. Specifically, we are interested in the following questions: (i) is there a specific CT and/or ultrasound imaging parameters that impact the accuracy of the system? (ii) how do alignment errors, located on a specific vertebra, propagate to adjacent vertebral levels? and (iii) can we identify patterns of ultrasound acquisitions that affect accuracy? In a controlled experimental study, we explore the feasibility of ultrasound-based neuronavigation for the lumbar spine. We report the results in terms of accuracy, robustness and effectiveness and discuss the usability in clinical conditions.

MATERIALS AND METHODS

Navigation System

The IGNS system is composed of three main components (**Figure 1**): an ultrasound scanner, a tracking camera and a computer station. The first component is an ultrasound unit with a linear probe (BK3500/14L3 probe, BK Medical, Peabody, MA, USA). The probe's contact surface is 14 mm wide and small enough to fit inside the surgical cavity to acquire intraoperative images. The second component is a tracking camera (FusionTrack 500, Atracsys, Puidoux, Switzerland). It is used to determine the spatial location of infrared light-reflecting spheres rigidly fixed to surgical instruments. In this study, the tracked instruments consist of a planar blunt probe PN960-556 (Medtronic, Dublin, Ireland) used as a pointer, the iUS linear probe and a rigid body reference. The instrument positions are expressed in the reference coordinate system, therefore accounting for patient movement during navigation. The third component is a computer station that runs IBIS[1], an open-source neuronavigation software developed in our laboratory (20). IBIS provides common navigation functionalities such as 3D data visualization, ultrasound probe calibration, ultrasound acquisitions, volume reconstruction and patient registration, and has been evaluated in the operating room for brain tumour resection (21, 22).

The iUS probe is calibrated prior to the experiments. This determines the spatial correspondence between the iUS image space (in pixel) and the patient space (in millimeters) with an accuracy ranging between 0.49 mm and 0.82 mm (23). The intraoperative procedure to establish navigation is as follows: First, the open cavity is filled with a saline solution to allow ultrasound image acquisition. The operator performs an axial iUS sweep along the caudo-cranial direction, starting from the inferior to the superior aspect of the vertebra (24). The data collected data are automatically provided to the IBIS station, and the CT-to-iUS spatial correspondence is computed by aligning the hyperechoic response produced by the bone surface on the iUS images with the precomputed posterior vertebral surface extracted from CT images (19, 25). Once the registration is completed, the tracked instruments are located on preoperative CT images for navigation.

Data

Lumbar spines of porcine cadavers are commonly used for validation of spinal instrumentation due to their similarity with human specimens and the limited ethical issues they involve (26, 27). For this study, a lumbosacral section of a 80 Kg pig, in which vertebrae L1 to L6 were present, was obtained

[1] Intra-operative Brain Imaging System: http://ibisneuronav.org/

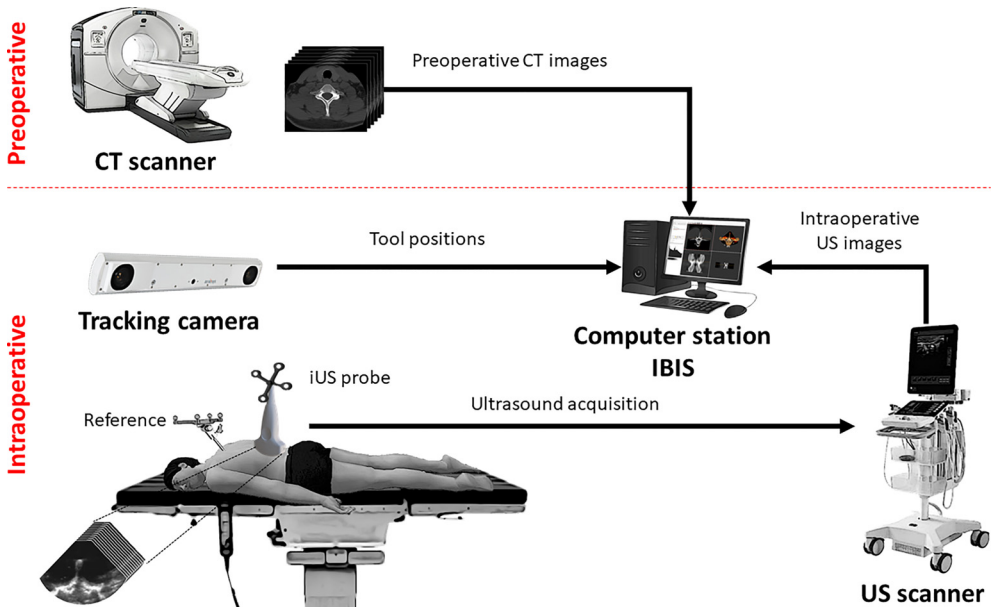

FIGURE 1 | Setup of the ultrasound-based image-guided neurosurgery system.

from a local butcher shop. The specimen was attached to a rigid frame to prevent intervertebral motion. A rigid body reference containing 4 infra-red reflective spheres was attached to the frame and serves as a dynamic reference object (DRO). The role of the DRO is two-fold. First, it serves as a reference coordinate space for the tracked instruments. The rigid frame ensures a fixed spatial relationship between the DRO and the specimen, allowing the instruments to be tracked with respect to the anatomy (see **Figures 2A–C**). Note that in spine surgery, the DRO is usually attached to the spinous process of the target vertebra, an adjacent vertebra or the iliac bone depending on the level of the target. Second, because the spheres are visible on the CT images, they are used to obtain a *ground truth alignment* for experiments. This procedure is similar to the one used by commercial systems that are based on intraoperative CT scanners. In this study, we compare the accuracy of our iUS-based neuronavigation system against the standard IGNS procedure based on intraoperative CT.

Before the experiment, the specimen was placed in a supine position and imaged using a clinical CT scanner (Aquilion ONE, Canon Medical, Otawara, Japan). Vertebral levels were manually identified on the CT scan. For each vertebral level, three corresponding CT volumes were reconstructed with a resolution of 0.5mm × 0.5mm × 0.5mm, 1mm × 1mm × 1mm, and 2mm × 2mm × 2mm. Then, the frame was flipped over to have the specimen in prone position and vertebrae L1 to L6 were exposed. Multiple iUS acquisitions were performed for each vertebral level with different depth and frequency parameters (see **Figure 2D**). Specifically, we investigated the effects of probe depth at 5 cm and 7 cm, and frequency of 6 and 12 MHz. The remaining ultrasound probe parameters were kept the same for all the acquisitions. For each depth–frequency combination, 5 similar independent iUS scans were acquired per vertebra yielding a total of 5 acquisitions × 2 frequencies × 2 depths × 6 vertebrae = 120 ultrasound scans. All the acquisitions were performed by the same operator. During iUS scanning, the probe was oriented in the antero-posterior direction and the 5 repetitions were performed with a slight but not significant variation in the left-right orientation and acquisition speed. This aims at reflecting the variability that may occur during a particular iUS acquisition protocol.

Ground Truth Alignment

A single ground truth alignment is used for all the vertebrae. The alignment is obtained using a rigidly fixed DRO, similar to the procedure employed in CT-based intraoperative navigation. The procedure consists in a pair-wise matching of the position of the spheres visible on CT images with their respective position obtained from the camera tracking. The spheres appear bright on CT images and can be precisely segmented using a thresholding technique. The coordinates of each sphere's center are then computed and used to obtain the spatial transform between the navigation space and the CT imaging space using a rigid-body landmark registration (28). This transform serves as the ground truth alignment when evaluating accuracy. Note that the validity of the ground truth alignment is subject to the assumptions that the specimen is fixed to the frame and that the spatial transform is exact. While violation of the former assumption would invalidate the ground truth, violation of the latter assumption could result in increasing ground truth misalignment as the distance from the DRO increases due to angular misalignment errors.

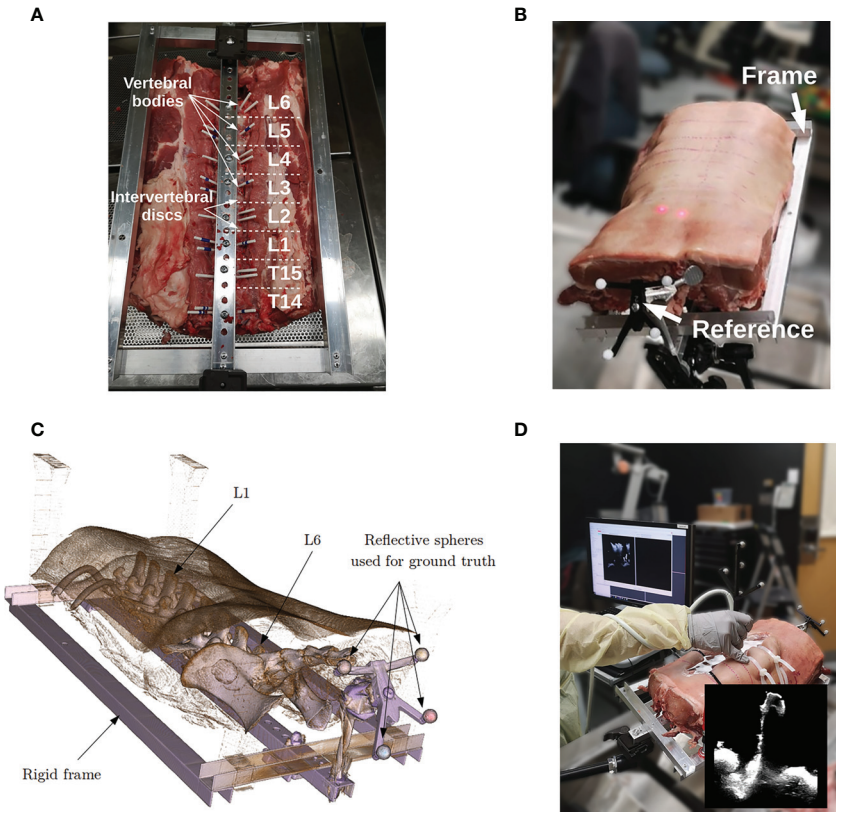

FIGURE 2 | Porcine cadaver data acquisition: **(A)** specimen in supine position attached to a rigid frame, **(B)** specimen in prone position redy for surgery, **(C)** CT volume rendering of the porcine cadaver, and **(D)** intraoperative ultrasound acquisition.

Performance Metrics

The IGNS system is evaluated according to three major criteria: accuracy, robustness and effectiveness. The *accuracy* is defined as the target registration error (TRE) resulting from the difference between the alignment obtained using the proposed iUS-based method and the ground truth alignment. For each vertebral level, the TRE is given by the root mean square of the Euclidean distance computed at 7 anatomical points located on the vertebra surface, corresponding to the apex of the spinous process, left and right laminae, left and right superior articular processes and tips of the left and right transverse processes. Note that the landmarks are identified on the CT images. Therefore, the TRE gives the error between the alignment obtained with the iUS-based neuronavigation and the one obtained with standard IGNS procedure based on intraoperative CT imaging (i.e., ground truth alignment). The alignment is considered satisfactory if the TRE is below 2 mm, which is the clinical threshold suggested for spinal navigation (29). The *robustness* is measured by the success rate (in %) defined as the fraction of acquisitions that achieved satisfactory alignment, (i.e., TRE <2mm). Finally, the *effectiveness* is measured by the overall computation time required to complete the registration.

The vertebral level where the TRE is computed indicates the accuracy of the alignment at that location. This is particularly true for angular errors, where a slight angular misalignment at L6, for example, can lead to a large error at L1. Note that for commercial intraoperative CT-based IGNS systems in which the alignment is performed using the DRO's reflective spheres, it is recommended to position the DRO near the vertebral levels receiving treatment. In our experiment, if an iUS acquisition covering a given vertebra yields a good result, we wish to identify how the accuracy propagates to other vertebral levels. Therefore, for each iUS acquisition, the TRE is computed on all vertebrae.

Ultrasound Acquisition Coverage

To gain insight into how the iUS acquisition affects the alignment outcome, we examine the vertebral anatomy *coverage* produced by the ultrasound scan. In other words, the coverage is defined as how much and what part of the vertebra surface was imaged during iUS acquisition. The goal of this metric is to investigate the relationship between the iUS acquisition and the success of the alignment. To obtain the coverage, we first manually segmented the vertebrae on each CT volume at the resolution of 0.5mm × 0.5mm × 0.5mm. For each vertebra, five labels were identified (see **Figure 3A**): the spinous process (SP), laminae (L), pedicles and vertebral body (VB), inferior and superior articular processes (AP), and transverse processes (TP). In addition to these labels, we include the coverage of the vertebrae located one

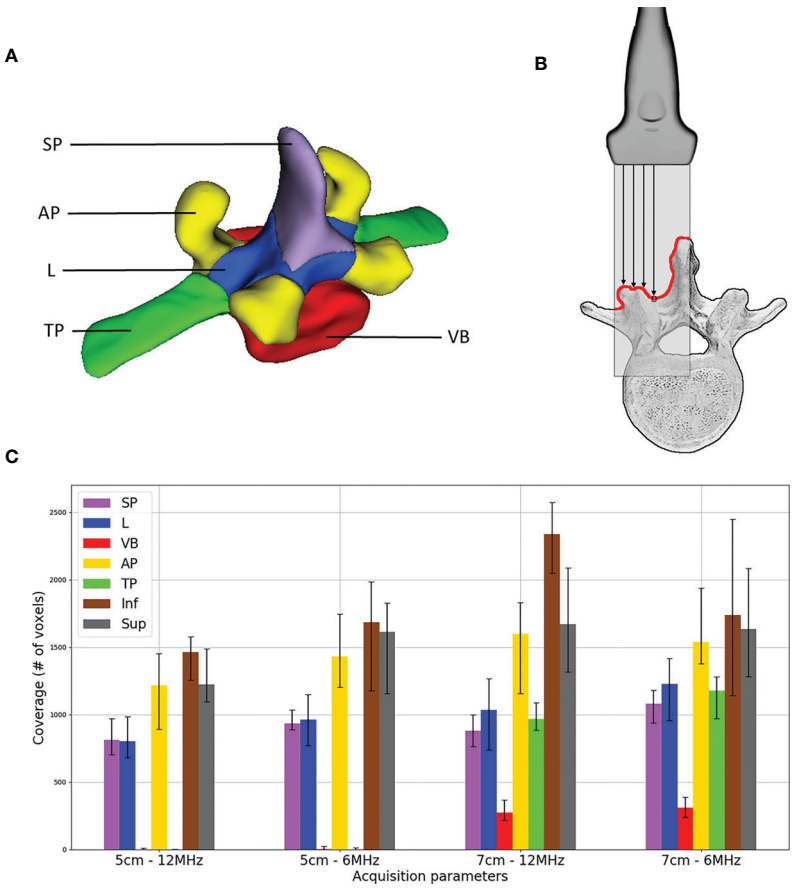

FIGURE 3 | Ultrasound acquisition coverage: **(A)** labels associated with vertebra segmentation – spinous process (SP), superior and inferior articular processes (AP), laminae (L), transverse processes (TP) and pedicles and vertebral body (VB); **(B)** illustration of coverage counting, only the first voxel encountered along ultrasound image columns is considered; and **(C)** median distribution of labels' coverage including voxels of one level inferior (Inf) and one level superior (Sup) vertebrae, error bars represent first and third quartiles.

level inferior and one level superior. This is because the acquisition starts at the inferior most part and ends at the superior most part of the vertebra, therefore we need to account for the existing overlap between vertebrae. Then, the CT segmentation is aligned with the iUS acquisition using the ground truth transform. Finally, the coverage is given by the sum of CT voxels within the segmentation that intersect with the iUS image planes. We assume no ultrasound penetration over bone tissues, therefore, only the first voxel encountered along the iUS image column is considered in our model (see **Figure 3B**).

Statistical Analysis

Two models were used to analyze the coverage effect on the alignment performance. The first model aims at understanding the impact that label combinations can have on the alignment outcome. Recall that the experimental design includes six vertebral levels, and for each level, two sub-groups of different frequencies and depths are constructed, each consisting of 5 repeated acquisitions. Therefore, a linear mixed-effect model is used (30). The model evaluates the TRE outcome considering every possible interaction between labels, and accounting for the group variance of vertebral levels and the sub-group variances of frequency and depth per level. The second model aims at understanding whether the coverage has an implication in causing level misalignments. The rationale is fact that coverage expresses the level location where the acquisition has been taken. In other words, if the acquisition is not centred on the correct vertebral level, we expect the coverage to be lower for the labels (SP, L, VB, AP, and TP) and higher for the adjacent levels (labels associated with inferior and superior levels). A binary response of *level misalignment* was created from the TRE results such as we associate a negative response to level misalignment if the TRE is lower than 10 mm and a positive response otherwise. Similar to the first model, we used a binomial mixed-effect model to account for group and sub-group variances of level, frequency and depth. However, because we are not interested in the different label interactions, a single independent variable representing the sum of all labels excluding adjacent levels is considered.

Intensity Profile

Ultrasound bone appearance varies significantly depending on the acquisition and probe positioning, for example in the case of occlusions caused by shadow artifacts. In order to gain insight into how the bone surface appears in ultrasound images, we analyzed the *intensity profile* of a line passing from the bone tissue to the cavity of L5, through the lamina. The intensity profile represents the values of image intensity along a line segment. Therefore, it is possible to observe changes in intensity as the line traverses the bone surface. We analyze the intensity profile of the 20 iUS acquisitions performed on the vertebra. The median intensity and the interquartile range are reported. To compare the same segment through different acquisitions, we first align the iUS acquisitions with the CT image using the ground truth alignment. Then, the intensity profile is computed using the same line position through all acquisitions.

RESULTS

Imaging Parameters

Table 1 shows the results obtained with the different CT resolutions and ultrasound depth and frequency parameters. For all the CT volume resolutions, the median TRE ranges from 1.42 mm to 1.58 mm. Out of the 120 acquisitions, 79 (65 %) to 84 (70 %) iUS scans were successfully aligned (i.e., TRE <2mm). No significant effect was found between the accuracy and the CT resolution ($F_{(2,10)} = 1.70$, $p = 0.232$). Although a slightly lower median TRE of 1.33 mm was achieved using a depth of 5 cm and a frequency of 12 MHz, there is no significant effect of depth ($F_{(1,5)} = 0.22$, $p = 0.659$) nor frequency ($F_{(1,5)} = 1.02$, $p = 0.359$) on the accuracy. Regarding effectiveness, CT and iUS imaging parameters did not affect the computation time. The overall computation time is 9.04 s ± 1.58 s.

We observed that for some acquisitions the iUS was aligned to the wrong vertebral level, mostly one vertebral level above or below the target level. For these *vertebral level mismatch* cases, the resulting TRE is very large, typically over 10 mm. All CT resolutions confounded, such cases represent 14 out of 120 (11.67 %) acquisitions and have a median TRE of 67.17 mm ± 15.73 mm. Note that the overall TRE results presented above include those cases. If these mismatch cases are removed, the overall median TRE for all experiments is reduced, from 1.43 mm to 1.29 mm, from 1.58 mm to 1.48 mm, and from 1.42 mm to 1.32 mm for each CT resolution. Vertebral level mismatch cases are distributed as follows: 1 case at L1 (5 %), 1 case at L2 (5 %), 1 case at L3 (5 %), 2 cases at L4 (10 %), 6 cases at L5 (30 %), and 3 cases at L6 (15 %). Because of the anatomical similarity between vertebrae, it is not trivial to identify a level misalignment by visual inspection.

Error Propagation

The alignment results obtained for each vertebra were used to compute the TRE across all other vertebral levels. **Figure 4A** shows the propagation of the TRE for each CT resolution. Each row corresponds to the location where the iUS acquisition was performed and each column corresponds to the location where the TRE was computed. The best alignment results are located on the diagonal, i.e., close to the vertebral levels that have been imaged and used to compute the registration. Note that along the diagonal, there is no consistent increase of the TRE as the measurements are done away from the DRO located at the most inferior part of the frame (near L6). This supports the assumption regarding the validity of the ground truth alignment as the angular error is negligible. On the other hand, the error increases linearly as it moves farther from the registered vertebral level (see **Figure 4B**). The distance between each two successive spinous processes was measured to be $d_{L6/5} = 69.36\ mm$, $d_{L5/4} = 35.33\ mm$, $d_{L4/3} = 38.21\ mm$, $d_{L3/2} = 39.38\ mm$, and $d_{L2/1} = 39.46\ mm$. For all CT resolutions, results for L1 show the worst performance with a median TRE of 3.01 *mm* ± 0.43 *mm* computed on L1, and increases to 7.96 *mm* ± 0.69 *mm* on the farthest vertebra L6 located at a distance of 221.74 mm away.

Coverage Results

A histogram of ultrasound acquisition coverage of the labels is shown in **Figure 3C**. Note that for the additional inferior and superior levels, the entire anatomy of the vertebra was considered as a single label, therefore resulting in a higher coverage value. Among all vertebra labels, AP showed the highest coverage values (mean 1485.5 voxels) for all the scans, followed by L (mean 1004.2 voxels) and SP (mean 944.1 voxels), respectively. Labels associated with VB and TP were only visible for acquisitions with an ultrasound depth of 7 cm. VB showed the lowest coverage values as it is only visible from the gap located in the intervertebral space.

TABLE 1 | Summary results of accuracy and computation time for different imaging parameters.

CT	US	US	Median	Successful		
Resolution	Depth	Frequency	TRE (mm)	IQR (mm)	acquisition (%)	Time (s)
0.5 mm × 0.5 mm × 0.5 mm	–	–	1.43	1.15	70.00	9.21
1 mm × 1 mm × 1 mm	–	–	1.58	1.83	65.83	8.49
2 mm × 2 mm × 2 mm	–	–	1.42	1.43	67.50	8.84
–	5 cm	6 MHz	1.47	1.76	68.89	8.33
–	5 cm	12 MHz	1.33	1.00	73.33	8.29
–	7 cm	6 MHz	1.68	1.23	64.44	9.74
–	7 cm	12 MHz	1.48	1.73	64.44	9.01

All parameters confounded are indicated by (–), TRE, target registration error; IQR, interquartile range, Successful acquisition: the fraction of iUS acquisitions achieving a TRE below 2 mm.

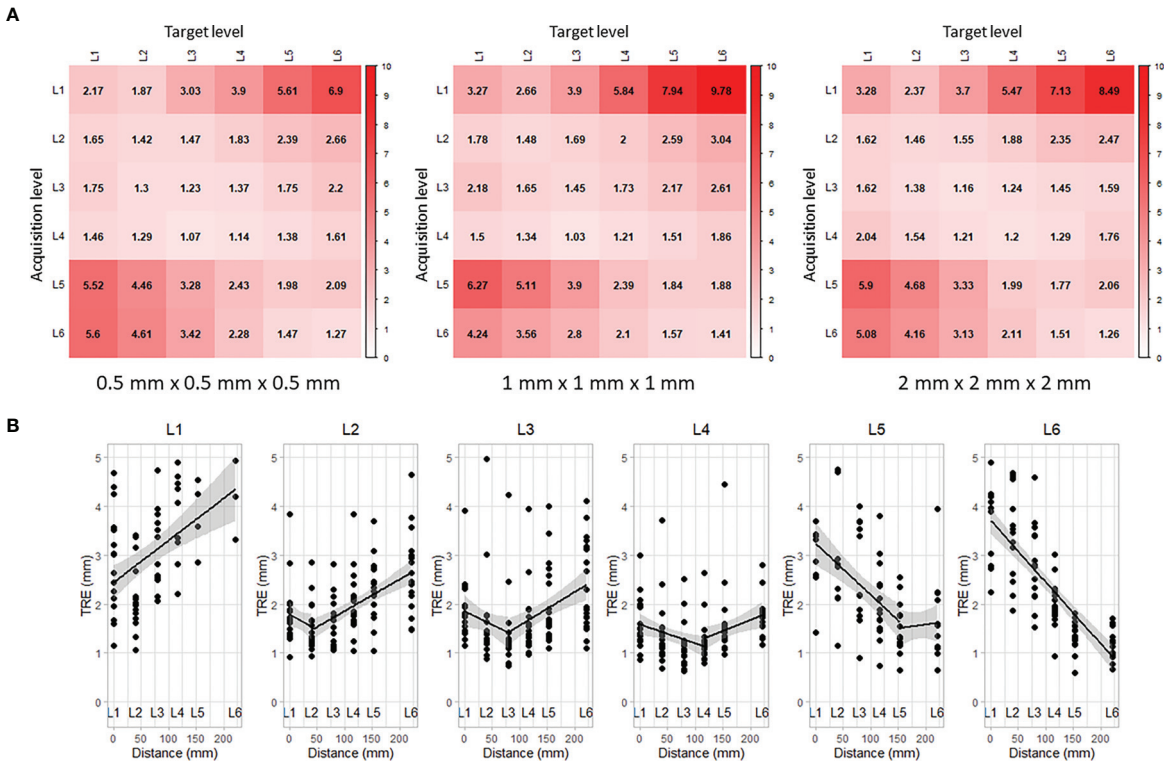

FIGURE 4 | Propagation of target registration error along vertebral levels: **(A)** rows correspond to the levels where iUS acquisitions were performed and columns correspond to the levels where TRE was measured, and **(B)** linear regression of the TRE accounting for the space between vertebral levels.

After removing the 14 outliers representing level misalignment cases, we fit the remaining TRE data with the model that includes all possible interactions between the labels. A significant relationship was found between the coverage amount of label L (p = 0.012) with negative correlation, as well as the combination of labels L and AP (p = 0.035) with positive interaction correlation, on the TRE measure. No significant effect was found for other label combinations. To identify the potential effect of coverage on causes of level misalignment, we fit the level misalignment outcomes to the binomial mixed-effect model, as described in Section 2.6. However, no statistically significant relationship was found between the acquisition coverage and level misalignment.

DISCUSSION

Effect of Imaging Parameters

We conducted a thorough experiment on a porcine cadaver to investigate the capabilities and limitations of our neuronavigation system for spine surgery. The system relies on optical trackers and intraoperative ultrasound imaging to efficiently establish patient alignment, which is then used to provide neuronavigation on preoperative CT images. In this study, we evaluated the alignment quality as the resolution of preoperative CT images varies from

0.5mm × 0.5mm × 0.5mm to 2mm × 2mm × 2mm. The overall median TRE ranges between 1.42 mm and 1.58 mm across all CT resolutions, which meets the clinical accuracy requirements of 2 mm for spinal navigation (29). Although a finer CT resolution provides a better representation of anatomical details, we found no significant impact on the quality of the final alignment. This can be explained by the intrinsic characteristics related to ultrasound bone imaging, specifically, the signal variation of ultrasound response near the bone-tissue interface. The intensity at the vertebral surface varies depending on signal strength, bone density and incidence angle of the ultrasound waves caused by the probe orientation with respect to the surface. **Figure 5** illustrates the distribution of the intensity profiles crossing the lamina of L5 for all 20 ultrasound acquisitions. While the vertebral surface on the CT image can be easily extracted, even with slice thickness of 2 mm, the intensities of the ultrasound images at the vertebral surface are more widely distributed, rendering the identification of the exact location of the vertebral surface challenging.

We investigated the effects that basic ultrasound parameters, including depth and frequency, have on the alignment quality. We first explore whether anterior structures of the vertebra, located deeper in the cavity, provide relevant features for the alignment. We then tested the effect of the probe frequency on the alignment. While low probe frequencies enable deeper tissue penetration and provide information on underlying vertebral

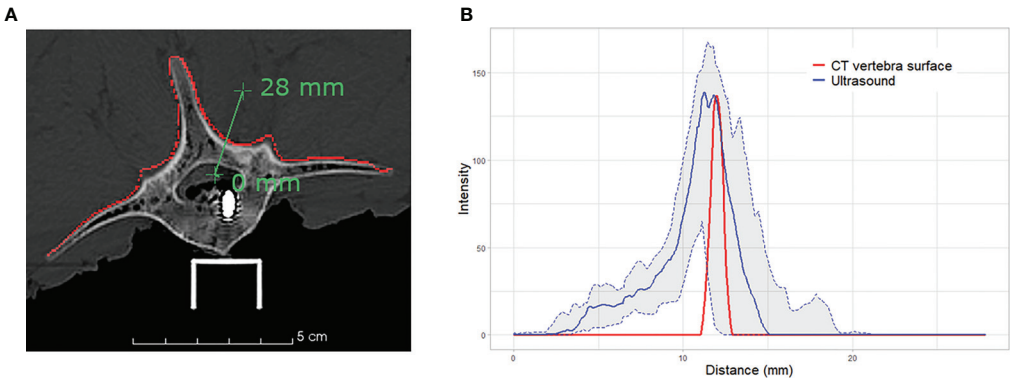

FIGURE 5 | Intensity profile across the vertebral surface of L5: **(A)** illustration of the profile line (green) crossing the vertebral surface (red) at the lamina on CT image; and **(B)** plot of the intensity profiles of CT vertebral surface (red), median intensity of 20 iUS acquisitions performed on L5 (blue) and the associated interquartile range (light grey).

structures, high probe frequencies provide a better image quality. In our experiment, increasing ultrasound depth and frequency did not show any significant improvement in the accuracy. The iUS acquisitions are performed in open surgery, in which the posterior part of the vertebra is exposed. The ultrasounds propagate through the saline solution in the cavity with negligible signal loss before encountering the bone surface. Therefore, signal loss usually associated with tissue absorption did not play a critical role in alignment accuracy.

The IGNS system was evaluated based on the alignment of a single vertebra at a time, meaning that the information used to establish the alignment is associated with one vertebral level in the pre- and intra-operative images. This intentional design is meant to avoid errors due to intervertebral motion caused by spine curvature changes, resulting from a typical preoperative CT scan in supine position while the iUS images are acquired in prone position during surgery. Assuming no spine curvature changes, we evaluated the propagation of the alignment error along the vertebral levels. Overall, the alignment accuracy was satisfactory for directly adjacent vertebral levels, i.e., one level superior and one level inferior to the vertebra level used to establish the alignment. The accuracy is sufficient for instrumentation of three vertebral levels per iUS alignment. This reduces the number of iUS acquisitions needed to establish navigation during surgery, decreasing considerably intraoperative time and surgical workflow interruptions. However, the best accuracy results were obtained at the vertebral level where the iUS acquisition was performed. Therefore, it is recommended to perform the alignment procedure on the vertebra being instrumented. The computation time is ∼10 seconds and we estimate the iUS acquisition time to be less than one minute, which makes the alignment procedure significantly faster than the standard intraoperative CT navigation, estimated to be 15–20 min. In addition, for surgeries involving several vertebral levels, the DRO needs to be re-positioned near the instrumented vertebral level. In such a case, the intraoperative CT procedure needs to be performed again.

Intraoperative Acquisition

The iUS acquisition plays a crucial role in the resulting quality of the alignment. In our IGNS system, the iUS acquisition is expected to be a linear scan from inferior to superior parts of the vertebra. This predefined constraint is used to initialize the alignment so that the iUS and the CT volumes are located in the same space and in the same orientation. We draw the reader's attention to the low accuracy results obtained with L1 (see **Figure 4**). This specific limitation has been caused by difficulties encountered while performing iUS acquisitions at L1. Because we could not extend the surgical opening beyond L1 without risking the perforation of the cavity, the width of the opening at that location was narrow, restricting the probe's motion. Note that this scenario is unlikely to happen during real surgery, as the vertebrae receiving treatment are more widely exposed. Nevertheless, this highlights an underlying limitation of iUS-based IGNS systems, in which the ultrasound probe physical dimensions need to be accounted for during data acquisition in open spine surgery. Probes with small size are to be preferred.

To understand which part of the vertebra provides the most relevant features for the alignment, we identified 5 regional vertebral labels and analyzed coverage data produced by the 120 iUS acquisitions performed during the experiment. Results revealed a significant relationship between the accuracy and the iUS coverage of laminae and superior and inferior articular processes. The negative correlation between the laminae coverage and the alignment error indicates that accuracy increases (error is reduced) with more laminae coverage. Similar results apply to the combination of laminae and articular processes coverage as a positive interaction was found between the two labels. This seems to be consistent with the fact that articular processes and laminae are the most prominent structures in posterior approaches for open spine surgery. Note that the coverage of the spinous process did not show a significant effect on accuracy. One would expect the spinous process to play a role in the alignment since it is the most exposed part of the vertebra. However, the shape of the spinous process forming a crest in the anterio-posterior direction does

not represent a good anatomical feature for the iUS acquisition. This is because most of the spinous process anatomy is in the same direction as the ultrasound beams produced by a posterior scan, resulting in low signal response along the spinous process. Note that one side of the spinous process can be imaged with the probe slightly tilted to the left or to the right of the vertebra.

Although we identified vertebral regions that provide relevant features, we have been unsuccessful to specifically determine the cause of alignment failures. From the ultrasound acquisitions, we found no particular pattern that seems to increase or decrease the alignment accuracy. To reduce scan variability, and perhaps increase robustness, a combination of multiple iUS acquisitions that allows the formation of a homogeneous ultrasound volume can be explored in the future.

Limitations

Regarding iUS acquisition, we used a linear ultrasound probe to collect intraoperative data. While linear probes have typically a higher frequency and thus a better depth image quality than curved probes, the resulting acquisitions have a smaller field of view, especially for imaging lateral parts of the vertebra. This limits the coverage of the transverse processes. In our experiment, only the proximal parts of the transverse processes were visible when the probe's depth was set to 7 cm. Future work will involve investigating the use of a curved probe for spinal IGNS, which would provide a wider field of view.

The model presented to quantify the ultrasound acquisition coverage has two major limitations. First, the model assumes no bone penetration, meaning that the coverage only accounts for the first voxel at the surface of the vertebra. While this allows identifying parts of the vertebra prominently exposed to the ultrasound, it does not account for underlying tissues that may result be imaged, especially for low frequency acquisitions. The second limitation involves the oversimplification of the ultrasound wave propagation. In our model, we assume the propagation to be linear along the ultrasound image columns, therefore, only accounting for the longitudinal ultrasound wave travel. In reality, the propagation has a transverse wave component that allows objects adjacent to the ultrasound image column to be imaged. Moreover, the oversimplification of the ultrasound wave does not consider the angular incidence of the beam on the bone surface. As a result, the model does not account for the intensity response of the ultrasound images. A more complex model would provide more accurate coverage information as it would include reflections and bone penetration which characterize the visibility of the vertebral surface on iUS images.

Finally, measurement of accuracy was carried out under the assumption of a rigid spine. The vertebrae were fixed to a metal frame to prevent intervertebral motion. Therefore, the DRO could be placed at a distant location, i.e., the edge of the frame, without invalidating the TRE measurements. In surgery, the spine curvature is subject to variation due to instrumentation, respiratory motion and patient positioning. The placement of the DRO for neuronavigation is critical as a distant DRO could result in large inaccuracies (31). Further work is needed to investigate how spine curvature changes may affect accuracy.

CONCLUSION

In this paper, an ultrasound-based neuronavigation system for spine surgery was evaluated on a porcine cadaver. The overall accuracy of the system ranges between 1.42 mm and 1.58 mm meeting the clinical accuracy requirement of 2 mm for spine navigation. The system demonstrated high robustness to different CT resolutions, ultrasound depth and frequency parameters. We analyzed multiple ultrasound acquisitions and identified both laminae and articular processes to provide relevant features for image alignment. However, the system suffers some limitations related to the intraoperative acquisitions with ultrasound. Fourteen out of the 120 trials resulted in a one-level-off misalignment. These misalignments can be difficult to identify visually and require particular attention. Additional work needs to be carried out to understand ultrasound acquisition patterns that yield the best alignment results.

DATA AVAILABILITY STATEMENT

The raw data supporting the conclusions of this article will be made available by the authors, without undue reservation.

ETHICS STATEMENT

The study involves a section of pig purchased from a local certified butcher. Ethical review and approval were not required for this study.

AUTHOR CONTRIBUTIONS

H-EG, CS, and LC contributed to conception and design of the study. H-EG and OR conducted experimentation. H-EG and LC contributed to data analysis. H-EG contributed to software development and wrote original manuscript. All authors contributed to the article and approved the submitted version.

FUNDING

This study was funded by grants from the Canadian Institutes of Health Research (No. 246067) and the Natural Sciences and Engineering Research Council of Canada (No. 396395).

REFERENCES

1. Yoshihara H, Yoneoka D. Trends in the surgical treatment for spinal metastasis and the in-hospital patient outcomes in the United States from 2000 to 2009. *Spine J* (2014) 14:1844–9. doi: 10.1016/j.spinee.2013.11.029
2. Fehlings MG, Nater A, Holmer H. Cost-effectiveness of surgery in the management of metastatic epidural spinal cord compression: a systematic review. *Spine* (2014) 39:S99–S105. doi: 10.1097/BRS.0000000000000525
3. Nasser R, Drazin D, Nakhla J, Al-Khouja L, Brien E, Baron EM, et al. Resection of spinal column tumors utilizing image-guided navigation: a multicenter analysis. *Neurosurgical Focus FOC* (2016) 41:E15. doi: 10.3171/2016.5.FOCUS16136
4. Ando K, Kobayashi K, Machino M, Ota K, Morozumi M, Tanaka S, et al. Computed tomography-based navigation system-assisted surgery for primary spine tumor. *J Clin Neurosci* (2019) 63:22–6. doi: 10.1016/j.jocn.2019.02.015
5. Nagashima H, Nishi T, Yamane K, Tanida A. Case report: osteoid osteoma of the c2 pedicle: surgical technique using a navigation system. *Clin Orthopaedics Related Research®* (2010) 468:283. doi: 10.1007/s11999-009-0958-8
6. Campos WK, Gasbarrini A, Boriani S. Case report: curetting osteoid osteoma of the spine using combined video-assisted thoracoscopic surgery and navigation. *Clin Orthopaedics Related Research®* (2013) 471:680–5. doi: 10.1007/s11999-012-2725-5
7. Sayari AJ, Pardo C, Basques BA, Colman MW. Review of robotic-assisted surgery: what the future looks like through a spine oncology lens. *Ann Trans Med* (2019) 7:224–4. doi: 10.21037/atm.2019.04.69
8. Tatsui CE, Lee SH, Amini B, Rao G, Suki D, Oro M, et al. Spinal Laser Interstitial Thermal Therapy: A Novel Alternative to Surgery for Metastatic Epidural Spinal Cord Compression. *Neurosurgery* (2016) 79:S73–82. doi: 10.1227/NEU.0000000000001444
9. Morassi LG, Kokkinis K, Evangelopoulos DS, Karargyris O, Vlachou I, Kalokairinou K, et al. Percutaneous radiofrequency ablation of spinal osteoid osteoma under ct guidance. *Br J Radiol* (2014) 87:20140003. doi: 10.1259/bjr.20140003
10. Wallace AN, Greenwood TJ, Jennings JW. Use of imaging in the management of metastatic spine disease with percutaneous ablation and vertebral augmentation. *Am J Roentgenol* (2015) 205:434–41. doi: 10.2214/AJR.14.14199
11. Yu F, Niu XH, Zhang Q, Zhao HT, Xu LH, Deng ZP. Radiofrequency ablation under 3d intraoperative iso-c c-arm navigation for the treatment of osteoid osteomas. *Br J Radiol* (2015) 88:20140535. doi: 10.1259/bjr.20140535
12. Mendelsohn D, Strelzow J, Dea N, Ford NL, Batke J, Pennington A, et al. Patient and surgeon radiation exposure during spinal instrumentation using intraoperative computed tomography-based navigation. *Spine J* (2016) 16:343–54. doi: 10.1016/j.spinee.2015.11.020
13. Woodard EJ, Leon SP, Moriarty TM, Quinones A, Zamani AA, Jolesz FA. Initial experience with intraoperative magnetic resonance imaging in spine surgery. *Spine* (2001) 26:410–7. doi: 10.1097/00007632-200102150-00018
14. Takahashi S, MoriKawa S, Saruhashi Y, MatsUsue Y, Kawakami M. Percutaneous transthoracic fenestration of an intramedullary neurenteric cyst in the thoracic spine with intraoperative magnetic resonance image navigation and thoracoscopy. *J Neurosurg: Spine* (2008) 9:488–92. doi: 10.3171/SPI.2008.9.11.488
15. Takahashi S, Saruhashi Y, Odate S, Matsusue Y, Morikawa S. Percutaneous aspiration of spinal terminal ventricle cysts using real-time magnetic resonance imaging and navigation. *Spine* (2009) 34:629–34. doi: 10.1097/BRS.0b013e31819b33d6
16. Tatsui CE, Nascimento CNG, Suki D, Amini B, Li J, Ghia AJ, et al. Image guidance based on mri for spinal interstitial laser thermotherapy: technical aspects and accuracy. *J Neurosurg: Spine* (2017) 26:605–12. doi: 10.3171/2016.9.SPINE16475
17. Gueziri HE, Santaguida C, Collins DL. The state-of-the-art in ultrasound-guided spine interventions. *Med Image Anal* (2020) 65:101769. doi: 10.1016/j.media.2020.101769
18. Prada F, Vetrano IG, Filippini A, Del Bene M, Perin A, Casali C, et al. Intraoperative ultrasound in spinal tumor surgery. *J Ultrasound* (2014) 17:195–202. doi: 10.1007/s40477-014-0102-9
19. Gueziri HE, Yan CX, Collins DL. Open-source software for ultrasound-based guidance in spinal fusion surgery. *Ultrasound Med Biol* (2020) 46(12):3353–68. doi: 10.1016/j.ultrasmedbio.2020.08.005
20. Drouin S, Kochanowska A, Kersten-Oertel M, Gerard IJ, Zelmann R, De Nigris D, et al. IBIS: an OR ready open-source platform for image-guided neurosurgery. *Int J Comput Assisted Radiol Surg* (2017) 12:363–78. doi: 10.1007/s11548-016-1478-0
21. Mercier L, Araujo D, Haegelen C, Del Maestro RF, Petrecca K, Collins DL. Registering pre- and postresection 3-dimensional ultrasound for improved visualization of residual brain tumor. *Ultrasound Med Biol* (2013) 39:16–29. doi: 10.1016/j.ultrasmedbio.2012.08.004
22. Gerard IJ, Kersten-Oertel M, Drouin S, MD JAH, Petrecca K, Nigris DD, et al. Combining intraoperative ultrasound brain shift correction and augmented reality visualizations: a pilot study of eight cases. *J Med Imaging* (2018) 5:1–12. doi: 10.1117/1.JMI.5.2.021210
23. Mercier L, Del Maestro RF, Petrecca K, Kochanowska A, Drouin S, Yan CX, et al. New prototype neuronavigation system based on preoperative imaging and intraoperative freehand ultrasound: system description and validation. *Int J Comput Assisted Radiol Surg* (2011) 6:507–22. doi: 10.1007/s11548-010-0535-3
24. Gueziri HE, Collins DL. Fast registration of ct with intra-operative ultrasound images for spine surgery. In: *Computational Methods and Clinical Applications for Spine Imaging*. Cham: Springer International Publishing (2018). p. 29–40. doi: 10.1007/978-3-030-13736-6_3
25. Gueziri HE, Drouin S, Yan CXB, Collins DL. Toward real-time rigid registration of intra-operative ultrasound with preoperative CT images for lumbar spinal fusion surgery. *Int J Comput Assisted Radiol Surg* (2019) 14:1933–43. doi: 10.1007/s11548-019-02020-1
26. Dath R, Ebinesan A, Porter K, Miles A. Anatomical measurements of porcine lumbar vertebrae. *Clin Biomech (Bristol Avon)* (2007) 22:607–13. doi: 10.1016/j.clinbiomech.2007.01.014
27. Sheng SR, Wang XY, Xu HZ, Zhu GQ, Zhou YF. Anatomy of large animal spines and its comparison to the human spine: a systematic review. *Eur Spine J* (2010) 19:46–56. doi: 10.1007/s00586-009-1192-5
28. Schroeder W, Martin K, Lorensen B. *The Visualization Toolkit An Object-Oriented Approach To 3D Graphics Fourth Edition*. New York, United States: Kitware (2006). doi: 10.1016/B978-012387582-2/50003-4
29. Cleary K, Anderson J, Brazaitis M, Devey G, DiGioia A, Freedman M, et al. Final report of the technical requirements for image-guided spine procedures workshop. *Comput Assisted Surg* (2000) 5:180–215. doi: 10.1002/1097-0150(2000)5:3<180::AID-IGS6>3.0.CO;2-C
30. Quené H, van den Bergh H. Examples of mixed-effects modeling with crossed random effects and with binomial data. *J Memory Lang* (2008) 59:413–25. doi: 10.1016/j.jml.2008.02.002
31. Quiñones-Hinojosa A, Kolen ER, Jun P, Rosenberg WS, Weinstein PR. Accuracy over space and time of computer-assisted fluoroscopic navigation in the lumbar spine in vivo. *Clin Spine Surg* (2006) 19:109–13. doi: 10.1097/01.bsd.0000168513.68975.8a

Conflict of Interest: The authors declare that the research was conducted in the absence of any commercial or financial relationships that could be construed as a potential conflict of interest.

frontiers in Oncology

REVIEW
published: 22 March 2021
doi: 10.3389/fonc.2021.659048

Current Limitations of Intraoperative Ultrasound in Brain Tumor Surgery

Andrej Šteňo, Ján Buvala, Veronika Babková, Adrián Kiss, David Toma and Alexander Lysak*

Department of Neurosurgery, Comenius University, Faculty of Medicine, University Hospital Bratislava, Bratislava, Slovakia

While benefits of intraoperative ultrasound (IOUS) have been frequently described, data on IOUS limitations are relatively sparse. Suboptimal ultrasound imaging of some pathologies, various types of ultrasound artifacts, challenging patient positioning during some IOUS-guided surgeries, and absence of an optimal IOUS probe depicting the entire sellar region during transsphenoidal pituitary surgery are some of the most important pitfalls. This review aims to summarize prominent limitations of current IOUS systems, and to present possibilities to reduce them by using ultrasound technology suitable for a specific procedure and by proper scanning techniques. In addition, future trends of IOUS imaging optimization are described in this article.

Keywords: intraoperative ultrasound, artifacts, pitfalls, training, neurosurgery

OPEN ACCESS

Edited by:
Francesco DiMeco, Fondazione IRCCS Istituto Neurologio Carlo Besta, Italy

Reviewed by:
Llewellyn Padayachy, University of Pretoria, South Africa
Giuseppe Maria Della Pepa, Fondazione Policlinico Universitario Agostino Gemelli IRCSS, Italy

****Correspondence:***
Andrej Šteňo
andrej.steno@fmed.uniba.sk

Specialty section:
This article was submitted to Neuro-Oncology and Neurosurgical Oncology, a section of the journal Frontiers in Oncology

Received: *26 January 2021*
Accepted: *03 March 2021*
Published: *22 March 2021*

Citation:
Šteňo A, Buvala J, Babková V, Kiss A, Toma D and Lysak A (2021) Current Limitations of Intraoperative Ultrasound in Brain Tumor Surgery. Front. Oncol. 11:659048. doi: 10.3389/fonc.2021.659048

INTRODUCTION

Standard conventional neuronavigation is a widespread tool for image guidance in brain tumor surgery. It has become standard of practice in many institutions for initial tumor localization, for surgical trajectory planning, and also for assessment of tumor margins during resection (1, 2). However, popularity of various intraoperative imaging methods continues to increase due to the well-known fact, that the accuracy of navigation may become unreliable after brain shift occurs (1, 3–5).

Intraoperative ultrasound (IOUS) has been used during resection of brain tumors for over four decades since early 1980s (6). However, despite the initial enthusiasm, this intraoperative imaging modality was not widely accepted, especially until the end of the millennium. There were various reasons for initial lack of acceptance of IOUS. First, the image quality of older IOUS systems was low. Second, oblique 2D IOUS views were unfamiliar to many neurosurgeons, used to evaluate computer tomography (CT) and magnetic resonance imaging (MRI) brain scans in standard three orthogonal planes—axial, coronal and sagittal. Third, visualization of large lesions in their full extent was problematic due to limited field of view of 2D IOUS probes. Fourth, as standard B-mode ultrasound does not selectively depict the MRI-contrast enhancing portion of diffuse high-grade gliomas, it could not be used for reliable identification and subsequent resection of this most malignant, enhancing glioma tissue. Fifth, many surgeons refused to change their surgical habits and perform horizontal craniotomies only in order to enable sufficient filling of resection cavity with fluid and appropriate ultrasound scanning. Sixth, difficulties in visualizing the bottom of the resection cavity due to IOUS artifacts were repeatedly reported, and this often resulted in insufficient visualization of tumor residua in this area. Seventh, distinct visualization of the entire sellar region during transsphenoidal approach was challenging.

Nowadays, some of these limitations can be minimized using modern IOUS equipment and proper methods of IOUS utilization. However, some pitfalls still persist, and solutions to overcome them are needed.

SUBOPTIMAL ULTRASOUND IMAGING

Image Quality

The main disadvantage of older two-dimensional (2D) IOUS systems was low image quality (7), mainly due to poor spatial resolution and dynamic range—identification of various brain structures was therefore challenging. Especially imaging of deeper structures such as thalamus and brainstem was insufficient, as low frequency probes of older IOUS systems offered very low spatial resolution. Insufficient imaging quality was evident especially when compared to MRI, which offered superior resolution and tissue differentiation (1).

Comparing to older devices, many new ultrasound systems have significantly better quality—one of the improvements is due to the ability of modern ultrasound systems to electronically and dynamically tune the frequency range of the imaging probe (8). Higher frequency means better image resolution, i.e. a better ability to differentiate two small targets as separate objects (8). However, the drawback of high frequency probes is the reduced penetration of acoustic waves in the tissue due to scattering and absorption (1), and thus insufficient visualization of deeper structures (8). As recommended by Unsgaard et al. (9), to obtain the best image, different probes should be used for imaging of lesions localized in different depth: a 5 MHz (4–8 MHz) probe gives optimal image quality at a distance of 2.5–6 cm from the probe tip, while for superficial lesions a 12 MHz linear probe is ideal as it provides the best image quality for the first few millimeters down to a depth of 4 cm (9). Using different probes for lesions at different depths in a series of 105 IOUS guided-surgeries, Mair et al. (10) introduced a grading system of ultrasonographic visibility for various intracerebral pathologies. Lesions difficult to visualize, having no clear border with normal brain represent Grade 1; lesions clearly identifiable, but with no clear border with normal tissue represent Grade 2; and lesions clearly identifiable, and with clear border represent Grade 3 (Grade 0 was considered for lesions not identifiable by IOUS). Only 8% out of 105 lesions were evaluated as grade 1, and none as grade 0.

Very good IOUS visualization of various non-irradiated brain lesions was repeatedly reported—predominantly of intra-axial tumors like gliomas and metastases (11–14), as well as of extra-axial tumors like meningiomas (11, 15). However, in patients who had received radiotherapy, the quality of ultrasound image often decreases (16). As evaluated by histopathology, a high-end intraoperative ultrasound system was proven to depict glioma (pseudo)borders at least as distinctly as a three-dimensional (3D) T2-weighted MRI image and better than a 3D T1-weighted MRI image (12). When high frequency ultrasound linear probe was used, the accuracy of residual low-grade glioma tissue detection by IOUS imaging was described to be comparable to high-field intraoperative MRI (17).

Nevertheless, the newest and perhaps the most detailed data presented by leading Norwegian group showed that MRI is superior in pre-resectional glioma visualization (18) as well as in visualization of small tumor remnants (19). This finding is important (**Figure 1**) despite the fact that in some cases glioma tissue may be better visualized by IOUS, as compared to high-field MRI (**Figure 2**).

Interestingly, in spite of reports from prominent neurosurgical centers stating that small deep-seated perforating lenticulostriate arteries (LSAs) cannot be identified by IOUS Doppler imaging (20, 21), these perforators may be in fact depicted (22) by power-Doppler. Using proper methodology and high-end IOUS devices, LSAs may be at least in some patients visualized comparably to MRI (figure). Hence, IOUS power Doppler imaging may serve as an important adjunct during resection of insular gliomas (**Figure 3**) (22). However, prospective studies are needed to evaluate real effectiveness of this relatively new method of intraoperative LSAs identification.

Anatomical Orientation and Large Lesions Visualization

Most neurosurgeons have extensive experience with the interpretation of CT and MRI images in three orthogonal planes—axial, coronal and sagittal. However, 2D IOUS image is dependent on the orientation of the ultrasound probe, and achieving IOUS scans in at least two exact orthogonal planes may be challenging, especially in small craniotomies (23). Because intraoperative 2D ultrasound views are mostly oblique (24), many neurosurgeons with little or no training/expertise may have considerable orientation problems during 2D IOUS-guided surgeries (25). Understanding the 2D ultrasound image is difficult particularly in areas with no cysts or ventricles visible (24). Another 2D IOUS problem is represented by the fact that ultrasound probes have a limited field of view. It is possible to evaluate only a section of brain tissue during 2D ultrasound scanning, and visualization of large lesions in their whole extent may be problematic.

These pitfalls together with aforementioned suboptimal image quality of older 2D IOUS systems caused preferable use of frameless neuronavigation based on preoperative CT or MRI for brain tumor-surgery guidance by many neurosurgeons (2, 26–31). Unlike 2D IOUS, frameless neuronavigation displays normal and pathological tissue in three orthogonal planes, and also enables preoperative planning of the craniotomy placement and surgical trajectory direction. Only a minority of neurosurgical centers continued in regular 2D IOUS use, mostly because of significant inaccuracy of neuronavigation after the occurrence of brain-shift, considering the fact that 2D IOUS offers a real-time imaging and is unaffected by brain-shift. Others solved the brain-shift problem by using intraoperative MRI for navigation data update (4, 5, 32); this solution however is much more expensive.

In order to simplify the interpretation of ultrasound imagery and allow quantification of brain-shift (33), some groups have

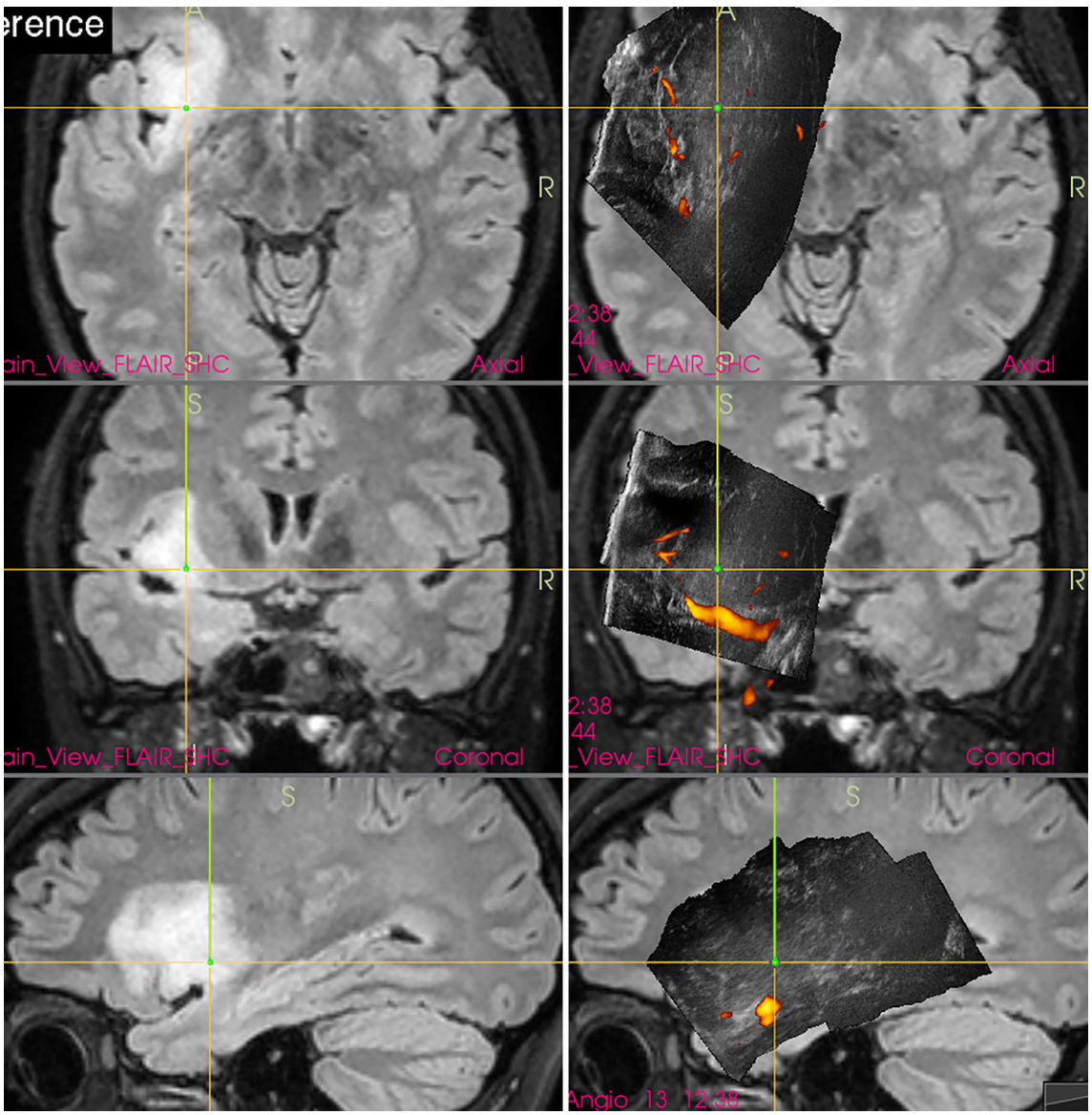

FIGURE 1 | Left-sided insular grade II astrocytoma **(Left column)** preoperative navigation 3D FLAIR MRI sequence (3-Tesla MRI scanner) **(Right column)** pre-resectional 3D IOUS image fused with navigation FLAIR MRI sequence. Note that the tumor tissue is only mildly hyperechoic and less distinctly visualized comparing to MRI. 3D, three-dimensional; IOUS, intraoperative ultrasound; FLAIR, fluid attenuated inversion recovery; MRI, magnetic resonance imaging.

connected ultrasound scanner to conventional neuronavigation, digitized the analog video signal from the scanner, and displayed a real-time 2D IOUS image on the navigation computer side by side with the corresponding MRI slice (**Figure 4**) (34–36). However, a much bigger step forward was the integration of neuronavigation and IOUS devices based on a digital interface between the ultrasound scanner and the navigation computer. This type of integration was the basis for the development of navigated 3D IOUS—a system that enables navigation using preoperative 3D MRI or CT data as well as intraoperative 3D ultrasound data (33). Three-dimensional ultrasound data is generated by summation of multiple 2D ultrasound images acquired by moving ultrasound probe freehand over the field of interest; the series of 2D IOUS images are then reconstructed to produce a 3D volume (37). These systems use ultrasound probes equipped with reflective marker reference frames and the position and orientation of the probe during the movement is tracked by means of a navigation camera system. After the scanning, 3D IOUS systems enable surgeons to visualize and navigate the whole volume of normal and pathological tissue that was scanned.

By means of combining frameless navigation with ultrasound, the navigated 3D IOUS systems solved prominent drawbacks of stand-alone conventional neuronavigation and 2D IOUS devices

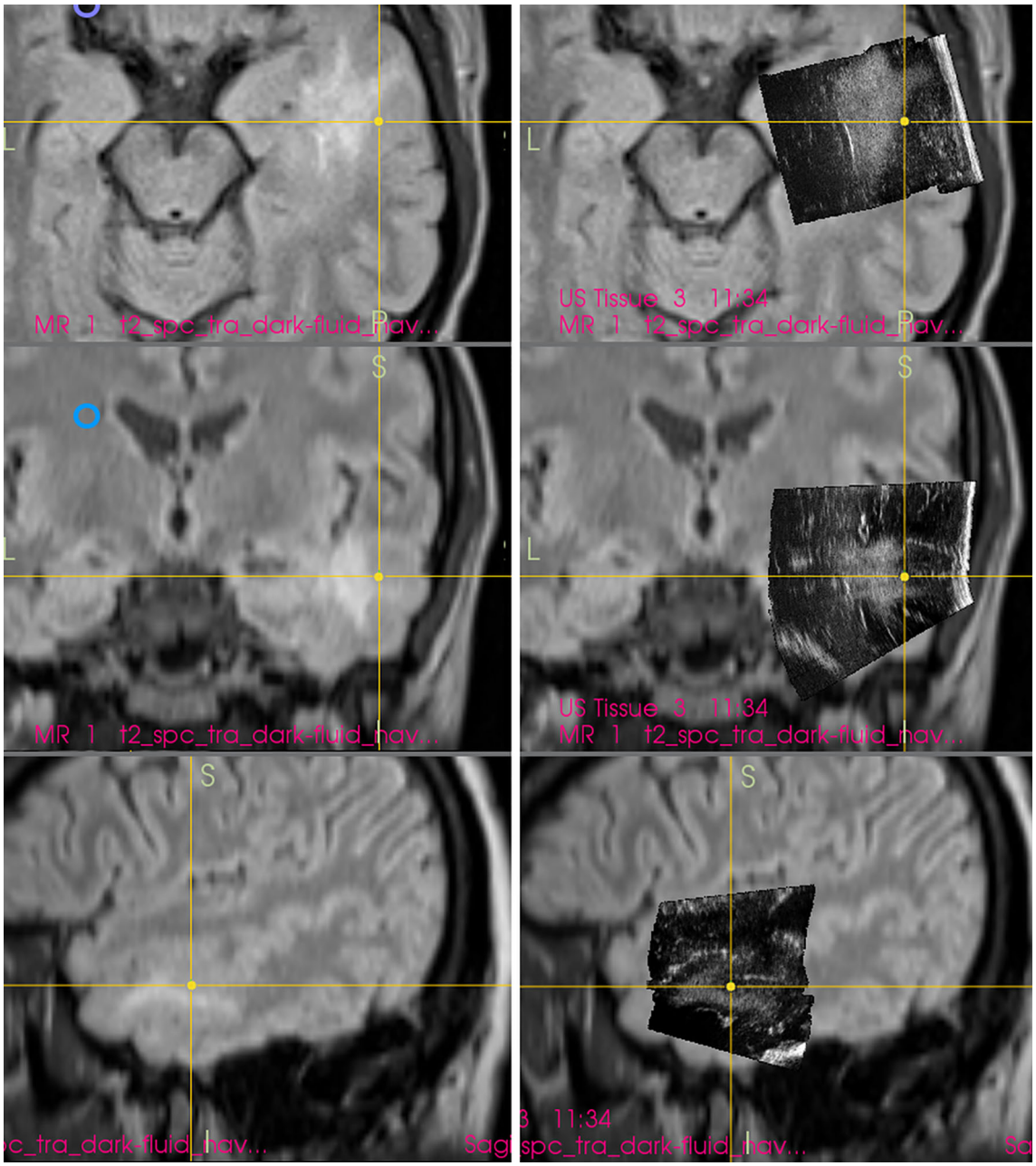

FIGURE 2 | Right-sided temporal grade II astrocytoma **(Left column)** preoperative navigation 3D FLAIR MRI sequence (1.5-Tesla MRI scanner) **(Right column)** pre-resectional 3D IOUS image fused with navigation FLAIR MRI sequence. Note that the hyperechoic tumor tissue is better visualized on IOUS image comparing to MRI. 3D, three-dimensional; FLAIR, fluid attenuated inversion recovery; MRI, magnetic resonance imaging; IOUS, intraoperative ultrasound.

—namely the brain-shift problem of navigation as well as the orientation and limited field of view problems of 2D IOUS (25). Even very large lesions, much larger than the ultrasound probe field of view, may be visualized in their whole extent using navigated 3D IOUS systems (**Figure 5**).

Automatic fusion with navigation MRI and/or CT sequence and rendering the ultrasound image in orthogonal planes make the recognition of normal and pathological structures much easier (38). In addition, navigated 3D IOUS provides almost real-time imaging and allows re-scanning of operating field as often as necessary, hence allows effective brain-shift compensation (25). Nevertheless, considering the fact that the "main" part of fused (combined) navigation-MRI/IOUS image is in fact ultrasound visualization of the operating field, knowledge of echogenicity of various normal and pathological brain structures is necessary.

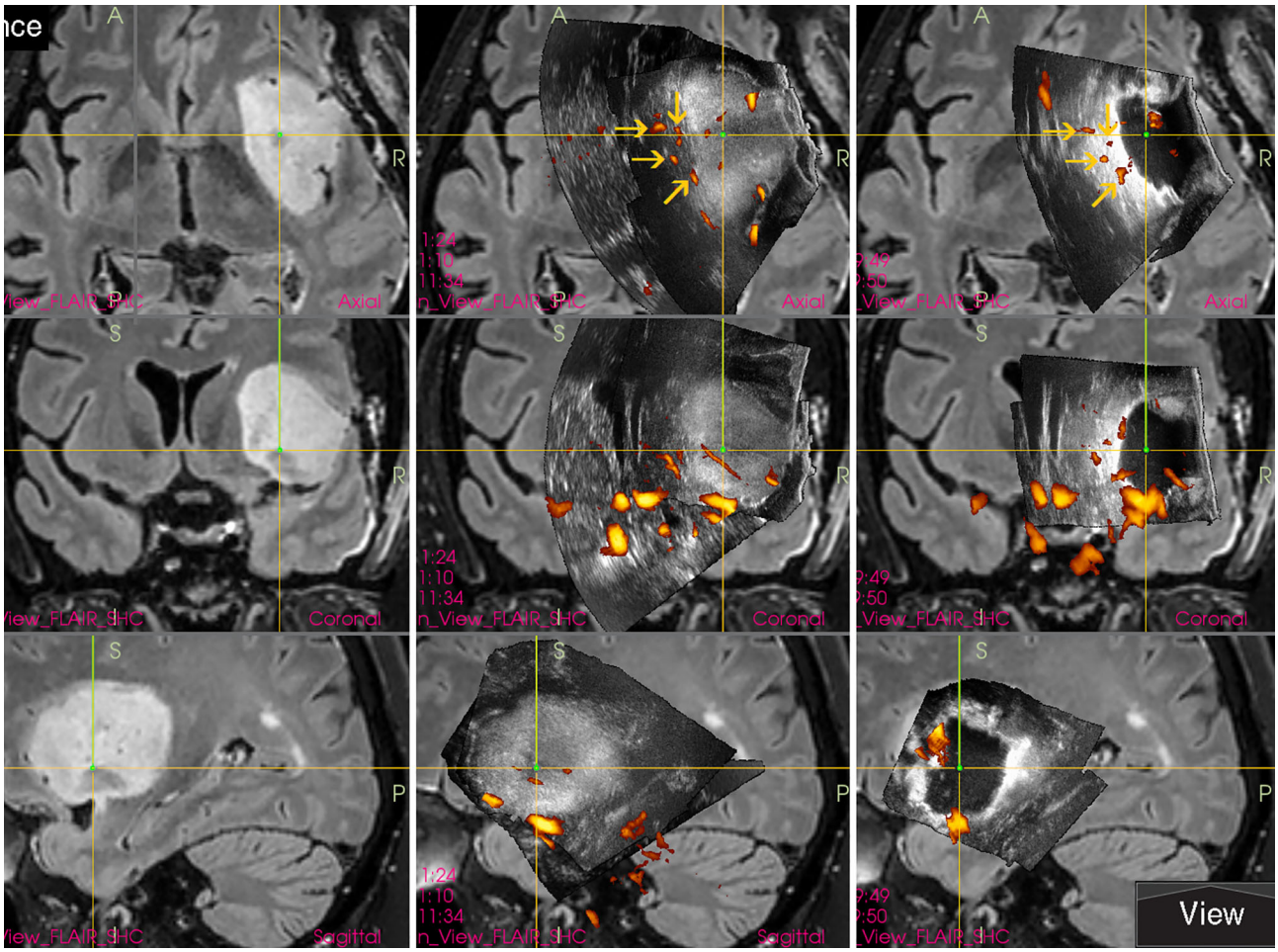

FIGURE 3 | Right-sided insular grade II astrocytoma **(Left column)** preoperative navigation 3D FLAIR MRI sequence **(Middle column)** pre-resectional 3D IOUS image fused with navigation FLAIR MRI sequence. Yellow arrows = lenticulostriate arteries visualized by 3D IOUS power-Doppler mode **(Right column)** 3D IOUS image acquired shortly before the end of resection. Note the close proximity of resection cavity bottom to the lenticulostriate arteries (arrows), intraoperative visualization of perforating arteries helped to prevent iatrogenic injury to them. 3D, three-dimensional; FLAIR, fluid attenuated inversion recovery; MRI, magnetic resonance imaging; IOUS, intraoperative ultrasound.

Another benefit of navigated 3D IOUS comparing to standard 2D IOUS is the fact that 3D IOUS is suitable for biopsies of deep-seated supratentorial lesions, as showed by the group of Moiyadi (39).

Selective Visualization of High-Grade Glioma Portion

Gross-total resection of high-grade gliomas is usually defined as a complete removal of contrast-enhancing glioma tissue evaluated on postoperative contrast-enhanced T1-weighted MRI (40). However, standard 2D or 3D IOUS based on B-mode ultrasound imaging often does not enable reliable selective identification of the most malignant portion of diffuse gliomas (**Figure 6**). Hence, intraoperative evaluation of the extent of resection of high-grade gliomas may be challenging when only B-mode IOUS is used, because both malignant tumor tissue and peritumoral edema, that is in fact usually a mixture of edema and infiltrating tumor cells (41), are hyperechoic.

A potential technique to differentiate between malignant glioma tissue and peritumoral edema is application of ultrasound contrast agents (42). Despite the fact that contrast-enhanced ultrasound (CEUS) agents, which are composed of small gaseous microbubbles, do not penetrate extravascularly (unlike MRI contrast agents which diffuse into the interstitium through disrupted blood–brain barrier), Prada et al. showed that glioblastoma contrast enhancement with CEUS is superimposable on that provided with preoperative gadolinium-enhanced T1-weighted MRI regarding location, margins, morphologic features, and dimensions, with a similar enhancement pattern (42). Hence, CEUS might play a decisive role in the process of maximizing glioblastoma

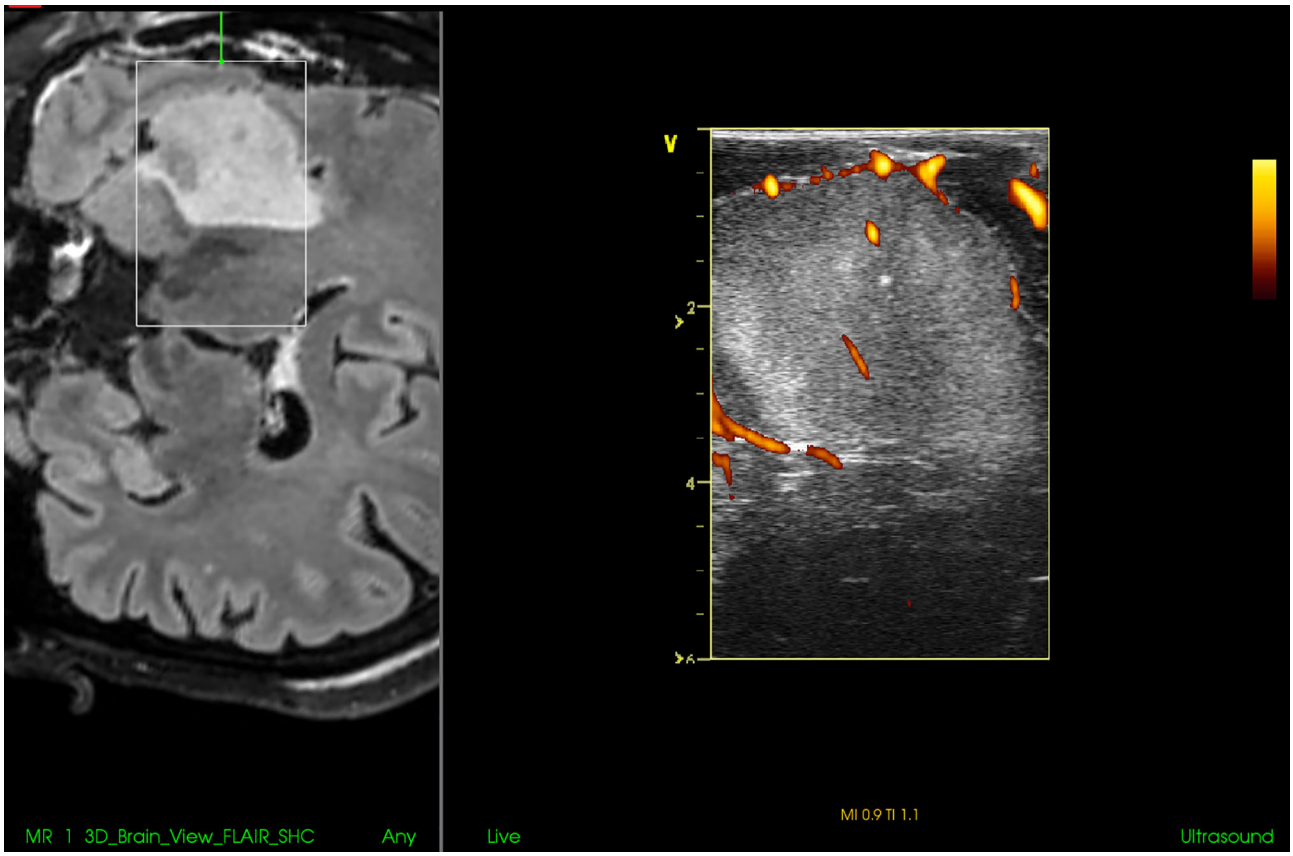

FIGURE 4 | Right-sided insular grade II astrocytoma. Visualization of the tumor before the resection using 12 MHz linear IOUS probe co-registrated with preoperative navigation 3D FLAIR MRI sequence. Note co-registration with navigation MRI facilitates anatomical orientation. 3D, three-dimensional; FLAIR, fluid attenuated inversion recovery; MRI, magnetic resonance imaging; IOUS, intraoperative ultrasound.

resection (43). Of note however, there is currently no commercially available navigated 3D IOUS system supporting CEUS, all IOUS devices enabling CEUS during brain surgeries are 2D.

Another technique to evaluate the extent of high-grade glioma tissue resection is utilization of B-mode IOUS together with 5-aminolevulinic acid (5-ALA) that enables selective malignant tissue visualization (44). In fact, these two methods can be complementary (45), and the combined use of both methods may minimize their pitfalls. Namely, a significant drawback of the intraoperative 5-ALA use is the fact that even a thin layer of intervening low-grade grade tissue is enough to lead to incorrect impression of complete high-grade tumor portion resection (46). Heterogeneous tumors with low-grade parts sometimes cannot be reliably resected by fluorescence-guided surgery alone, in these cases the additional use of intraoperative imaging is required (45, 47). At least in some cases, B-mode IOUS may help to identify larger high-grade glioma residua, and that despite the very challenging differentiation between high-grade tissue and surrounding edema without CEUS (**Figure 7**). In addition, the fact that some high-grade glioma patients may benefit from further resection of T2 abnormality (48, 49) that can be visualized by B-mode ultrasound but not by 5-ALA, underscores the potential benefit of simultaneous use of both methods.

Combination of IOUS and 5-ALA may be potentially useful also when focally malignized low-grade gliomas with no or non-significant contrast-enhancement are resected (50). In such cases, 3D IOUS provides adequate visualization of the whole hyperechoic tumor, while the small foci of anaplasia can be intraoperatively identified by 5-ALA fluorescence using the methodology pioneered by Widhalm et al. (51). This approach helps to achieve an extensive resection of glioma tissue and at the same time helps to identify anaplastic foci in order to avoid a sampling error.

ULTRASOUND ARTIFACTS

Perhaps the most important pitfall of all neurosurgical ultrasound devices is various ultrasound artifacts (52–54).

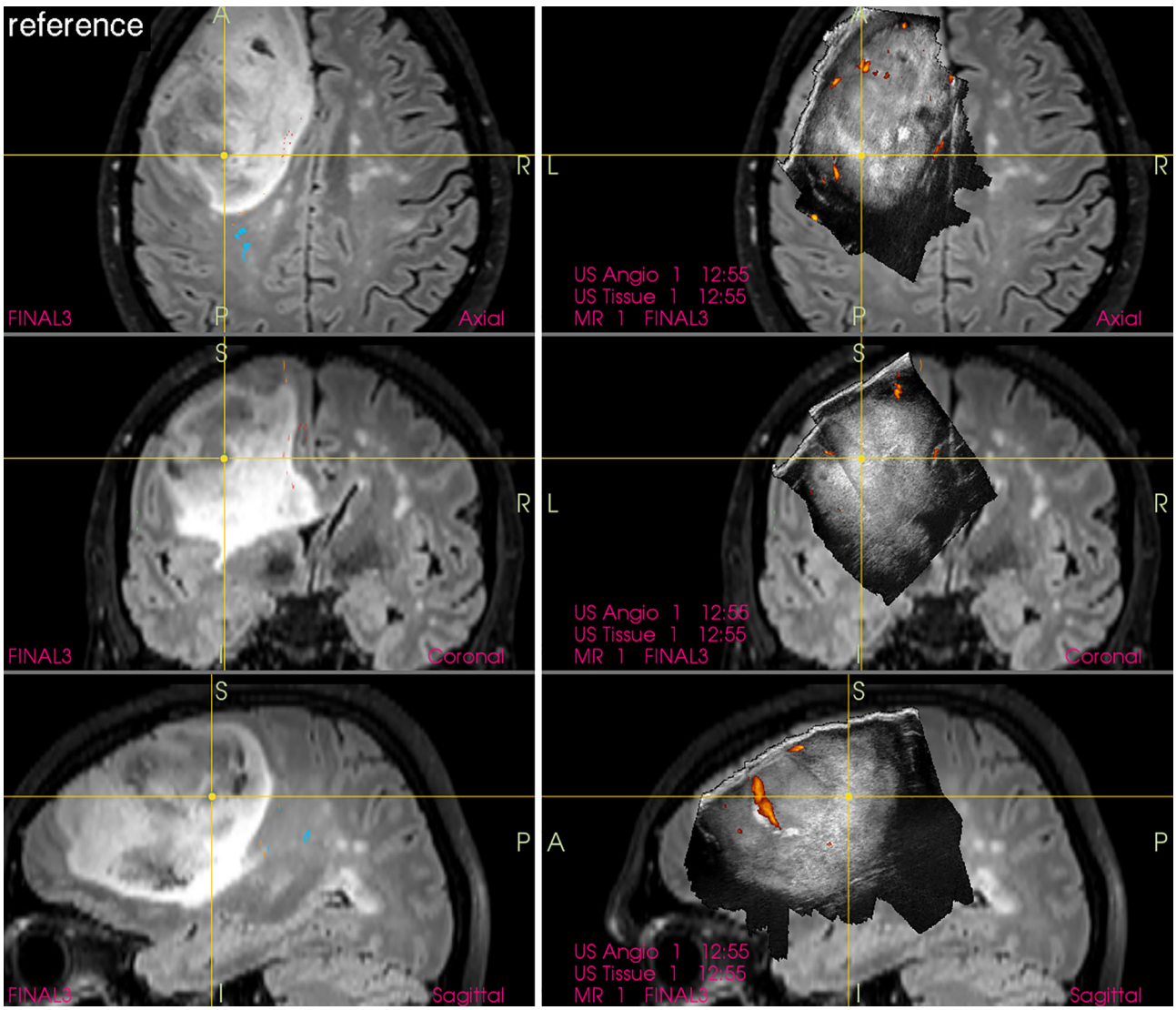

FIGURE 5 | Left-sided frontal grade II astrocytoma **(Left column)** preoperative navigation 3D FLAIR MRI sequence (3-Tesla MRI scanner) **(Right column)** pre-resectional 3D IOUS image fused with navigation FLAIR MRI sequence. Note visualization of the entire tumor on 3D IOUS image despite its large size. 3D, three-dimensional; FLAIR, fluid attenuated inversion recovery; MRI, magnetic resonance imaging; IOUS, intraoperative ultrasound.

From practical point of view, the most prominent problem is the acoustic enhancement artifacts (AEAs). These artifacts appear at the bottom of the resection cavity after some tumor debulking (13, 55), when ultrasound probe is placed at the level of brain surface and ultrasound waves penetrate through a higher column of saline solution. The appearance of AEAs is due to a large difference between a very low attenuation of acoustic waves in saline solution and high attenuation of acoustic waves in (normal or pathological) tissue (55, 56). Because AEAs are, similarly as the majority of brain tumors, hyperechoic, the ultrasonic depiction of medial tumor borders after some tumor debulking may be challenging (53). Acoustic enhancement artifacts are especially significant during resections of voluminous tumors and large resection cavities, as the degree of enhancement depends on the distance that ultrasound waves have traveled in saline. Importantly, AEAs may often preclude the detection of tumor remnants at the bottom of the resection cavity and make IOUS unreliable (**Figure 8**) (52). Understandably, this happens mostly towards the end of resection, when brain-shift usually occurs and intraoperative imaging is needed most (53).

Several methods that enable differentiation between AEAs and tumor remnants and estimate the extent of resection were presented: The first possibility is to evaluate the bottom of the resection cavity by moving the probe. In real-time 2D IOUS, the location of the AEAs in the image will

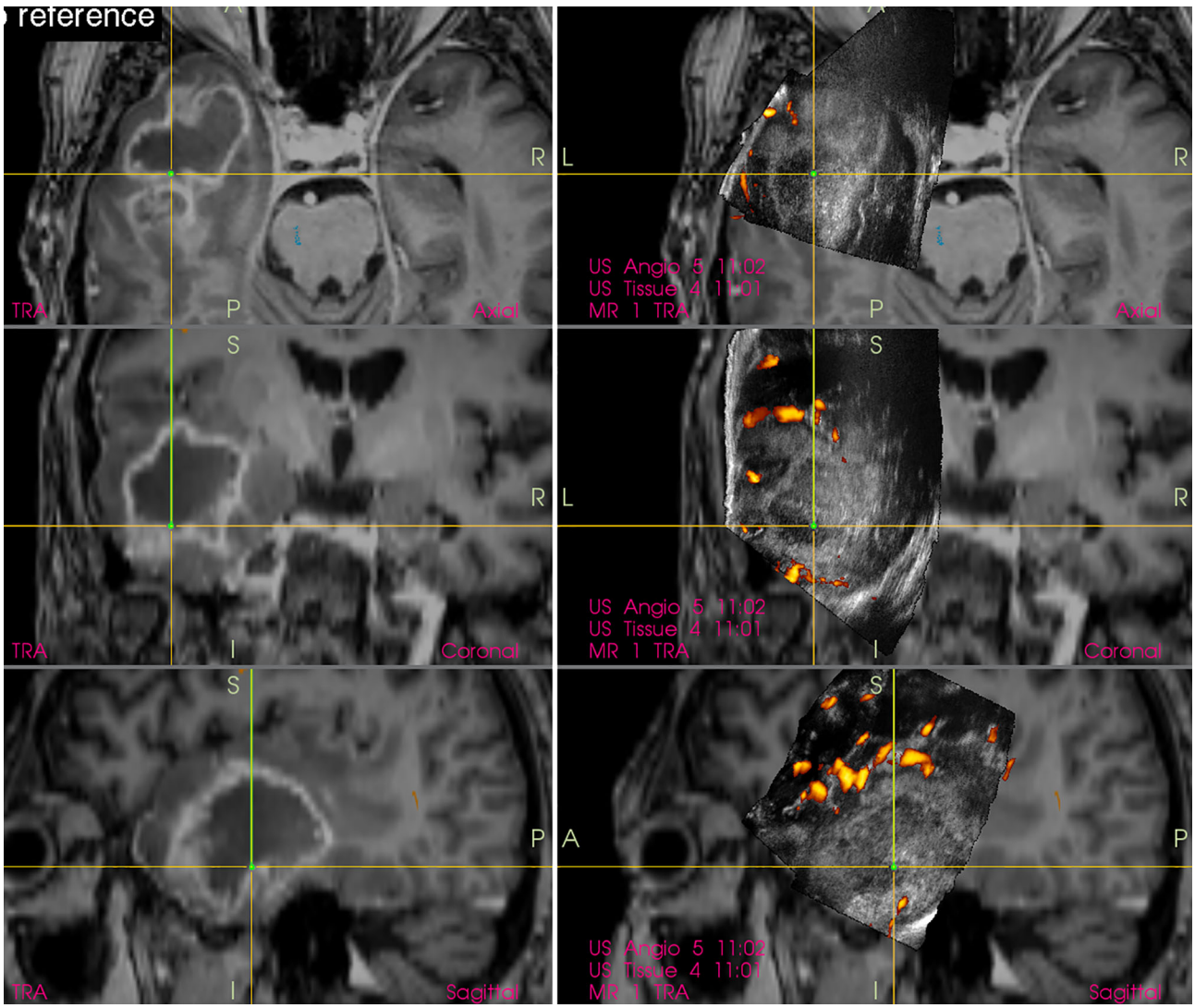

FIGURE 6 | Right-sided temporal glioblastoma **(Left column)** preoperative navigation 3D contrast-enhanced T1-weighted MRI sequence displaying high-grade tumor showing typical ring enhancement **(Right column)** pre-resectional 3D IOUS image fused with navigation MRI. Note that the hyperechoic high-grade tumor tissue is not selectively identifiable on the IOUS image, as the surrounding edematous and infiltrated brain (non-enhancing on MRI) is hyperechoic as well. 3D, three-dimensional; MRI, magnetic resonance imaging; IOUS, intraoperative ultrasound.

move when the position and angle of ultrasound probe has changed (55).

Another possibility to indirectly distinguish AEAs and residual tumor is a comparison between pre-resectional and updated ultrasound image, performed during or after resection. If the hyperechoic area is localized in a region where no tumor was present before the resection, it is most probably a bright artifact and not a real tumor remnant (55, 57).

Thirdly, AEAs may be minimized by inserting a small ultrasound probe into the resection cavity (13, 55, 57, 58). By doing so, the column of saline solution between the tip of the miniature probe and scanned tissue at the bottom of resection cavity is smaller than when scanning with a larger probe placed at the level of the brain surface. Shortening the column of saline solution reduces the AEAs at the bottom of resection cavity, and the structures in the medial part of resection cavity can be distinctly depicted (**Figure 9**). However, this method is not without limitations. Small probes have a very limited field of view (43), which may be a significant limiting factor predominantly when these probes are used with 2D IOUS systems (59). Under such circumstances the anatomical orientation may be difficult (43). On the other hand, when used with navigated 3D IUOS, this pitfall may be at least partially minimized, as described by our group (59). Nevertheless, artifacts reduction using mini-probes is certainly not ideal. While frequently allowing depiction of tumor

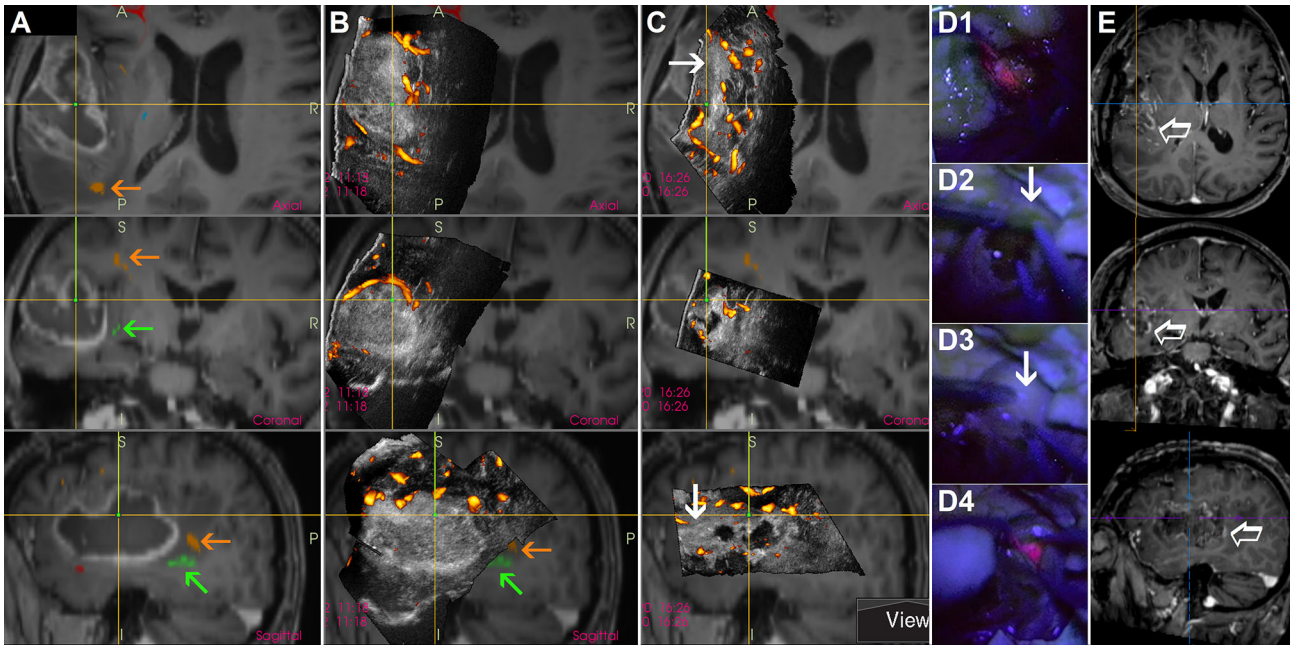

FIGURE 7 | Awake resection of a left-sided temporal glioblastoma guided by direct electrical stimulation, navigated intraoperative 3D IOUS and 5-aminolevulinic acid **(A)** preoperative navigation 3D contrast-enhanced T1-weighted MRI sequence with implemented tractography. Orange arrows = arcuate fascicle. Green arrows = inferior fronto-occipital fascicle **(B)** Pre-resectional 3D IOUS image fused with navigation MRI. Orange arrows = arcuate fascicle. Green arrows = inferior fronto-occipital fascicle **(C)** 3D IOUS image acquired during the resection. Despite the absence of red fluorescence in the anterior part of the resection cavity at the time of IOUS scanning, ultrasound image showed a large nodular tumor residuum in this area (arrows) **(D1)** Distinct red fluorescence observed shortly after the resection beginning **(D2, D3)** Absence of red fluorescence in the anterior part of the resection cavity. Arrow—presumably high grade tumor part identified using actual 3D IOUS scans **(D4)** Distinct red fluorescence after cortical resection **(E)** Postoperative MRI performed 72 hours after the surgery. Empty arrow—contrast-enhancing residual tumor intentionally left in place, electrical stimulation of inferior fronto-occipital fascicle in this area elicited semantic paraphasias. 3D, three-dimensional; MRI, magnetic resonance imaging; IOUS, intraoperative ultrasound.

remnants, it is sometimes problematic to maintain the same distance between the tip of the mini-probe and the resection cavity bottom; when this distance becomes larger AEAs appear (**Figure 9**). Next, while some linear probes used for intracavitary visualization allow high resolution imaging (17), image quality of other mini-probes is far from ideal. In addition, even small probes may be too bulky to be safely inserted into the resection cavity in between deliberated bridging veins, which may hinder mini-probe insertion (60).

A new solution for this longstanding problem may be minimizing the AEAs by utilizing the artifact reducing acoustic coupling fluid. This fluid was developed by the group of G. Unsgaard (55, 56); because the fluid attenuates ultrasound energy similarly to normal brain tissue, the AEAs are minimized. Promising results of phase one clinical study were recently published (61).

CHALLENGING PATIENT POSITIONING

During scanning the operating field with the ultrasound probe placed at the level of brain surface the resection cavity has to be filled with fluid, most often saline solution (9). If air becomes trapped in the resection cavity, the adequate visualization is compromised. At the interface with structures characterized by very low acoustic impedance (such as entrapped air), the sound will be completely reflected and cannot propagate beyond these interfaces—an "acoustic vacuum" will be created (62). Therefore, the position of the patient's head should enable horizontal position of the craniotomy; in that way fluid will fill a whole resection cavity. However, horizontal placement of the craniotomy may not be optimal in every type of surgery—for example in awake resections of tumors growing close to the Rolandic area and/or supplementary motor area performed in semi-sitting position (which is most comfortable for patients) (**Figure 10**). In order to keep the fluid within the resection cavity in cases when the craniotomy is not placed horizontally, a miniature barrier made from bone-vax may be effectively used (50) (**Figure 11**). This "miniature dam" allows sufficient filing of the resection cavity with fluid and appropriate scanning. Another possible solution in cases with non-horizontal placement of the craniotomy is insertion of the hockey stick-shaped ultrasound probe into the resection cavity, as described by Coburger et al. (17).

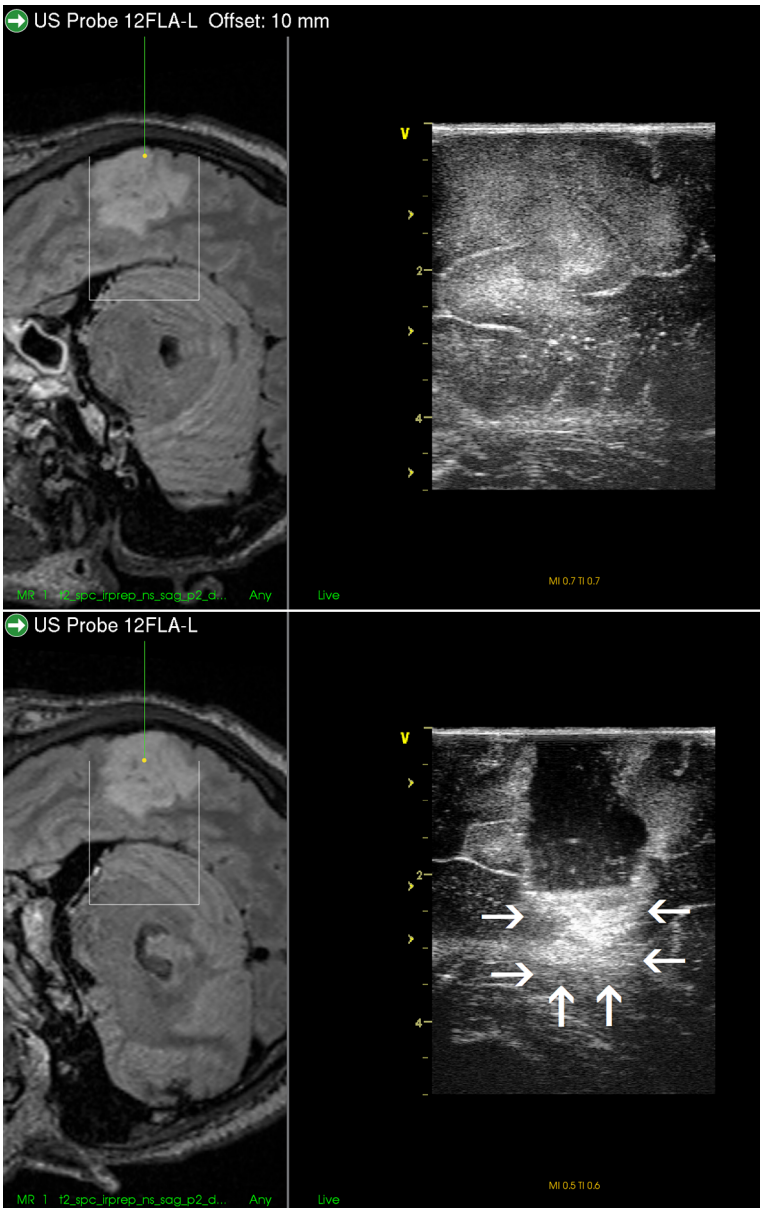

FIGURE 8 | Right-sided temporal grade II oligodendroglioma **(Upper row)** visualization of the tumor before the resection using 12 MHz linear probe co-registrated with preoperative navigation 3D FLAIR MRI sequence **(Lower row)** visualization of the tumor after resection of the central tumor part. Note clear visualization of the tumor residua on the sides of the resection cavity, and large acoustic enhancement artifact at the resection cavity-bottom precluding identification of potential tumor remnant in this area. 3D, three-dimensional; FLAIR, fluid attenuated inversion recovery; MRI, magnetic resonance imaging.

ULTRASOUND VISUALIZATION OF SELLAR REGION

Despite the fact that a variety of IOUS transducers have been applied to transsphenoidal surgery, the significance of endonasal IOUS in the context of transsphenoidal tumor surgeries is still unclear (1). While several reports describe IOUS as a useful adjunct during transsphenoidal resections of microadenomas (63–65) as well of macroadenomas (66–72), IOUS imaging is generally not considered to be a comparable alternative to intraoperative MRI during resections of sellar tumors (73). There are several pitfalls of IOUS use during trassphenoidal procedures, especially during resections of macroadenomas and giant pituitary adenomas. Firstly, while preoperative imaging of these lesions usually includes coronal T1- and T2-weighted and sagittal T1-weighted MRI scans, as well as coronal and sagittal postcontrast T1-weighted MRI scans (74), only very few reports describe ultrasound imaging

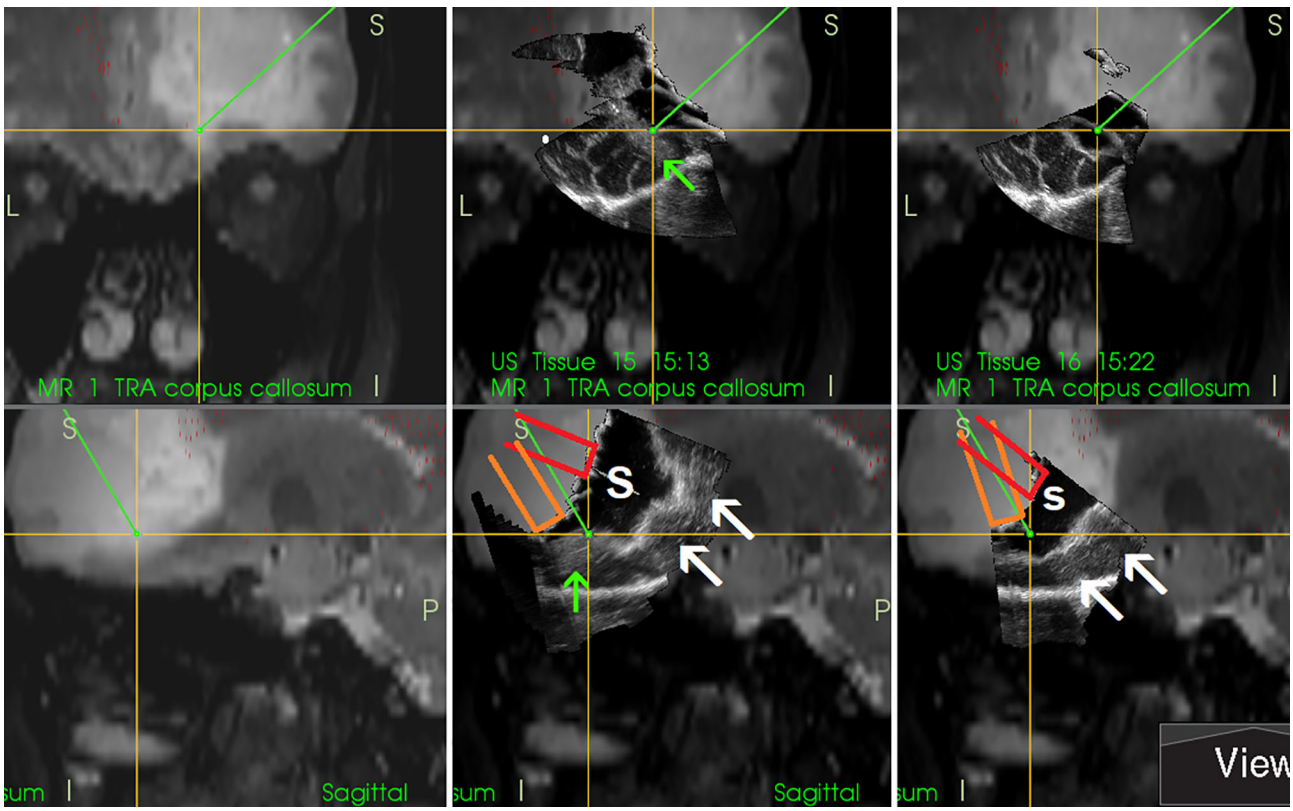

FIGURE 9 | Right-sided frontal grade II oligo-astrocytoma **(Left column)**—3D T2-weighted navigation sequence **(Middle column)** 3D IOUS image fused with navigation MRI. The tip of the pointer (green line) points at small tumor residuum (green arrow) visualized by miniprobe inserted into the resection cavity. Red and orange lines: schematic depiction of the miniprobe position within the resection cavity during the scanning. Note that acoustic enhancement artifacts appeared when the distance between the probe-tip and the scanned tissue became larger (arrows) **(Right column)** The same intraoperative situation as shown in the middle column, 3D IOUS image was acquired after resection of identified tumor residuum. 3D, three-dimensional; MRI, magnetic resonance imaging; IOUS, intraoperative ultrasound; S, hypoechoic saline solution within the resection cavity.

both in sagittal and coronal planes (66, 67). On the contrary, numerous IOUS probes used for intraoperative imaging during transsphenoidal procedures offer nonintuitive imaging planes most neurosurgeons are unfamiliar with (69). Secondly, imaging results and interpretation are highly dependent on the skills of the investigator and the resolution of many transducers is low (73). Thirdly—there is currently no commercially available ultrasound device that would enable 3D IOUS reconstructions and image rendering in orthogonal planes, which might improve the surgeon's ability to understand ultrasound imaging of the sellar region (1).

Nevertheless, the available IOUS devices may still offer some important benefits during resections of pituitary tumors. Most importantly, based on the differentiation of the audio signal of a micro-Doppler probe together with neuronavigation, the position of the internal carotid artery within the adenoma-invaded cavernous sinus may be identified and an injury with brisk arterial bleeding can be avoided (73, 75). In addition, the position of the carotid artery may be identified also by its visualization using small, side-looking, high-frequency ultrasound probe (68). Next, some IOUS systems enable visualization of suprasellar space, and identification and further resection of residual suprasellar adenoma tissue (**Figure 12**) (67). This may be of particular importance during resection of giant adenomas, as the suprasellar tumor portion may be unintentionally left in place in spite of endoscope utilization. Identification of unnoticed large suprasellar residua using intraoperative imaging might be crucial to prevent hemorrhagic infarction of the tumor, compression of the hypothalamus and potentially fulminant course (76, 77). Lastly, in spite of aforementioned limitations, current IOUS use may contribute to better surgical results as compared to transsphenoidal resections without intraoperative imaging (72).

FUTURE PERSPECTIVES

Despite the fact that more than four decades have passed since IOUS was initially introduced during a brain tumor resection (6), this intraoperative imaging method still needs substantial improvement to achieve widespread acceptance. Nevertheless,

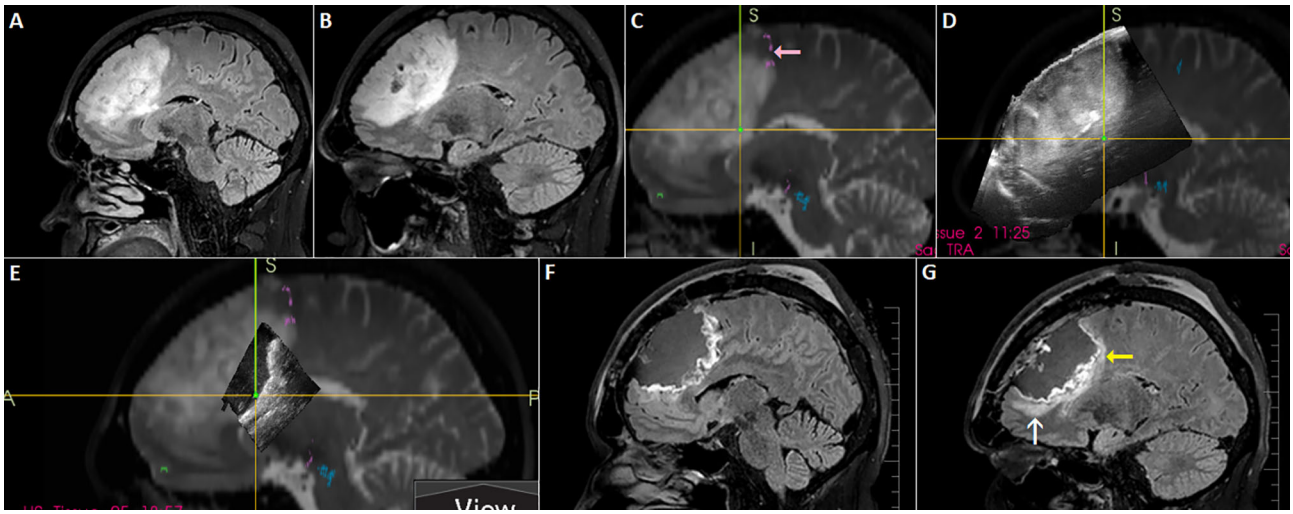

FIGURE 10 | Left-sided frontal oligodendroglioma resected in a semi-sitting position. **(A, B)** Preoperative sagittal FLAIR MRI sequence **(C)** 3D T2 sequence fused with tractography. Note involvement of tracts originating in pre-supplemetary motor area (pink arrow) **(D)** 3D IOUS image fused with navigation MRI **(E)** Incomplete filling of the resection cavity with saline due to non-horizontal placement of the craniotomy resulted in insufficient scanning of anterior part of the resection cavity **(F, G)** Postoperative sagittal FLAIR MRI sequence showing resectable residuum (white arrow), as well as residual tumor involving eloquent tracts (yellow arrow). 3D, three-dimensional; FLAIR, fluid attenuated inversion recovery; MRI, magnetic resonance imaging; IOUS, intraoperative ultrasound.

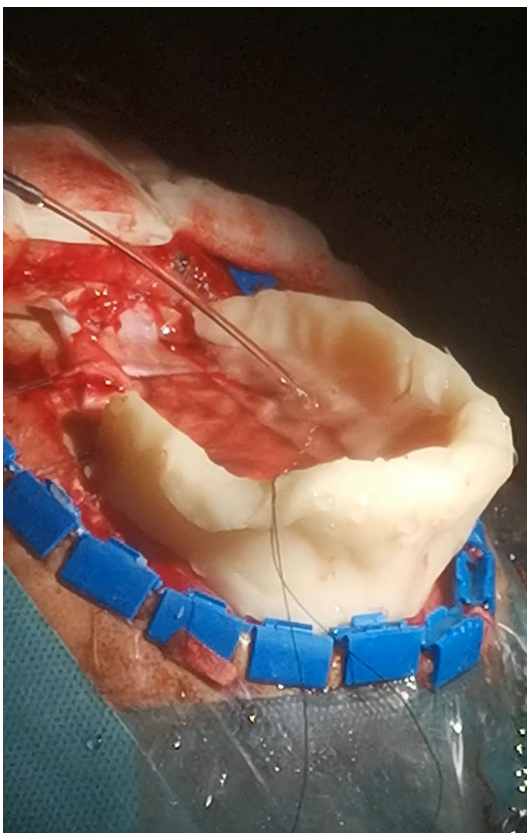

FIGURE 11 | Bone-wax mini-barrier used during removal of a precentral tumor performed in semi-sitting position.

the development of neurosurgical IOUS since the beginning of the millennium was substantial, and some pitfalls are close to reasonable solutions. On the contrary, other drawbacks need further development of the neurosurgical IOUS technology.

The prominent problem regarding ultrasound acoustic enhancement artifacts, maybe the biggest drawback of all neurosurgical IOUS devices, might soon be minimized by acoustic coupling fluid mimicking brain tissue.

Introduction of CEUS in order to guide resections of brain tumors made identification and subsequent resection of contrast enhancing malignant glioma tissue much easier. However, an important limitation is the fact that only very few commercially available ultrasound devices dedicated to neurosurgery enable CEUS, and none of them is 3D.

Interpretation of IOUS image during transsphenoidal tumor resections could be significantly easier, if new ultrasound transducers enabling distinct visualization of the sellar region in sagittal and coronal planes were developed, considering the fact that these (and not the oblique) planes are familiar to most pituitary surgeons. Development of new elongated thin ultrasound probes dedicated for intracavitary scanning might be also helpful during identification of residual glioma tissue. The important aspect of the development of new IOUS probes is the achievement of sterile intraoperative working conditions. A neurosurgical IOUS probe can be either sterilized or, if sterilization is not possible, covered with sterile sheath containing sterile coupling gel (1). Sterilization protocols of IOUS probes that contact brain tissue and cerebrospinal fluid must strictly respect regional regulations. If sterile covers are used, they should be fit tightly to the probe (1) in order to minimize the artifacts and to not alter the (special) probe shape and/or significantly enlarge the actual probe volume.

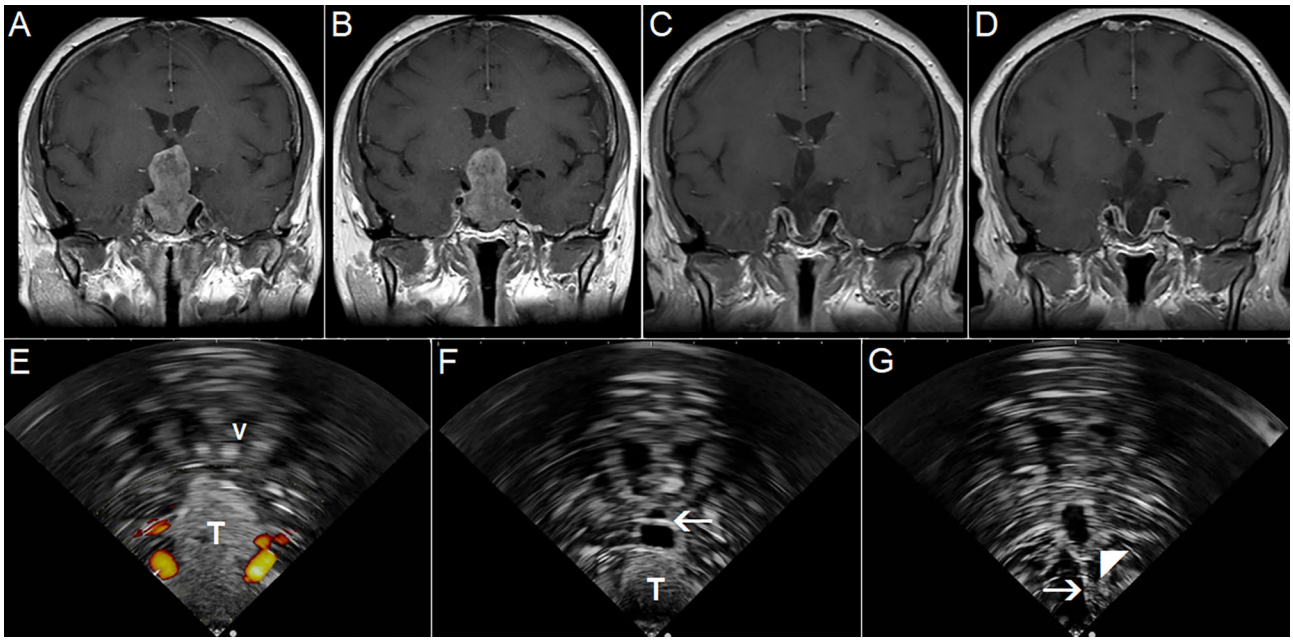

FIGURE 12 | Pituitary macroadenoma invading left cavernous sinus **(A, B)** Preoperative coronal contrast-enhanced T1 MRI sequence **(C, D)** Postoperative coronal contrast-enhanced T1 MRI sequence, small tumor residuum was intentionally left in the left cavernous sinus **(E)** Pre-resectional 2D IOUS image using flexible mini-probe, note distinct depiction of the tumor tissue as well as visualization of upper segments of carotid arteries by power-Doppler mode **(F)** Intraoperative 2D IOUS image after partial tumor resection. Note partial decompression of the third ventricle with depicted interthalamic adhesion (arrow) **(G)** 2D IOUS image after tumor resection, note pituitary stalk is distinctly visible (arrow) as well as the floor of the 3rd ventricle (arrowhead). 2D, two-dimensional; MRI, magnetic resonance imaging; IOUS, intraoperative ultrasound; V, lateral ventricle; T, tumor.

Introduction of navigated 3D IOUS reduced anatomical orientation problems caused by nonintuitive oblique planes during many types of brain surgeries by rendering IOUS images in orthogonal planes. Nevertheless, only a few studies examining effectiveness of navigated 3D IOUS utilization during transsphenoidal surgeries and CEUS-guided brain tumor resections were reported (78, 79). Research in this area should continue and result into commercially available navigated 3D IOUS systems enabling both aforementioned types of intraoperative imaging.

Correct positioning of patients before IOUS-guided resections in order to allow sufficient filling of resection cavity with fluid may be challenging; utilization of alternative adjuncts such as mini-barriers may be required. However, it is necessary to emphasize that patient positioning during intraoperative MRI-guided surgeries on the MRI table is sometimes also less-than-ideal, especially during awake tumor resections (80). Regarding awake procedures, it is worth noting that IOUS is a less time-consuming imaging modality than intraoperative MRI (50). This might be an important factor during procedures performed in conscious patients, as awake tumor resections have limited duration due to patient fatigue (81). Comparative studies examining effectiveness of both imaging modalities during awake resections should be conducted.

Traditional perception of intraoperative ultrasound as a modality with low image quality is slowly being overcome by innovation of ultrasound devices and ultrasound transducers. New high frequency IOUS probes may have strikingly high-resolution image. Visualization of tiny perforating arteries using power-Doppler mode seems to be at least comparable to MRI devices (**Figure 13**) (22).

Of note, as IOUS is strongly investigator-dependent, sufficient knowledge on ultrasound imaging of normal and pathological brain structures, as well as proper training are crucial for successful course of IOUS-guided resections (82). Recent IOUS simulation methods e.g. "virtual probes" (82) or IOUS-simulation smartphone applications (82), and practice on phantom (83) or animal (84) models under supervision of expert sonographers are recommended in order to refine scanning and surgical techniques (1). As showed recently by group of DiMeco, current high-end 2D IOUS systems integrated with neuronavigation may be in experienced hands of a significant benefit in terms of both extent of brain tumor resections and neurological outcomes (85). However, further prospective studies are necessary to evaluate impact of IOUS on surgical results (86, 87).

Lastly, algorithms allowing brain shift compensation based on preoperative MRI-to-IOUS rigid registration were already presented and their effectiveness was evaluated both during and after surgical procedures (88). While the rigid registration improved the alignment of the MRI and IOUS image volumes, considering the fact that brain-shift is a nonlinear process, deformable registration has the potential to further improve the results (88). Future sophisticated fusion algorithms

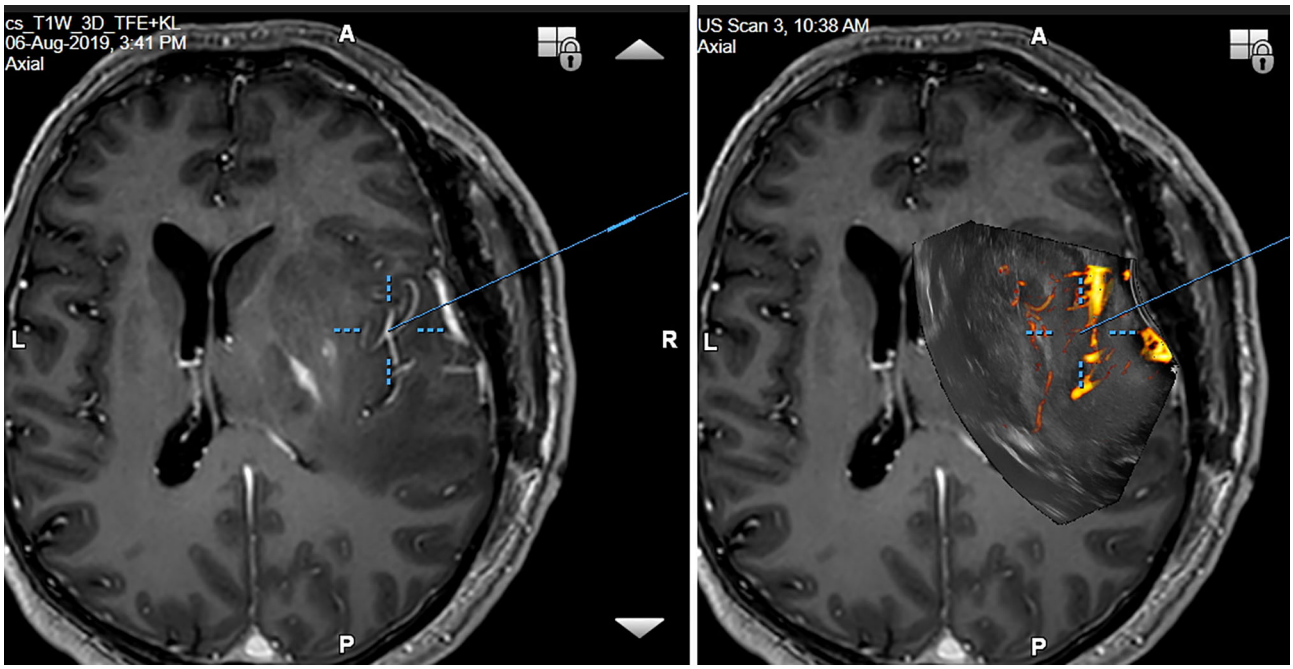

FIGURE 13 | Right-sided temporo-insular glioma (reoperation after previous urgent brainstem decompression) **(Left column)** preoperative navigation 3D contrast-enhanced T1-weighted MRI sequence (3-Tesla MRI scanner) **(Right column)** pre-resectional 3D IOUS image fused with navigation MRI using a high-end navigated 3D IOUS system. Note the excellent visualization of perforating lenticulostriate arteries under the infiltrated right insula. 3D, three-dimensional; MRI, magnetic resonance imaging; IOUS, intraoperative ultrasound.

might use IOUS image as anatomical reference, similarly to intraoperative CT, and enable deformation of preoperative 3D MRI image into "virtual intraoperative MRI" (89).

AUTHOR CONTRIBUTIONS

AŠ—manuscript writing, figure development, literature review, and data acquisition. JB—data acquisition and manuscript editing and review. VB—data acquisition and manuscript editing and review. AK—data acquisition and manuscript editing and review. DT—data acquisition and manuscript editing and review. AL—data acquisition and manuscript editing and review. All authors contributed to the article and approved the submitted version.

FUNDING

This work was supported by the Scientific grant agency of the Ministry of education of the Slovak republic and the Slovak academy of sciences (VEGA) in the form of grant (number 1/0719/18)

REFERENCES

1. Sastry R, Bi WL, Pieper S, Frisken S, Kapur T, Wells W3rd, et al. Applications of Ultrasound in the Resection of Brain Tumors. *J Neuroimaging* (2017) 27 (1):5–15. doi: 10.1111/jon.12382
2. Dasenbrock HH, See AP, Smalley RJ, Bi WL, Dolati P, Frerichs KU, et al. Frameless Stereotactic Navigation during Insular Glioma Resection using Fusion of Three-Dimensional Rotational Angiography and Magnetic Resonance Imaging. *World Neurosurg* (2019) 126:322–30. doi: 10.1016/j.wneu.2019.03.096
3. Gerard IJ, Kersten-Oertel M, Petrecca K, Sirhan D, Hall JA, Collins LC. Brain shift in neuronavigation of brain tumors. A review. *Med Image Anal* (2017) 35:403–20. doi: 10.1016/j.media.2016.08.007
4. Nimsky C. Intraoperative MRI in glioma surgery: proof of benefit? *Lancet Oncol* (2011) 12(11):982–3. doi: 10.1016/S1470-2045(11)70219-4
5. Nimsky C, Ganslandt O, Cerny S, Hastreiter P, Greiner G, Fahlbusch R. Quantification of, visualization of, and compensation for brain shift using intraoperative magnetic resonance imaging. *Neurosurgery* (2000) 47:1070–80. doi: 10.1097/00006123-200011000-00008
6. Rubin JM, Mirfakhraee M, Duda EE, Dohrmann GJ, Brown F. Intraoperative ultrasound examination of the brain. *Radiology* (1980) 137(3):831–2. doi: 10.1148/radiology.137.3.6255514
7. Unsgaard G, Gronningsaeter A, Ommedal S, Nagelhus Hernes TA. Brain operations guided by real-time two-dimensional ultrasound: new possibilities as a result of improved image quality. *Neurosurgery* (2002) 51(2):402–11. doi: 10.1227/01.NEU.0000019873.66709.0D
8. Unsgaard G, Rygh OM, Selbekk T, Müller TB, Kolstad F, Lindseth F, et al. Intra-operative 3D ultrasound in neurosurgery. *Acta Neurochir* (2006) 148 (3):235–53. doi: 10.1007/s00701-005-0688-y
9. Unsgård G, Solheim O, Lindseth F, Selbekk T. Intra-operative imaging with 3D ultrasound in neurosurgery. *Acta Neurochir Suppl* (2011) 109:181–6. doi: 10.1007/978-3-211-99651-5_28
10. Mair R, Heald J, Poeata I, Ivanov M. A practical grading system of ultrasonographic visibility for intracerebral lesions. *Acta Neurochir* (2013) 155(12):2293–8. doi: 10.1007/s00701-013-1868-9

11. Velthoven VV. Intraoperative ultrasound imaging: comparison of pathomorphological findings in US versus CT, MRI and intraoperative findings. *Acta Neurochir Suppl* (2003) 85:95–9. doi: 10.1007/978-3-7091-6043-5_13
12. Unsgaard G, Selbekk T, Brostrup Müller T, Ommedal S, Torp SH, Myhr G, et al. Ability of navigated 3D ultrasound to delineate gliomas and metastases–comparison of image interpretations with histopathology. *Acta Neurochir* (2005) 147(12):1259–69. doi: 10.1007/s00701-005-0624-1
13. Šteňo A, Karlík M, Mendel P, Čík M, Šteňo J. Navigated three-dimensional intraoperative ultrasound-guided awake resection of low-grade glioma partially infiltrating optic radiation. *Acta Neurochir* (2012) 154(7):1255–62. doi: 10.1007/s00701-012-1357-6
14. Moiyadi AV, Shetty PM, Mahajan A, Udare A, Sridhar E. Usefulness of three-dimensional navigable intraoperative ultrasound in resection of brain tumors with a special emphasis on malignant gliomas. *Acta Neurochir* (2013) 155 (12):2217–25. doi: 10.1007/s00701-013-1881-z
15. Solheim O, Selbekk T, Lindseth F, Unsgård G. Navigated resection of giant intracranial meningiomas based on intraoperative 3D ultrasound. *Acta Neurochir* (2009) 151(9):1143–51. doi: 10.1007/s00701-009-0395-1
16. Solheim O, Selbekk T, Jakola AS, Unsgård G. Ultrasound-guided operations in unselected high-grade gliomas–overall results, impact of image quality and patient selection. *Acta Neurochir* (2010) 152(11):1873–86. doi: 10.1007/s00701-010-0731-5
17. Coburger J, Scheuerle A, Thal DR, Engelke J, Hlavac M, Wirtz CHR, et al. Linear array ultrasound in low-grade glioma surgery: histology-based assessment of accuracy in comparison to conventional intraoperative ultrasound and intraoperative MRI. *Acta Neurochir* (2015) 157(2):195–206. doi: 10.1007/s00701-014-2314-3
18. Ravn Munkvold BK, Bø HK, Jakola AS, Reinertsen I, Berntsen EM, Unsgård G, et al. Tumor Volume Assessment in Low-Grade Gliomas: A Comparison of Preoperative Magnetic Resonance Imaging to Coregistered Intraoperative 3-Dimensional Ultrasound Recordings. *Neurosurgery* (2018) 83(2):288–96. doi: 10.1093/neuros/nyx392
19. Ravn Munkvold BK, Jakola AS, Reinertsen I, Sagberg LM, Unsgård G, Solheim O. The Diagnostic Properties of Intraoperative Ultrasound in Glioma Surgery and Factors Associated with Gross Total Tumor Resection. *World Neurosurg* (2018) 115:e129–36. doi: 10.1016/j.wneu.2018.03.208
20. Duffau H. A personal consecutive series of surgically treated 51 cases of insular WHO Grade II glioma: advances and limitations. *J Neurosurg* (2009) 110:696–708. doi: 10.3171/2008.8.JNS08741
21. Jakola AS, Berntsen EM, Christensen P, Gulati S, Unsgård G, Kvistad KA, et al. Surgically acquired deficits and diffusion weighted MRI changes after glioma resection—a matched case-control study with blinded neuroradiological assessment. *PLoS One* (2014) 9:e101805. doi: 10.1371/journal.pone.0101805
22. Šteňo A, Jezberová M, Hollý V, Timárová G, Šteňo J. Visualization of lenticulostriate arteries during insular low-grade glioma surgeries by navigated 3D ultrasound power Doppler: technical note. *J Neurosurg* (2016) 125(4):1016–23. doi: 10.3171/2015.10.JNS151907
23. Prada F, Del Bene M, Moiraghi A, DiMeco F. "Echographic brain semeiology and topographic anatomy according to surgical approaches". In: F Prada, L Solbiati, A Martegani, F DiMeco, editors. *Intraoperative Ultrasound (IOUS) in Neurosurgery: From Standard B-Mode to Elastosonography*. Cham: Springer International Publishing (2016). p. 29–39.
24. Bozinov O, Burkhardt JK, Fischer CM, Kockro RA, Bernays RL, Bertalanffy H. Advantages and limitations of intraoperative 3D ultrasound in neurosurgery. Technical note. *Acta Neurochir Suppl* (2011) 109:191–6. doi: 10.1007/978-3-211-99651-5_30
25. Unsgaard G, Ommedal S, Muller T, Gronningsaeter A, Nagelhus Hernes TA. Neuronavigation by intraoperative three-dimensional ultrasound: initial experience during brain tumor resection. *Neurosurgery* (2002) 50(4):804–12. doi: 10.1097/00006123-200204000-00022
26. Wirtz CR, Albert FK, Schwaderer M, Heuer C, Staubert A, Tronnier VM, et al. The benefit of neuronavigation for neurosurgery analyzed by its impact on glioblastoma surgery. *Neurol Res* (2000) 22(4):354–60. doi: 10.1080/01616412.2000.11740684
27. Kurimoto M, Hayashi N, Kamiyama H, Nagai S, Shibata T, Asahi T, et al. Impact of neuronavigation and image-guided extensive resection for adult patients with supratentorial malignant astrocytomas: a single-institution retrospective study. *Minim Invasive Neurosurg* (2004) 47(5):278–83. doi: 10.1055/s-2004-830093
28. Bello L, Gallucci M, Fava M, Carrabba G, Giussani C, Acerbi F, et al. i Intraoperative subcortical language tract mapping guides surgical removal of gliomas involving speech areas. *Neurosurgery* (2007) 60(1):67–80. doi: 10.1227/01.NEU.0000249206.58601.DE
29. Mert A, Kiesel B, Wöhrer A, Martínez-Moreno M, Minchev G, Furtner J. at al. Introduction of a standardized multimodality image protocol for navigation-guided surgery of suspected low-grade gliomas. *Neurosurg Focus* (2015) 38(1): E4. doi: 10.3171/2014.10.FOCUS14597
30. Pinsker MO, Nabavi A, Mehdorn HM. Neuronavigation and resection of lesions located in eloquent brain areas under local anesthesia and neuropsychological-neurophysiological monitoring. *Minim Invasive Neurosurg* (2007) 50(5):281–4. doi: 10.1055/s-2007-985825
31. Chang EF, Smith JS, Chang SM, Lamborn KR, Prados MD, Butowski N, et al. Preoperative prognostic classification system for hemispheric low-grade gliomas in adults. *J Neurosurg* (2008) 109(5):817–24. doi: 10.3171/JNS/2008/109/11/0817
32. Senft C, Bink A, Franz K, Vatter H, Gasser T, Seifert V. Intraoperative MRI guidance and extent of resection in glioma surgery: a randomised, controlled trial. *Lancet Oncol* (2011) 12(11):997–1003. doi: 10.1016/S1470-2045(11)70196-6
33. Gronningsaeter A, Kleven A, Ommedal S, Aarseth TE, Lie T, Lindseth F, et al. SonoWand, an ultrasound-based neuronavigation system. *Neurosurgery* (2000) 47(6):1373–9. doi: 10.1097/00006123-200012000-00021
34. Hata N, Dohi T, Iseki H, Takakura K. Development of a frameless and armless stereotactic neuronavigation system with ultrasonographic registration. *Neurosurgery* (1997) 41(3):608–13. doi: 10.1097/00006123-199709000-00020
35. Koivukangas J, Louhisalmi Y, Alakuijala J, Oikarinen J. Ultrasound-controlled neuronavigator-guided brain surgery. *J Neurosurg* (1993) 79(1):36–42. doi: 10.3171/jns.1993.79.1.0036
36. Trobaugh JW, Richard WD, Smith KR, Bucholz RD. Frameless stereotactic ultrasonography: method and applications. *Comput Med Imaging Graph* (1994) 18(4):235–46. doi: 10.1016/0895-6111(94)90048-5
37. Moiyadi AV, Unsgård G. "Navigable ultrasound, 3D ultrasound and fusion imaging in neurosurgery". In: F Prada, L Solbiati, A Martegani, F DiMeco, editors. *Intraoperative Ultrasound (IOUS) in Neurosurgery: From Standard B-Mode to Elastosonography*. Cham: Springer International Publishing (2016). p. 135–45.
38. Lindseth F, Kaspersen JH, Ommedal S, Langø T, Bang J, Hokland J, et al. Multimodal image fusion in ultrasound-based neuronavigation: improving overview and interpretation by integrating preoperative MRI with intraoperative 3D ultrasound. *Comput Aided Surg* (2003) 8(2):49–69. doi: 10.3109/10929080309146040
39. Patil AD, Singh V, Sukumar V, Shetty PM, Moiyadi AV. Comparison of outcomes of free-hand 2-dimensional ultrasound-guided versus navigated 3-dimensional ultrasound-guided biopsy for supratentorial tumours: a single-institution experience with 125 cases. *Ultrasonography* (2019) 38(3):255–63. doi: 10.14366/usg.18036
40. Sanai N, Polley MY, McDermott MW, Parsa AT, Berger MS. An extent of resection threshold for newly diagnosed glioblastomas. *J Neurosurg* (2011) 115 (1):3–8. doi: 10.3171/2011.2.jns10998
41. Kotrotsou A, Elakkad A, Sun J, Thomas GA, Yang D, Abrol S, et al. Multi-center study finds postoperative residual non-enhancing component of glioblastoma as a new determinant of patient outcome. *J Neurooncol* (2018) 139(1):125–33. doi: 10.1007/s11060-018-2850-4
42. Prada F, Vitale V, Del Bene M, Boffano C, Sconfienza LM, Pinzi V, et al. Contrast-enhanced MR Imaging versus Contrast-enhanced US: A Comparison in Glioblastoma Surgery by Using Intraoperative Fusion Imaging. *Radiology* (2017) 285(1):242–9. doi: 10.1148/radiol.2017161206
43. Prada F, Del Bene M, Fornaro R, Vetrano IG, Martegani A, Aiani L, et al. Identification of residual tumor with intraoperative contrast-enhanced ultrasound during glioblastoma resection. *Neurosurg Focus* (2016) 40(3):E7. doi: 10.3171/2015.11.FOCUS15573
44. Stummer W, Pichlmeier U, Meinel T, Wiestler OD, Zanella F, Reulen HJ. ALA-Glioma Study Group Fluorescence-guided surgery with 5-aminolevulinic acid for resection of malignant glioma: a randomised

controlled multicentre phase III trial. *Lancet Oncol* (2006) 7(5):392–401. doi: 10.1016/S1470-2045(06)70665-9
45. Moiyadi A, Shetty P. Navigable intraoperative ultrasound and fluorescence-guided resections are complementary in resection control of malignant gliomas: one size does not fit all. *J Neurol Surg A Cent Eur Neurosurg* (2014) 75(6):434–41. doi: 10.1055/s-0034-1372436
46. Eyüpoglu IY, Hore N, Savaskan NE, Grummich P, Roessler K, Buchfelder M, et al. Improving the extent of malignant glioma resection by dual intraoperative visualization approach. *PLoS One* (2012) 7(9):e44885. doi: 10.1371/journal.pone.0044885
47. Tsugu A, Ishizaka H, Mizokami Y, Osada T, Baba T, Yoshiyama M, et al. Impact of the combination of 5-aminolevulinic acid-induced fluorescence with intraoperative magnetic resonance imaging-guided surgery for glioma. *World Neurosurg* (2011) 76(1-2):120–7. doi: 10.1016/j.wneu.2011.02.005
48. Beiko J, Suki D, Hess KR, Fox BD, Cheung V, Cabral M, et al. IDH1 mutant malignant astrocytomas are more amenable to surgical resection and have a survival benefit associated with maximal surgical resection. *Neuro Oncol* (2014) 16(1):81–91. doi: 10.1093/neuonc/not159
49. Li YM, Suki D, Hess K, Sawaya R. The influence of maximum safe resection of glioblastoma on survival in 1229 patients: Can we do better than gross-total resection? *J Neurosurg* (2016) 124(4):977–88. doi: 10.3171/2015.5.JNS142087
50. Šteňo A, Giussani C, Riva M. "Multimodal imaging in glioma surgery". In: F Prada, L Solbiati, A Martegani, F DiMeco, editors. *Intraoperative Ultrasound (IOUS) in Neurosurgery: From Standard B-Mode to Elastosonography*. Cham: Springer International Publishing (2016). p. 81–97.
51. Widhalm G, Wolfsberger S, Minchev G, Woehrer A, Krssak M, Czech T, et al. 5-Aminolevulinic acid is a promising marker for detection of anaplastic foci in diffusely infiltrating gliomas with nonsignificant contrast enhancement. *Cancer* (2010) 116(6):1545–52. doi: 10.1002/cncr.24903
52. Petridis AK, Anokhin M, Vavruska J, Mahvash M, Scholz M. The value of intraoperative sonography in low grade glioma surgery. *Clin Neurol Neurosurg* (2015) 131:64–8. doi: 10.1016/j.clineuro.2015.02.004
53. Hentschel SJ, Lang FF. Surgical resection of intrinsic insular tumors. *Neurosurgery* (2005) 57(1 Suppl):176–83. doi: 10.1227/01.neu.0000163603.70972.ab
54. Gerganov VM, Samii A, Giordano M, Samii M, Fahlbusch R. Two-dimensional high-end ultrasound imaging compared to intraoperative MRI during resection of low-grade gliomas. *J Clin Neurosci* (2011) 18(5):669–73. doi: 10.1016/j.jocn.2010.08.017
55. Selbekk T, Jakola AS, Solheim O, Johansen TF, Lindseth F, Reinertsen I, et al. Ultrasound imaging in neurosurgery: approaches to minimize surgically induced image artefacts for improved resection control. *Acta Neurochir* (2013) 155:973–80. doi: 10.1007/s00701-013-1647-7
56. Jakola AS, Jørgensen A, Selbekk T, Michler RP, Solheim O, Torp SH, et al. Animal study assessing safety of an acoustic coupling fluid that holds the potential to avoid surgically induced artifacts in 3D ultrasound guided operations. *BMC Med Imaging* (2014) 14:11. doi: 10.1186/1471-2342-14-11
57. Steno A, Matejcik V, Steno J. Intraoperative ultrasound in low-grade glioma surgery. *Clin Neurol Neurosurg* (2015) 135:96–9. doi: 10.1016/j.clineuro.2015.05.012
58. Coburger J, Konig RW, Scheuerle A, Engelke J, Hlavac M, Thal DR, et al. Navigated high frequency ultrasound: description of technique and clinical comparison with conventional intracranial ultrasound. *World Neurosurg* (2014) 82:366–75. doi: 10.1016/j.wneu.2014.05.025
59. Steno A, Matejcik V, Steno J. Letter to the editor: identification of residual glioma using ultrasound miniprobes. *Neurosurg Focus* (2016) 41:E15. doi: 10.3171/2016.5.FOCUS16180
60. Šteňo A, Hollý V, Mendel P, Šteňová V, Petričková Ľ, Timárová G, et al. Navigated 3D-ultrasound versus conventional neuronavigation during awake resections of eloquent low-grade gliomas: a comparative study at a single institution. *Acta Neurochir* (2018) 160(2):331–42. doi: 10.1007/s00701-017-3377-8
61. Unsgård G, Sagberg LM, Müller S, Selbekk T. A new acoustic coupling fluid with ability to reduce ultrasound imaging artefacts in brain tumour surgery-a phase I study. *Acta Neurochir* (2019) 161(7):1475–86. doi: 10.1007/s00701-019-03945-x
62. Martegani A, Mattei L, Aiani L. "US Physics, Basic Principles, and Clinical Application". In: F Prada, L Solbiati, A Martegani, F DiMeco, editors. *Intraoperative Ultrasound (IOUS) in Neurosurgery: From Standard B-Mode to Elastosonography*. Cham: Springer International Publishing (2016). p. 9–17.
63. Ram Z, Shawker TH, Bradford MH, Doppman JL, Oldfield EH. Intraoperative ultrasound-directed resection of pituitary tumors. *J Neurosurg* (1995) 83 (2):225–30. doi: 10.3171/jns.1995.83.2.0225
64. Watson JC, Shawker TH, Nieman LK, DeVroom HL, Doppman JL, Oldfield EH. Localization of pituitary adenomas by using intraoperative ultrasound in patients with Cushing's disease and no demonstrable pituitary tumor on magnetic resonance imaging. *J Neurosurg* (1998) 89(6):927–32. doi: 10.3171/jns.1998.89.6.0927
65. Knappe UJ, Engelbach M, Konz K, Lakomek HJ, Saeger W, Schönmayr R, et al. Ultrasound-assisted microsurgery for Cushing's disease. *Exp Clin Endocrinol Diabetes* (2011) 119(4):191–200. doi: 10.1055/s-0029-1241207
66. Arita K, Kurisu K, Tominaga A, Kawamoto H, Iida K, Mizoue T, et al. Transsellar color Doppler ultrasonography during transsphenoidal surgery. *Neurosurgery* (1998) 42(1):81–5. doi: 10.1097/00006123-199801000-00016
67. Ishikawa M, Ota Y, Yoshida N, Iino Y, Tanaka Y, Watanabe E. Endonasal ultrasonography-assisted neuroendoscopic transsphenoidal surgery. *Acta Neurochir* (2015) 157(5):863–8. doi: 10.1007/s00701-015-2382-z
68. Solheim O, Selbekk T, Løvstakken L, Tangen GA, Solberg OV, Johansen TF, et al. Intrasellar ultrasound in transsphenoidal surgery: a novel technique. *Neurosurgery* (2010) 66(1):173–85. doi: 10.1227/01.NEU.0000360571.11582.4F
69. Solheim O, Johansen TF, Cappelen J, Unsgård G, Selbekk T. Transsellar Ultrasound in Pituitary Surgery With a Designated Probe: Early Experiences. *Oper Neurosurg* (2016) 1;12(2):128–34. doi: 10.1227/NEU.0000000000001108
70. Marcus HJ, Vercauteren T, Ourselin S, Dorward NL. Intraoperative Ultrasound in Patients Undergoing Transsphenoidal Surgery for Pituitary Adenoma: Systematic Review. *World Neurosurg* (2017) 106:680–5. doi: 10.1016/j.wneu.2017.07.054
71. Alomari A, Jaspers C, Reinbold WD, Feldkamp J, Knappe UJ. Use of intraoperative intracavitary (direct-contact) ultrasound for resection control in transsphenoidal surgery for pituitary tumors: evaluation of a microsurgical series. *Acta Neurochir* (2019) 161(1):109–17. doi: 10.1007/s00701-018-3747-x
72. Alshareef M, Lowe S, Park Y, Frankel B. Utility of intraoperative ultrasonography for resection of pituitary adenomas: a comparative retrospective study. *Acta Neurochir* (2021). doi: 10.1007/s00701-020-04674-2
73. Buchfelder M, Schlaffer SM. Novel Techniques in the Surgical Treatment of Acromegaly: Applications and Efficacy. *Neuroendocrinology* (2016) 103 (1):32–41. doi: 10.1159/000441980
74. Soto-Ares G, Cortet-Rudelli C, Assaker R, Boulinguez A, Dubest C, Dewailly D, et al. MRI protocol technique in the optimal therapeutic strategy of non-functioning pituitary adenomas. *Eur J Endocrinol* (2002) 146(2):179–86. doi: 10.1530/eje.0.1460179
75. Fernandez-Miranda JC, Zwagerman NT, Abhinav K, Lieber S, Wang EW, Snyderman CH, et al. Cavernous sinus compartments from the endoscopic endonasal approach: anatomical considerations and surgical relevance to adenoma surgery. *J Neurosurg* (2018) 129(2):430–41. doi: 10.3171/2017.2.JNS162214
76. Kurwale NS, Ahmad F, Suri A, Kale SS, Sharma BS, Mahapatra AK, et al. Postoperative pituitary apoplexy: preoperative considerations toward preventing nightmare. *Br J Neurosurg* (2012) 26(1):59–63. doi: 10.3109/02688697.2011.591947
77. Zaidi HA, De Los Reyes K, Barkhoudarian G, Litvack ZN, Bi WL, Rincon-Torroella J, et al. The utility of high-resolution intraoperative MRI in endoscopic transsphenoidal surgery for pituitary macroadenomas: early experience in the Advanced Multimodality Image Guided Operating suite. *Neurosurg Focus* (2016) 40(3):E18. doi: 10.3171/2016.1.FOCUS15515
78. Askeland C, Solberg OV, Bakeng JB, Reinertsen I, Tangen GA, Hofstad EF, et al. CustusX: an open-source research platform for image-guided therapy. *Int J Comput Assist Radiol Surg* (2016) 11(4):505–19. doi: 10.1007/s11548-015-1292-0
79. Arlt F, Chalopin C, Müns A, Meixensberger J, Lindner D. Intraoperative 3D contrast-enhanced ultrasound (CEUS): a prospective study of 50 patients with brain tumours. *Acta Neurochir* (2016) 158(4):685–94. doi: 10.1007/s00701-016-2738-z
80. Maldaun MVC, Khawja SN, Levine NB, Rao G, Lang FF, Weinberg JS, et al. Awake craniotomy for gliomas in a high-field intraoperative magnetic

resonance imaging suite: analysis of 42 cases. *J Neurosurg* (2014) 121(4):810–7. doi: 10.3171/2014.6.JNS132285

81. Duffau H, Capelle L, Denvil D, Sichez N, Gatignol P, Taillandier L, et al. Usefulness of intraoperative electrical subcortical mapping during surgery for low-grade gliomas located within eloquent brain regions: functional results in a consecutive series of 103 patients. *J Neurosurg* (2003) 98(4):764–78. doi: 10.3171/jns.2003.98.4.0764
82. Perin A, Prada FU, Moraldo M, Schiappacasse A, Galbiati TF, Gambatesa E, et al. USim: A New Device and App for Case-Specific, Intraoperative Ultrasound Simulation and Rehearsal in Neurosurgery. *A Preliminary Study Oper Neurosurg* (2018) 14(5):572–8. doi: 10.1093/ons/opx144
83. Singh V, Shaikh S, Shetty P, Moiyadi A. Customized Low-Cost Model for Hands-on Training in Intraoperative Ultrasound for Neurosurgeons: Our Experience and Review of Literature. *World Neurosurg* (2020) 143:564–71.e2. doi: 10.1016/j.wneu.2020.07.044
84. Vavruska J, Buhl R, Petridis AK, Maslehaty H, Scholz M. Evaluation of an intraoperative ultrasound training model based on a cadaveric sheep brain. *Surg Neurol Int* (2014) 9(5):46. doi: 10.4103/2152-7806.130314
85. Moiraghi A, Prada F, Delaidelli A, Guatta R, May A, Bartoli A, et al. Navigated Intraoperative 2-Dimensional Ultrasound in High-Grade Glioma Surgery: Impact on Extent of Resection and Patient Outcome. *Oper Neurosurg* (2020) 18(4):363–73. doi: 10.1093/ons/opz203
86. Sweeney JF, Smith H, Taplin A, Perloff E, Adamo MA. Efficacy of intraoperative ultrasonography in neurosurgical tumor resection. *J Neurosurg Pediatr* (2018) 21(5):504–10. doi: 10.3171/2017.11.PEDS17473
87. Fountain DM, Bryant A, Barone DG, Waqar M, Hart MG, Bulbeck H, et al. Intraoperative imaging technology to maximise extent of resection for glioma: a network meta-analysis. *Cochrane Database Syst Rev* (2021) 1:CD013630. doi: 10.1002/14651858.CD013630.pub2
88. Iversen DH, Wein W, Lindseth F, Unsgård G, Reinertsen I. Automatic Intraoperative Correction of Brain Shift for Accurate Neuronavigation. *World Neurosurg* (2018) 120:e1071–8. doi: 10.1016/j.wneu.2018.09.012
89. Riva M, Hiepe P, Frommert M, Divenuto I, Gay LG, Sciortino T, et al. Intraoperative Computed Tomography and Finite Element Modelling for Multimodal Image Fusion in Brain Surgery. *Oper Neurosurg* (2020) 18(5):531–41. doi: 10.1093/ons/opz196

Conflict of Interest: The authors declare that the research was conducted in the absence of any commercial or financial relationships that could be construed as a potential conflict of interest.

frontiers in Oncology

ORIGINAL RESEARCH
published: 21 April 2021
doi: 10.3389/fonc.2021.660805

Intraoperative Ultrasound-Assisted Extent of Resection Assessment in Pediatric Neurosurgical Oncology

Andrea Carai[1], Alessandro De Benedictis[1], Tommaso Calloni[2], Nicola Onorini[1], Giovanni Paternò[1], Franco Randi[1], Giovanna Stefania Colafati[3], Angela Mastronuzzi[4] and Carlo Efisio Marras[1]*

[1] Neurosurgery Unit, Department of Neurological and Psychiatric Sciences, IRCCS Bambino Gesù Children's Hospital, Rome, Italy, [2] School of Neurosurgery, University of Milan-Bicocca, Milan, Italy, [3] Neuro-Radiology Unit, Department of Imaging, IRCCS Bambino Gesù Children's Hospital, Rome, Italy, [4] Department of Hematology/Oncology, Cell and Gene Therapy, IRCCS Bambino Gesù Children's Hospital, Rome, Italy

OPEN ACCESS

Edited by:
Francesco DiMeco,
Fondazione IRCCS Istituto Neurologio Carlo Besta, Italy

Reviewed by:
Giovanni Raffa,
University of Messina, Italy
Matteo Zoli,
IRCCS Institute of Neurological Sciences of Bologna (ISNB), Italy

***Correspondence:**
Alessandro De Benedictis
alessandro.debenedictis@opbg.net

Specialty section:
This article was submitted to Neuro-Oncology and Neurosurgical Oncology, a section of the journal Frontiers in Oncology

Received: 29 January 2021
Accepted: 16 March 2021
Published: 21 April 2021

Citation:
Carai A, De Benedictis A, Calloni T, Onorini N, Paternò G, Randi F, Colafati GS, Mastronuzzi A and Marras CE (2021) Intraoperative Ultrasound-Assisted Extent of Resection Assessment in Pediatric Neurosurgical Oncology. Front. Oncol. 11:660805. doi: 10.3389/fonc.2021.660805

Central nervous system tumors represent the most frequent solid malignancy in the pediatric population. Maximal safe surgical resection is a mainstay of treatment, with significant prognostic impact for the majority of histotypes. Intraoperative ultrasound (ioUS) is a widely available tool in neurosurgery to assist in intracerebral disease resection. Despite technical caveats, preliminary experiences suggest a satisfactory predictive ability, when compared to magnetic resonance imaging (MRI) studies. Most of the available evidence on ioUS applications in brain tumors derive from adult series, a scenario that might not be representative of the pediatric population. We present our preliminary experience comparing ioUS-assisted resection assessment to early post-operative MRI findings in 154 consecutive brain tumor resections at our pediatric neurosurgical unit. A high concordance was observed between ioUS and post-operative MRI. Overall ioUS demonstrated a positive predictive value of 98%, a negative predictive value of 92% in assessing the presence of tumor residue compared to postoperative MRI. Overall, sensibility and specificity were 86% and 99%, respectively. On a multivariate analysis, the only variable significantly associated to unexpected tumor residue on postoperative MRI was histology. Tumor location, patient positioning during surgery, age and initial tumor volume were not significantly associated with ioUS predictive ability. Our data suggest a very good predictive value of ioUS in brain tumor resective procedures in children. Low-grade glioma, high-grade glioma and craniopharyngioma might represent a setting deserving specific endeavours in order to improve intraoperative extent of resection assessment ability.

Keywords: intraoperative ultrasound, neurosurgical oncology, extent of resection, brain tumor, children

INTRODUCTION

Several studies have demonstrated that extent of resection is a crucial prognostic factor for achieving the best outcome in neurosurgical oncology (1).

For this reason, previous investigations have focused on the possible contribution of intraoperative imaging techniques in improving surgical results (2). In this context, intraoperative ultrasonography (ioUS) is a promising tool to assist the surgeon in accomplishing several tasks, including target localization, volume and margin delineation, real-time brain shift evaluation and assessment of extent of resection (3, 4). Progressive technological improvement has allowed the differentiation of distinct tissue patterns, including necrosis, hemorrhage, and cystic components of tumors (5–7). Moreover, ioUS offers significant advantages in terms of availability, versatility and costs in comparison to other intraoperative imaging modalities, such as MRI and CT (8).

However, available evidence is mainly based on adult case series, which might fail to account for population specific features of pediatric disease (9, 10).

In this study, we report our experience on the use of ioUS in series of pediatric patients undergoing brain tumor resection.

MATERIALS AND METHODS

All patients undergoing ultrasound assisted brain tumor resection at the Neurosurgery Unit of the Bambino Gesù Children's Hospital from January 2018 to June 2020 were included in the study.

Extent of resection was evaluated according to latest recommendation of the International Society of Pediatric Oncology (SIOP), integrating a surgical grading with a MRI grading. Surgical impression on resection was therefore graded from SR0 to SR3 as follows: SR0 (complete resection), SR1 (rim-like residual), SR2 (bulky residual), SR3 (biopsy). Radiological assessment was graded MR0 to MR3: MR0 (complete resection), MR1 (rim-like residual ≤ 3 mm), MR2 (residual > 3 mm in any section), MR3 (residual > 50% of initial volume) (11) **(Table 1)**

Planned resection (pSR) was defined during multidisciplinary neuro-oncology board meetings. Unless a bioptic procedure was indicated, maximal safe resection was always planned.

TABLE 1 | Extent of resection as evaluated intraoperatively and on postoperative contrast-enhanced MRI to be performed within 48 h (max, 72 h) after surgery.

SR 0	Total resection, no residue
SR 1	Suspected residue, possible local invasion
SR 2	Solid residuum (to be defined by postoperative MRI)
SR 3	Tumor volume unchanged, biopsy
MR 0	No visible tumor
MR 1	Rim enhancement or signal abnormality (matching the tumor) at the operation site only ("Rim"), ≤ 3 mm in any of the dimensions and equivocal for tumor residue
MR 2	Residual tumor measuring > 3 mm in all 3 dimensions (greater than MR1, less than MR3)
MR 3	No significant change to preoperative tumor size ("minimal change")

Adapted from Gnekow (11).

All children underwent navigated craniotomy (Medtronic S7) and microsurgical resection of the lesion. Intraoperative ultrasound (BK 5000, BK Medical, Peabody, MA) equipped with a 5- to 10-MHz convex probe (Craniotomy probe N13C5, BK Medical) was used before and after dural opening to confirm the relationship of the lesion to brain landmarks (**Figures 1B** and **2B**), during resection at surgeon's discretion, at the end of resection to confirm the microsurgical impression of reaching the planned resection (SR) (**Figures 1D** and **2D**). To reduce inter-operator variability, intraoperative evaluations in our series were only performed by three surgeons sharing the case series, each having at least a 5-year experience in ioUS use (AC, ADB, CEM).

Post-operative imaging was performed on a 3T Siemens MRI machine (**Figures 1A, C**, **2A, C**). All scans were reviewed by an experienced pediatric neuroradiologist (GSC) blinded to the intraoperative impression.

The agreement between intraoperative ultrasound evaluation and MRI was measured with Fleiss' kappa agreement (12). The Chi-square test was used to analyze associations between categorical variables, which were expressed as absolute numbers and percentages. Multivariate logistic regression analysis was performed to identify predictors for discordance between intraoperative ultrasound evaluation and MRI (the model included as variables age at intervention, diameter of the lesion, localization of the tumor and surgical position). Statistical analyses were performed using GraphPad Prism, version 9.0 (GraphPad Software, San Diego, California, USA, www.graphpad.com).

IRB approval was obtained for this retrospective study, including waiver of consent from participating patients.

RESULTS

Our series (**Table 2**) included 154 patients, mean age was 8.6 years with a median of 8.2. Average tumor diameter was 36.18 mm with a median of 34 mm.

The most frequent tumor location was found to be the posterior fossa (46 cerebellum, 6 IVth ventricle, 10 brainstem, and 4 cerebello-pontine angle). Hemispheric lesions were 58: 19 frontal, 29 temporal, 7 parietal, 2 cingular and 1 occipital. Additional deep tumor locations were less frequent and included: 12 intraventricular, 4 thalamic, 6 sellar and 8 pineal.

Patient positioning during surgery was determined based on lesion location, therefore the most frequently used was the supine position (84). In posterior fossa and pineal region tumors, the prone (49) and sitting (21) position were also used.

Most frequent histology was low-grade glioma (81), followed by medulloblastoma (17), ependymoma (12) and high-grade glioma (10). Additional tumor subtypes included craniopharyngioma (6), germ cell tumors (5), choroid plexus tumors (3) and other less common tumors (20). Due to heterogeneity of the histologies and tumor locations, for statistical purposes, we had to group the cases into broader categories (**Table 2**).

In children with a central nervous system tumor, the most frequently planned procedure was a complete resection (pSR0 in 111 cases) and a "near total" resection (pSR1 in 15 cases). In 26 cases

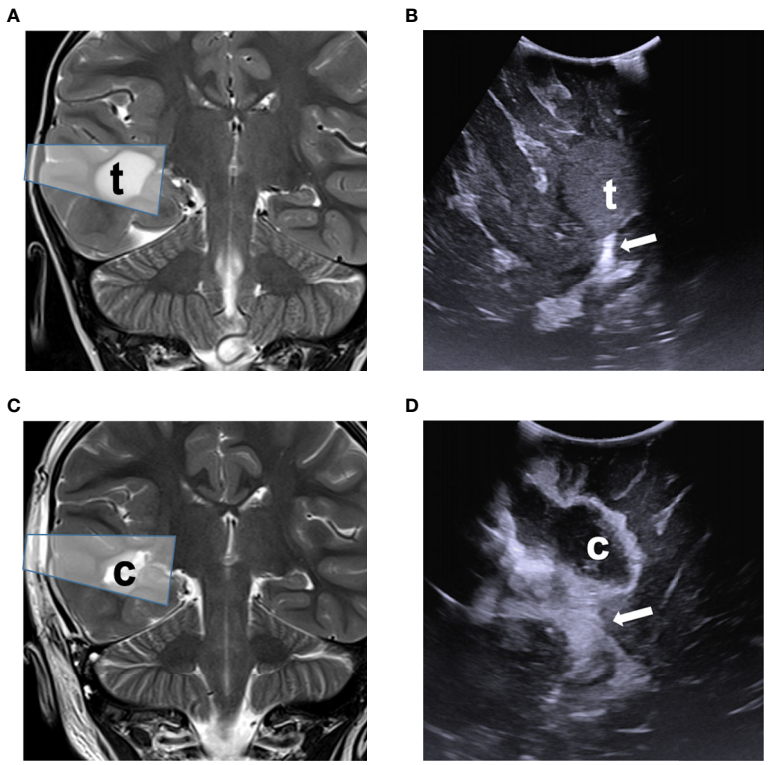

FIGURE 1 | Comparison of ioUS with pre- and post-operative MRI images of a right temporal low-grade glioma. Pre-operative **(A)** and post-operative **(C)** coronal T2-weighted MRI sequence demonstrating the lesion (t) and surgical cavity (c) with ioUS approximate field of view (shaded box). Intraoperative US view of the same is shown before dural opening **(B)** and after resection **(D)**, documenting the spatial relationship with the choroid plexus (white arrow).

a debulking procedure was planned (pSR2), while a biopsy was rarely indicated (pSR3 in two cases).

At the time of surgery, extent of resection was estimated by integrating microscopic evidence, neuronavigation information and intraoperative ultrasound assessment. Ultrasound assessment was possible in all cases, despite some technical limitations were anticipated in selected settings including parietal lesions (10) sitting position (13) and large tumor size (14).

Intraoperative assessment confirmed achievement of a planned SR0 in 95% of cases (SR0 106/111, SR1 5/111), pSR1 in 100% (15/15), pSR2 in 96% (SR2 25/26, SR3 1/26) and pSR3 in 100% of cases (2/2). In five cases the surgery was stopped despite the fact the assessment of a lower than planned EOR (SR1 instead of pSR0). Four of these patients had a LGG arising from or infiltrating the brainstem, the other patient had a recurrent posterior fossa ependymoma with infiltration of the lower cranial nerves which was not fully predictable on preoperative imaging. The child in which a biopsy was obtained instead of a subtotal resection (SR3 instead of pSR2) had a very large (133 mm in diameter) high-grade glioma infiltrating the third ventricle walls and thalamus bilaterally.

Post-operative MR confirmed intraoperative assessment in 87% of cases, stratified as follows: SR0 in 92% of cases (MR0 97/106, MR1 5/106, MR2 4/106), SR1 in 47% of cases (MR0 in 1/19, MR1 in 9/19, MR2 in 9/19), SR2 in 100% (25/25) and SR3 in 100% (MR3 3/3).

Overall, in this cohort of pediatric brain tumors, when used to assess the Extent of Resection as compared to early post-operative MRI, ioUS was found to have sensibility of 86%, specificity of 99%, negative predictive value of 92% and positive predictive value of 98%.

Concordance analysis between intraoperative ultrasound evaluation and MRI showed substantial agreement (kappa = 0.758) (12). In details, intraoperative ultrasound evaluation underestimated tumor residual. Overestimation occurred only in a single case. Low-grade gliomas (underestimation: 15/81, 18.5%), high-grade gliomas (underestimation: 2/10, 20%) and CRF (underestimation: 1/6, 16.6%) were associated with US underestimation ($p = 0.034$). In order to correct for confounding factors, multivariate logistic regression analysis was performed, showing only histology as associated with discordance of the two imaging tests (odds ratio, 1.604; 95% CI, 1.126–2.623; $p = 0.0234$).

Bivariate statistical analysis did show a statistically significant correlation between ioUS failure to accurately assess residual tumor and histology. No correlation was found for other clinical variables, including age, tumor diameter, lesion location, and patient positioning during surgery (**Table 3**).

DISCUSSION

Intraoperative imaging is an emerging tool in the neurosurgical armamentarium with a growing body of evidence to support

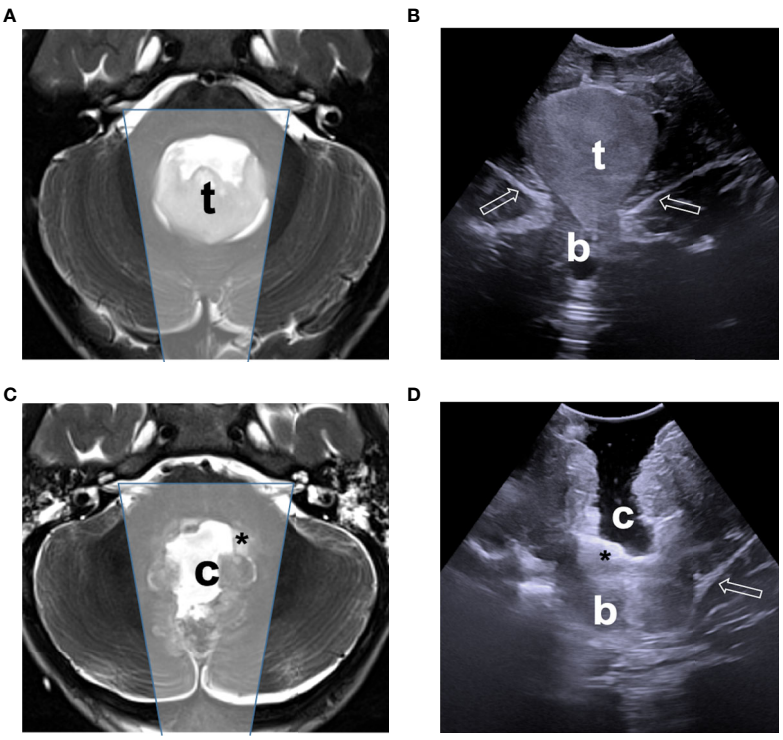

FIGURE 2 | Comparison of ioUS with pre- and post-operative MRI images of a IV ventricle low-grade glioma. Pre-operative **(A)** and post-operative **(C)** axial T2-weighted MRI sequence demonstrating the lesion (t), and the surgical cavity (c), tumor residue (asterisk) respectively, with approximate ioUS field of view (shaded box). Intraoperative US view of the same is shown before dural opening **(B)** and after resection **(D)**, documenting the presence of a small tumor remnant (asterisk) which was intentionally left in place to avoid damage to the IV ventricle floor structures.

TABLE 2 | Study population.

Features of patient population and disease			
Average Age	Years:	8, 6	
Sex	M	93	60,39%
	F	61	39,61%
Average Diameter	mm	36, 18	
Histology	LGG	81	52,60%
	HGG	10	6,49%
	Embryonal	22	14,29%
	Ependymoma	12	7,79%
	Craniopharyngioma	6	3,90%
	Choroid P. tumors	3	1,95%
	Other	20	12,99%
Site	PCF	66	42,86%
	Hemispheric	58	37,66%
	Intraventricular	12	7,79%
	Pineal	8	5,19%
	Sella	6	3,90%
	Thalamus	4	2,60%
Patient position during surgery	Prone	84	54,55%
	Supine	49	31,82%
	Sitting	21	13,64%

its advantages for lesion targeting and extent of resection evaluation.

In the setting of pediatric neurosurgical oncology, control over the extent of resection is paramount. In this scenario, the introduction of real time intraoperative imaging, in addition to direct inspection of the microsurgical field integrated with neuronavigation data and intraoperative monitoring information has the potential to significantly improve surgical orientation. Indeed, while the aim of surgery is generally to achieve complete resection, in particular cases this may not desirable, making precise intraoperative assessment of residual disease a fundamental tool to tailor surgical resection.

The neuro-oncological pediatric population has several peculiarities when compared to adults, including a larger variety of histological subtypes and frequent lesion location in the posterior fossa. Therefore, generalization of available evidence concerning the use of ioUS, mostly derived from the adult population, might not be obvious.

TABLE 3 | Multivariate statistical analysis based on patients' age, tumor diameter, histology, site, and position during surgery.

	p value
Age	0.7505
Diameter	0.8741
Histology	**0.0234**
Site	0.9966
Position	0.3713

Bolding is meant to underline the only statistically significant value.

As mentioned above, when used to assess the Extent of Resection compared to early post-operative MRI, in this series ioUS was found to have sensibility of 86% negative predictive value of 92%, with a specificity of 99% and positive predictive value of 98%. This trend for higher PPV than NPV has also been found in adults (15), underlying a residue found at ioUS is more likely to result in MRI evidence of tumor residue than negative ioUS is to result in radiologic GTR.

The data concerning the use of ioUS as an aid in detecting tumor residues in pediatric brain tumor resection is sparse and based on small series. Even more scattered is evidence regarding clinical variables associated to ioUS diagnostic yield, including lesion site and histology.

Smith and colleagues discussed the use of ioUS in resection of pediatric brain tumors: in a series of 62 patients, GTR was planned in 82%. Surgery was stopped when microscopy and ioUS demonstrated complete resection. In 71% of the patients, the GTR was subsequently confirmed by postoperative MRI, while in 11% a residue was diagnosed with MRI which ioUS failed to detect. Notably, the specificity of iOUS appeared to be particularly low in parietal tumors (55%), which the authors did not offer possible explanations for (10).

In a mixed cohort of children and adults, the same group described 42 false ioUS-based diagnoses of GTR out of 217 intended GTR procedures (19.35%). False negatives occurred mostly in the setting of surgery for glioblastoma possibly as a result of the difficulties in detecting the margins of these highly invasive lesions. No information concerning the location of the false negatives was provided, nor stratification of the results based on age (2).

El Betagy and colleagues published two papers concerning ioUS use in brain tumor resection in children. In the first one they described 25 patients, 14 of which underwent GTR with no additional data about planned extent of resection. The ability of ioUS in detecting tumor residue was claimed to be comparable to that of MRI (16). In a follow-up paper, 60 patients operated for posterior cranial fossa lesions in the prone position were divided into two groups, 30 to be operated with the aid of ioUS and 30 without. The use of iOUS resulted in a 16% increase in GTR achievement (96% vs 80%), while allowing a lower incidence of cerebellar mutism (3% vs 20%) without significant increase of the operative time. They reported ioUS usefulness in detecting residue in the region of the rostral vermis and the lateral recesses of the fourth ventricle (17). No information was provided concerning the patients' randomization process.

Concerning pediatric posterior fossa lesions, a paper by Nagaty and colleagues described 23 surgeries performed with the aid of ioUS, in 11 of which GTR was achieved. The accuracy of ioUS was not compared to postoperative MRI, beside the fact that the average size of residuals diagnosed by ioUS and by MRI were similar (18).

Ulrich and colleagues described a series of 22 patients, in 19 of which a GTR was planned. On postoperative MRI, out of the 19 planned GTR procedures, a residual was diagnosed in a single case of IV ventricle medulloblastoma, which the iOUS failed to detect.

Our data confirm the high sensibility and specificity of ioUS in detecting the extent of residual disease in a pediatric brain tumor series in what is, to the best of our knowledge, the largest pediatric series published to date.

The pivotal role of accurate assessment of residual tumor is in children is underlined by the introduction by the International Society for Paediatric Oncology (11) of a new scale to quantify both the operator's assessment and the post-operative imaging data. Our decision to assess residual disease according to this classification might account for some of the differences in extent of resection rate compared to previously reported series.

In our series, ioUS underestimated resection in 18 cases (12%), Notably, in five (3%) cases, it suggested a complete resection (SR0) had been accomplished while MR later showed a linear residual smaller than 3 mm in diameter (MR1) and in nine (6%) cases, it suggested a linear residual (SR1) instead of a nodular one (SR2). Further, 4 (3%) cases ioUS suggested complete resection (SRO) while a nodular residual (SR2) had been left behind. Notably, even if all patients were operated with the aid of intraoperative monitoring, resection was never interrupted because of neurophysiological data.

We did not find significant association between residual underestimation and either prone, supine or sitting positioning, While the inability to fill the tumor cavity with saline in sitting positioning has raised questions about ioUS reliability in this setting (13), the sitting position does not appear to correlate with false negatives in our experience.

A well-described technical pitfall of ioUS in the neuro-oncological setting is presence of artifacts when exploring tissue surrounding large cavities, due to the difference in sound propagation between saline solution and brain (14). Possible countermeasures include the use of small probes inserted in the surgical cavity, at the price of a limited field of view (14) and ongoing development of acoustic coupling gels as saline alternatives (19). Despite these concerns, in our analysis, tumor size did not correlate with ioUS failure to detect lesion residue.

Anecdotally, the single case of residue overestimation (0.6%) in our series was a large frontal tumor in which artifacts from tissue manipulation where misinterpreted as linear residual disease (SR1) not confirmed at the post-operative MR (MR0).

The only variable significantly associated with an unexpected tumor residue on the postoperative MRI was histology ($p = 0.0234$). In particular, all the false negatives in this series were LGG, HGG, and craniopharyngioma (CFR).

Most of the literature concerning ioUS as an aid in residue identification, which stems from mostly adult series, compares ioUS sensitivity in is generally reported to have higher sensitivity in the detection of residues of HGG than LGG (15, 20). In this series, while certain histologies were associated with residue, no significant difference was apparent between LGG and HGG. We believe similarity in echogenicity and microscopic appearance to brain parenchyma in the case of the former and peritumoral edema and infiltrating pattern, typically found in the latter, might have lessened the ability to distinguish the tumor remnants from the surrounding tissue. Identification of tumor residues in the sellar and parasellar region carries unique challenges due to the geometry of the cavity with respect to the major tumor axes and the high rate of artifacts due to the

closeness of osteo-dural and vascular structures, while we did not find a statistical significance for tumor residue in the sellar region compared to other tumor locations, we believe these factor did play a role in the single case of residue in a CFR.

The low sensitivity of ioUS in parietal lesions reported by Smith and colleagues was not apparent in this series (10). Tumor location indeed did not associate with undetected residue on multivariate analysis.

While lesion location did not reach significance on multivariate analysis, the subgroup in which ioUS failed to accurately assess residual showed a high percentage of brainstem infiltrating lesions (50%) and posterior temporal lobe location with tumor residual on the wall of the resection cavity (49%). Intriguingly, these two conditions found in 89% of cases of underestimation of tumor residue share some technical challenges for ioUS despite US probe positioning at the top of the resection cavity. We speculate that inaccuracy in the posterior fossa might depend on peculiar echogenicity of brainstem and proximity of bone walls, while residual location on a wall of the resection cavity, artifacts from ventricular structures, proximity of middle fossa floor and tangential direction of the US probe to the surgical cavity might contribute in temporal lobe resections.

We speculate that the use of more advanced US techniques, such as contrast-enhanced (21) and navigated (22) ultrasound, which were not used in this series, might allow an even more reliable assessment of the extent of resection, as a growing body of evidence suggests.

CONCLUSIONS

Maximal safe resection of brain tumors is a critical step of treatment in the pediatric population. Intraoperative extent of resection can be accurately assessed by ioUS in the vast majority of cases.

Further technical refinement and application of additional intraoperative advanced visualization tools might help overcome this limitation contributing to a more precise intraoperative residual detection in the future.

DATA AVAILABILITY STATEMENT

The original contributions presented in the study are included in the article, further inquiries can be directed to the corresponding authors.

ETHICS STATEMENT

The studies involving human participants were reviewed and approved by the Institutional Review Board at the Ospedale Pediatric Bambino Gesù. Written informed consent from the participants' legal guardian/next of kin was not required to participate in this study in accordance with the national legislation and the institutional requirements.

AUTHOR CONTRIBUTIONS

CM: manuscript conception and revision. AC and AD: data revision and interpretation, manuscript drafting, and revision. TC: data collection and revision and manuscript drafting. GP and NO: data collection. GC: imaging data interpretation. AM and FR: manuscript revision. All authors contributed to the article and approved the submitted version.

FUNDING

This research was funded by the Ministero della Salute- Ricerca Corrente to Ospedale Pediatrico Bambino Gesù, IRCCS.

ACKNOWLEDGMENTS

The authors would like to thank Pietro Merli, MD, for his essential contribution in designing and reviewing the statistical analysis.

REFERENCES

1. Neidert MC, Hostettler IC, Burkhardt J-K, Mohme M, Held U, Kofmehl R, et al. The influence of intraoperative resection control modalities on survival following gross total resection of glioblastoma. *Neurosurg Rev* (2016) 39:401–9. doi: 10.1007/s10143-015-0698-z
2. Sweeney JF, Smith H, Taplin AL, Perloff E, Adamo MA. Effcacy of intraoperative ultrasonography in neurosurgical tumor resection. *J Neurosurgery: Pediatr* (2018) 21:504–10. doi: 10.3171/2017.11.PEDS17473
3. Chacko AG, Kumar NKS, Chacko G, Athyal R, Rajshekhar V, Unsgaard G. Intraoperative ultrasound in determining the extent of resection of parenchymal brain tumours - A comparative study with computed tomography and histopathology. *Acta Neurochirurgica* (2003) 145:743–8. doi: 10.1007/s00701-003-0009-2
4. Mair R, Heald J, Poeata I, Ivanov M. A practical grading system of ultrasonographic visibility for intracerebral lesions. *Acta Neurochir* (2013) 155:2293–8. doi: 10.1007/s00701-013-1868-9
5. Miller D, Knake S, Bauer S, Krakow K, Pagenstecher A, Sure U, et al. Intraoperative ultrasound to define focal cortical dysplasia in epilepsy surgery. *Epilepsia* (2008) 49:156–8. doi: 10.1111/j.1528-1167.2007.01268.x
6. Akeret K, Bellut D, Huppertz HJ, Ramantani G, König K, Serra C, et al. Ultrasonographic features of focal cortical dysplasia and their relevance for epilepsy surgery. *Neurosurgical Focus* (2018) 45:1–10. doi: 10.3171/2018.6.FOCUS18221
7. Prada F, Gennari AG, Quaia E, D'Incerti L, de Curtis M, DiMeco F, et al. Advanced intraoperative ultrasound (ioUS) techniques in focal cortical dysplasia (FCD) surgery: A preliminary experience on a case series. *Clin Neurol Neurosurgery* (2020) 198:106188. doi: 10.1016/j.clineuro.2020.106188
8. Hammoud MA, Ligon BL, Elsouki R, Shi WM, Schomer DF, Sawaya R. Use of intraoperative ultrasound for localizing tumors and determining the extent of resection: A comparative study with magnetic resonance imaging. *J Neurosurgery* (1996) 84:737–41. doi: 10.3171/jns.1996.84.5.0737
9. Ulrich NH, Burkhardt JK, Serra C, Bernays RL, Bozinov O. Resection of pediatric intracerebral tumors with the aid of intraoperative real-time 3-D ultrasound. *Child's Nervous System* (2012) 28:101–9. doi: 10.1007/s00381-011-1571-1

10. Smith H, Taplin A, Syed S, Adamo MA. Correlation between intraoperative ultrasound and postoperative MRI in pediatric tumor surgery. *J Neurosurgery: Pediatr* (2016) 18:578–84. doi: 10.3171/2016.5.PEDS15739
11. Gnekow AK, Kandels D, van TC, AA A, Opocher E, Stokland T, et al. SIOP-E-BTG and GPOH Guidelines for Diagnosis and Treatment of Children and Adolescents with Low Grade Glioma. *Klin Padiatr* (2019) 231:107–35. doi: 10.1055/a-0889-8256
12. Landis JR, Koch GG. The Measurement of Observer Agreement for Categorical Data. *Biometrics* (1977) 33:159. doi: 10.2307/2529310
13. Unsgaard G, Rygh OM, Selbekk T, Müller TB, Kolstad F, Lindseth F, et al. Intra-operative 3D ultrasound in neurosurgery. *Acta Neurochirurgica* (2006) 148:235–53. doi: 10.1007/s00701-005-0688-y
14. Selbekk T, Jakola AS, Solheim O, Johansen TF, Lindseth F, Reinertsen I, et al. Ultrasound imaging in neurosurgery: Approaches to minimize surgically induced image artefacts for improved resection control. *Acta Neurochirurgica* (2013) 155:973–80. doi: 10.1007/s00701-013-1647-7
15. Trevisi G, Barbone P, Treglia G, Mattoli MV, Mangiola A. Reliability of intraoperative ultrasound in detecting tumor residual after brain diffuse glioma surgery: a systematic review and meta-analysis. *Neurosurg Rev* (2020) 43:1221–33. doi: 10.1007/s10143-019-01160-x
16. El Beltagy MA, Aggag M, Kamal M. Role of intraoperative ultrasound in resection of pediatric brain tumors. *Child's Nervous System* (2010) 26:1189–93. doi: 10.1007/s00381-010-1091-4
17. El Beltagy MA, Atteya MME. The benefits of navigated intraoperative ultrasonography during resection of fourth ventricular tumors in children. *Child's Nervous System* (2013) 29:1079–88. doi: 10.1007/s00381-013-2103-y
18. Nagaty A, Elsabaa A, Anwer H. Efficacy of Intraoperative Ultrasound in Resection of Posterior Fossa Lesions. *Int J Neurosurgery* (2019) 3:13. doi: 10.11648/j.ijn.20190302.11
19. Unsgård G, Sagberg LM, Müller S, Selbekk T. A new acoustic coupling fluid with ability to reduce ultrasound imaging artefacts in brain tumour surgery—a phase I study. *Acta Neurochirurgica* (2019) 161:1475–86. doi: 10.1007/s00701-019-03945-x
20. Mahboob S, McPhillips R, Qiu Z, Jiang Y, Meggs C, Schiavone G, et al. Intraoperative Ultrasound-Guided Resection of Gliomas: A Meta-Analysis and Review of the Literature. *World Neurosurgery* (2016) 92:255–63. doi: 10.1016/j.wneu.2016.05.007
21. Prada F, Vetrano IG, DelBene M, Mauri G, Sconfienza LM, DiMeco F. Letter to the Editor Regarding "The Diagnostic Properties of Intraoperative Ultrasound in Glioma Surgery and Factors Associated with Gross Total Tumor Resection." *World Neurosurgery* (2019) 125:553–4. doi: 10.1016/j.wneu.2018.12.179
22. Shetty P, Yeole U, Singh V, Moiyadi A. Navigated ultrasound-based image guidance during resection of gliomas: practical utility in intraoperative decision-making and outcomes. *Neurosurgical Focus* (2021) 50:E14. doi: 10.3171/2020.10.FOCUS20550

Conflict of Interest: The authors declare that the research was conducted in the absence of any commercial or financial relationships that could be construed as a potential conflict of interest.

frontiers in Oncology

ORIGINAL RESEARCH
published: 03 May 2021
doi: 10.3389/fonc.2021.656519

Challenges and Opportunities of Intraoperative 3D Ultrasound With Neuronavigation in Relation to Intraoperative MRI

Dhiego Chaves De Almeida Bastos[*†], *Parikshit Juvekar*[†], *Yanmei Tie*, *Nick Jowkar*, *Steve Pieper*, *Willam M. Wells*, *Wenya Linda Bi*, *Alexandra Golby*, *Sarah Frisken*[‡] *and Tina Kapur*[‡]

Department of Neurosurgery, Brigham and Women's Hospital, Harvard Medical School, Boston, MA, United States

OPEN ACCESS

Edited by:
Francesco DiMeco, Fondazione Istituto Neurologio Carlo Besta (IRCCS), Italy

Reviewed by:
Aliasgar Moiyadi, Tata Memorial Hospital, India
Yubo Wang, First Affiliated Hospital of Jilin University, China

***Correspondence:**
Dhiego Chaves De Almeida Bastos
dhiegomed@yahoo.com.br

[†]*These authors share first authorship*

[‡]*These authors share senior authorship*

Specialty section:
This article was submitted to Neuro-Oncology and Neurosurgical Oncology, a section of the journal Frontiers in Oncology

Received: *20 January 2021*
Accepted: *09 April 2021*
Published: *03 May 2021*

Citation:
Bastos DCA, Juvekar P, Tie Y, Jowkar N, Pieper S, Wells WM, Bi WL, Golby A, Frisken S and Kapur T (2021) Challenges and Opportunities of Intraoperative 3D Ultrasound With Neuronavigation in Relation to Intraoperative MRI. Front. Oncol. 11:656519. doi: 10.3389/fonc.2021.656519

Introduction: Neuronavigation greatly improves the surgeon's ability to approach, assess and operate on brain tumors, but tends to lose its accuracy as the surgery progresses and substantial brain shift and deformation occurs. Intraoperative MRI (iMRI) can partially address this problem but is resource intensive and workflow disruptive. Intraoperative ultrasound (iUS) provides real-time information that can be used to update neuronavigation and provide real-time information regarding the resection progress. We describe the intraoperative use of 3D iUS in relation to iMRI, and discuss the challenges and opportunities in its use in neurosurgical practice.

Methods: We performed a retrospective evaluation of patients who underwent image-guided brain tumor resection in which both 3D iUS and iMRI were used. The study was conducted between June 2020 and December 2020 when an extension of a commercially available navigation software was introduced in our practice enabling 3D iUS volumes to be reconstructed from tracked 2D iUS images. For each patient, three or more 3D iUS images were acquired during the procedure, and one iMRI was acquired towards the end. The iUS images included an extradural ultrasound sweep acquired before dural incision (iUS-1), a post-dural opening iUS (iUS-2), and a third iUS acquired immediately before the iMRI acquisition (iUS-3). iUS-1 and preoperative MRI were compared to evaluate the ability of iUS to visualize tumor boundaries and critical anatomic landmarks; iUS-3 and iMRI were compared to evaluate the ability of iUS for predicting residual tumor.

Results: Twenty-three patients were included in this study. Fifteen patients had tumors located in eloquent or near eloquent brain regions, the majority of patients had low grade gliomas (11), gross total resection was achieved in 12 patients, postoperative temporary deficits were observed in five patients. In twenty-two iUS was able to define tumor location, tumor margins, and was able to indicate relevant landmarks for orientation and guidance. In sixteen cases, white matter fiber tracts computed from preoperative dMRI were overlaid on the iUS images. In nineteen patients, the EOR (GTR or STR) was predicted by iUS and confirmed by iMRI. The remaining four patients where iUS was not

able to evaluate the presence or absence of residual tumor were recurrent cases with a previous surgical cavity that hindered good contact between the US probe and the brain surface.

Conclusion: This recent experience at our institution illustrates the practical benefits, challenges, and opportunities of 3D iUS in relation to iMRI.

Keywords: ultrasound, 3D, neurosurgery, iMRI = intraoperative MRI, tumor

INTRODUCTION

Maximal safe resection of high-grade and low-grade gliomas has been established as an important prognostic factor with a strong correlation to survival (1–4). Image-guidance using computerized navigation on the basis of preoperative MRI is the current standard in the surgical management of brain tumors. Although neuronavigation greatly improves the surgeon's ability to approach, assess and operate on brain tumors, navigation based on preoperative MRI loses its accuracy as the surgery progresses, owing to substantial brain shift and deformation (5–8). Intraoperative MRI (iMRI) partially addresses this inherent problem of neuronavigation based on preoperative imaging when used serially during the surgery to provide anatomical updates reflective of the changing tissue structure (9, 10).

The first iMRI system, developed in the 1990s by General Electric in collaboration with physicians at Brigham and Women's Hospital, was designed as a 'double donut' configuration with the surgeon standing in the aperture between the two halves of the magnet. This provided the surgeon full access to the head without the need to move the patient in and out of the bore of the scanner (11). This system integrated navigation with continuous multi-oblique image plane acquisitions. This design mandated a low field strength magnet of 0.5T and was limited by the resultant poor image quality when compared to preoperative diagnostic MRI scanners of field strengths typically ranging from 1.5T to 3T. To improve image quality and resolution, higher field, closed configuration magnets are necessary, requiring either moving the patient deep into the bore of the magnet or moving the magnet to the patient on the operating room table. This requirement makes it impractical to acquire multiple images to update neuronavigation as tumor resection progresses and tissue deformation ensues, due to the time cost associated with each iMRI imaging session. Thus, the common practice in iMRI guided brain tumor surgery is to perform a single iMRI imaging session near the end of intended resection for identifying any residual tumor.

Intraoperative ultrasound (iUS) is a powerful alternative to iMRI for monitoring brain shift and updating neuronavigation during surgery. The main advantage of iUS is that it causes minimal disruption to the surgical workflow while providing real-time information to the surgeon and is much less expensive and resource intensive than iMRI (12). 2D iUS has the disadvantage of a steep learning curve and an increased cognitive burden necessitated to integrate the orientation of 2D images to the 3D anatomy of the surgical field. Thus, it can be difficult for surgeons to maximally benefit from 2D iUS in neurosurgical procedures. Integrating preoperative MRI with 3D iUS in neuronavigation helps resolve these orientation challenges of 2D iUS (13–15; Geirmund 16–18).

In this report, we present the challenges and opportunities in the use of 3D iUS during brain tumor resection in an advanced image-guided operating environment with multimodal preoperative MRI, neuronavigation and iMRI. We describe how we use preoperative MRI, iMRI, and 3D iUS intraoperatively and discuss the current and future impact of these imaging modalities on neurosurgical practice.

MATERIALS AND METHODS

We retrospectively evaluated patients who underwent image-guided brain tumor resection in the Advanced Multi-modal Image-Guided Operating (AMIGO) Suite (19, 20) at Brigham and Women's Hospital in Boston, USA, between June 2020 and November 2020, where both iUS and iMRI were employed to guide the resection. We selected cases representative of patients at higher risk of post-operative neurological complications due to the location of the tumor in or near the eloquent cortex or patients where intraoperative imaging was required to guide resection. The cases were individually analyzed and the roles of iUS and iMRI at multiple time points were compared. Clinical, demographic, histopathological and radiological information was manually collected from the patients' electronic medical records. Tumors were classified according to the World Health Organization (WHO) 2016 Classification of Gliomas and cIMPACT-NOW updates 4, 6 and 7 (21–24). Additionally, tumors were classified into one of 3 categories based on proximity to functional cortex (non-eloquent [Grade I], near-eloquent [Grade II], and eloquent [Grade III]) (25). Extent of resection (EOR) was classified by a neuroradiologist as gross total resection (GTR) or subtotal resection (STR) based on a postoperative MRI performed within 48 hours after surgery. We also describe three cases in greater detail and note the nuances in our experience of using iUS in neurosurgical practice. The study was approved by the Mass General Brigham Institutional Review Board and written informed consent was obtained from all patients included in this study. The surgical procedures in this series were performed either by W.L.B or A.G, both neurosurgeons with extensive experience in image-guided neurosurgery using iUS and iMRI.

Cohort Selection

The study was conducted between June 2020 and December 2020 when an extension of a commercially available navigation software was introduced in our practice enabling 3D iUS volumes to be reconstructed from tracked 2D iUS images. During this period, a total of 23 cases were performed in the AMIGO suite by the study surgeons. Preoperatively, MR images were acquired using a 3T MRI scanner (Magnetom Prisma/Skyra, Siemens Healthineers, Erlangen, Germany) and a 20-channel Siemens head-coil. Structural MR imaging included a 3D T1-weighted post-contrast sequence, a 2D T2-weighted sequence, a 3D MP2RAGE sequence, and a 3D T2-weighted FLAIR sequence. Patients with lesions in or near eloquent areas underwent blood oxygen level-dependent (BOLD) fMRI with a single-shot 2D echo-planar imaging (EPI) sequence with the appropriate tasks paradigms for language and motor mapping, according to our institutional protocol (26). Preoperative Diffusion MRI (dMRI) was acquired in all patients and Brainlab Fibertracking software module (Brainlab Elements, Munich, Germany) was used for tractography in patients who had lesions in close proximity to eloquent white matter tracts. Relevant fMRI activations were used as seed regions to generate fiber tracts, either individually or in combination, as deemed clinically appropriate. All MR images were imported into a neuronavigation system (Brainlab, Munich, Germany) for presurgical planning.

3D Intraoperative Ultrasound (iUS)

iUS was performed using a 2D neuro-cranial curvilinear transducer on a cart-based ultrasound system (N13C5, BK5000, Analogic Corporation, Peabody, MA, USA). This sterilizable transducer has a contact surface area of 29x10 mm and frequency range of 13-5 MHz. The ultrasound probe was tracked with the Brainlab Curve navigation system (Brainlab, Munich, Germany). Similar to optical tracking of other surgical instruments, a fiducial array was attached to the ultrasound transducer and tracked relative to a reference array attached to the head fixation device (HFD100, IMRIS, Minnetonka, MN, USA). This allowed the navigation software to localize the acquired 2D iUS slices and orient them at the transducer tip. During image acquisition, the imaging plane of the transducer was oriented as close as possible to one of the three cardinal axes of the head, determined by the size and shape of the craniotomy (e.g., when the largest dimension of the craniotomy was along the anteroposterior axis, the transducer was placed in a coronal or sagittal orientation depending on the surgeon's view preference). The 2D probe was slowly swept across the craniotomy to acquire a sequence of tracked 2D images. A 3D iUS volume was created from the tracked images at a resolution of 0.2 mm x 0.2 mm x 0.2 mm using an automated ultrasound reconstruction extension at the backend of the navigation software (Digital Ultrasound Integration, Brainlab, Munich, Germany). The 3D iUS volume was overlaid on preoperative imaging, providing insight into brain shift and possible registration errors. For each patient, three or more 3D iUS volumes were acquired during the procedure, and one iMRI was acquired after significant resection towards the end of the procedure. The iUS images included: an extradural image acquired immediately after the craniotomy and before dural incision (iUS-1); an intradural image acquired immediately after the dural opening (iUS-2); and a third image acquired immediately before the iMRI acquisition (iUS-3) (S. 27).

Intraoperative MRI (iMRI)

iMRI was performed using a 3T wide-bore (70 cm) MRI scanner (Magnetom Verio, Siemens Healthineers, Erlangen, Germany) after significant resection to evaluate the presence of any residual tumor. A temporary closure was performed prior to the iMRI acquisition. The total time required to obtain iMRI including preparation for scanning, MR safety check, image acquisition, and repreparing for surgery t was 1-1.5 hours per session. In some of the surgeries, clinical needs necessitated imaging sessions at 2 distinct surgical timepoints. The Brainlab registration module was used to automatically register iMRI to preoperative MRI (rigid registration). This allows us to compare iMRI in the same coordinate space as iUS.

Comparison of iUS to Neuronavigation and iMRI

iUS-1 and iUS-2 were used to provide a real-time assessment of the lesion extension, location and local anatomy and to confirm navigation accuracy. iUS-3 was qualitatively compared to iMRI to evaluate how well the iUS could image residual tumor and predict the extent of the resection. The presence or absence of residual tumor on iUS-3, as per the attending neurosurgeon, was recorded prior to the acquisition of the iMRI. The assessment of the residual tumor in iMRI was also made by the attending neurosurgeon in consultation with a neuroradiologist.

RESULTS

We compared the clinical utility of iUS with preoperative MRI and iMRI in twenty-three patients (15 men, 8 women; age range 28-83 years) who underwent image-guided brain tumor resection in the AMIGO suite (**Table 1**). In seven patients, the tumors were located in eloquent brain regions, eight near-eloquent brain regions, and eight in a deep-seated non-eloquent brain region. Thirteen patients had newly diagnosed tumors, while ten patients underwent resection for recurrent tumors. Five patients had *IDH1*-mutant grade 3 gliomas, three patients had an integrated histological and molecular diagnosis of glioblastoma multiforme, ten had grade 2 gliomas, one had brain metastases from a non-small cell lung carcinoma, one had a diagnosis of radiation necrosis and one had a central nervous system lymphoma. GTR was achieved in twelve patients (in the other patients, subtotal resection was expected due to the unfavorable location of tumors in the eloquent cortex). Temporary postoperative deficits were observed in five patients, all of whom had tumors in eloquent or near-eloquent regions. **Table 2** summarizes tumor pathology along with

TABLE 1 | Summary of patient demographics, and preoperative clinical and radiological aspects of brain tumors.

#	Sex (Age, years)	Tumor Location	Recurrent	Eloquence	Related White Matter Tracts	Contrast Enhancing
1	Male (61)	Right frontal	No	Near Eloquent	CST[1]	No
2	Male (28)	Left medial temporal	No	Near Eloquent	IFOF[2], Arcuate, visual fibers	No
3	Female (53)	Left cingulate gyrus	No	Near Eloquent	CST[1], Frontal Aslant Tract	No
4	Male (58)	Left Insula	No	Eloquent	CST[1], Arcuate	No
5	Male (45)	Right temporal-Recurrent	Yes	Non-eloquent	–	Yes
6	Male (36)	Left insula	Yes	Eloquent	CST[1], Arcuate	No
7	Male (58)	Left frontal	No	Eloquent	CST[1]	Yes
8	Female (34)	Right Insula-Recurrent	No	Eloquent	IFOF[2], Uncinate	No
9	Male (83)	Right frontal	No	Eloquent	CST[1]	Yes
10	Male (52)	Left temporal	No	Near Eloquent	CST[1], Arcuate	Yes
11	Female (56)	Left frontal	Yes	Non-eloquent	–	Yes
12	Female (32)	Left temporal	Yes	Near Eloquent	Arcuate, IFOF	No
13	Female (49)	Left frontal	Yes	Non-eloquent	–	Yes
14	Male (45)	Right frontal	No	Near Eloquent	CST	No
15	Female (45)	Right parietal	Yes	Near Eloquent	CST	No
16	Male (42)	Left frontal	Yes	Non-eloquent	–	Yes
17	Female (23)	Left occipito-parietal	Yes	Non-eloquent	–	Yes
18	Male (48)	Right frontal	Yes	Non-eloquent	–	Yes
19	Male (52)	Right temporal	No	Non-eloquent	IFOF	No
20	Male (42)	Right precentral gyrus	No	Eloquent	CST	No
21	Female (23)	Right temporal	No	Non-eloquent	–	Yes
22	Male (69)	Left frontal	Yes	Eloquent	Arcuate, CST	No
23	Male (54)	Left frontal/insula	No	Near Eloquent	IFOF, Arcuate	No

[1]Corticospinal Tract; [2]Inferior fronto-occipital fascicle.

intraoperative details of the tumor resection and the postoperative patient outcomes.

In all cases, iUS images acquired at two time points were visually compared with either preoperative MRI or iMRI. In nineteen patients, the iUS and iMRI findings regarding the status of the resection (GTR or STR) were concordant. In all these patients, iUS was able to define tumor location, tumor margins and was able to indicate relevant landmarks for orientation and guidance. The remaining four patients where iUS was not able to evaluate the presence or absence of residual tumor were recurrent cases with a previous surgical cavity that hindered good contact between the US probe and the brain surface. In sixteen cases, white matter fiber tracts computed from preoperative dMRI were overlaid on the iUS images. **Table 2** summarizes the imaging characteristics of iUS at iUS-1, iUS-2 and iUS-3. We discuss three of these cases in detail below.

Case 1

A 61-year-old right-handed man presented with new onset focal seizures, manifesting as dysarthria, and left-sided facial twitching. Brain MRI revealed a non-enhancing mass in the right frontal lobe anterior to the precentral gyrus (**Figure 1**). The lip pursing task from the preoperative fMRI showed BOLD activations in the pre- and postcentral gyri, 1 cm posterior to the T2-hyperintense lesion (**Figure 1C**). The activations corresponding to the left hand were superior to the activations for lip pursing along the pre- and postcentral gyri, distant from the lesion. Language activations indicated left lateralized language function. White matter tractography seeded from motor fMRI BOLD activation areas was used to generate the right corticospinal tract (**Figures 1D, E**).

A right frontotemporal craniotomy with transcranial and direct cortical motor mapping was performed. After the craniotomy, an extradural ultrasound (iUS-1) confirmed a homogeneously hyperechoic mass, expanding the gyrus anterior to the prefrontal gyrus (**Figures 2** and **3A**). Overlaying iUS-1 on the preoperative MRI showed a mismatch by one gyrus (approximately 1.5 cm) between the segmented tumor on MRI and the tumor observed in the iUS (**Figure 2**). After the dural opening, iUS (iUS-2) was performed and the margins of the tumor were blurrier than iUS-1 (**Figure 3B**). The iUS (US-1 and US-2) in this case was used to precisely localize the area of the abnormality and the gyral anatomy. Cortical mapping was used directly over the planned resection sites and did not evoke any motor responses. Microsurgical resection proceeded with serial checks of the ultrasound to evaluate progress, especially as resection approached the posterior and medial margin of the lesion in close relation to the descending motor fibers (**Figure 3C**). Continuous subcortical motor mapping was also performed during the resection with a monopolar stimulating suction (Drytouch single-use Frazier Monopolar Stimulation Suction Probe, Neurovision Medical Products, Ventura CA). When a complete resection had been achieved per the surgeon's estimate, a final iUS sweep (iUS-3) was acquired that suggested the absence of any residual tumor (**Figure 3D**) which was corroborated by the iMRI for confirmation of GTR. The patient had no postoperative neurological deficits and was discharged home after two days. Pathology revealed a glioblastoma multiforme.

Case 2

A 28-year-old right-handed man presented with episodes of anxiety and fear lasting 20-30 seconds, with an initial diagnosis

TABLE 2 | Summary of Intraoperative and Postoperative Imaging Findings.

#	Lesion echogenicity	Predura US Anatomical Landmark	US1 confirms navigation MRI	Residual Tumor (US)	Residual Tumor (iMRI)	Extent of Resection	Postop Deficits	Tumor Pathology
1	Homogeneous hyperechoic	Sulci	Yes	No	No	GTR[1]	None	GBM**
2	Heterogeneous hyperechoic	Tentorium, brainstem, cerebellum	Yes	Yes	Yes	STR[2]	Temporary word findings and reading difficulty	Anaplastic Astrocytoma *IDH1*mutant, Grade 3
3	Homogenous hyperechoic	Falx, cingulate sulcus, lateral ventricles, callosum sulcus	Yes	Yes	Yes	STR	SMA* syndrome	GBM**
4	Homogeneous hyperechoic	Sylvian fissure	Yes	Yes	Yes	STR	Temporary aphasia	Diffuse Astrocytoma *IDH1*mutant, Grade 2
5	Heterogeneous hyperechoic	Lateral ventricle, tentorium	Yes	Yes	Yes	STR	None	Anaplastic Oligodendroglioma, Grade 3
6	Homogeneous hyperechoic	Sylvian fissure, ventricles	Yes	Yes	Yes	STR	None	Anaplastic Astrocytoma *IDH1*mutant, Grade 3
7	Hypoechoic cyst + hyperechogenic margins	Falx, ventricles	Yes	No	No	GTR	None	Metastasis (NSCLC[T])
8	Heterogeneous hyperechoic	Sylvian fissure, Falx	Yes	Yes	Yes	STR	None	Diffuse Astrocytoma *IDH1*mutant, Grade 2
9	Isoechoic with surrounding hyperechoic edema	Lateral ventricles, Falx	Yes	No	No	GTR	Temporary UE[3] paresis	Lymphoma
10	Heterogeneous hyperechoic solid component & hypoechogenic cyst	Occipitotemporal sulcus	Yes	Yes	Yes	GTR	No	Oligodendroglioma, Grade 2
11	Heterogeneous hyperechoic	Orbital gyri	Yes	Yes	Yes	GTR	No	Radiation necrosis
12	Heterogeneous hyperechoic	Tentorium, brainstem, cerebellum	Yes	Yes	Yes	STR	No	Diffuse Astrocytoma *IDH1*mutant, Grade 2
13	Nonvisible (large surgical cavity)	Ventricles	No	Not visible (previous resection cavity)	Yes	GTR	No	Anaplastic Oligodendroglioma, Grade 3
14	Homogeneous hyperechoic	Sylvian fissure	Yes	Yes	Yes	STR	No	Oligodendroglioma, Grade 2
15	Heterogeneous hyperechoic (hard to visualize)	Lateral ventricles	Yes	Not visible (previous resection cavity)	No	GTR	No	Oligodendroglioma, Grade 2
16	Heterogeneous hyperechoic	Lateral ventricles	Yes	Yes	Yes	STR	No	Oligodendroglioma, Grade 2
17	Heterogeneous hyperechoic	Falx	Yes	Not visible (previous resection cavity)	No	GTR	No	Grade 2 low grade glioma with ependymoma differentiation, IDH1 wildtype
18	Homogeneous hyperechoic	Lateral ventricles	Yes	Not visible (blurry)	Yes	GTR	No	Anaplastic Astrocytoma *IDH1*mutant, Grade 3
19	Homogeneous hyperechoic	Sylvian fissure	Yes	Yes	Yes	GTR	No	Oligodendroglioma, Grade 2
20	Homogeneous hyperechoic	Sulci	Yes	Yes	Yes	GTR	No	Oligodendroglioma, Grade 2
21	Hypoechoic cyst + hyperechogenic margins	Sylvian fissure	Yes	No	No	GTR	No	Ganglioglioma, grade I
22	Heterogeneous hyperechoic	Lateral ventricles	Yes	Yes	Yes	STR	No	Anaplastic Oligodendroglioma, Grade 3
23	Heterogeneous hyperechoic	Lateral ventricles	Yes	Yes	Yes	STR	Status epilepticus	GBM

*[1]Gross total resection; [2]Subtotal resection; [T]Non small cell lung cancer; [3]Upper extremity; *Supplementary motor area; **Glioblastoma multiforme.*

of post-traumatic stress disorder. Escalating frequency of these episodes prompted imaging evaluation, which revealed a large left non-enhancing mass in the mid- and posterior medial temporal lobe. Preoperative language fMRI showed BOLD activations in the putative receptive language areas of the left superior temporal gyrus, within 1 cm of the T2-hyperintense lesion. Visual tasks were used to map the primary visual cortex using fMRI. The AF, IOFF/IFOF, ILF, FAT and Optic Radiations (OR) were created on the tractography software using fMRI BOLD activation areas as seed ROIs, consistent with their expected anatomical locations. An unexpected fiber bundle running through the middle of the posterior aspect of the lesion was suspected to be related to the visual pathway (**Figure 4**).

A left temporal craniotomy was performed, with subsequent extradural ultrasound (iUS-1) which confirmed presence of a

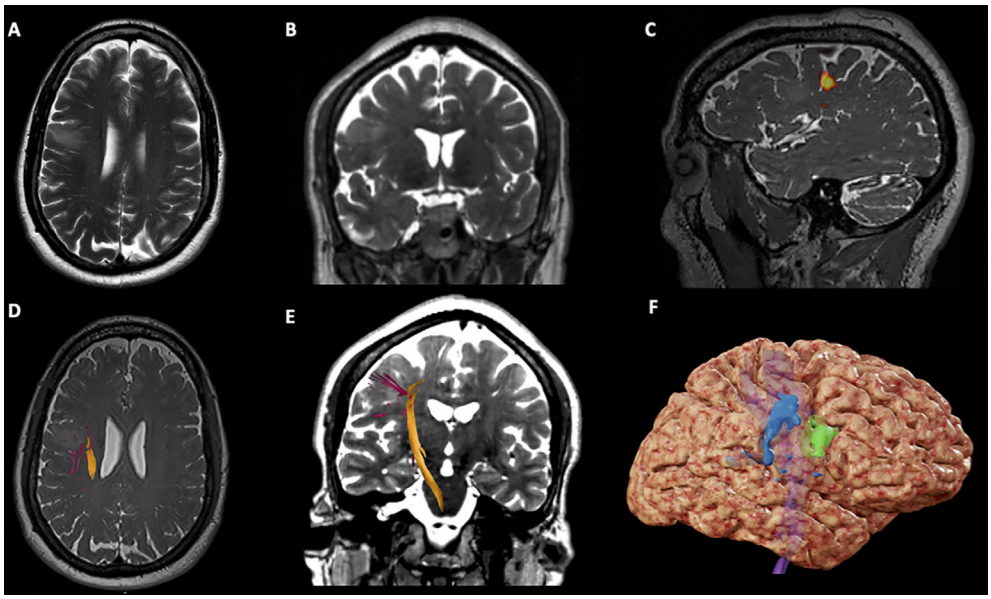

FIGURE 1 | Case 1 Surgical Plan. **(A)** Axial T2-weighted imaging showing an hypointensity in the right middle frontal gyrus, anterior to the precentral gyrus; **(B)** Coronal T2-weighted imaging showing an hypointensity in the right middle frontal gyrus; **(C)** Sagittal T2*-weighted imaging showing BOLD activation for lip purse test (yellow) on the lateral aspect of the right precentral gyrus; **(D)** Axial T2*-weighted imaging showing the right Corticospinal Tract (CST) on the deep and posterior margins of the tumor; **(E)** Coronal T2-weighted imaging showing the right CST descending from the precentral gyrus in the posterior aspect of the tumor; **(F)** 3D brain reconstruction showing the BOLD activation for lip purse segmented (in blue), the segmented tumor (green) and the CST deep (in purple).

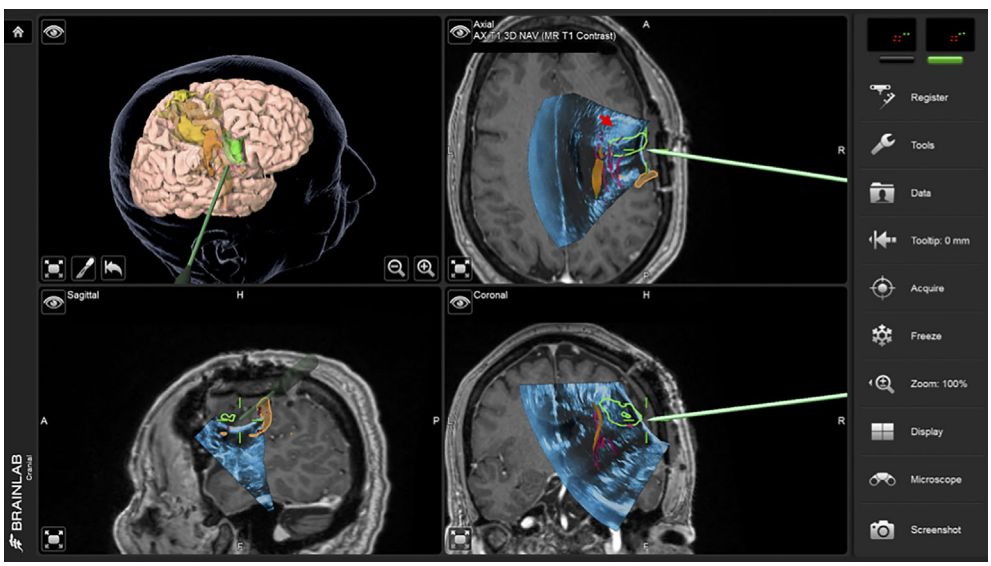

FIGURE 2 | Case 1 intraoperative screen capture with the 3D surgical plan reconstruction with fMRI BOLD activation segmented in orange, tumor in green and Corticospinal Tract in yellow (the upper left panel), and the three orthogonal planes with 3D iUS-1 overlaid on preoperative MP2Rage. Notice the mismatch between the segmented tumor on MRI (green segmentation) and observed tumor on iUS (red arrowhead), placing the tumor site over the sulcus between the gyri making it difficult to know which gyrus was the tumor actually located.

heterogeneous hyperechoic mass within the exposed area (**Figure 4A**). Relatively immobile reference landmarks, such as the tentorium, the brainstem, the cerebellum, and the cerebral aqueduct, were visualized as additional correlative landmarks. The dura was opened and an intradural ultrasound was performed to confirm the tumor location (**Figure 4B**). A linear pial incision, in the inferior temporal gyrus and parallel to the gyrus, was fashioned followed by dissection until the tumor was

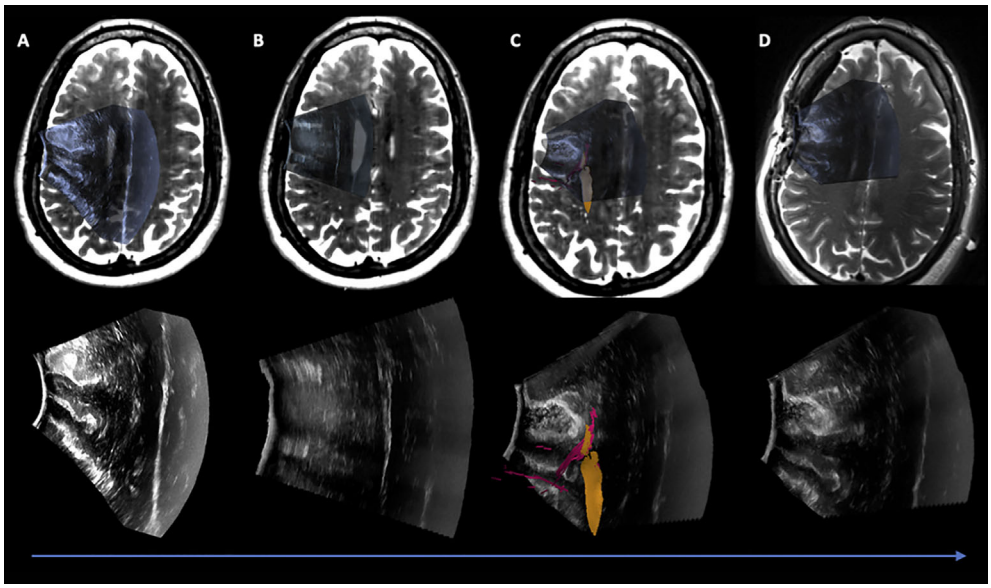

FIGURE 3 | Case 1 Post hoc manually aligned preoperative axial T2-weighted imaging with **(A)** iUS-1, **(B)** iUS-2, **(C)** iUS-3 with right Corticospinal Tract (yellow) and Frontal Aslant Tract (red), and **(D)** iMRI axial T2-weighted imaging manually aligned with iUS-3. On D it is possible to observe a gross total resection on iUS and confirmed by iMRI.

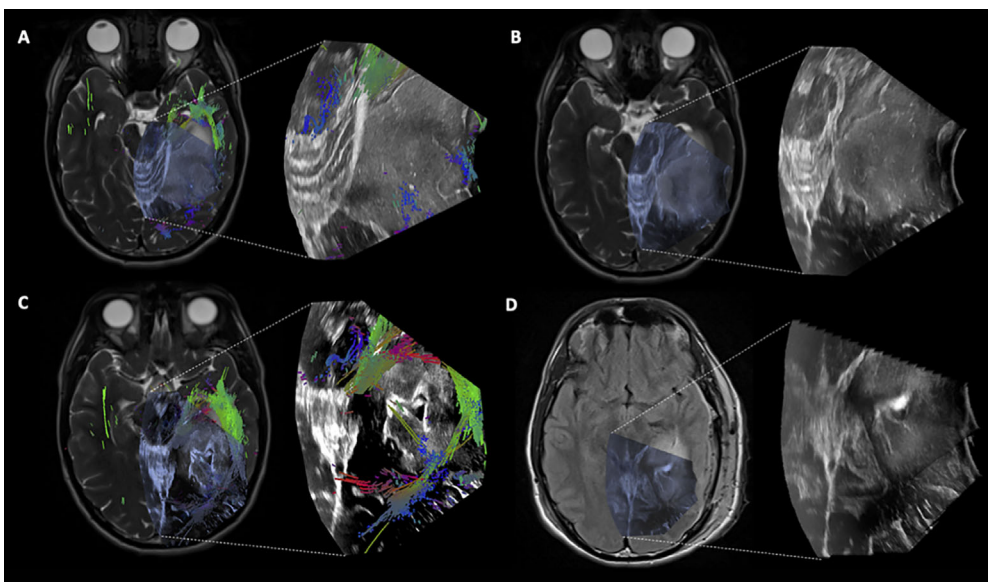

FIGURE 4 | Case 2 Post hoc manually aligned preoperative axial T2-weighted imaging with **(A)** iUS-1, **(B)** iUS-2, **(C)** iUS-3 with multiple tracts around and inside the tumor, and **(D)** iMRI axial T2-FLAIR imaging manually aligned with iUS-3 without the overlaid tracts. Notice on C the presence of tracts running through the tumor. On D, it is possible to notice the presence of residual tumor in the posterolateral margin as well as posteriorly along the medial margin in the vicinity of the coursing tracts through the tumor.

encountered. The tumor was extirpated centripetally, using multiple ultrasound sweeps to serially assess resection progress. At one point, the tracts within the tumor were localized using iUS and preserved (**Figures 4C** and **5**). When the initial resection goals were accomplished to the surgeon's satisfaction, iUS-3 was performed, which suggested possible residual tumor at the posterolateral margin as well as posteriorly along the medial margin in the vicinity of the coursing tracts through the tumor

(**Figure 4D**). iMRI confirmed the iUS findings (**Figure 4D**). The patient was re-draped, and the resection of the remaining tumor in the posterolateral aspect of the cavity was completed. The patient exhibited mild temporary word finding and reading difficulty early post-operatively. Three weeks after surgery, his preoperative anxiety attacks were nearly resolved and he only had minor word finding difficulties. On his 3-months follow-up, the patient was back to his baseline and seizure free. Pathology was compatible with a grade 3 *IDH1*-mutant anaplastic astrocytoma.

Case 3

A 53-year-old woman presented with a partial motor seizure, with postictal transient right-sided hemiparesis. Brain MRI showed a non-enhancing deep-seated lesion in the left cingulate gyrus, extending to the mid-/posterior corpus callosum inferiorly and to the paracentral gyrus superiorly. Preoperative fMRI of hand clenching, finger tapping, and toe wiggling tasks showed BOLD activations in the anatomically expected M1 location and more anteriorly in the superior frontal gyrus. DTI tractography using fMRI BOLD activation areas as seed ROIs was used to generate the left CST and the left FAT. A 3D rendering of preoperative T1 post-contrast MRI reconstruction highlighted two prominent cortical veins entering the superior sagittal sinus in the planned craniotomy. Taken together, preoperative imaging suggested a narrow window for a safe operative corridor to the tumor.

A left frontal craniotomy with transcranial and direct cortical motor evoked potentials as well as subcortical motor mapping was planned. The patient was positioned supine with head neutral and 30° neck flexion. Via a linear incision a craniotomy was performed to expose the superior sagittal sinus and coronal suture. iUS-1 confirmed adequate exposure of the tumor (**Figure 6**). A second iUS (iUS-2) was performed after the dura mater was opened to validate the continued accuracy of neuronavigation; there was a potential for a brain shift in the anteroposterior direction due to cerebrospinal fluid (CSF) drainage but none was observed. We attempted an interhemispheric dissection, which was limited by the bridging veins merging with the sinus along its length, prompting pursuit of a transcortical approach instead. The cortical entry point was defined between the two hand and foot activation areas connected by the corticospinal tract and the frontal aslant tract, using a combination of motor mapping and navigating the iUS-2 volume with the preoperative MRI (**Figure 6B**). The anterior-most and superficial part of the tumor was well differentiated from the surrounding brain, but the posterior and deeper portion was only partially distinguishable. Surgical resection was pursued posteriorly until subcortical stimulation of motor tract responses reached a threshold of 2.5 mA. A third iUS sweep (iUS-3) indicated some residual tumor in the anterior-most part of the cavity, cloaked by a sheath of arachnoid in the cingulate sulcus (**Figure 7A**). iMRI at this point confirmed residual tumor in both the anterior and posterior aspects of the surgical cavity (**Figure 7B**). Additional microscopic resection of the anterior residual tumor was achieved. In the early postoperative period, the patient exhibited right-sided hemiparesis, most prominent on lower extremity with preserved tone, with near-complete recovery by postoperative Day 10 barring minor gait apraxia, and a full recovery after 3 weeks consistent with a supplementary motor syndrome. Pathology was compatible with glioblastoma multiforme

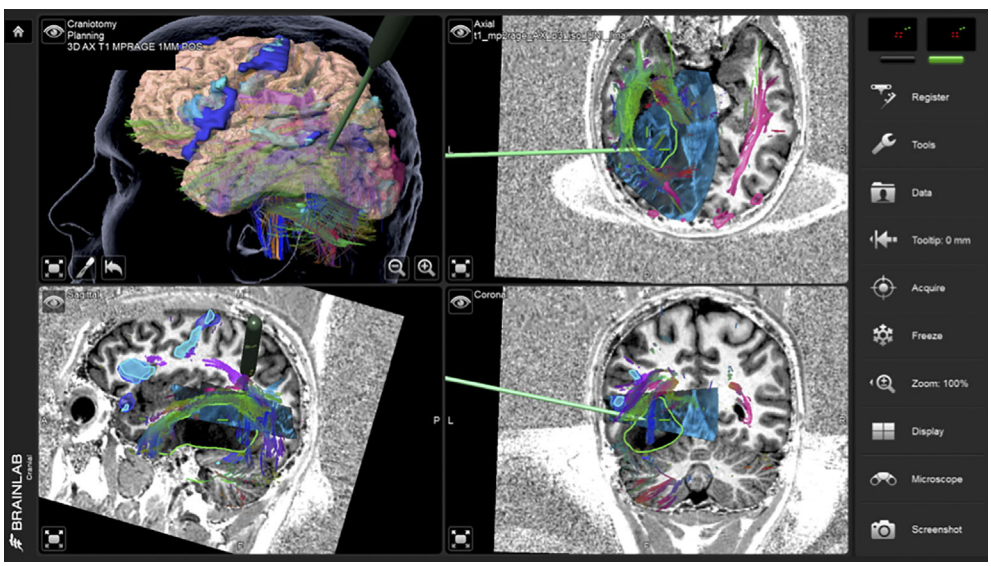

FIGURE 5 | Case 2 intraoperative screen capture with the 3D surgical plan reconstruction with fMRI BOLD activation segmented in dark and light blue and tumor in green (upper left panel), and the three orthogonal planes with 3D iUS-3 overlaid on preoperative MP2Rage. Notice the navigation probe in close proximity to the tracts running through the tumor. In order to preserve these tracts, no further resection medially was performed.

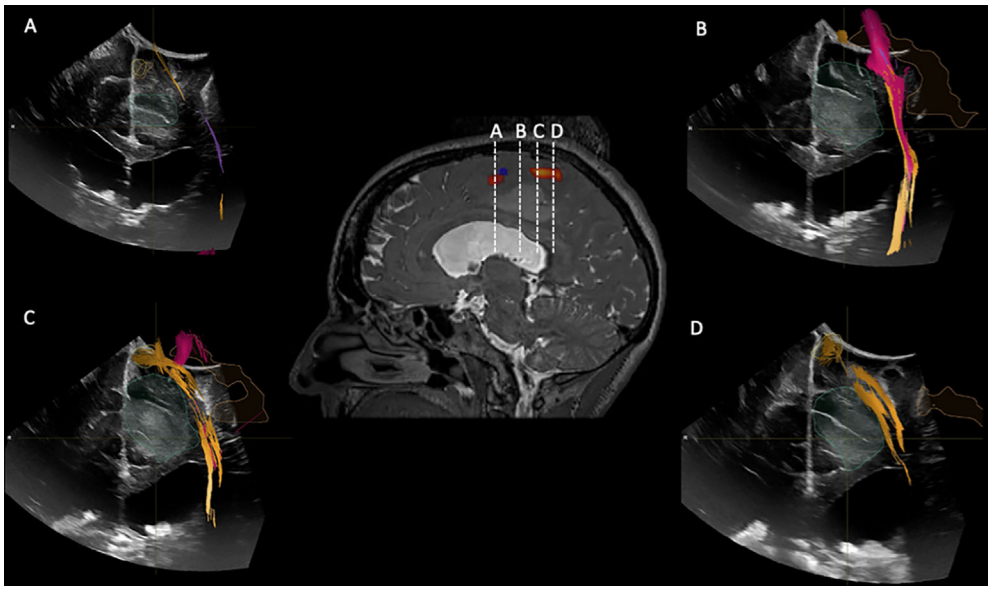

FIGURE 6 | iUS1 in Case 3. Central panel shows a sagittal T2*-weighted imaging with fMRI BOLD activations for lower extremity (red) and upper extremity (blue). **(A)** Coronal iUS-1 showing the most anterior part of the tumor; **(B)** coronal iUS-1 showing the only possible surgical corridor that avoids the fMRI BOLD activations areas and Corticospinal Tract (CST); **(C)** Coronal iUS-1 overlaid with fMRI BOLD activation for lower extremity and CST superior to the tumor; **(D)** coronal iUS-1 with overlay of CST superior to the tumor.

DISCUSSION

2D and 3D iUS Compared to Preoperative MRI

In the present paper, the locations and margins of the tumors as shown by iUS were in agreement with preoperative MRI. This is consistent with findings in the literature of significant correlation between 2D US and preoperative MRI (28, 29). While there is additional literature on the ability of iUS to provide better tumor delineation than T1-weighted MRI iUS, (30; G. 31), we have not systematically studied this.

iUS and Navigation

Navigated 3D iUS was able to provide real-time information regarding brain shift, possible problems with registration and to identify potential surgical entry points in all cases. Since we used iUS-1 and iUS-2 to validate neuronavigation on preoperative MRI, we were able to recognize rigid mismatches and avoid errors such as incision of the incorrect gyrus that could have happened if we had navigated solely on the preoperative MRI (Case 1). iUS allowed us to enhance neuronavigation by providing important information regarding the best window between two functional areas to proceed with a corticectomy (Case 3). A recent study of 210 glioma patients reported that serially acquired navigated iUS played an important role in assessing resection progress (32).

iUS to Measure and Monitor Brain Shift

An important advantage of iUS is its ability to monitor brain shift over the course of surgical resection and to provide real-time anatomical information that reflects the current intraoperative state. In our cohort, we observed minimal brain shift between iUS-1 and iUS-2, but as the surgical resection progressed, the mismatch between the preoperative MRI on the navigation system and the iUS became evident, rendering neuronavigation suboptimal for clinical decision-making. Therefore, the only true, real-time image-guidance available to us was from iUS. While we have not employed any non-rigid registration methods in this study, we and others have developed several that have continued to move the field forward for registration of MRI-MRI and MRI-iUS volumes (6, 27, 33–37).

Concordance Between iUS and iMRI

Our study showed a concordance rate of 100% between iUS and iMRI findings in predicting the EOR in patients where good contact between the US probe and the brain surface was possible; on iUS-3 four patients showed no residual tumor and fifteen patients showed residual tumor, all confirmed by iMRI. These results are similar to the earliest study that revealed a 100% concordance rate between the two imaging modalities (28). (38) showed in a study of 20 GBM surgeries that tumor detection sensitivity using a navigated linear array ultrasound transducer is significantly higher (78% vs. 24%) compared to using a curved array transducer, while specificity is reduced (from 58% vs 96%). A more recent study in both adult and pediatric patients with brain tumors using iUS showed 81% concordance, with 19% false-negative results (39). The main hurdle in using iUS to establish the EOR is the difficulty by the end of the surgery to assess if a hyperechoic area is truly residual tumor, since the

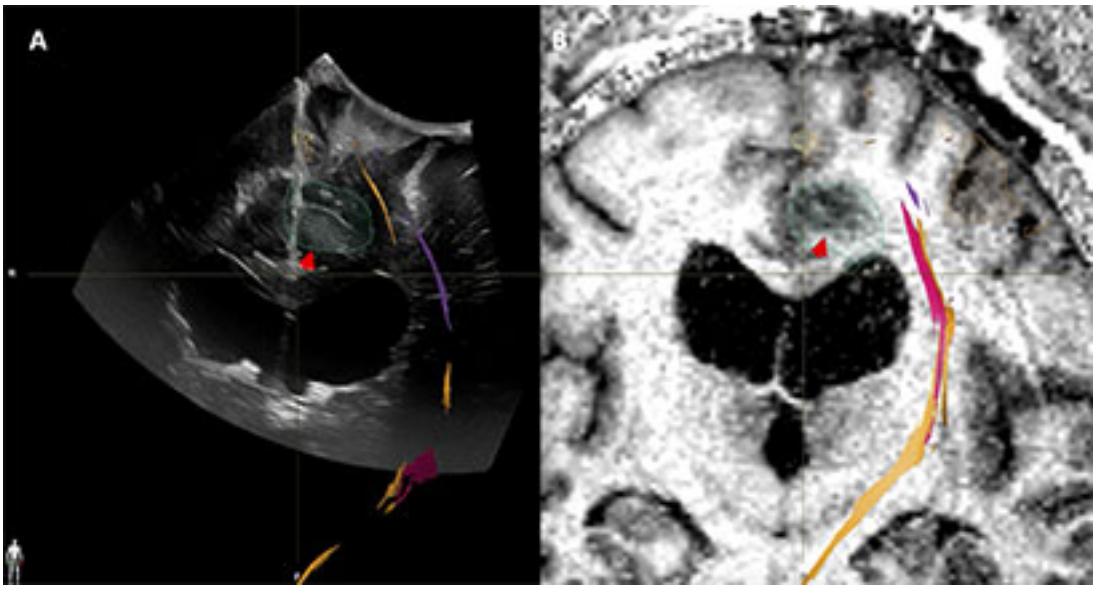

FIGURE 7 | Case3. iUS3 **(A)** showing unexpected residual tumor (red arrowhead) under the arachnoid fold which was confirmed by iMRI **(B)**.

enhancement artifact caused by differences in attenuation of the resection cavity fluid and the surrounding brain is a significant surgically induced ultrasound artifact (40). Although we noticed this artifact in some of our cases, we were able to confirm the iUS findings using iMRI because all the cases were performed in the AMIGO suite. A potential solution to this problem is a coupling fluid that attenuates ultrasound energy like the normal brain and reduces enhancement artifacts, which has been studied though is not yet commercially available (40).

Limitation of iUS Imaging

In patients with large resection cavities, either new or previous, contact between iUS probe and the brain surface can be difficult or impossible to achieve, particularly in cases where the head position does not favor retention of fluid in the cavity. In such cases we were unable to obtain 2D and hence 3D iUS.

Challenges in Creating 3D iUS Volume

Although 3D iUS provides us with a powerful surgical tool, creating these volumes poses some challenges. It is difficult to maintain a uniform speed of probe translation while collecting 2D images for a volume. This task becomes more difficult later in the surgery when the resection cavity is filled with fluid and subtle variations in the steadiness of the transducer leads to artifacts in the resultant 3D volume.

CONCLUSION

The impact of iUS on neurosurgical practice continues to evolve in the face of improved transducers, neuronavigation systems, and surgical technique. This review of the recent experience at our institution illustrates the practical benefits of iUS in relation to iMRI, and the challenges encountered in a range of tumor resection cases.

DATA AVAILABILITY STATEMENT

The raw data supporting the conclusions of this article will be made available by the authors, without undue reservation.

ETHICS STATEMENT

The studies involving human participants were reviewed and approved by Mass General Brigham Institutional Review Board. The patients/participants provided their written informed consent to participate in this study. Written informed consent was obtained from the individual(s) for the publication of any potentially identifiable images or data included in this article.

AUTHOR CONTRIBUTIONS

Data collection: DB, PJ. Data interpretation: DB, PJ, AG, WB, TK, SF. Manuscript: DB, PJ, AG, WB, TK, SF, SP. Manuscript editing: DB, PJ, AG, WB, TK, SF, YT, SP, WW. Bibliography editor: DB, NJ, TK. Images editor: DB, PJ. All authors contributed to the article and approved the submitted version.

ACKNOWLEDGMENTS

P41EB015898, P41EB015902, P41EB028741, R01EB027134, R21CA198740, Jennifer Oppenheimer Cancer Research Initiative.

REFERENCES

1. Lacroix M, Abi-Said D, Fourney DR, Gokaslan ZL, Shi W, DeMonte F, et al. A Multivariate Analysis of 416 Patients With Glioblastoma Multiforme: Prognosis, Extent of Resection, and Survival. *J Neurosurg* (2001) 95(2):190–8. doi: 10.3171/jns.2001.95.2.0190
2. McGirt MJ, Chaichana KL, Attenello FJ, Weingart JD, Than K, Burger PC, et al. Extent of Surgical Resection is Independently Associated With Survival in Patients With Hemispheric Infiltrating Low-Grade Gliomas. *Neurosurgery* (2008) 63(4):700–7. doi: 10.1227/01.NEU.0000325729.41085.73
3. Sanai N, Polley M-Y, McDermott MW, Parsa AT, Berger MS. An Extent of Resection Threshold for Newly Diagnosed Glioblastomas. *J Neurosurg* (2011) 115(1):3–8. doi: 10.3171/2011.2.JNS10998
4. Smith JS, Chang EF, Lamborn KR, Chang SM, Prados MD, Cha S, et al. Role of Extent of Resection in the Long-Term Outcome of Low-Grade Hemispheric Gliomas. *J Clin Oncol* (2008) 26(8):1338–45. doi: 10.1200/JCO.2007.13.9337
5. Dorward NL, Alberti O, Velani B, Gerritsen FA, Harkness WF, Kitchen ND, et al. Postimaging Brain Distortion: Magnitude, Correlates, and Impact on Neuronavigation. *J Neurosurg* (1998) 88(4):656–62. doi: 10.3171/jns.1998.88.4.0656
6. Nabavi A, Black PM, Gering DT, Westin CF, Mehta V, Pergolizzi RSJR, et al. Serial Intraoperative Magnetic Resonance Imaging of Brain Shift. *Neurosurgery* (2001) 48(4):787–97; discussion 797–8. doi: 10.1227/00006123-200104000-00019
7. Nimsky C, Ganslandt O, Cerny S, Hastreiter P, Greiner G, Fahlbusch R. Quantification of, Visualization of, and Compensation for Brain Shift Using Intraoperative Magnetic Resonance Imaging. *Neurosurgery* (2000) 47(5):1070–9; discussion 1079–80. doi: 10.1097/00006123-200011000-00008
8. Orringer DA, Golby A, Jolesz F. Neuronavigation in the Surgical Management of Brain Tumors: Current and Future Trends. *Expert Rev Med Devices* (2012) 9(5):491–500. doi: 10.1586/erd.12.42
9. Golby A. ed. *Image-Guided Neurosurgery, 1st Edition*. Cambridge, Massachusetts, USA: Academic Press (2015). pp. 536.
10. Zhang J, Chen X, Zhao Y, Wang F, Li F, Xu B. Impact of Intraoperative Magnetic Resonance Imaging and Functional Neuronavigation on Surgical Outcome in Patients With Gliomas Involving Language Areas. *Neurosurg Rev* (2015) 38(2):319–30; discussion 330. doi: 10.1007/s10143-014-0585-z
11. Schenck JF, Jolesz FA, Roemer PB, Cline HE, Lorensen WE, Kikinis R, et al. Superconducting Open-Configuration MR Imaging System for Image-Guided Therapy. *Radiology* (1995) 195(3):805–14. doi: 10.1148/radiology.195.3.7754014
12. Dohrmann GJ, Rubin JM. History of Intraoperative Ultrasound in Neurosurgery. *Neurosurg Clinics N Am* (2001) 12(1):155–166. doi: 10.1016/s1042-3680(18)30074-3
13. Gronningsaeter A, Kleven A, Ommedal S, Aarseth TE, Lie T, Lindseth F, et al. SonoWand, an Ultrasound-Based Neuronavigation System. *Neurosurgery* (2000) 47(6):1373–9; discussion 1379–80. doi: 10.1093/neurosurgery/47.6.1373
14. Nagelhus Hernes TA, Lindseth F, Selbekk T, Wollf A, Solberg OV, Harg E, et al. Computer-Assisted 3D Ultrasound-Guided Neurosurgery: Technological Contributions, Including Multimodal Registration and Advanced Display, Demonstrating Future Perspectives. *Int J Med Robot Comput Assist Surg: MRCAS* (2006) 2(1):45–59. doi: 10.1002/rcs.68
15. Sergeeva O, Uhlemann F, Schackert G, Hergeth C, Morgenstern U, Steinmeier R. Integration of Intraoperative 3d-Ultrasound in a Commercial Navigation System. *Zentralbl für Neurochirurg* (2006) 67(04):197–203. doi: 10.1055/s-2006-942186
16. Unsgaard G, Ommedal S, Muller T, Gronningsaeter A, Nagelhus Hernes TA. Neuronavigation by Intraoperative Three-Dimensional Ultrasound: Initial Experience During Brain Tumor Resection. *Neurosurgery* (2002) 50(4):804–812; discussion 812. doi: 10.1097/00006123-200204000-00022
17. Unsgård G, Lindseth F. 3D Ultrasound–Guided Resection of Low-Grade Gliomas: Principles and Clinical Examples. *Neurosurg Focus* (2019) 47(6):E9. doi: 10.3171/2019.9.FOCUS19605
18. Yeole U, Singh V, Mishra A, Shaikh S, Shetty P, Moiyadi A. Navigated Intraoperative Ultrasonography for Brain Tumors: A Pictorial Essay on the Technique, its Utility, and its Benefits in Neuro-Oncology. *Ultrason* (2020) 39(4):394–406. doi: 10.14366/usg.20044
19. FA Jolesz, ed. *Intraoperative Imaging and Image-Guided Therapy*. New York: Springer Science & Business Media (2014). doi: 10.1007/978-1-4614-7657-3
20. Tempany CMC, Jayender J, Kapur T, Bueno R, Golby A, Agar N, et al. Multimodal Imaging for Improved Diagnosis and Treatment of Cancers. *Cancer* (2015) 121(6):817–27. doi: 10.1002/cncr.29012
21. Ellison DW, Hawkins C, Jones DTW, Onar-Thomas A, Pfister SM, Reifenberger G, et al. cIMPACT-NOW Update 4: Diffuse Gliomas Characterized by MYB, MYBL1, or FGFR1 Alterations or BRAFV600E Mutation. *Acta Neuropathol* (2019) 137(4):683–7. doi: 10.1007/s00401-019-01987-0
22. Ellison DW, Aldape KD, Capper D, Fouladi M, Gilbert MR, Gilbertson RJ, et al. cIMPACT-NOW Update 7: Advancing the Molecular Classification of Ependymal Tumors. *Brain Pathol* (2020) 30(5):863–6. doi: 10.1111/bpa.12866
23. Louis DN, Wesseling P, Aldape K, Brat DJ, Capper D, Cree IA, et al. cIMPACT-NOW Update 6: New Entity and Diagnostic Principle Recommendations of the cIMPACT-Utrecht Meeting on Future CNS Tumor Classification and Grading. *Brain Pathol* (2020) 30(4):844–56. doi: 10.1111/bpa.12832
24. Wesseling P, Capper D. Who 2016 Classification of Gliomas. *Neuropathol Appl Neurobiol* (2018) 44(2):139–50. doi: 10.1111/nan.12432
25. Sawaya R, Hammoud M, Schoppa D, Hess KR, Wu SZ, Shi WM, et al. Neurosurgical Outcomes in a Modern Series of 400 Craniotomies for Treatment of Parenchymal Tumors. *Neurosurgery* (1998) 42(5):1044–55; discussion 1055–6. doi: 10.1097/00006123-199805000-00054
26. Unadkat P, Fumagalli L, Rigolo L, Vangel MG, Young GS, Huang R, et al. Functional MRI Task Comparison for Language Mapping in Neurosurgical Patients. *J Neuroimaging* (2019) 29(3):348–56. doi: 10.1111/jon.12597
27. Frisken S, Luo M, Machado I, Unadkat P, Juvekar P, Bunevicius A, et al. Preliminary Results Comparing Thin Plate Splines With Finite Element Methods for Modeling Brain Deformation During Neurosurgery Using Intraoperative Ultrasound. *Proc SPIE Int Soc Opt Eng* (2019) 10951:1095120. doi: 10.1117/12.2512799
28. Hammoud MA, Ligon BL, elSouki R, Shi WM, Schomer DF, Sawaya R. Use of Intraoperative Ultrasound for Localizing Tumors and Determining the Extent of Resection: A Comparative Study With Magnetic Resonance Imaging. *J Neurosurg* (1996) 84(5):737–41. doi: 10.3171/jns.1996.84.5.0737
29. Solheim O, Selbekk T, Jakola AS, Unsgård G. Ultrasound-Guided Operations in Unselected High-Grade Gliomas–Overall Results, Impact of Image Quality and Patient Selection. *Acta Neurochirurg* (2010) 152(11):1873–86. doi: 10.1007/s00701-010-0731-5
30. LeRoux PD, Winter TC, Berger MS, Mack LA, Wang K, Elliott JP. A Comparison Between Preoperative Magnetic Resonance and Intraoperative Ultrasound Tumor Volumes and Margins. *J Clin Ultrasound: JCU* (1994) 22(1):29–36. doi: 10.1002/jcu.1870220107
31. Unsgaard G, Selbekk T, Brostrup Müller T, Ommedal S, Torp SH, Myhr G, et al. Ability of Navigated 3D Ultrasound to Delineate Gliomas and Metastases – Comparison of Image Interpretations With Histopathology. *Acta Neurochirurg* (2005) 147(12):1259–69. doi: 10.1007/s00701-005-0624-1
32. Shetty P, Yeole U, Singh V, Moiyadi A. Navigated Ultrasound-Based Image Guidance During Resection of Gliomas: Practical Utility in Intraoperative Decision-Making and Outcomes. *Neurosurg Focus* (2021) 50(1):E14. doi: 10.3171/2020.10.FOCUS20550
33. Archip N, Clatz O, Whalen S, Kacher D, Fedorov A, Kot A, et al. Non-Rigid Alignment of Pre-Operative MRI, fMRI, and DT-MRI With Intra-Operative MRI for Enhanced Visualization and Navigation in Image-Guided Neurosurgery. *NeuroImage* (2007) 35(2):609–24. doi: 10.1016/j.neuroimage.2006.11.060
34. Comeau RM, Sadikot AF, Fenster A, Peters TM. Intraoperative Ultrasound for Guidance and Tissue Shift Correction in Image-Guided Neurosurgery. *Med Phys* (2000) 27(4):787–800. doi: 10.1118/1.598942
35. Letteboer MMJ, Willems PWA, Viergever MA, Niessen WJ. Brain Shift Estimation in Image-Guided Neurosurgery Using 3-D Ultrasound. *IEEE Trans Bio Med Eng* (2005) 52(2):268–76. doi: 10.1109/TBME.2004.840186
36. Machado I, Toews M, Luo J, Unadkat P, Essayed W, George E, et al. Non-rigid Registration of 3D Ultrasound for Neurosurgery Using Automatic Feature Detection and Matching. *Int J Comput Assist Radiol Surg* (2018) 13(10):1525–38. doi: 10.1007/s11548-018-1786-7

37. Risholm P, Pieper S, Samset E, Wells WM,3. Summarizing and Visualizing Uncertainty in non-Rigid Registration. *Med Image Comput Comput Assist Interv: MICCAI Int Conf Med Image Comput Comput Assist Interv* (2010) 13 (Pt 2):554–61. doi: 10.1007/978-3-642-15745-5_68
38. Coburger J, Scheuerle A, Kapapa T, Engelke J, Thal DR, Wirtz CR, et al. Sensitivity and Specificity of Linear Array Intraoperative Ultrasound in Glioblastoma Surgery: A Comparative Study With High Field Intraoperative MRI and Conventional Sector Array Ultrasound. *Neurosurg Rev* (2015) 38 (3):499–509. doi: 10.1007/s10143-015-0627-1
39. Sweeney JF, Smith H, Taplin A, Perloff E, Adamo MA. Efficacy of Intraoperative Ultrasonography in Neurosurgical Tumor Resection. *J Neurosurg Pediatr* (2018) 21(5):504–10. doi: 10.3171/2017.11.PEDS17473
40. Selbekk T, Jakola AS, Solheim O, Johansen TF, Lindseth F, Reinertsen I, et al. Ultrasound Imaging in Neurosurgery: Approaches to Minimize Surgically Induced Image Artefacts for Improved Resection Control. *Acta Neurochirurg* (2013) 155(6):973–80. doi: 10.1007/s00701-013-1647-7

Conflict of Interest: The authors declare that the research was conducted in the absence of any commercial or financial relationships that could be construed as a potential conflict of interest.

frontiers in Oncology

ORIGINAL RESEARCH
published: 19 May 2021
doi: 10.3389/fonc.2021.649797

Intraoperative B-Mode Ultrasound Guided Surgery and the Extent of Glioblastoma Resection: A Randomized Controlled Trial

Fatih Incekara[1,2]*, *Marion Smits*[2], *Linda Dirven*[3,4], *Eelke M. Bos*[1], *Rutger K. Balvers*[1], *Iain K. Haitsma*[1], *Joost W. Schouten*[1] *and Arnaud J. P. E. Vincent*[1]

[1] Department of Neurosurgery, Erasmus MC - University Medical Center Rotterdam, Rotterdam, Netherlands, [2] Department of Radiology and Nuclear Medicine, Erasmus MC - University Medical Center Rotterdam, Rotterdam, Netherlands, [3] Department of Neurology, Leiden University Medical Center, Leiden, Netherlands, [4] Department of Neurology, Haaglanden Medical Center, The Hague, Netherlands

OPEN ACCESS

Edited by:
Francesco DiMeco,
Fondazione IRCCS Istituto Neurologio Carlo Besta, Italy

Reviewed by:
Massimiliano Del Bene,
Dipartimento di Neurochirurgia, Istituto Neurologico Carlo Besta (IRCCS), Italy
Francesco Prada,
Fondazione IRCCS Istituto Neurologio Carlo Besta, Italy

***Correspondence:**
Fatih Incekara
f.incekara@erasmusmc.nl

Specialty section:
This article was submitted to Neuro-Oncology and Neurosurgical Oncology, a section of the journal Frontiers in Oncology

Received: 05 January 2021
Accepted: 09 April 2021
Published: 19 May 2021

Citation:
Incekara F, Smits M, Dirven L, Bos EM, Balvers RK, Haitsma IK, Schouten JW and Vincent AJPE (2021) Intraoperative B-Mode Ultrasound Guided Surgery and the Extent of Glioblastoma Resection: A Randomized Controlled Trial. Front. Oncol. 11:649797. doi: 10.3389/fonc.2021.649797

Background: Intraoperative MRI and 5-aminolaevulinic acid guided surgery are useful to maximize the extent of glioblastoma resection. Intraoperative ultrasound is used as a time- and cost-effective alternative, but its value has never been assessed in a trial. The goal of this randomized controlled trial was to assess the value of intraoperative B-mode ultrasound guided surgery on the extent of glioblastoma resection.

Materials and Methods: In this randomized controlled trial, patients of 18 years or older with a newly diagnosed presumed glioblastoma, deemed totally resectable, presenting at the Erasmus MC (Rotterdam, The Netherlands) were enrolled and randomized (1:1) into intraoperative B-mode ultrasound guided surgery or resection under standard neuronavigation. The primary outcome of this study was complete contrast-enhancing tumor resection, assessed quantitatively by a blinded neuroradiologist on pre- and post-operative MRI scans. This trial was registered with ClinicalTrials.gov (NCT03531333).

Results: We enrolled 50 patients between November 1, 2016 and October 30, 2019. Analysis was done in 23 of 25 (92%) patients in the intraoperative B-mode ultrasound group and 24 of 25 (96%) patients in the standard surgery group. Eight (35%) of 23 patients in the intraoperative B-mode ultrasound group and two (8%) of 24 patients in the standard surgery group underwent complete resection (p=0.036). Baseline characteristics, neurological outcome, functional performance, quality of life, complication rates, overall survival and progression-free survival did not differ between treatment groups (p>0.05).

Conclusions: Intraoperative B-mode ultrasound enables complete resection more often than standard surgery without harming patients and can be considered to maximize the extent of glioblastoma resection during surgery.

Keywords: glioblastoma, extent of resection, intraoperative ultrasound, randomized controlled trial, image guided neurosurgery

INTRODUCTION

Patients with glioblastoma have a poor prognosis with a median overall survival of 15 months, despite surgical resection with concomitant and adjuvant chemoradiotherapy (1). Complete resection of contrast-enhancing tumor on T1-weighted post-contrast MRI has consistently been associated with longer overall survival (2, 3). It is shown that intraoperative technologies, specifically 5-aminolevulinic acid or intraoperative MRI guided surgery, are useful to maximize tumor resection during glioblastoma surgery (4–6). Although intraoperative MRI has been associated with higher rates of complete glioblastoma resection, its use is expensive and time-consuming (6).

Intraoperative ultrasound guidance is used during glioblastoma surgery as a time- and cost-effective intraoperative imaging alternative (7). Retrospective studies have shown that intraoperative B-mode ultrasound has the potential to support the surgeon to maximize the extent of glioblastoma resection (8–10). In addition, advanced ultrasound techniques such as contrast enhanced ultrasound, Doppler and elastopgraphy have the potential to better identify residual tumor volumes during glioma surgery (11–14). As Jenkinson et al. showed in a Cochrane review however, the value of intraoperative ultrasound to maximize tumor resection has never been assessed in a randomized controlled trial (4).

We therefore initiated the first randomized controlled trial assessing the value of intraoperative B-mode ultrasound guided surgery on the extent of glioblastoma resection.

MATERIALS AND METHODS

In this randomized controlled trial, patients of 18 years or older with a newly diagnosed, contrast-enhancing presumed glioblastoma, deemed totally resectable, presented at the Erasmus MC (Rotterdam, The Netherlands) were enrolled. Exclusion criteria were tumors located in the basal ganglia, cerebellum, brain stem or crossing the midline thereby prohibiting complete resection; multifocal tumors; patients with a Karnofsky performance status < 60 or with pre-existing neurological deficits (e.g. aphasia, hemiparesis). The study was approved by the Medical Ethical Committee of Erasmus MC (MEC-2015-46). All patients gave written informed consent prior to participation. This trial was reported following the CONSORT guidelines and registered with ClinicalTrials.gov (NCT03531333).

Randomization and Intervention

We randomly assigned patients (1:1) into intraoperative B-mode ultrasound guided surgery (intervention) or resection under standard neuronavigation (control). Randomization was done *via* www.sealedenvelope.com with use of random computer-generated blocks of four by a research assistant who was not otherwise involved with this study. Neurosurgeons and patients were not blinded for treatment allocation. The primary outcome assessor, an independent neuroradiologist, was blinded for treatment group allocation.

Intraoperative ultrasound guidance was performed with the BK Medical Flex Focus 800 ultrasound system alone or integrated with a neuronavigation system (Brainlab, Munich, Germany). The BK Medical craniotomy 8862 transducer was used, which is a convex array transducer with a sector angle of 66° and a contact surface of 29 x 6mm. B-mode, 2-D ultrasound imaging was used without additional usage of advanced ultrasound modalities such as 3-D imaging, contrast-enhanced imaging or elastography. Intraoperative ultrasound was used before opening of the dura to locate the tumor, during tumor resection and to locate any residual tumor in the surgical cavity. Resection was continued until no residual tumor suspected, hyperechoic lesion as seen on ultrasound images was observed in the surgical cavity, or until further resection was deemed unsafe.

Standard surgery was performed with conventional neurosurgical techniques, such as neuronavigation system, cavitational ultrasonic surgical aspiration and surgical microscope. After wound closure, surgeons were asked in both treatment groups to estimate whether complete tumor resection was achieved (yes or no). Surgery time was measured from skin incision to wound closure. Standard adjuvant chemo-and or radiotherapy and clinical follow-up with periodic MRI scans were followed for patients in both groups (15).

Outcome Measures

The primary outcome of this study was complete resection of contrast-enhancing tumor on early postoperative MRI. All patients underwent 1.5T or 3T MRI scanning with and without gadolinium-based contrast agent one day before surgery and within 48 hours after surgery. One blinded, independent, highly experienced neuroradiologist assessed the tumor localization and extent of tumor resection by volumetrically measuring initial and residual contrast-enhancing tumor volumes. First, pre- and post-operative T1-weighted contrast scans were loaded into Brainlab Elements. Using the SmartBrush tool, semi-automatic tumor assessment of all tumor involved contrast enhancement on preoperative scans and on post-operative scans (excluding small vessels or blood in the surgical cavity) was performed. Tumor localization in terms of eloquence was rated following the Sawaya classification (grade 1: non-eloquent, grade 2: near eloquent, grade 3; eloquent) (16). Complete resection was defined as ≥ 99% resection of contrast-enhancing tumor volume.

Secondary outcomes were: extent of tumor resection (%); neurological status on the National Institutes of Health Stroke Scale (NIHSS) within one week after surgery; functional status on Karnofsky performance scale seven weeks, three months and six months after surgery; change over time in health-related quality of life (EORTC QLQ-C-30 (10) and QLQ-BN20 (17–19) questionnaire) from baseline up to six months after surgery; complication rates; overall survival and progression free survival. EORTC scoring procedures were followed to calculate scale scores (20). Three QLQ-C30 scales (global health, physical functioning, cognitive functioning) and two QLQBN-20 scales (motor dysfunction and communication deficits) were preselected for analysis. A change over time of ≥10 points were classified as clinically meaningful changes (21). Complications

were classified according to the US National Cancer Institute common toxicity criteria (CTCAE, version 4.0). Overall survival was defined as time from surgery to death and progression-free survival was defined as time from surgery till clinical or radiological progression following the RANO criteria (22).

Statistical Analysis

Sample size calculation was performed for the primary outcome based on retrospective studies on intraoperative ultrasound and standard surgery as described in the trial protocol (**Supplemental Material**). Based on complete resection rates of the conventional treatment arm as reported by Stummer et al. we estimated that in the standard surgery group 36% of patients would have complete tumor resection (5). With an estimated effect size of 40% increase of complete resection proportion, power of 80% and significance level at 0.05, we calculated that each group had to include 23 patients. To account for the possibility of drop-out or missing data, we increased the sample size to 25 patients per treatment arm and a total of 50 patients.

Statistical analyses were performed with SPSS 25.0 statistical software (IBM Corp.). Descriptive statistics were tested between treatment arms with the Chi Squared test or Fisher Exact test in case of categorical variables and with the Mann-Whitney U test in case of continuous non-normal distributed data. Survival data were compared between treatment groups with log rank tests and Kaplan Meier estimates and analyzed with multivariable Cox proportional-hazards models. Linear Mixed Models were used to compare health-related quality of life scores over time between treatment arms.

RESULTS

We enrolled 50 patients between November 1, 2016 and October 30, 2019. Two patients who were diagnosed with metastases after surgery in the ultrasound group and one patient who received a biopsy instead of surgery in the control group were excluded from all further analyses (**Figure 1**). Patient and tumor baseline characteristics did not differ between treatment groups (**Table 1**). Eight (35%) of 23 patients in the intraoperative ultrasound group and two (8%) of 24 patients in the standard surgery group had complete resection of contrast-enhancing tumor (odds ratio 5.9 (95% CI 1.1-31.6), p=0.036; proportion difference 27% (95% CI,

TABLE 1 | Baseline characteristics.

	Intraoperative ultrasound (n=23)	Resection under standard neuronavigation (n=24)
Age, median years (IQR)	62 (54-71)	64 (57-70)
Sex		
Male	14 (61%)	14 (58%)
Female	9 (39%)	10 (42%)
KPS, median (IQR)	90 (80-100)	90 (80-100)
Tumor localization*		
Non-eloquent	8 (35%)	8 (33%)
Near eloquent	6 (26%)	6 (25%)
Eloquent	9 (39%)	10 (42%)
Tumor volume, median cm^3 (IQR)	38.6 (16.9-60.1)	32.3 (17.2-44.6)
NIHSS, median (IQR)	1 (0-1)	0 (0-2)
Quality of life, mean (SD)**		
Global health status	75 (24)	77 (17)
Physical functioning	88 (15)	91 (16)
Cognitive functioning	88 (16)	85 (21)
Motor dysfunction	12 (18)	10 (21)
Communication deficit	17 (24)	9 (14)

*Data are No. (%), unless stated otherwise. *Sawaya Grading System **For global health status, physical functioning and cognitive functioning, a higher score represents better functioning. For motor dysfunction and communication deficit, a higher score represents more problems.*

KPS, Karnofsky performance status; IDH, isocitrate dehydrogenase; MGMT, methylguanine; DNA, methyltransferase; NIHSS, National Institutes of Health stroke score.

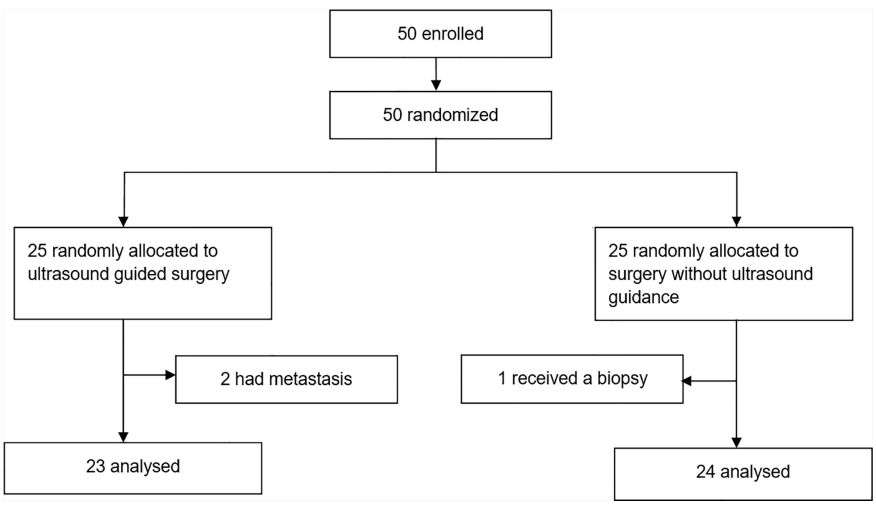

FIGURE 1 | Flowchart.

2.8-47.7), p=0.024). Median extent of resection was 97% (IQR 89-100) with intraoperative ultrasound and 95% (IQR 79-98) with standard surgery (p=0.151, **Table 2**). Median residual tumor volume was 0.9 cm^3 (IQR 0.2-3.4) with intraoperative ultrasound and 1.4 cm^3 (IQR 0.7-6.4) with standard surgery (p=0.205). Patient outcome of both treatment groups are presented in **Table 3**.

Intraoperative ultrasound was used four times (range two to nine) on average per surgery. In the operating room, surgeons estimated that complete tumor resection was achieved in 15 (65%) of 23 patients when intraoperative ultrasound was used and in 17 (71%) of 23 patients without the use of intraoperative ultrasound (p=0.680). However, cases in which complete resection was thought to be achieved corresponded with radiological complete resection in only two (11.8%) of 17 in the standard surgery group and in seven (46.7%) of 15 patients in the intraoperative ultrasound group (proportion difference 34.9%, 95% CI 3.5-59.6, p=0.031; odds ratio 6.6, 95% CI 1.1-39.3, p=0.049). Median surgery time with intraoperative ultrasound guided surgery (177 minutes, IQR 135-255) was comparable to standard surgery (179 minutes, IQR 146-227, p=0.907).

Secondary outcome in terms of overall survival, progression free survival and health-related quality of life did not differ between treatment arms (p>0.05, details available as **Supplemental Material**). Median Karnofsky performance status seven weeks and three months after surgery was 90 (IQR 70/80-100) in both treatment groups. Six months after surgery, Karnofsky performance status was 60 or below in three patients (17%) who underwent intraoperative ultrasound surgery and in seven patients (37%) who underwent standard surgery (p=0.269). Neurological outcome as measured using the NIHSS scale within one week after surgery did not significantly differ between treatment groups (NIHSS 0 (IQR 0-2), p=0.825). In the intraoperative ultrasound *vs.* standard surgery groups, 16 (70%) respectively 19 (79%) patients had the same neurological status on the NIHSS scale after surgery as before surgery and five (22%) respectively three (13%) patients had neurological improvement.

TABLE 2 | Surgery outcome.

	Intraoperative ultrasound (n=23)	Resection under standard neuronavigation (n=24)	p value
Resection			0.036*
Complete	8 (35%)	2 (8%)	
Incomplete	15 (65%)	22 (92%)	
Extent of resection, median (IQR), %	97 (89-100)	95 (79-98)	0.151
Residual tumor volume, median (IQR), cm^3	0.9 (0.2-3.4)	1.4 (0.7-6.4)	0.205
Surgery time, median (IQR), minutes	177 (135-255)	179 (146-227)	0.907
Blood loss, median (IQR), ml	150 (0-400)	125 (58-200)	0.729

Data are n or n (%), unless stated otherwise.
**Significant, p value <0.05.*

TABLE 3 | Patient outcome.

	Intraoperative ultrasound (n=23)	Resection under standard neuronavigation (n=24)	p value
IDH mutation			0.494
Mutated	0 (0%)	0 (0%)	
Wildtype	19 (83%)	17 (71%)	
Unknown	4 (17%)	7 (29%)	
MGMT promotor methylation			0.347
Methylated	6 (26%)	7 (29%)	
Unmethylated	13 (57%)	9 (38%)	
Unknown	4 (17%)	8 (33%)	
Adjuvant therapy			0.148
None	3 (13%)	2 (8%)	
Chemo or radiotherapy	3 (13%)	0 (0%)	
Chemoradiation*	17 (74%)	22 (92%)	
NIHSS post-operative, median (IQR)	0 (0-2)	0 (0-2)	0.825
KPS after surgery, median (IQR)			
Seven weeks	90 (90-100)	90 (80-100)	0.412
Three months	90 (80-100)	90 (70-100)	0.540
Six months	90 (70-90)	70 (60-90)	0.228
Quality of life change, baseline *vs.* six months**			
Global health status	-2 (35)	-14 (28)	0.344
Physical functioning	-8 (31)	-13 (18)	0.267
Cognitive functioning	-11 (32)	-2 (30)	0.893
Motor dysfunction	2 (21)	5 (20)	0.893
Communication deficit	1 (26)	-6 (22)	0.609
Overall survival, median (95% CI), days	377 (247-507)	372 (320-424)	0.751
Progression-free survival, median (95% CI), days	227 (107-347)	233 (153-313)	0.937

*Data are n or n (%), unless stated otherwise. *Stupp protocol **A change of ≥10 points is considered to be clinically relevant.*
KPS, Karnofsky performance status; IDH, isocitrate dehydrogenase; MGMT, methylguanine; DNA, methyltransferase; NIHSS, National Institutes of Health stroke score.

Four (9%) of all 47 patients had new or worsened neurological deficits: two (8%) patients who underwent intraoperative ultrasound guided surgery (one patient with hemiparesis and one with delirium and superior sagittal sinus thrombosis) and two patients (8%) who underwent standard surgery (one patient with aphasia and one with postoperative hemorrhage). Characteristics of these patients are presented in more detail in **Table 4**. Frequency of new or worsened neurological deficits did not significantly differ between treatment groups (p=0.591).

DISCUSSION

This is the first randomized controlled trial that assessed the value of intraoperative B-mode ultrasound guided surgery on the extent of glioblastoma resection. Our trial showed that intraoperative B-mode ultrasound guided surgery enables complete contrast-enhancing tumor resections more often than standard surgery, without harming patients in terms of neurological outcome, functional performance or health-related quality of life.

Complete resection of contrast-enhancing tumor during glioblastoma surgery has consistently been associated with

TABLE 4 | Details of patients with complications.

Patient number	Sex	Age	Treatment group	NIHSS before surgery	NIHSS after surgery	CTCAE grade	Details of complication	Treatment of complication	KPS Seven weeks-three months-six months	Survival (days)
1	Male	75	Resection under standard neuronavigation	1	5	2	Aphasia	None	80-80-70	377
7	Male	65	Resection under standard neuronavigation	0	2	4	Postoperative hemorrhage	Emergency craniotomy	80-80-60	361
30	Male	59	Intraoperative ultrasound	1	9	2	Delirium and a sagittal sinus thrombosis	Haldol for delirium; Fraxiparine for thrombosis	n/a	36
35	Male	43	Intraoperative ultrasound	0	14	3	Left sided hemiparesis and central facial palsy	None	50-40-n/a	172

NIHSS, National Institutes of Health Stroke Scale; CTCAE, Common Terminology Criteria for Adverse Events grading v.4.0; KPS, Karnofsky Performance Status; n/a, not applicable.

longer overall survival (2, 3, 23, 24). It is shown that 5-aminolevulinic acid and intraoperative MRI guided surgery improves the extent of glioblastoma resection (4–6, 25–27).

An alternative potentially cost- and time-effective technology that is used to acquire real-time imaging and apply brain shift correction during neuro-oncological surgery is intraoperative ultrasound guidance (7). Retrospective studies have suggested that intraoperative ultrasound increase the extent of tumor resection during surgery (8–10). These studies however, included different glioma subtypes and held different definitions of gross total resection, thereby introducing some degree of selection and confounding biases. No randomized controlled trial was performed to date to assess the value of intraoperative ultrasound to maximize the extent of glioblastoma resection (4).

When compared to intraoperative MRI, intraoperative ultrasound has two advantages; it is less expensive and, as shown in our trial, it does not prolong surgery time. Surgeons could rapidly control for residual tumor in the resection cavity multiple times during surgery without prolonging surgery time. The interpretation of intraoperative ultrasound images might be more challenging than intraoperative MRI images, however, the integration of an intraoperative ultrasound systems with a standard neuronavigation system (as used in our trial) enables surgeons to overlay intraoperative ultrasound images on navigational preoperative MRI scans, which may facilitate the interpretation of ultrasound images and consequently the accuracy of complete tumor resection estimation. Importantly, we observed that when intraoperative ultrasound was used, surgeons were able to estimate complete tumor resection in the operating room significantly more accurately than with standard surgery without ultrasound guidance, as confirmed on post-operative MRI.

Complete tumor resection as a primary outcome has some aspects that need careful consideration. Several definitions of complete tumor resection exist across studies, both qualitatively as quantitatively (2, 25). Studies defined complete tumor resection as no residual contrast-enhancing tumor on a post-operative MRI scan (24, 28), which is a relatively stringent definition (if quantitatively assessed) and may result in false positive assessment of the presence of residual tumor due to non-specific contrast enhancement such as ischemia, small vessels, a non-specific tissue response, or by T1-hyperintense blood in the surgical cavity that is incorrectly interpreted as enhancement. In our trial, this was mitigated by overlaying the identically acquired and registered pre- and post-contrast T1w sequences to exclude any T1-hyperintense areas from the residual tumor delineation. To take interpretation varieties into account, some studies defined complete tumor resection as contrast-enhancing residual tumor smaller than 0.175 cm^3 following Stummer et al. (5, 6) while others have used extent of resection cut-off percentages, such as 95%, 97% or 98% (27, 29–32). In relation to this, it is known that residual tumor assessment of glioblastoma has a low interobserver agreement, introducing some degree of subjectivity when distinguishing contrast-enhancing residual tumor from non-specific contrast enhancement (33). In this trial, complete tumor resection was defined as more than 99% resection of contrast-enhancing tumor volume, accepting residual contrast-enhancing volume smaller than one percent to account for the non-tumor related post-surgical reactive enhancement amongst others, which is present even on early (within 48h) post-operative MRI scans (34). Even then, our complete resection proportion is lower than that reported in conventional treatment arms of previous trials, however the median extent of resection in both groups were high (97% in intraoperative ultrasound *vs.* in 95% standard surgery) (5, 6). This indicates that the low proportion of complete resection could partially be explained by a possible stringent interpretation of small contrast-enhancing voxels in the surgical cavity rather than surgical performance, as described earlier. This may have led to false positive interpretation of residual contrast enhanced tumor (i.e. false negative complete resection outcomes) in our trial. Importantly, we included only glioblastoma that were deemed complete resectable prior to surgery, which could partially explain the high median extent of resection percentages in both treatment groups (97% with ultrasound guidance and 95% with standard surgery). Our hypothesis in this trial was that in these totally resectable deemed glioblastoma, intraoperative ultrasound would be useful to resect the last small tumor portions and thus to actually achieve complete resection

more often. As mentioned earlier, since only high resection cut-off percentages (e.g. >97% and >98%) (25, 28) are associated with survival benefit, we chose complete resection, rather than resection percentage as primary outcome.

A limitation of this trial is that it was not double-blinded, however, complete resection of contrast-enhancing tumor, our primary outcome, was assessed by an independent, blinded neuroradiologist.

Another limitation of this trial is that only 2-D, B-mode intraoperative ultrasound imaging was used in our trial without the use of advanced ultrasound techniques. Earlier studies have shown that intraoperative B-mode ultrasound enables gross total resection of contrast enhancing tumor more frequently (8–10). Tumor detection however, is dependent on factors such as surgeon experience, resolution and used probe. As Coburger et al. showed, a linear array ultrasound probe is superior in detecting tumor than conventional ultrasound probe. This is even more relevant, since it is shown that the detection of especially smaller residual volumes (<1cm^3) becomes a challenge. Advanced ultrasound techniques such as contrast enhanced ultrasound, Doppler ultrasound and elastography have the potential to improve tumor detection during surgery (11). Prada et al. showed that next to B-mode imaging, contrast enhanced ultrasound to be useful and highly specific in the identification of residual tumor (12, 13). Finally, it is also shown that elastography could better discriminate between different tissues and was able to identify lesion margins sharper compared to B-mode (14). Future studies that include such advanced ultrasound techniques to study the potential of supporting the surgeon to safely maximize the extent of glioblastoma resection are desired. Our trial did not show any overall survival benefit for patients who underwent intraoperative ultrasound. It should be noted however, that our trial did not aim and was not designed or powered to show differences in overall survival. Although complete glioblastoma resection is associated with survival benefit, future trials on image guidance with a suited design and larger sample size are still needed to show any potential clinical benefit directly in the trial itself for patients with glioblastoma.

In conclusion, this randomized controlled trial showed that intraoperative ultrasound guided surgery enables complete contrast-enhancing tumor resections more often than standard surgery, without harming patients in terms of neurological outcome, functional performance or health-related quality of life. Intraoperative ultrasound is a safe and useful intraoperative imaging alternative and, just as intraoperative MRI or 5-aminolevulinic acid guided surgery, can be considered to maximize the extent of contrast-enhancing glioblastoma resection.

DATA AVAILABILITY STATEMENT

The original contributions presented in the study are included in the article/**Supplementary Materials**, further inquiries can be directed to the corresponding author.

ETHICS STATEMENT

The studies involving human participants were reviewed and approved by Medical Ethical Committee of Erasmus MC (MEC-2015-46). The patients/participants provided their written informed consent to participate in this study.

AUTHOR CONTRIBUTIONS

Study design, clinical data collection: FI and AV. Primary outcome assessor: MS. Data interpretation: all authors. All authors contributed to the article and approved the submitted version.

FUNDING

This study was supported by a grant from the Coolsingel Foundation (project number 105517), The Netherlands. The funders had no role in the design, execution or writing of this trial.

SUPPLEMENTARY MATERIAL

The Supplementary Material for this article can be found online at: https://www.frontiersin.org/articles/10.3389/fonc.2021.649797/full#supplementary-material

REFERENCES

1. Stupp R, Hegi ME, Mason WP, van den Bent MJ, Taphoorn MJB, Janzer RC, et al. Effects of Radiotherapy With Concomitant and Adjuvant Temozolomide Versus Radiotherapy Alone on Survival in Glioblastoma in a Randomised Phase III Study: 5-Year Analysis of the EORTC-NCIC Trial. *Lancet Oncol* (2009) 10(5):459–66. doi: 10.1016/S1470-2045(09)70025-7
2. Brown TJ, Brennan MC, Li M, Church EW, Brandmier NJ, Rakszaw ski KL, et al. Association of the Extent of Resection With Survival in Glioblastoma: A Systematic Review and Meta-Analysis. *JAMA Oncol* (2016) 2(11):1460–9. doi: 10.1001/jamaoncol.2016.1373
3. Molinaro AM, Hervey-Jumper S, Morshed RA, Young J, Han SJ, Chunduru P, et al. Association of Maximal Extent of Resection of Contrast-Enhanced and Non-Contrast-Enhanced Tumor With Survival Within Molecular Subgroups of Patients With Newly Diagnosed Glioblastoma. *JAMA Oncol* (2020) 6 (4):495–503. doi: 10.1001/jamaoncol.2019.6143
4. Jenkinson MD, Barone DG, Bryant A, Vale L, Bulbeck H, Law rie TA, et al. Intraoperative Imaging Technology to Maximise Extent of Resection for Glioma Review. *Cochrane Database Syst Rev* (2018) 1:CD012788. doi: 10.1002/14651858.CD012788.pub2
5. Stummer W, Pichlmeier U, Meinel T, Wiestler OD, Zanella F, Reulen HJ, et al. Fluorescence-Guided Surgery With 5-Aminolevulinic Acid for Resection of Malignant Glioma: A Randomised Controlled Multicentre Phase III Trial. *Lancet Oncol* (2006) 7(5):392–401. doi: 10.1016/S1470-2045(06)70665-9
6. Senft C, Bink A, Franz K, Vatter H, Gasser T, Seifert V, et al. Intraoperative MRI Guidance and Extent of Resection in Glioma Surgery: A Randomised,

Controlled Trial. *Lancet Oncol* (2011) 12(11):997–1003. doi: 10.1016/S1470-2045(11)70196-6
7. Unsgaard G, Ommedal S, Muller T, Gronningsaeter A, Nagelhus Hernes TA. Neuronavigation by Intraoperative Three-Dimensional Ultrasound: Initial Experience During Brain Tumor Resection. *Neurosurgery* (2002) 50(4):804–12; discussion 812. doi: 10.1097/00006123-200204000-00022
8. Mahboob S, McPhillips R, Qiu Z, Jiang Y, Meggs C, Schiavone G, et al. Intraoperative Ultrasound-Guided Resection of Gliomas: A Meta-Analysis and Review of the Literature. *World Neurosurg* (2016) 92:255–63. doi: 10.1016/j.wneu.2016.05.007
9. Solheim O, Selbekk T, Jakola AS, Unsgård G. Ultrasound-Guided Operations in Unselected High-Grade Gliomas-Overall Results, Impact of Image Quality and Patient Selection. *Acta Neurochir* (2010) 152(11):1873–86. doi: 10.1007/s00701-010-0731-5
10. Moiraghi A, Prada F, Delaidelli A, Guatta R, May A, Bartoli A, et al. Navigated Intraoperative 2-Dimensional Ultrasound in High-Grade Glioma Surgery: Impact on Extent of Resection and Patient Outcome. *Oper Neurosurg (Hagerstown)* (2020) 18(4):363–73. doi: 10.1093/ons/opz203
11. Del Bene M, Perin A, Casali C, Legnani F, Saladino A, Mattei L, et al. Advanced Ultrasound Imaging in Glioma Surgery: Beyond Gray-Scale B-Mode. *Front Oncol* (2018) 8:576. doi: 10.3389/fonc.2018.00576
12. Prada F, Del Bene M, Fornaro R, Vetrano IG, Martegani A, Aiani L, et al. Identification of Residual Tumor With Intraoperative Contrast-Enhanced Ultrasound During Glioblastoma Resection. *Neurosurg Focus* (2016) 40(3):E7. doi: 10.3171/2015.11.FOCUS15573
13. Prada F, Vitale V, Del Bene M, Boffano C, Sconfienza LM, Pinzi V, et al. Contrast-Enhanced MR Imaging Versus Contrast-enhanced Us: A Comparison in Glioblastoma Surgery by Using Intraoperative Fusion Imaging. *Radiology* (2017) 285(1):242–9. doi: 10.1148/radiol.2017161206
14. Prada F, Del Bene M, Rampini A, Mattei L, Casali C, Vetreno IG, et al. Intraoperative Strain Elastosonography in Brain Tumor Surgery. *Oper Neurosurg (Hagerstown)* (2019) 17(2):227–36. doi: 10.1093/ons/opy323
15. Stupp R, Mason WP, Van Den Bent MJ, Weller M, Fisher B, Taphoorn MJB, et al. Radiotherapy Plus Concomitant and Adjuvant Temozolomide for Glioblastoma. *N Engl J Med* (2005) 352(10):987–96. doi: 10.1056/NEJMoa043330
16. Sawaya R, Hammoud M, Schoppa D, Hess KR, Wu SZ, Shi WM, et al. Neurosurgical Outcomes in a Modern Series of 400 Craniotomies for Treatment of Parenchymal Tumors. *Neurosurgery* (1998) 42(5):1044–55; discussion 1055-1046. doi: 10.1097/00006123-199805000-00054
17. Aaronson NK, Ahmedzai S, Bergman B, Bullinger M, Cull A, Duez NJ, et al. The European Organization for Research and Treatment of Cancer QLQ-C30: A Quality-of-Life Instrument for Use in International Clinical Trials in Oncology. *J Natl Cancer Inst* (1993) 85(5):365–76. doi: 10.1093/jnci/85.5.365
18. Osoba D, Aaronson NK, Muller M, Sneeuw K, Hsu MA, Yung WK, et al. The Development and Psychometric Validation of a Brain Cancer Quality-of-Life Questionnaire for Use in Combination With General Cancer-Specific Questionnaires. *Qual Life Res* (1996) 5(1):139–50. doi: 10.1007/BF00435979
19. Taphoorn MJ, Claassens L, Aaronson NK, Coens C, Mauer M, Osoba D, et al. An International Validation Study of the EORTC Brain Cancer Module (EORTC QLQ-BN20) for Assessing Health-Related Quality of Life and Symptoms in Brain Cancer Patients. *Eur J Cancer* (2010) 46(6):1033–40. doi: 10.1016/j.ejca.2010.01.012
20. Fayers PM AN, Bjordal K, Groenvold M, Curran D, Bottomley A. *The EORTC QLQ-C30 Scoring Manual. 3rd ed*. Brussels, Belgium: European Organisation for Research and Treatment of Cancer (2001).
21. Taphoorn MJ, Stupp R, Coens C, Osoba D, Kortmann R, van den Bent M, et al. Health-Related Quality of Life in Patients With Glioblastoma: A Randomised Controlled Trial. *Lancet Oncol* (2005) 6(12):937–44. doi: 10.1016/S1470-2045(05)70432-0
22. Wen PY, Macdonald DR, Reardon DA, Cloughesy TF, Sorensen AG, Galanis E, et al. Updated Response Assessment Criteria for High-Grade Gliomas: Response Assessment in Neuro-Oncology Working Group. *J Clin Oncol* (2010) 28(11):1963–72. doi: 10.1200/JCO.2009.26.3541
23. Pessina F, Navarria P, Cozzi L, Ascolese AM, Simonelli M, Santoro A, et al. Maximize Surgical Resection Beyond Contrast-Enhancing Boundaries in Newly Diagnosed Glioblastoma Multiforme: Is it Useful and Safe? A Single Institution Retrospective Experience. *J Neurooncol* (2017) 135(1):129–39. doi: 10.1007/s11060-017-2559-9
24. Li YM, Suki D, Hess K, Sawaya R. The Influence of Maximum Safe Resection of Glioblastoma on Survival in 1229 Patients: Can We do Better Than Gross-Total Resection? *J Neurosurg* (2016) 124(4):977–88. doi: 10.3171/2015.5.JNS142087
25. Kubben PL, ter Meulen KJ, Schijns OEMG, ter Laak-Poort MP, van Overbeeke JJ, van Santbrink H. Intraoperative MRI-guided Resection of Glioblastoma Multiforme: A Systematic Review. *Lancet Oncol* (2011) 12(11):1062–70. doi: 10.1016/S1470-2045(11)70130-9
26. Ferraro N, Barbarite E, Albert TR, Berchmans E, Shah AH, Bregy A, et al. The Role of 5-Aminolevulinic Acid in Brain Tumor Surgery: A Systematic Review. *Neurosurg Rev* (2016) 39(4):545–55. doi: 10.1007/s10143-015-0695-2
27. Hatiboglu MA, Weinberg JS, Suki D, Rao G, Prabhu SS, Shah K, et al. Impact of Intraoperative High-Field Magnetic Resonance Imaging Guidance on Glioma Surgery: A Prospective Volumetric Analysis. *Neurosurgery* (2009) 64(6):1073–81. doi: 10.1227/01.NEU.0000345647.58219.07
28. Gessler F, Bernstock JD, Braczynski A, Lescher S, Baumgarten P, Harter PN, et al. Surgery for Glioblastoma in Light of Molecular Markers: Impact of Resection and MGMT Promoter Methylation in Newly Diagnosed IDH-1 Wild-Type Glioblastomas. *Neurosurgery* (2018) 84(1):190–7. doi: 10.1093/neuros/nyy049
29. Lacroix M, Abi-Said D, Fourney DR, Gokaslan ZL, Shi W, DeMonte F, et al. A Multivariate Analysis of 416 Patients With Glioblastoma Multiforme: Prognosis, Extent of Resection, and Survival. *J Neurosurg* (2001) 95(2):190–8. doi: 10.3171/jns.2001.95.2.0190
30. Chaichana KL, Jusue-Torres I, Navarro-Ramirez R, Raza SM, Pascual-Gallego M, Ibrahim A, et al. Establishing Percent Resection and Residual Volume Thresholds Affecting Survival and Recurrence for Patients With Newly Diagnosed Intracranial Glioblastoma. *Neuro Oncol* (2014) 16(1):113–22. doi: 10.1093/neuonc/not137
31. Grabowski MM, Recinos PF, Nowacki AS, Schroeder JL, Angelov L, Barnett GH, et al. Residual Tumor Volume Versus Extent of Resection: Predictors of Survival After Surgery for Glioblastoma. *J Neurosurg* (2014) 121(5):1115–23. doi: 10.3171/2014.7.JNS132449
32. Incekara F, Smits M, van der Voort SR, Dubbink HJ, Atmodimedjo PN, Kros JM, et al. The Association Between the Extent of Glioblastoma Resection and Survival in Light of MGMT Promoter Methylation in 326 Patients With Newly Diagnosed IDH-Wildtype Glioblastoma. *Front Oncol* (2020) 10:1087. doi: 10.3389/fonc.2020.01087
33. Kubben PL, Postma AA, Kessels AG, van Overbeeke JJ, van Santbrink H. Intraobserver and Interobserver Agreement in Volumetric Assessment of Glioblastoma Multiforme Resection. *Neurosurgery* (2010) 67(5):1329–34. doi: 10.1227/NEU.0b013e3181efbb08
34. Bette S, Gempt J, Huber T, Boeckh-Behrens T, Ringel F, Meyer B. Patterns and Time Dependence of Unspecific Enhancement in Postoperative Magnetic Resonance Imaging After Glioblastoma Resection. *World Neurosurg* (2016) 90:440–7. doi: 10.1016/j.wneu.2016.03.031

Conflict of Interest: MS reports an honorarium received from Parexel Ltd (paid to institution) and speaker fees from GE Healthcare (paid to institution).

The remaining authors declare that the research was conducted in the absence of any commercial or financial relationships that could be construed as a potential conflict of interest.

frontiers in Oncology

ORIGINAL RESEARCH
published: 18 August 2021
doi: 10.3389/fonc.2021.656020

Utilizing Intraoperative Navigated 3D Color Doppler Ultrasound in Glioma Surgery

Benjamin Saß[1*], *Mirza Pojskic*[1], *Darko Zivkovic*[1], *Barbara Carl*[1,2], *Christopher Nimsky*[1,3] *and Miriam H. A. Bopp*[1,3]

[1] Department of Neurosurgery, University of Marburg, Marburg, Germany, [2] Department of Neurosurgery, Helios Dr. Horst Schmidt Kliniken, Wiesbaden, Germany, [3] Center for Mind, Brain and Behavior (CMBB), Marburg, Germany

Background: In glioma surgery, the patient's outcome is dramatically influenced by the extent of resection and residual tumor volume. To facilitate safe resection, neuronavigational systems are routinely used. However, due to brain shift, accuracy decreases with the course of the surgery. Intraoperative ultrasound has proved to provide excellent live imaging, which may be integrated into the navigational procedure. Here we describe the visualization of vascular landmarks and their shift during tumor resection using intraoperative navigated 3D color Doppler ultrasound (3D iUS color Doppler).

Methods: Six patients suffering from glial tumors located in the temporal lobe were included in this study. Intraoperative computed tomography was used for registration. Datasets of 3D iUS color Doppler were generated before dural opening and after tumor resection, and the vascular tree was segmented manually. In each dataset, one to four landmarks were identified, compared to the preoperative MRI, and the Euclidean distance was calculated.

Results: Pre-resectional mean Euclidean distance of the marked points was 4.1 ± 1.3 mm (mean ± SD), ranging from 2.6 to 6.0 mm. Post-resectional mean Euclidean distance was 4.7. ± 1.0 mm, ranging from 2.9 to 6.0 mm.

Conclusion: 3D iUS color Doppler allows estimation of brain shift intraoperatively, thus increasing patient safety. Future implementation of the reconstructed vessel tree into the navigational setup might allow navigational updating with further consecutive increasement of accuracy.

Keywords: intraoperative ultras, color Doppler ultrasound, intraoperative imaging, brain shift, glioma

OPEN ACCESS

Edited by:
Francesco DiMeco, Fondazione IRCCS Istituto Neurologio Carlo Besta, Italy

Reviewed by:
Massimiliano Del Bene, Dipartimento di Neurochirurgia, Istituto Neurologico Carlo Besta (IRCCS), Italy
Andrej Steno, Comenius University, Slovakia

***Correspondence:**
Benjamin Saß
sassb@med.uni-marburg.de

Specialty section:
This article was submitted to Neuro-Oncology and Neurosurgical Oncology, a section of the journal Frontiers in Oncology

Received: *20 January 2021*
Accepted: *23 July 2021*
Published: *18 August 2021*

Citation:
Saß B, Pojskic M, Zivkovic D, Carl B, Nimsky C and Bopp MHA (2021) Utilizing Intraoperative Navigated 3D Color Doppler Ultrasound in Glioma Surgery. Front. Oncol. 11:656020. doi: 10.3389/fonc.2021.656020

INTRODUCTION

Gliomas are the most common primary brain tumors representing 27% of all brain and central nervous system (CNS) tumors and 80% of malignant brain tumors in the United States (US) population (1). The broad category of gliomas encompasses tumors of astrocytic, oligodendrocytic, or ependymal origin and is classified by the World Health Organization (WHO) into four grades, depending on histological and molecular characteristics (2). Grade I tumors, typically

seen in children, are potentially curable when resected, whereas low-grade gliomas (WHO grade II), which are mostly seen in young adults, progress eventually to high-grade gliomas (3). The majority of gliomas (55.1%) are glioblastomas WHO grade IV, which occur with an incidence of 3.4 per 100,000 (1). The main cornerstones of glioma therapy include surgery for histological diagnosis and tumor removal, radiotherapy, and pharmacotherapy (4). There is an ongoing debate on the appropriate resection strategy, mainly driven by the demonstration of glioma cells within regions appearing to be normal brain tissue on cerebral magnetic resonance tomography (MRI) (5) and computed tomography (CT) (6, 7) and even in histologically normal brain regions (8). Several studies have proved the extent of resection (EOR) and the residual tumor volume in glioma surgery to be important factors influencing the patient's outcome as measured in progression-free survival and overall survival (9–12). Thus, it is common practice to resect as much tumor as possible while preserving neurological functions (13).

Prerequisite for this is the localization of pathological tissue as well as eloquent brain areas during the neurosurgical procedure, which can be realized using neuronavigational systems. These systems commonly utilize preoperative imaging, to which the patient is registered (14). Intraoperative imaging modalities such as computed tomography (iCT) (15–17), magnetic resonance tomography (iMRI) (18–20), and ultrasound (iUS) (21–23) can be integrated into these systems, improving safety and accuracy. Besides the possibility of instant resection control, intraoperative imaging can help the neurosurgeon to deal with brain shift, a well-described phenomenon, which is mostly due to brain swelling, loss of cerebrospinal fluid, tumor reduction, brain retraction, and influences of gravity after craniotomy and dural opening (24, 25). First efforts to estimate the extent of brain deformation date back to the 1980s (26). Since then various attempts have been made to approach this issue including optical scanning (27) and navigated pointer based surface displacement measurements (28, 29), a stereotactic system with integrated operative microscope and video analysis (24), iMRI (30, 31), and iUS (32–34). Brain shift has been shown to occur during the whole operative procedure, which can be partially addressed by serial MRI acquisitions as demonstrated by Nabavi et al. (35). The main limitations of iMRI are its restricted availability, structural requirements, time consumption, and high costs (36, 37). None of these drawbacks apply for iUS, which can be performed without significant interruption of the surgical procedure, is nowadays widely available, straightforward in use, and cost-effective (38). Modern ultrasound systems can be fully integrated into neuronavigational setups (39, 40) and are able to provide the neurosurgeon with information about resection extent in glioma surgery (40, 41) and brain deformation (39).

First descriptions of brain shift measurements utilizing iUS were published in the late 1990s, when specific, easily identifiable structures like the ventricles were marked in preoperative and intraoperative imaging to evaluate brain shifting (32–34). In 2003 Keles et al. analyzed pre- and postresectional navigated iUS for brain shift correction and determination of resection extent (42). By that time iUS image quality and integration into navigational setups were rather poor, but improved successively the following years (39, 40, 43). In 2010 Ohue et al. described a new US-linked navigation system with improved imaging quality, which they used to quantify brain deformation at different anatomical (ventricles, meninges, sulci) or pathological structures (tumor boundaries) before and after dural opening and after tumor resection (22). These structures were identified in intraoperative brightness modulation (B-mode) ultrasound, whereas vessels can be visualized better in color or power Doppler mode. Already in 2001, Slomka et al. described a voxel-based registration of 3D Doppler ultrasound and preoperative MRI datasets using an iterative algorithm searching for the best geometric match in six cases (44). Rasmussen et al. examined postoperative automatic fusion of magnetic resonance angiogram (MRA) and intraoperative 3D Doppler ultrasound (i3D US Doppler) in five cases and found satisfactory results in terms of accuracy and time expenditure (45). In 2007 Reinertsen et al. intensified research in this respect and validated retrospectively an algorithm in five patients that used vascular centerlines extracted from both modalities to eventually achieve non-linear registration (46). The aforementioned investigations were feasibility studies outside the operating theater, and it took until 2014 to implement intraoperative use, when Reinertsen et al. reported an ultrasound-based registration method to correct for brain shift running during surgery. They performed semi-automatic registration based on MRA and i3D US Doppler datasets, in which the vascular tree was segmented, in seven cases (three vascular and four tumor procedures) and reported their method to be fully integrated into the neuronavigational system and ready to use (37). I3D US Doppler can also be sufficiently co-registered to other vascular imaging modalities, such as 3D digital subtraction angiography (DSA), as shown in 37 vascular cases by Podlesek et al., who utilized a curved linear array transducer capable of generating 3D volumes, which is typically used for endocavitary examinations in obstetrical, gynecological, and urological applications. They described iUS to be a valuable adjunct to established intraoperative vascular imaging modalities like indocyanine green angiography (ICG), although they did not integrate iUS into the navigational setup (47). Mohammadi et al. proposed and tested in a phantom and animal model a new approach for brain shift estimation utilizing a combination of surface imaging (stereo vision) and iUS Doppler, which were both registered to preoperative MRI respectively MRA datasets (48, 49). However, this approach has so far not entered clinical practice.

In our institution, i3D US datasets are routinely acquired during brain tumor resections, adding intraoperative live imaging to our multimodal neuronavigational setup. We have shown for brain metastasis that i3D US clearly delineates tumor boundaries and thereby allows pathologically based estimation of brain shift (50). Whilst tumor contours clearly identifiable with i3D US allow object analyzation and consecutive brain shift estimation in metastasis surgery, this becomes more challenging

in glioma surgery, where tumor boundaries are often not well defined in iUS. In the presented prospective work, we focused on brain shift estimation in glioma surgery utilizing preoperative MRI (preMRI) and i3D US Doppler datasets for the visualization of vascular structures. We designed this work as a proof-of-concept study to examine how the analysis of the vascular shift can be implemented in the preexisting navigational setup with as little workaround as possible to make it easily applicable for intraoperative use.

MATERIALS AND METHODS

To allow good visualization of vessels in i3D US, we only included patients suffering from gliomas and one case of a dysembroplastic neuroepithelial tumor (DNET), which were operated utilizing a temporal craniotomy. For more details see **Table 1**. Informed consent was obtained from all patients. Ethics approval was granted for prospective archiving clinical and technical data applying intraoperative imaging and navigation (study no. 99/18).

All patients underwent MRI imaging within a few days before surgery, typically including contrast-enhanced imaging and time-of-flight (ToF) sequences for vascular imaging. Preoperative imaging was transferred to the navigational system (Brainlab, Munich, Germany), consisting of a ceiling-mounted double monitor (Curve, Brainlab, Munich, Germany), a wall-mounted double display (Buzz, Brainlab, Munich, Germany), and navigational software.

All procedures were conducted under general anesthesia, and all patients received 40 mg of dexamethasone. After narcosis induction, the patients were positioned, the head placed horizontally and fixed to the OR (operating room) table using a radiolucent Doro head clamp with metallic pins. The pins were placed in such a way that in between intraoperative computed tomography (iCT) scanning for registration was possible without significant artifacts. A reference array with four reflective markers was attached to the head clamp. Although not necessary for registration, three fiducial markers were placed on the patient's head within the scanning range allowing registration accuracy measurements. After a 90° rotation of the OR table to the 32-slice mobile CT scanner (AIRO, Brainlab, Munich), a low-dose registration scan (0.042 mSv) of 62 mm scan length was performed. During the scanning process the navigational camera detected reflected markers permanently attached to the AIRO-scanner and the reference array. The dataset was automatically transferred to the navigational system and fused to the preoperative imaging data to establish patient registration. After rotating the OR table back, the registration accuracy was checked by placing the tip of the navigational pointer in the divot of each of the three fiducial markers, which allowed calculation of the target registration error (TRE) as the Euclidean offset of the pointer tip. The reference array was removed and replaced by a sterile one after surgical skin preparation and sterile draping. Further details on the setup using iCT as an registration device were published before (51).

After team time-out, the skin was incised, and the temporalis muscle dissected. Subsequently, 125 ml of 15% mannitol were administered, and a temporal craniotomy performed. First sets of i3D US and i3D US Doppler data were acquired before dural opening using the ultrasound device bk5000 (bk medical, Herlev, Denmark) with a high resolution, small footprint transducer (N13C5, bk medical, Herlev, Denmark), which has a convex contact surface of 29 × 10 mm, a frequency range of 5–13 MHz, and is fully immersible and sterilizable. The pre-calibrated US probe was equipped with a reference array with three reflective markers. Saline was used as a coupling fluid, and the probe was swept gently over the dural layer for image acquisition. The generated 0.3 mm 2D slices were automatically transferred to the navigational system and transformed to co-registered 3D datasets. During the further surgical procedure, the i3D US and i3D US Doppler datasets were displayed either in an overlay view, side-by-side, or as standalone. After tumor resection, another set of US Doppler images was acquired in the same way in six cases.

For analysis of the vascular displacement, the vascular tree was segmented manually using a threshold-based filtering approach or outlined manually in ToF or T1 contrast-enhanced sequences. Because currently, the software does not allow threshold-based segmentation in i3D US Doppler datasets, in ultrasound images the vascular structures were segmented manually with the smart brush application (Brainlab navigational software, Munich, Germany), which is a computer-assisted outlining tool, allowing accelerated object segmentation. Representative, easily identifiable structures, such as vascular bifurcations, were marked in each dataset. To gain information on the brain deformation before dural opening, the Euclidean distance of the defined landmarks in preoperative MRI (preMRI) and pre-resectional i3D US Doppler was calculated. The brain shift occurring during the operative course was determined using the distance of the

TABLE 1 | Patient characteristics and tumor volume.

Case	Age [Years]	Diagnosis	Tumor volume [cm^3]
1	62.4	GBM	47.8
2	37.0	DA	71.5
3	40.8	GBM	39.9
4	71.4	DA*	67.5
5	35.2	DNET	20.4
6	55.6	GBM	41.3

GBM, glioblastoma; DA, diffuse astrocytoma; DA, DA with molecular features of a glioblastoma WHO grade IV; DNET, dysembroplastic neuroepithelial tumor.*

corresponding structures in post-resectional i3D US Doppler compared to preMRI.

GraphPad Prism 8.4.3 (GraphPad Software, San Diego, USA) for MacOS was used for statistical analysis. Under the assumption of normally distributed data, a paired t-test was used for further analysis. A p-value <0.05 was considered statistically significant.

RESULTS AND DISCUSSION

Six patients with temporal glial tumors were included in this study. The mean ± standard deviation (SD) patient age was 50.4 ± 14.9 years, ranging from 35.2 to 71.4 years. The mean ± SD tumor volume was 48.07 ± 19.00 cm^3 (range: 20.4 to 71.5 cm^3). Histopathological workup revealed glioblastoma in three cases. One case was classified as a diffuse astrocytary glioma with molecular features of a glioblastoma WHO grade IV, and one patient was diagnosed with WHO grade II diffuse astrocytoma. We also included one patient with a temporal DNET. The mean TRE was 0.82 ± 0.11 mm (mean ± SD), depicting an excellent registration accuracy. Patient characteristics and tumor volume are summarized in **Table 1**.

The generation of 3D iUS Doppler image sets was straightforward. Pre-resectional 3D iUS Doppler was performed in all cases before dural opening. In case no. 3, the 3D iUS Doppler image set was corrupted by artifacts, primarily caused by dural thickening, permitting no reliable identification of bifurcations or other prominent vascular structures. In all other cases, one to four vascular anatomic points were identified and the Euclidean distance to the corresponding preMRI data calculated (**Figure 1**). For each case the mean Euclidean distance of the marked points was calculated, ranging from 2.6 to 6.0 mm (mean ± SD = 4.1 ± 1.3 mm). Post-resectionally, 3D iUS Doppler was conducted in all six cases. Here, we found a Euclidean distance of 4.7. ± 1.0 mm (mean ± SD), ranging from 2.9 to 6.0 mm. All measurements are shown in **Table 2**. Interestingly, apart from one measured value in case no. 2, the measured Euclidean distances within each case did not vary much, suggesting that the mean value can give a good indication for the estimation of the local brain deformation. Interestingly, according to our measurements the extent of pre-resectional and post-resectional shift of vascular landmarks is similar (mean of differences: 0.55 mm), without statistically significant differences (p = 0.625; paired t-test), as shown in an illustrative example in **Figure 2**. This is in contrast to the generally accepted assumption that the main shifting occurs after durotomy, as shown by Hill et al., who found a dural displacement of only 1.2 ± 2.0 mm (mean ± SD) after craniotomy, but a brain shift of 4.4 ± 1.9 mm (immediately after dural opening) and of 5.6 ± 1.9 mm (approximately 1 h later), respectively (29). On the other hand, Ohue et al. described a displacement of tumor margins of 3.4 ± 1.9 mm (mean ± SD) after craniotomy but before durotomy, which increased to 5.1 ± 2.7 mm, when the dura mater was opened (22). Similar findings were reported by Lettboer et al., who found the main displacement after craniotomy but reported an additional shift of only 0.2 mm once the dural layer was opened (52). Regarding the pre-durotomy shift, our results are well in line with those of Ohue et al. and Lettboer et al., but one would expect more additional brain deformation after tumor resection as demonstrated, for example, by Roberts et al., who found a mean displacement of 1 cm (24). Yet there is a high variability in the extent of brain shift (25), and particularly deeper located structures are less prone to shifting (25, 53), which could also apply for the vascular structures and thus explain our results. Sastry et al. attributed the observation of a rather small post-durotomy shift to registration errors (38). In an earlier study, we determined the accuracy of the co-registration of the precalibrated ultrasound probe, using a tracked ultrasound phantom containing wires, and found an offset of 1.33 ± 0.33 (mean ± SD) (50). Given this and the here calculated high registration accuracy, we consider the influence of the registrational inaccuracies to be minor on our results. Care has to be taken when interpreting our results of the rather small brain shift of deeper located vessels in this study, as in many surgical situations already a little spatial offset of vascular structures could have devastating effects, if not considered by the surgeon. With that in mind, Šteňo et al. described the visualization of lenticulostriate arteries during the resection of insular low-grade gliomas using navigated 3D power Doppler and found this to be a promising approach to increase safety during the surgical course (54).

During surgery the main region of interest with respect to brain shift is the tumor surrounding area, and the actual brain deformation present there might be underestimated by measuring the movement of distant vascular landmarks. In our study, i3D US color Doppler did not depict small peritumoral vessels with such a high resolution that allowed analysis of shifting when compared to preMRI. Regarding this, a reasonable alternative to color Doppler is power Doppler, which does not measure the velocity and direction of the Doppler signal (and thus blood flow) but the power (amplitude) of the signal (55). Power Doppler allows detection of smaller vessels with less blood flow (55, 56), such as peritumoral vascular structures, and is less prone to typical color Doppler limitations and artifacts, like angle dependency or aliasing. Color Doppler is angle dependent, because it depicts the velocity along the ultrasound beam direction and not the true blood flow velocity, and thus, it is not able to detect flow perpendicular to the ultrasound beam. Aliasing occurs when the pulse rate limitation of the ultrasound transducer is exceeded or with inadequate velocity scale settings, resulting in incorrect pixel values. Neither applies for power Doppler, because it is not based on velocity measurements (55, 57). Additionally, power Doppler has less noise artifacts, which can be influenced by Doppler gain settings (38, 57). On the other hand, the power Doppler signal has a tendency to extend beyond the borders of vessels, which consequently appear thicker than they actually are, and the visualization of too many surgically not important vessels might result in rather confusing imaging (58).

Recently, contrast-enhanced ultrasound (CEUS) has been introduced as a real-time imaging in neurosurgical procedures, facilitating identification of pathological tissue and tumor blood

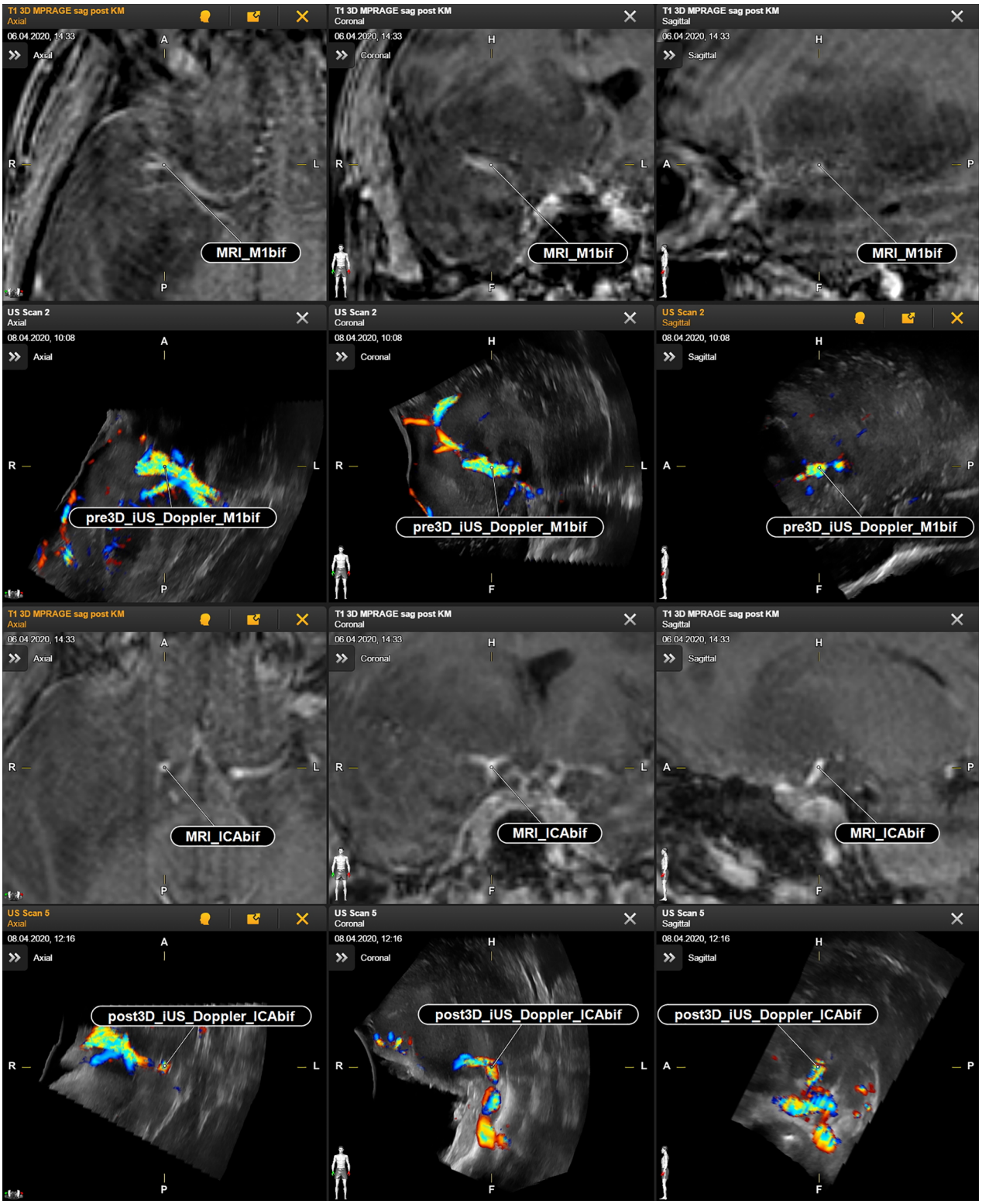

FIGURE 1 | Case no. 2. Identification of vascular anatomic landmarks in MRI and navigated reformatted 3D iUS Doppler. First and second row: preoperative MRI and corresponding pre-resectional 3D iUS Doppler in axial, coronal, and sagittal plane. Third and fourth row: preoperative MRI and corresponding post-resectional 3D iUS Doppler in axial, coronal, and sagittal plane. CAbif, internal carotid artery bifurcation; M1bif, M1bifurcation; pre3D iUS Doppler, pre-resectional 3D iUS Doppler; post3D iUS Doppler, post-resectional 3D iUS Doppler.

TABLE 2 | Measurements.

Case	pre3D iUS Doppler *vs.* preMRI			post3D iUS Doppler *vs.* preMRI		
	Vascular Structure	Euclidean Distance [mm]	Mean Euclidean Distance [mm]	Vascular Structure	Euclidean distance [mm]	Mean Euclidean Distance [mm]
1	ICAbif	5.1	6.0	ICAbif	4.9	5.0
	M1bif	6.9		M1bif	5.0	
2	ICAbif	3.8	3.5	ICAbif	2.4	2.9
	M1bif	3.4		M1bif	3.4	
	M2bif	4.9		M2bif	3.0	
	M1cont	1.86		M1cont	2.9	
3	–	–	–	ACIbif	5.2	5.2
				Basilar tip	5.1	
4	ICAbif	4.5	4.3	ICAbif	3.4	4.5
	M1bif	4.0		M1bif	5.5	
5	–		4.0	ICAbif	6.2	6.0
	M1bif	4.0		M1bif	5.7	
6	ICAbif	3.2	2.6	ICAbif	6.2	4.8
	M1bif	2.0		Basilar tip	4.1	
				A2	4.2	

A2, A2 segment of anterior cerebral artery; ICAbif, internal carotid artery bifurcation; M1bif, M1bifurcation segment of the MCA; M1cont, vascular contact of M1 to another vascular branch; M2, M2 segment of MCA; MCA, middle cerebral artery; pre3D iUS Doppler, pre-resectional 3D iUS Doppler; post3D iUS Doppler, post-resectional 3D iUS Doppler.

supply (59). Ilunga-Mbuyamba et al. acquired intraoperative CEUS and compared it to preoperative MRI data, using an algorithm for image registration. They described a good delineation of smaller vessels and used those data to estimate brain shift (60).

Our study was partially limited by the quality of the 3D iUS Doppler datasets, hampering the identification of landmarks. Additionally, we were confronted with several problems when segmenting the vascular tree. Preoperative MRI segmentation of the vessels was performed automatically in TOF or T1 contrast-enhanced sequences, or, alternatively, using the computer-assisted segmentation *via* the smart brush tool, depending on the quality of the auto-segmented objects. However, in 3D iUS Doppler ultrasound, neither automatic segmentation nor generation of objects using simple thresholding is currently available in the navigational software. Therefore, the vascular tree had to be manually segmented with the smart brush tool, which turned out to be a challenging and time-consuming procedure due to artifacts in the reconstructed and reformatted datasets. Whilst a rough segmentation and identification of vascular landmarks could be performed during surgery by either a neurosurgeon or a trained computer scientist experienced in this field within 5–10 minutes, thorough segmentation using the smart brush tool was more complex and not feasible during the surgical procedure at this stage. Segmentation of small perivascular vessels in ultrasound datasets, which could have been localized with power Doppler or CEUS, using the smart brush tool, and manual identification of corresponding landmarks (e.g., vascular bifurcation) in the peritumoral region would have prolonged the whole procedure dramatically, if even possible. Thus, we focused on greater vascular structures, which could be identified in color Doppler and did not include power Doppler or CEUS analysis. Nevertheless, given a future implementation of automatic ultrasound segmentation into the navigational software, both share a great potential in the field of local brain shift estimation by delineating small peritumoral vessels.

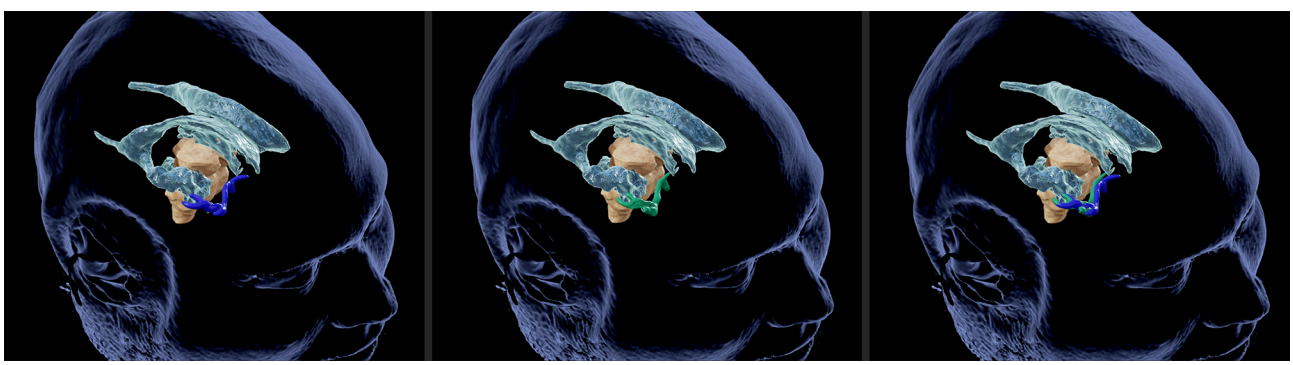

FIGURE 2 | Illustrative case no. 2. 3D view of vascular landmarks segmented in MRI (left) and US (middle). Combined presentation of both segmentations (right) depicts the spatial overlap.

Another option would have been to utilize third-party applications for the analysis of the vessel tree and to transfer the data back to the navigational system. This would allow deeper exploration of approaches, as the one proposed by Reinertsen et al., who used vascular centerlines for the calculation of brain deformation (37, 46). However, here we focused on the built-in features of the navigational system to test for intraoperative applicability. To increase usability and efficiency, the analysis tools should be implemented into the navigational software itself, e.g., for automatic identification and correction of brain shift after 3D iUS Doppler acquisition.

This work involved only patients with temporal mass lesions. We chose this approach to allow good visualization of the vascular tree encompassing, if available, the internal carotid artery, the A1/A2 segment of the anterior cerebral artery, and the M1/M2 segment of the medial cerebral artery, and to make our result more comparable to each other. On the other hand, this patient inclusion criterion makes it difficult to generalize the study results to differently located tumors, in which visualization of the vascular tree may be less successful. Eventually, this study cannot describe the impact of 3D iUS Doppler on every kind of brain tumor resection, but only for those cases in which the deeply located vascular structures are easily depictable in Doppler imaging. Finally, due to the limited number of identified corresponding anatomical landmarks, the here described approach does not allow full correction of brain shift within the navigational system yet. Identification of more representative landmarks or vascular segments would allow fusion of preoperative and intraoperative imaging as shown by Rasmussen et al., who have found satisfactory results in five cases of automatic multimodal fusion of preMRI and i3D US Doppler postoperatively and proposed intraoperative use of their technique (45).

Despite these limitations, we found 3D iUS Doppler to be a valuable adjunct to our multimodal navigational setup. In the current setup, identification of vascular landmarks in color Doppler imaging allows intraoperatively estimation of local brain shift and thus increases safety during resection. Future implementation of automatic segmentation in ultrasound imaging or the possibility of generating objects *via* simple thresholding would facilitate further analysis of the vascular anatomy and brain shift and might allow navigational updating using 3D iUS Doppler datasets. Under these conditions, the advantages of power Doppler mode and CEUS could be fully exploited, and it will be of great interest to find out which type of vascular imaging contributes best and most feasibly to the determination of brain shift.

DATA AVAILABILITY STATEMENT

The original contributions presented in the study are included in the article/supplementary material. Further inquiries can be directed to the corresponding author.

ETHICS STATEMENT

The studies involving human participants were reviewed and approved by Ethikkommission der Philipps Universität Marburg, Fachbereich Medizin. The patients/participants provided their written informed consent to participate in this study.

AUTHOR CONTRIBUTIONSN

Conceptualization, MB, CN, BS. Methodology, MB and BS. Validation, BC, CN, and MP. Investigation, MB, BS, and DZ. Resources, MB, BC, CN, MP, BS, and DZ. Data curation, MB and BS. Writing—original draft preparation, BS. Writing—review and editing, MB and CN. Visualization, MB and BS. Supervision, MB, CN, and BS. Project administration, MB. All authors contributed to the article and approved the submitted version.

REFERENCES

1. Ostrom QT, Gittleman H, Fulop J, Liu M, Blanda R, Kromer C, et al. CBTRUS Statistical Report: Primary Brain and Central Nervous System Tumors Diagnosed in the United States in 2008-2012. *Neuro Oncol* (2015) 17(Suppl 4):iv1–62. doi: 10.1093/neuonc/nov189
2. Sharma A, Graber JJ. Overview of Prognostic Factors in Adult Gliomas. *Ann Palliat Med* (2021) 10(1):863–74. doi: 10.21037/apm-20-640
3. Claus EB, Walsh KM, Wiencke JK, Molinaro AM, Wiemels JL, Schildkraut JM, et al. Survival and Low-Grade Glioma: The Emergence of Genetic Information. *Neurosurg Focus* (2015) 38(1):E6. doi: 10.3171/2014.10.FOCUS12367
4. Weller M, van den Bent M, Tonn JC, Stupp R, Preusser M, Cohen-Jonathan-Moyal E, et al. European Association for Neuro-Oncology (EANO) Guideline on the Diagnosis and Treatment of Adult Astrocytic and Oligodendroglial Gliomas. *Lancet Oncol* (2017) 18(6):e315–29. doi: 10.1016/S1470-2045(17)30194-8
5. Pallud J, Varlet P, Devaux B, Geha S, Badoual M, Deroulers C, et al. Diffuse Low-Grade Oligodendrogliomas Extend Beyond MRI-Defined Abnormalities. *Neurology* (2010) 74(21):1724–31. doi: 10.1212/WNL.0b013e3181e04264
6. Kelly PJ, Daumas-Duport C, Kispert DB, Kall BA, Scheithauer BW, Illig JJ. Imaging-Based Stereotaxic Serial Biopsies in Untreated Intracranial Glial Neoplasms. *J Neurosurg* (1987) 66(6):865–74. doi: 10.3171/jns.1987.66.6.0865
7. Burger PC, Heinz ER, Shibata T, Kleihues P. Topographic Anatomy and CT Correlations in the Untreated Glioblastoma Multiforme. *J Neurosurg* (1988) 68(5):698–704. doi: 10.3171/jns.1988.68.5.0698
8. Silbergeld DL, Chicoine MR. Isolation and Characterization of Human Malignant Glioma Cells From Histologically Normal Brain. *J Neurosurg* (1997) 86(3):525–31. doi: 10.3171/jns.1997.86.3.0525
9. Brown TJ, Brennan MC, Li M, Church EW, Brandmeir NJ, Rakszawski KL, et al. Association of the Extent of Resection With Survival in Glioblastoma: A Systematic Review and Meta-Analysis. *JAMA Oncol* (2016) 2(11):1460–9. doi: 10.1001/jamaoncol.2016.1373
10. Grabowski MM, Recinos PF, Nowacki AS, Schroeder JL, Angelov L, Barnett GH, et al. Residual Tumor Volume Versus Extent of Resection: Predictors of Survival After Surgery for Glioblastoma. *J Neurosurg* (2014) 121(5):1115–23. doi: 10.3171/2014.7.JNS132449

11. Kreth FW, Thon N, Simon M, Westphal M, Schackert G, Nikkhah G, et al. Gross Total But Not Incomplete Resection of Glioblastoma Prolongs Survival in the Era of Radiochemotherapy. *Ann Oncol* (2013) 24(12):3117–23. doi: 10.1093/annonc/mdt388
12. Li YM, Suki D, Hess K, Sawaya R. The Influence of Maximum Safe Resection of Glioblastoma on Survival in 1229 Patients: Can We do Better Than Gross-Total Resection? *J Neurosurgery* (2016) 124(4):977–88. doi: 10.3171/2015.5.JNS142087
13. Almeida JP, Chaichana KL, Rincon-Torroella J, Quinones-Hinojosa A. The Value of Extent of Resection of Glioblastomas: Clinical Evidence and Current Approach. *Curr Neurol Neurosci Rep* (2015) 15(2):517. doi: 10.1007/s11910-014-0517-x
14. Bayer S, Maier A, Ostermeier M, Fahrig R. Intraoperative Imaging Modalities and Compensation for Brain Shift in Tumor Resection Surgery. *Int J BioMed Imaging* (2017) 2017:6028645. doi: 10.1155/2017/6028645
15. Uhl E, Zausinger S, Morhard D, Heigl T, Scheder B , Rachinger W, et al. Intraoperative Computed Tomography With Integrated Navigation System in a Multidisciplinary Operating Suite. *Neurosurgery* (2009) 64(5 Suppl 2):231–9discussion 9–40. doi: 10.1227/01.NEU.0000340785.51492.B5
16. Hosoda T, Takeuchi H, Hashimoto N, Kitai R, Arishima H, Kodera T, et al. Usefulness of Intraoperative Computed Tomography in Surgery for Low-Grade Gliomas: A Comparative Study Between Two Series Without and With Intraoperative Computed Tomography. *Neurol Med Chir (Tokyo)* (2011) 51 (7):490–5. doi: 10.2176/nmc.51.490
17. Barbagallo GMV, Palmucci S, Visocchi M, Paratore S, Attina G, Sortino G, et al. Portable Intraoperative Computed Tomography Scan in Image-Guided Surgery for Brain High-Grade Gliomas: Analysis of Technical Feasibility and Impact on Extent of Tumor Resection. *Oper Neurosurg (Hagerstown)* (2016) 12(1):19–30. doi: 10.1227/NEU.0000000000001112
18. Senft C, Bink A, Franz K, Vatter H, Gasser T, Seifert V. Intraoperative MRI Guidance and Extent of Resection in Glioma Surgery: A Randomised, Controlled Trial. *Lancet Oncol* (2011) 12(11):997–1003. doi: 10.1016/S1470-2045(11)70196-6
19. Kuhnt D, Ganslandt O, Schlaffer SM, Buchfelder M, Nimsky C. Quantification of Glioma Removal by Intraoperative High-Field Magnetic Resonance Imaging: An Update. *Neurosurgery* (2011) 69(4):852–62discussion 62–3. doi: 10.1227/NEU.0b013e318225ea6b
20. Kuhnt D, Bauer MH, Nimsky C. Brain Shift Compensation and Neurosurgical Image Fusion Using Intraoperative MRI: Current Status and Future Challenges. *Crit Rev BioMed Eng* (2012) 40(3):175–85. doi: 10.1615/CritRevBiomedEng.v40.i3.20
21. Gerganov VM, Samii A, Giordano M, Samii M, Fahlbusch R. Two-Dimensional High-End Ultrasound Imaging Compared to Intraoperative MRI During Resection of Low-Grade Gliomas. *J Clin Neurosci* (2011) 18 (5):669–73. doi: 10.1016/j.jocn.2010.08.017
22. Ohue S, Kumon Y, Nagato S, Kohno S, Harada H, Nakagawa K, et al. Evaluation of Intraoperative Brain Shift Using an Ultrasound-Linked Navigation System for Brain Tumor Surgery. *Neurol Med Chir (Tokyo)* (2010) 50(4):291–300. doi: 10.2176/nmc.50.291
23. Gronningsaeter A, Kleven A, Ommedal S, Aarseth TE, Lie T, Lindseth F, et al. SonoWand, an Ultrasound-Based Neuronavigation System. *Neurosurgery* (2000) 47(6):1373–9discussion 9–80. doi: 10.1093/neurosurgery/47.6.1373
24. Roberts DW, Hartov A, Kennedy FE, Miga MI , Paulsen KD. Intraoperative Brain Shift and Deformation: A Quantitative Analysis of Cortical Displacement in 28 Cases. *Neurosurgery* (1998) 43(4):749–58discussion 58–60. doi: 10.1097/00006123-199810000-00010
25. Nimsky C, Ganslandt O, Cerny S, Hastreiter P, Greiner G, Fahlbusch R. Quantification of, Visualization of, and Compensation for Brain Shift Using Intraoperative Magnetic Resonance Imaging. *Neurosurgery* (2000) 47 (5):1070–9. doi: 10.1097/00006123-200011000-00008
26. Kelly PJ, Kall BA, Goerss S, Earnest FT. Computer-Assisted Stereotaxic Laser Resection of Intra-Axial Brain Neoplasms. *J Neurosurg* (1986) 64(3):427–39. doi: 10.3171/jns.1986.64.3.0427
27. MA Audette, K Siddiqi, TM Peters eds. *Level-Set Surface Segmentation and Fast Cortical Range Image Tracking for Computing Intrasurgical Deformations*. Berlin, Heidelberg: Springer Berlin Heidelberg (1999). doi: 10.1007/10704282_86
28. Dorward NL, Alberti O, Velani B, Gerritsen FA, Harkness WF, Kitchen ND, et al. Postimaging Brain Distortion: Magnitude, Correlates, and Impact on Neuronavigation. *J Neurosurg* (1998) 88(4):656–62. doi: 10.3171/jns.1998.88.4.0656
29. Hill DL, Maurer CRJr., Maciunas RJ, Barwise JA, Fitzpatrick JM, Wang MY. Measurement of Intraoperative Brain Surface Deformation Under a Craniotomy. *Neurosurgery* (1998) 43(3):514–26. doi: 10.1097/00006123-199809000-00066
30. Wirtz CR, Bonsanto MM, Knauth M, Tronnier VM, Albert FK, Staubert A, et al. Intraoperative Magnetic Resonance Imaging to Update Interactive Navigation in Neurosurgery: Method and Preliminary Experience. *Comput Aided Surg* (1997) 2(3-4):172–9. doi: 10.3109/10929089709148110
31. Nimsky C, Ganslandt O, Hastreiter P, Fahlbusch R. Intraoperative Compensation for Brain Shift. *Surg Neurol* (2001) 56(6):357–64. doi: 10.1016/S0090-3019(01)00628-0
32. Bucholdz RD, Yeh DD, Trobaugh J, McDurmount LL, Sturm CD, Baumann C, et al eds. *The Correction of Stereotactic Inaccuracy Caused by Brain Shift Using an Intraoperative Ultrasound Device*. Berlin, Heidelberg: Springer Berlin Heidelberg (1997). 10.1007/BFb0029268
33. Jodicke A, Deinsberger W, Erbe H, Kriete A, Boker DK. Intraoperative Three-Dimensional Ultrasonography: An Approach to Register Brain Shift Using Multidimensional Image Processing. *Minim Invasive Neurosurg* (1998) 41 (1):13–9. doi: 10.1055/s-2008-1052008
34. Comeau RM, Fenster A, Peters TM. Intraoperative US in Interactive Image-Guided Neurosurgery. *Radiographics* (1998) 18(4):1019–27. doi: 10.1148/radiographics.18.4.9672984
35. Nabavi A, Black PM, Gering DT, Westin CF, Mehta V, Pergolizzi RSJr., et al. Serial Intraoperative Magnetic Resonance Imaging of Brain Shift. *Neurosurgery* (2001) 48(4):787–97discussion 97–8. doi: 10.1227/00006123-200104000-00019
36. Nimsky C, Ganslandt O, von Keller B, Romstock J, Fahlbusch R. Intraoperative High-Field-Strength MR Imaging: Implementation and Experience in 200 Patients. *Radiology* (2004) 233(1):67–78. doi: 10.1148/radiol.2331031352
37. Reinertsen I, Lindseth F, Askeland C, Iversen DH, Unsgard G. Intra-Operative Correction of Brain-Shift. *Acta Neurochir (Wien)* (2014) 156(7):1301–10. doi: 10.1007/s00701-014-2052-6
38. Sastry R, Bi WL, Pieper S, Frisken S, Kapur T, Wells W3rd, et al. Applications of Ultrasound in the Resection of Brain Tumors. *J Neuroimaging* (2017) 27 (1):5–15. doi: 10.1111/jon.12382
39. Unsgaard G, Ommedal S, Muller T, Gronningsaeter A, Nagelhus Hernes TA. Neuronavigation by Intraoperative Three-Dimensional Ultrasound: Initial Experience During Brain Tumor Resection. *Neurosurgery* (2002) 50(4):804–12:discussion 12. doi: 10.1097/00006123-200204000-00022
40. Tronnier VM, Bonsanto MM, Staubert A, Knauth M, Kunze S, Wirtz CR. Comparison of Intraoperative MR Imaging and 3D-Navigated Ultrasonography in the Detection and Resection Control of Lesions. *Neurosurg Focus* (2001) 10(2):E3. doi: 10.3171/foc.2001.10.2.4
41. Munkvold BKR, Jakola AS, Reinertsen I, Sagberg LM, Unsgard G, Solheim O. The Diagnostic Properties of Intraoperative Ultrasound in Glioma Surgery and Factors Associated With Gross Total Tumor Resection. *World Neurosurg* (2018) 115:e129–e36. doi: 10.1016/j.wneu.2018.03.208
42. Keles GE, Lamborn KR, Berger MS. Coregistration Accuracy and Detection of Brain Shift Using Intraoperative Sononavigation During Resection of Hemispheric Tumors. *Neurosurgery* (2003) 53(3):556–62discussion 62–4. doi: 10.1227/01.NEU.0000080949.44837.4C
43. Pallatroni H, Hartov A, McInerney J, Platenik LA, Miga MI, Kennedy FE, et al. Coregistered Ultrasound as a Neurosurgical Guide. *Stereot Funct Neuros* (1999) 73(1-4):143–7. doi: 10.1159/000029775
44. Slomka PJ, Mandel J, Downey D, Fenster A. Evaluation of Voxel-Based Registration of 3-D Power Doppler Ultrasound and 3-D Magnetic Resonance Angiographic Images of Carotid Arteries. *Ultrasound Med Biol* (2001) 27 (7):945–55. doi: 10.1016/S0301-5629(01)00387-8
45. Rasmussen IAJr., Lindseth F, Rygh OM, Berntsen EM, Selbekk T, Xu J, et al. Functional Neuronavigation Combined With Intra-Operative 3D Ultrasound: Initial Experiences During Surgical Resections Close to Eloquent Brain Areas and Future Directions in Automatic Brain Shift Compensation of Preoperative Data. *Acta Neurochir (Wien)* (2007) 149(4):365–78. doi: 10.1007/s00701-006-1110-0
46. Reinertsen I, Lindseth F, Unsgaard G, Collins DL. Clinical Validation of Vessel-Based Registration for Correction of Brain-Shift. *Med Image Anal* (2007) 11(6):673–84. doi: 10.1016/j.media.2007.06.008

47. Podlesek D, Meyer T, Morgenstern U, Schackert G, Kirsch M. Improved Visualization of Intracranial Vessels With Intraoperative Coregistration of Rotational Digital Subtraction Angiography and Intraoperative 3D Ultrasound. *PloS One* (2015) 10(3):e0121345. doi: 10.1371/journal.pone.0121345
48. Mohammadi A, Ahmadian A, Azar AD, Sheykh AD, Amiri F, Alirezaie J. Estimation of Intraoperative Brain Shift by Combination of Stereovision and Doppler Ultrasound: Phantom and Animal Model Study. *Int J Comput Assist Radiol Surg* (2015) 10(11):1753–64. doi: 10.1007/s11548-015-1216-z
49. Mohammadi A, Ahmadian A, Rabbani S, Fattahi E, Shirani S. A Combined Registration and Finite Element Analysis Method for Fast Estimation of Intraoperative Brain Shift; Phantom and Animal Model Study. *Int J Med Robot* (2017) 13(4):1–8. doi: 10.1002/rcs.1792
50. Saß B, Carl B, Pojskic M, Nimsky C, Bopp M. Navigated 3d Ultrasound in Brain Metastasis Surgery: Analyzing the Differences in Object Appearances in Ultrasound and Magnetic Resonance Imaging. *Appl Sci* (2020) 10(21):7798. doi: 10.3390/app10217798
51. Carl B, Bopp M, Sass B, Nimsky C. Intraoperative Computed Tomography as Reliable Navigation Registration Device in 200 Cranial Procedures. *Acta Neurochir (Wien)* (2018) 160(9):1681–9. doi: 10.1007/s00701-018-3641-6
52. Letteboer MM, Willems PW, Viergever MA, Niessen WJ. Brain Shift Estimation in Image-Guided Neurosurgery Using 3-D Ultrasound. *IEEE Trans BioMed Eng* (2005) 52(2):268–76. doi: 10.1109/TBME.2004.840186
53. Ganser KA, Dickhaus H, Staubert A, Bonsanto MM, Wirtz CR, Tronnier VM, et al. Quantification of Brain Shift Effects in MRI Images. *BioMed Tech (Berl)* (1997) 42 Suppl:247–8. doi: 10.1515/bmte.1997.42.s2.247
54. Steno A, Jezberova M, Holly V, Timarova G, Steno J. Visualization of Lenticulostriate Arteries During Insular Low-Grade Glioma Surgeries by Navigated 3D Ultrasound Power Doppler: Technical Note. *J Neurosurg* (2016) 125(4):1016–23. doi: 10.3171/2015.10.JNS151907
55. Anderson T, McDicken WN. The Difference Between Colour Doppler Velocity Imaging and Power Doppler Imaging. *Eur J Echocardiogr* (2002) 3 (3):240–4. doi: 10.1053/euje.3.3.240
56. Martinoli C, Pretolesi F, Crespi G, Bianchi S, Gandolfo N, Valle M, et al. Power Doppler Sonography: Clinical Applications. *Eur J Radiol* (1998) 27 Suppl 2:S133–40. doi: 10.1016/S0720-048X(98)00054-0
57. Pozniak MA, Zagzebski JA, Scanlan KA. Spectral and Color Doppler Artifacts. *Radiographics* (1992) 12(1):35–44. doi: 10.1148/radiographics.12.1.1734480
58. Rygh OM, Nagelhus Hernes TA, Lindseth F, Selbekk T, Brostrup Muller T, Unsgaard G. Intraoperative Navigated 3-Dimensional Ultrasound Angiography in Tumor Surgery. *Surg Neurol* (2006) 66(6):581–92: discussion 92. doi: 10.1016/j.surneu.2006.05.060
59. Prada F, Del Bene M, Mattei L, Lodigiani L, DeBeni S, Kolev V, et al. Preoperative Magnetic Resonance and Intraoperative Ultrasound Fusion Imaging for Real-Time Neuronavigation in Brain Tumor Surgery. *Ultraschall Med* (2015) 36(2):174–86. doi: 10.1055/s-0034-1385347
60. Ilunga-Mbuyamba E, Avina-Cervantes JG, Lindner D, Cruz-Aceves I, Arlt F, Chalopin C. Vascular Structure Identification in Intraoperative 3d Contrast-Enhanced Ultrasound Data. *Sensors (Basel)* (2016) 16(4):1–14. doi: 10.3390/s16040497

Conflict of Interest: CN and MB are consultants for Brainlab.

The remaining authors declare that the research was conducted in the absence of any commercial or financial relationships that could be construed as a potential conflict of interest.

Publisher's Note: All claims expressed in this article are solely those of the authors and do not necessarily represent those of their affiliated organizations, or those of the publisher, the editors and the reviewers. Any product that may be evaluated in this article, or claim that may be made by its manufacturer, is not guaranteed or endorsed by the publisher.

Advantages of publishing in Frontiers

OPEN ACCESS
Articles are free to read for greatest visibility and readership

FAST PUBLICATION
Around 90 days from submission to decision

HIGH QUALITY PEER-REVIEW
Rigorous, collaborative, and constructive peer-review

TRANSPARENT PEER-REVIEW
Editors and reviewers acknowledged by name on published articles

Frontiers
Avenue du Tribunal-Fédéral 34
1005 Lausanne | Switzerland

Visit us: www.frontiersin.org
Contact us: frontiersin.org/about/contact

REPRODUCIBILITY OF RESEARCH
Support open data and methods to enhance research reproducibility

DIGITAL PUBLISHING
Articles designed for optimal readership across devices

FOLLOW US
@frontiersin

IMPACT METRICS
Advanced article metrics track visibility across digital media

EXTENSIVE PROMOTION
Marketing and promotion of impactful research

LOOP RESEARCH NETWORK
Our network increases your article's readership